

Dissertation

submitted to the

Combined Faculty of the Natural Sciences and
Mathematics of the Ruperto-Carola-University of
Heidelberg, Germany

for the degree of

Doctor of Natural Sciences

Put forward by

Christophe Pixius

born in

Wiltz, Luxembourg

Oral examination: 04.07.2023

ON THE PERTURBATIVE TREATMENT OF INTERACTIONS IN
KINETIC FIELD THEORY
APPLICATIONS TO COSMIC STRUCTURE FORMATION

Refereed by:

Prof. Dr Matthias Bartelmann

Prof. Dr. Björn Malte Schäfer

ABSTRACT

We present the results of applying a perturbative treatment of the interaction operator in the canonical formulation of kinetic field theory (KFT) to cosmic structure formation. The KFT formalism, developed in a series of publications [1–4], allows for the description of equilibrium and non-equilibrium classical many-body systems. The usefulness of KFT for analytical calculations of cosmic structure formation stems from the fact that it circumvents approximations such as the single-stream approximation, which cause more common hydrodynamical frameworks such as Eulerian and Lagrangian perturbation theory to break down at small scales where non-linear structures are forming. This work focuses on a systematic treatment of perturbation theory, which corresponds to an expansion in perturbative corrections to the free phase-space trajectories of the classical point-particles of the system in canonical KFT. We show how diagrams for this perturbation theory can be constructed and evaluated and investigate the different choices for defining free particle trajectories and the corresponding interactions. Results for the dark matter power spectrum are presented and discussed for two such choices, Newtonian and Zel’dovich trajectories. We find that the choice of free trajectories has a substantial impact on the strength of perturbative corrections and specifically that Newtonian trajectories are not well suited to be applied in the canonical formulation of KFT.

ZUSAMMENFASSUNG

Wir stellen die Resultate der Anwendung einer störungstheoretische Behandlung des Wechselwirkungsoperators in der kanonischen Formulierung der kinetischen Feldtheorie (KFT) auf kosmische Strukturbildung vor. Der KFT Formalismus, welcher in einer Reihe von Publikationen [1–4] entwickelt wurde, erlaubt die Beschreibung klassischer Vielteilchensysteme innerhalb und außerhalb des Gleichgewichtszustandes. Die Nützlichkeit der KFT zur analytischen Berechnung kosmischer Strukturbildung ist dadurch begründet, dass sie es einem erlaubt die Einzelstromnäherung, welche andere weitverbreitete Methoden wie die Eulersche und Lagrangesche Störungstheorie auf kleinen Skalen, wo sich nichtlineare Strukturen bilden, zusammenbrechen lässt, zu umgehen. Der Schwerpunkt dieser Arbeit liegt in einer systematischen Auswertung der Störungstheorie in kanonischer KFT, welche einer perturbativen Entwicklung in den, durch Wechselwirkungen verursachten, Korrekturen der klassischen Teilchentrajektorien des Systems entspricht. Wir zeigen wie Diagramme für diese Störungstheorie konstruiert und ausgewertet werden können, und untersuchen die Auswirkung verschiedener Wahlen für die Definition freier Teilchentrajektorien und den entsprechenden Wechselwirkungen. Für zwei dieser Wahlen, welche Newton- und Zel’dovich-Trajektorien entsprechen werden Resultate für das Dunkle-Materie-Leistungsspektrum vorgestellt und diskutiert. Wir finden eine erhebliche Auswirkung der Wahl freier Teilchentrajektorien auf die Stärke der störungstheoretischen Korrekturen und zeigen, dass Newtonsche Trajektorien sich nicht für Rechnungen in der kanonischen Störungstheorie eignen.

“If you are out to describe the truth, leave elegance to the tailor.”

— Ludwig Boltzmann

ACKNOWLEDGEMENTS

This work was supported by the Luxembourg National Research Fund (FNR) under the AFR PhD program. Thank you for the funding support that made this thesis possible.

It is my great pleasure to start this work by thanking all the people who have supported me over the years that saw this thesis come to light.

First and foremost, I want to express my deepest gratitude to my supervisor Matthias Bartelmann, who showed nothing but support for my decisions. His unshakable optimism, fascination for physics, and drive to share his profound knowledge with the world are unceasing sources of inspiration and motivation. Thank you for the amazing work you are doing!

I also want to thank Björn Malte Schäfer for graciously accepting to be my co-corrector and for enlightening me and the entire institute with his many insightful and funny stories during afternoon breaks.

Additionally, I want to offer my thanks to Prof. Cornelis Dullemond and Prof. Monica Dunford, for agreeing to be part of my disputation as examiners.

My deepest thanks go to Elena Kozlikin, Tristan Daus and Iris Feldt for the uncountable exciting and thought-provoking discussions we had at the institute, at the boulder gym and in Fontainebleau. You never know what expects you when you open the door to their office, but you know it will be good. For his exciting insights about cosmology and sharing his quirky knowledge about typesetting, obscure programming languages and the details of the German criminal code, I want to express my gratitude to my (unfortunately only recent) office mate Marvin Sipp. Of course, I should also mention that Marvin, Elena and Tristan read parts of this thesis and provided incredibly constructive and insightful feedback. Thank you so much for your help!

Special thanks also go to Ricardo Waibel for the incredible work he put into organizing the “KFT week” which brought together and sparked discussions among all the researchers engaged in this fascinating field. In this context, my thanks also go to Robert Lilow and Stefan Zentarra for offering their deep insights into KFT and to Johannes Schwinn who shared his experience as a PhD candidate with me and supported me as a friend.

I realize that I could go on and on, thanking every single person at the institute for creating a genuinely awe-inspiring atmosphere of kindness and scientific spirit on the second floor of Philosophenweg 12. Let me, therefore, give a big shout-out to all the members of the Bartelmann, Schäfer and Heisenberg groups for helping to create and maintain this truly unique spirit and for providing a steady supply of cakes.

A big thank-you also to all my former flatmates from Oberdorfstraße who made the Covid lockdown feel so much more bearable. In particular, I want to thank Sonja for the countless intriguing conversations about KFT, physics and life in general, and Daniel for teaching me some humility in chess (or was it the other way around?).

Last but certainly not least, I want to thank my family, my friends and my fantastic partner Inu for their continued love and support, which helped me to pursue my passion. The last years have truly been a great journey, and knowing that you all got my back made it that much more enjoyable.

And now, to quote Dr. Sheldon Cooper, *“Let’s put on our thinking cap, shall we?”*

CONTENTS

1	INTRODUCTION	1
1.1	Motivation	1
1.2	Notation and Fourier convention	2
I	FOUNDATIONS	5
2	COSMOLOGY AND LARGE SCALE STRUCTURE FORMATION	7
2.1	The cosmological standard model	7
2.1.1	The Friedmann equation	7
2.1.2	Observations	8
2.2	Cosmic structures - a statistical description	10
2.2.1	The two-point correlation function	10
2.2.2	The power spectrum	11
2.3	Structures in the early universe	11
2.3.1	Planting the seeds	12
2.3.2	Evolution through matter-radiation equality	12
2.4	Eulerian perturbation theory	14
2.4.1	Equations of motion	14
2.4.2	Linear growth	15
2.4.3	Initial conditions and the linear power spectrum	16
2.4.4	Beyond linear growth	17
2.5	Lagrangian perturbation theory	18
2.5.1	Equations of motion	19
2.5.2	First-order result and the Zel'dovich approximation	20
2.5.3	The power spectrum in the Zel'dovich approximation	21
2.6	Simulations and the halo model	22
2.7	Discussion	23
3	KINETIC FIELD THEORY	25
3.1	General setting and notation	25
3.2	From the probability density to the generating functional	26
3.3	General particle trajectories and the interaction operator	28
3.3.1	Free phase-space trajectories	30
3.3.2	Fully interacting phase-space trajectories	30
3.4	Essential macroscopic operators	31
3.4.1	The density operator	31
3.4.2	Interactions and the response field operator	33
3.5	Canonical perturbation theory	36
3.6	A toy model for canonical perturbation theory	39
3.6.1	Setting	39
3.6.2	Interactions and diagrams	40
3.6.3	Topologies of diagrams	42
3.6.4	Special case: harmonic interaction potential	43
3.7	Discussion	45
4	KINETIC FIELD THEORY FOR COSMIC STRUCTURE FORMATION	47
4.1	The continuum limit	47

4.2	Initial conditions	47
4.2.1	Probability density	48
4.2.2	KFT correlation functions with cosmological initial conditions	50
4.2.3	Expanding in the initial power spectrum	55
4.3	Diagrammatic approach to canonical perturbation theory	57
4.3.1	Motivation	57
4.3.2	Density operators	58
4.3.3	Response field contractions	59
4.3.4	Rules for the construction and evaluation of diagrams	60
4.3.5	Including initial correlations	63
4.4	Phase-space trajectories in an expanding universe	64
4.4.1	The Lagrangian of a particle in expanding space-time	64
4.4.2	Hamiltonian and equations of motion	64
4.4.3	Zel'dovich trajectories	66
4.5	The KFT power spectrum in the Zel'dovich approximation	70
4.6	Discussion	71
II	RESULTS	73
5	ANALYTICAL RESULTS FOR THE TWO-POINT FUNCTION	75
5.1	Linear growth from Newtonian trajectories	75
5.1.1	Non-vanishing diagrams	75
5.1.2	Evaluation of non-vanishing diagrams	77
5.1.3	Formal resummation	78
5.1.4	Truncation at a finite order	79
5.2	Linear growth from Zel'dovich trajectories	81
5.3	Discussion	84
6	GOING BEYOND LINEAR GROWTH	87
6.1	Results for Newtonian trajectories	87
6.1.1	First and second-order perturbative corrections	88
6.1.2	Evaluation of higher orders	90
6.1.3	Results for the dark matter power spectrum	92
6.2	Results for Zel'dovich trajectories	94
6.2.1	Evaluation of particle interactions	95
6.2.2	Evaluation of the counter-operator	96
6.2.3	Results for the dark matter power spectrum	97
6.2.4	Remarks on the evaluation	98
6.3	Discussion	100
7	CONCLUSION	103
III	APPENDIX	107
A	DETAILED CALCULATIONS FOR EULERIAN AND LAGRANGIAN PERTURBATION THEORY	109
A.1	Transforming the time coordinate in the Euler-Poisson system	109
A.2	First order LPT solution equation	110
A.3	Derivation of the power spectrum in the Zel'dovich approximation	110
B	PARTICLE TRAJECTORIES	113
B.1	Derivation of general particle trajectories	113
B.2	Phase-space trajectories in cosmology - Newtonian trajectories	114
B.3	Phase-space trajectories in cosmology - Zel'dovich trajectories	115

C	EFFECT OF RESPONSE FIELD OPERATORS	117
D	TRADITIONAL DIAGRAMS OF CANONICAL PERTURBATION THEORY	121
	D.1 Construction of diagrams	121
	D.2 Evaluation of diagrams	123
E	DERIVATION OF THE COUNTER-OPERATOR	127
F	DERIVATION OF PARTICLE DYNAMICS IN COSMOLOGY FROM GENERAL REL- ATIVITY	131
	F.1 Ingredients	131
	F.2 The dynamics of the metric	132
	F.3 Particle dynamics	134
G	LAPLACE TRANSFORMS	137
	G.1 Some basic facts	137
	G.2 Application	137
	BIBLIOGRAPHY	139

INTRODUCTION

1.1 MOTIVATION

Although cosmology is a comparatively young science, it has seen tremendous progress throughout its relatively short history. Starting with the early discovery of cosmic expansion due to the works of Friedman, Lemaître, Hubble, and others in the 1920s, cosmology has evolved into a precision science due to crucial developments such as the discovery of the cosmic microwave background (CMB) radiation in 1964 [5], the first measurement of CMB anisotropies by COBE in 1992 [6] and the definitive measurement of cosmic acceleration in 1998 [7, 8], to name just a few.

These and many more discoveries and paradigm shifts have led us to the current standard Λ CDM model of cosmology, postulating a universe containing not only radiation and visible matter but also a predominantly unknown component called dark energy (which might well be a cosmological constant Λ), driving the current cosmic acceleration, and an unknown dark matter component dictating the formation of large-scale structures. Although the Λ CDM model is hugely successful in matching observational data and has been constrained to extremely high precision by modern CMB observations [9], many open questions remain. While the physical nature of dark energy and dark matter have been a mystery for decades, additional challenges have arisen more recently with an emerging tension between the values of the Hubble constant H_0 (quantifying the current rate of cosmic expansion) inferred by CMB and local supernova observations [10]. Addressing these outstanding problems requires more data and a better understanding of the underlying models. Nowadays, a large variety of measurements are used to put further constraints on the current cosmological model, and with larger and more precise surveys planned for the coming years, a more profound theoretical understanding of the observed objects is in need. Among these observations are surveys probing the large-scale structure of the universe. Comparing observations and theoretical predictions of distinct features, such as baryonic acoustic oscillations, in the spatial distribution of galaxies allows us to infer further information about the cosmological model and put constraints on its parameters.

But beyond its practical usefulness, cosmic structure formation is an interesting physical problem in its own right, as it represents an example of a classical statistical system far from equilibrium. The predominant analytical methods to calculate the evolution of cosmic structures are based on the equations of hydrodynamics, thus describing the cosmic matter content as a self-gravitating fluid. Around the turn of the century, two approaches emerged for the analytical treatment of cosmic structure formation, Standard (Eulerian) Perturbation Theory (SPT) and Lagrangian Perturbation Theory (LPT) corresponding to the Eulerian and the Lagrangian picture of fluid dynamics (see the review of Bernardeau et al. [11]). The seminal papers of Crocce and Scoccimarro [12, 13] in

2006 sparked a renewed interest in SPT by introducing the community to more powerful techniques of field theory. Since then, a broad panoply of advanced non-perturbative methods of quantum field theory (QFT), such as the use of an effective action and renormalization group techniques, have been proposed for SPT [14–16]. Nevertheless, as was noted early on in [17], theories building on the basic assumptions of SPT are bound to break down below certain length scales. In parallel to the developments of analytical methods for cosmic structure formation, more and more powerful simulations are becoming available [18], allowing us to tackle the problem from a different angle. Indeed, simulations of cosmic structure formation allow for a calculation of cosmic structures down to much smaller scales than analytical methods. Unfortunately, they come at a high computational and financial cost and are not suitable for efficiently exploring large ranges of cosmic models.

It is in this context that Kinetic Field Theory (KFT), which has recently been developed as a new analytical method to describe the large-scale cosmic structure formation and takes ideas from both numerical simulations and previous analytical methods, was introduced in a series of papers [1–3]. Building upon earlier developments in statistical field theory [19–21], KFT aims to describe the evolution of cosmic structures based on the motion of classical particles in phase-space. At its very basis, there are no a priori assumptions that would invalidate the application of KFT at any length scale, making it a promising candidate for a consistent analytical treatment of non-linear cosmic structure formation. In this work, we will explore the possibilities of the most basic formulation of KFT—canonical KFT—and the resulting canonical perturbation theory. Whereas many works on KFT have been published since its development in 2015, a systematic look at canonical perturbation theory is so far lacking, even though the latter is useful for at least two reasons. First, we will see that if applied correctly, canonical perturbation theory in KFT can be a powerful tool to explore the evolution of cosmic structures in the non-linear regime. Second, a proper understanding of canonical KFT can help build an intuition for more advanced KFT methods such as resummed KFT (rKFT) [22] or the grand-canonical formulation of KFT [4].

After a thorough introduction to the standard analytical approaches to cosmic structure formation in [Chapter 2](#), we will therefore give a detailed introduction into the canonical formulation of KFT [Chapter 3](#) focussing on building an intuition for the perturbative treatment of particle interactions with the help of a toy model. [Chapter 4](#) is dedicated to the specialization of KFT to cosmic structure formation by demonstrating how initial conditions and particle trajectories are obtained for the cosmological application of KFT. In particular, we will establish a new diagrammatic language for canonical KFT and show how Zel’dovich trajectories can be introduced consistently. While in [Chapter 5](#), we explore the application of canonical perturbation theory to the linear growth of the dark matter power spectrum, [Chapter 6](#) treats the non-linear behaviour of the power spectrum. We draw our conclusions in [Chapter 7](#).

1.2 NOTATION AND FOURIER CONVENTION

Since we will be confronted with a lot of three-dimensional integrals both in configuration and in Fourier space we introduce the following shorthand notation

$$\int_{\mathbb{R}^3} d^3q f(\mathbf{q}) =: \int_{\mathbf{q}} f(\mathbf{q}), \quad \int_{\mathbb{R}^3} \frac{d^3k}{(2\pi)^3} g(\mathbf{k}) =: \int_{\mathbf{k}} g(\mathbf{k}). \quad (1.1)$$

Fourier transforms will be commonly used throughout this thesis. We assume that the concept is known to the reader and merely state the convention that we employ in this work. The Fourier transform of a function $f(\mathbf{q})$, as well as its backtransform are defined by

$$f(\mathbf{k}) := \int_{\mathbf{q}} f(\mathbf{q}) e^{-i\mathbf{k}\cdot\mathbf{q}}, \quad f(\mathbf{q}) := \int_{\mathbf{k}} f(\mathbf{k}) e^{i\mathbf{k}\cdot\mathbf{q}}. \quad (1.2)$$

The Fourier transform of unity is the Dirac-delta distribution

$$\int_{\mathbf{q}} e^{-i\mathbf{k}\cdot\mathbf{q}} = (2\pi)^3 \delta_D(\mathbf{k}). \quad (1.3)$$

Part I

FOUNDATIONS

 COSMOLOGY AND LARGE SCALE STRUCTURE FORMATION

2.1 THE COSMOLOGICAL STANDARD MODEL

The standard model of cosmology has evolved over the past century, starting with the first symmetric solutions to Einstein's field equations by Alexander Friedmann, the observations of Edwin Hubble of the redshift of distant nebulae and the work by Georges Lemaître who connected Friedmann's solution to observations, to name just a few. Since then, cosmology has come a long way, evolving into a precision science at the latest with the observation of the Cosmic Microwave Background (CMB) radiation. This section presents a narrow selection of aspects of our cosmological model relevant to properly understanding cosmic structure formation. A more detailed discussion can be found in most cosmology textbooks, e. g. [23–25].

2.1.1 *The Friedmann equation*

The theory at the basis of modern cosmology is general relativity, where spacetime is described as a smooth manifold curved by its energy-momentum content. Classical particles moving under the influence of gravity, in turn, follow geodesics on this curved manifold. The equations relating curvature and the energy-momentum tensor of some content of spacetime are Einstein's field equations

$$G_{\mu\nu} + \Lambda g_{\mu\nu} = \frac{8\pi G}{c^4} T_{\mu\nu}, \quad (2.1)$$

which contain the spacetime geometry and the cosmological constant Λ on the lhs and the energy-momentum content on the right. Since Einstein's field equations are inherently non-linear, they are impossible to solve analytically without further symmetry assumptions or approximation schemes. In the standard model of cosmology, we assume the maximally symmetric case of a spatially **homogeneous** and **isotropic** spacetime, leaving but a single free parameter in the line element

$$ds^2 = g_{\mu\nu} dx^\mu dx^\nu = -c^2 dt^2 + a^2(t) g_{ij} dx^i dx^j. \quad (2.2)$$

The function $a(t)$ is called the scale factor and indicates how physical distances change with cosmic time t . Since we compare relative changes in distances over time, the absolute value of the scale factor is irrelevant for us, such that we can fix $a_0 = a(t_0) = 1$ where t_0 is the present cosmic time. Using these symmetry assumptions and including the energy-momentum tensors of non-relativistic matter and radiation on the rhs of (2.1). In standard cosmology, where the universe contains non-relativistic matter, radiation, and a cosmological constant Einstein's equations reduce to the Friedmann equation

$$H^2(a) = H_0^2 \left(\Omega_{r,0} a^{-4} + \Omega_{m,0} a^{-3} + \Omega_{k,0} a^{-2} + \Omega_{\Lambda,0} \right), \quad (2.3)$$

which relates the scale factor's time evolution to the universe's overall matter content. Here $H(a) = \frac{\dot{a}}{a}$ is the Hubble-Lemaître function, $H_0 = H(a_0)$ is its present value and the dimensionless density parameters $\Omega_{i,0}$ are obtained from the physical densities $\rho_i(a_0)$ by

$$\Omega_{i,0} = \frac{\rho_i(a_0)}{\rho_{\text{crit},0}} \quad \text{with} \quad \rho_{\text{crit},0} = \frac{3H_0^2}{8\pi G}. \quad (2.4)$$

The critical density $\rho_{\text{crit},0}$ is the density of a spatially flat universe at t_0 . In (2.3) we distinguish between non-relativistic matter with density parameter $\Omega_{\text{m},0}$, radiation (or ultra-relativistic matter) $\Omega_{\text{r},0}$, spatial curvature $\Omega_{\text{k},0}$ and the cosmological constant $\Omega_{\Lambda,0}$. Note that (2.3) evaluated at a_0 leads to $\Omega_{\text{k},0} = 1 - \Omega_{\text{m},0} - \Omega_{\text{r},0} - \Omega_{\Lambda,0}$, explaining the geometric interpretation of the critical density.

From the different scaling of the terms in (2.3) with the scale factor a we can infer that the universe's expansion history can be divided into different phases. Observations of the velocities of distant galaxies indicate that we live in an expanding universe, such that the scale factor becomes smaller as we go back in time. These observations suggests that there should have been a period in the early universe where the Hubble-Lemaître function was dominated by the radiation content, followed by matter domination, curvature and finally, the cosmological constant. By equating different terms, we can get a rough value for the scale factor where a transition from the domination of one form of energy to another took place. Of course, without knowing the values of the individual density parameters, we cannot know for sure if and when all these expansion epochs took place. This is a question only observations can address, which we talk about after having introduced the notion of cosmological redshift. Recession velocities of distant galaxies can only be determined indirectly via the shift they induce in the spectral lines in galaxy spectra. The redshift is defined by

$$z := \frac{\nu_e}{\nu_o} - 1, \quad (2.5)$$

where ν_e and ν_o are the emitted and observed frequencies, respectively. In cosmology, these frequencies are related, respectively, to the scale factor at the time of emission and observation. Since all our observations take place at $a_0 = 1$, this gives us a one-to-one relation between the scale factor $a(t)$ at some time t in the past and the corresponding redshift an event at this time would be observed with

$$a(t) = \frac{1}{1+z}. \quad (2.6)$$

The redshift is zero at t_0 by definition and increases as we go back in cosmic history.

2.1.2 Observations

First, one might ask whether the simple model of a spatially homogeneous and isotropic spacetime truly describes the actual universe we live in. After all, the world in our immediate surroundings is certainly not following such tight symmetry constraints. However, observations of cosmic structures confirm that homogeneity and isotropy appear to be fulfilled to a very high degree once we consider large cosmological scales.

Beyond confirming large-scale isotropy, observations allow us to determine the parameters entering Friedmann's equation (2.3). Observations in cosmology require extremely sophisticated measurement devices and techniques and involve advanced data analysis

methods. The most groundbreaking discovery, which started the age of precision cosmology, was the detection of the CMB signal in 1965 [5]. Until this day, measurements of the temperature fluctuations in the CMB are providing us with the most precise estimates for the values of the cosmological parameters. According to the latest analysis of CMB data by the Planck Collaboration [9], assuming vanishing spatial curvature¹ $\Omega_{k,0}$, the parameters in (2.3) take the values

$$\begin{aligned}\Omega_{m,0} &= 0.3111 \pm 0.0056 & \Omega_{r,0} &= (9.182 \pm 0.175) \cdot 10^{-5} \\ \Omega_{\Lambda,0} &= 0.6886 \pm 0.0056 & h &= 0.6766 \pm 0.0042,\end{aligned}\tag{2.7}$$

where h is defined such that $H_0 = 100h \text{ km(sMpc)}^{-1}$. There are several additional parameters that can be extracted from the CMB, but discussing them all would go far beyond the scope of this section. We should note, however, that extracting parameter values from CMB data can only be done within the scope of a specific class of cosmological models. CMB measurements are therefore often referred to as ‘model dependent’ observations, in contrast to local measurements, e. g. of the Hubble constant using observations of redshifts of type Ia supernovae, which can yield values for a limited number of cosmological parameters independent of specific model assumptions.

An exciting consequence of CMB measurements and observations of the velocity of galaxies in galaxy clusters [26] is that the majority of the matter content of the universe consists of an unknown form of matter which does not couple to electromagnetism and is therefore referred to as *dark matter*². Observations from Planck [9] suggest that the contribution of visible matter to the overall matter content lies around 16%, making the majority of gravitating matter in the universe dark matter. The fundamental nature of dark matter and the cosmological constant are among the most pressing challenges of modern physics. For dark matter, there are different candidates, most notably a selection of fundamental particles beyond the standard model of particle physics or primordial black holes (PBHs). Different fundamental particle candidates, such as WIMPS (weakly interacting massive particle), axions, or entire dark sectors, have emerged and run out of fashion over the years [27]. PBHs are still in the running as well, but weak-lensing surveys, gravitational wave observations (or the lack thereof) and bounds due to evaporation have already put tight constraints on their permitted mass range [28]. The discussion about the cosmological constant and whether it is the manifestation of a dynamical dark energy is even more unclear. Many models have been proposed, but for now, no compelling evidence heavily favours any of them. Ultimately, we must acknowledge that we do not know the answers to these questions yet.

Luckily, we can be agnostic about the precise physical origin of the dark components of the universe since we do not need microscopic properties of dark matter to describe its effect on the formation of cosmic structures. For our purpose, it is sufficient to assume that dark matter exists and acts like an ensemble of classical non-relativistic particles

¹ This assumption can be tested precisely by a combination of baryon-acoustic oscillation and CMB measurements. Even if the curvature parameter is not wholly vanishing, it will never make an appreciable contribution to the universe’s expansion history since it scales with a^{-2} . Due to this scaling, curvature therefore takes over after matter domination, but due to its small values is immediately overpowered by the cosmological constant. This is in contrast to radiation, which has a minimal density parameter at current times as well but dominated in the early universe due to its a^{-4} -dependence.

² This is to date the most successful and widespread explanation among cosmologists since it can explain a wide range of observations with very few assumptions. Nonetheless, alternatives to the dark matter paradigm, such as modifications of Newtonian dynamics (MOND) or General Relativity, are actively investigated.

on cosmological scales. Dark energy will be treated as a cosmological constant which drives accelerated expansion at the current cosmic epoch.

2.2 COSMIC STRUCTURES - A STATISTICAL DESCRIPTION

2.2.1 *The two-point correlation function*

Although the assumptions of homogeneity and isotropy seem to be fulfilled on large cosmic scales, smaller scales exhibit fluctuations w. r. t. this highly symmetrical background. These structures play an essential role in advancing our understanding of the universe since they allow us to extract information on various cosmological parameters. As we have mentioned above, the main contribution to the matter content in our universe comes from dark matter, making it the most crucial component in large-scale structure formation. Additionally, once the universe has cooled down sufficiently to allow for the presence of neutral atoms, structures in baryonic matter³ essentially follow those of dark matter on large cosmic scales. In contrast, baryonic effects such as pressure due to a finite cross-section and cooling due to the coupling to electromagnetism are relevant only on small scales. For our description of cosmic structure formation, it is therefore sufficient to treat the entire cosmic matter content as a collisionless gas with density

$$\rho_m(\mathbf{q}, t) = \bar{\rho}_m(t)(1 + \delta(\mathbf{q}, t)), \quad (2.8)$$

where we introduced the density contrast $\delta(\mathbf{q}, t)$ as a fluctuation of the matter density w. r. t. the background density $\bar{\rho}(t)$. As in (2.2) t denotes cosmic time and \mathbf{q} the position vector in comoving coordinates, i. e. the physical position vector scaled with the scale factor a .

Since we care little about the exact location of large conglomerates of matter but rather about their relative distribution, the discussion of large-scale structures has to be statistical. A key statistical quantity of the matter field is the two-point correlation function of the density contrast

$$\xi_\delta(q, t) = \langle \delta(\mathbf{q}_0, t) \delta(\mathbf{q}_0 + \mathbf{q}, t) \rangle, \quad (2.9)$$

where q is the norm of the comoving distance vector \mathbf{q} and $\langle \dots \rangle$ denotes the ensemble average⁴. Note that homogeneity and isotropy are inherited by the density field in a statistical way. Even though, on small scales, the system is neither homogeneous nor isotropic around a single point, the fluctuations behave so that they fulfil both conditions when taking the ensemble average. Due to statistical homogeneity, the two-point correlation function is independent of the absolute positions \mathbf{q}_0 , whereas statistical isotropy additionally restricts the dependence to the absolute comoving distance q between the points, independent of the direction.

³ Cosmologists tend to use the word baryonic matter as an umbrella term for anything that is not dark matter.

⁴ It might appear bizarre to refer to an ensemble average in the context of cosmology since there is but a single universe to perform observations on. Indeed, to extract statistical quantities from observations, isotropy allows us to take averages over different positions on the celestial sphere, which should then be equivalent to ensemble averages. As theorists, we can be content with imagining a large set of universes which are different realisations of our universe and averaging over these.

2.2.2 The power spectrum

The Fourier transform of the two-point correlation function (2.9) is the density fluctuation power spectrum

$$P_\delta(k, t) = \int_{\mathbf{q}} \xi_\delta(q, t) e^{-i\mathbf{k}\cdot\mathbf{q}}, \quad (2.10)$$

which is related to the two-point function in Fourier space by

$$\langle \delta(\mathbf{k}, t) \delta(\mathbf{k}', t) \rangle = (2\pi)^3 \delta_D(\mathbf{k} + \mathbf{k}') P_\delta(k, t). \quad (2.11)$$

Due to its relation to the density correlation function, the dark matter power spectrum contains information on the clustering behaviour of dark matter. As we will see, working with the power spectrum instead of the correlation function is significantly more convenient since the equations governing the dynamics of the density contrast allow for a simpler description in Fourier space. Therefore, the dark matter power spectrum is the most natural quantity to start with, to understand cosmic structure formation. If dark matter density fluctuations follow a Gaussian random field, it is also the only non-vanishing cumulant of the underlying probability density. From observations of the CMB [9], we have strong evidence that fluctuations in the matter field in the early universe were, if not Gaussian, then at least very close to it.

Predicting the power spectrum at $z = 0$ for a large range of scales is, at the same time, a significant challenge and of crucial importance for modern cosmology. Although numerical simulations can reproduce small-scale structures, even considering baryonic feedback effects, they yield limited physical insights into the physical processes of structure formation. Unfortunately, for low redshift the evolution of cosmic structures on length scales $l \lesssim 8 h^{-1} \text{ Mpc}$ is governed by non-linear dynamics and therefore extremely difficult to calculate analytically. We aim to walk down a few steps on the long road to a complete description of non-linear structure formation in this work, but before thinking about late-time evolution, it pays off to start at the beginning.

2.3 STRUCTURES IN THE EARLY UNIVERSE

To motivate the initial conditions underlying late-time cosmic structure formation, we want to give a short overview of the most important ideas that can explain the creation of cosmic structures in the very early universe and their evolution shortly after that. Many of the ideas in this section are discussed in greater depth in [23]. An essential concept in the following considerations is the comoving Hubble horizon. The Hubble-Lemaître function H has the dimension of inverse time, such that the quantity $r_H = c/H$, where c is the speed of light is a natural cosmic length scale, quantifying the distance between two points that can still be in causal contact⁵. The comoving Hubble horizon, which plays a crucial role in the behaviour of Fourier modes of the density field in the early stages of cosmic structure formation, is then given by $c/(aH)$.

⁵ The Hubble horizon is not a physical horizon per se but gives a reasonable estimate for the actual particle horizon, i. e. the maximum physical distance between two points which can still be in causal contact, and appears as a natural length scale in the equations of structure formation, e. g. in [Appendix F](#)

2.3.1 *Planting the seeds*

The most widely spread theory for the earliest epoch of cosmic expansion is inflation. The main reason for the success of this model is that, in addition to its simplicity, it not only solves cosmological puzzles such as the flatness and the horizon problems but also makes a prediction for cosmic structures. The simplest inflationary model can be summarized as a scalar field—the inflaton—driving exponential expansion while slowly relaxing to its vacuum state. At this stage of cosmic history, nothing is assumed to exist in the universe except for said inflaton field. While primarily driving inflation, the scalar field exhibits quantum fluctuations around its false vacuum value. Exponential expansion implies a shrinking comoving Hubble horizon, so modes of the quantum fluctuations can exit the horizon, freeze in and become classical fluctuations on top of the homogeneous background. Once the period of exponential expansion ends, we enter an epoch called reheating, supposedly induced by oscillations of the inflaton field around its true vacuum. During reheating, the energy that is still stored in the inflaton is assumed to be converted into standard model particles and dark matter. The fluctuations that were imprinted onto the scalar field during the inflationary epoch are imprinted onto the initial conditions of the emerging standard model fields. A key prediction of the inflationary model is that scalar fluctuations follow a (nearly) Gaussian random field (GRF) described by the primordial power spectrum

$$P_{(\text{prim.})}(k) \propto k^{n_s}. \quad (2.12)$$

The exponent n_s is the spectral index and should be close to but smaller than one. In fact, how close the spectral index is to unity is directly related to the duration of the inflationary epoch; for example, an infinitely long inflationary epoch would result in n_s precisely equal to one. Measurements of the cosmic microwave background (CMB)⁶ indicate that $n_s \approx 0.965$ and the relative amplitude of fluctuations was initially very small. Standard model particles and dark matter were thus produced in an almost entirely homogeneous fashion, with tiny fluctuations in their density imprinted on them due to quantum fluctuations in the inflaton field.

It should be noted that inflation is one of many models capable of solving the flatness and horizon problems and predicting the primordial power spectrum. Additionally, within the inflationary paradigm, there is a broad panoply of proposed models for the inflaton field and currently minimal opportunity to test their predictions. And even in the simplest scalar field model, many open questions remain; for example, the exact mechanism behind the reheating process is currently completely unknown. Therefore, the handwavy explanation we provided here should be taken with a gigantic grain of salt. On the other hand, the most important take-home message of this section is the prediction of (nearly) Gaussian primordial fluctuations with a power spectrum following (2.12), which is predicted by a wide variety of early-universe models and supported by current observations [9].

2.3.2 *Evolution through matter-radiation equality*

After reheating, the universe entered a radiation-dominated phase, i. e. the Hubble expansion was controlled mainly by the energy density of radiation. During this period,

⁶ One should note that CMB measurements can only be interpreted within a cosmological model, i. e. they are model-dependent.

the behaviour of Fourier modes of the density fluctuations (density modes) depends on the modes' comoving wavelength relative to the comoving Hubble horizon. Throughout inflation, the comoving Hubble horizon was shrinking, pushing all density modes that are relevant today beyond the Hubble horizon. Once the exponential expansion is over, density modes start re-entering the horizon, starting with shorter wavelengths and moving towards longer ones. As we transition from the radiation-dominated epoch to matter domination, the time evolution of density modes inside the comoving Hubble horizon changes since radiation pressure slowly ceases to suppress their growth. As a result, modes that enter the horizon after matter-radiation equality show a different behaviour from those that entered before, a feature which is directly imprinted onto the density fluctuation power spectrum. From the scale factor $a_{\text{eq}}=2.95 \cdot 10^{-4}$ at matter radiation equality [9] we can derive the comoving wavenumber of those modes that entered the comoving Hubble horizon at the time of the transition. A short calculation reveals that the corresponding wavenumber is

$$k_{\text{eq}} = \sqrt{\frac{2\Omega_{\text{m},0}H_0^2}{a_{\text{eq}}c^2}} \approx 0.015 h \text{ Mpc}^{-1} \quad (2.13)$$

This scale offers a qualitative explanation for the behaviour of the density fluctuation power spectrum after matter-radiation equality. For a quantitative result, we must solve the underlying relativistic Boltzmann equations coupled with Einstein's field equations. Since fluctuations remain relatively small throughout this period, linearized equations where different Fourier modes evolve independently are an excellent approximation of all length scales of interest. The solution for the fluctuations of non-relativistic matter can thus be encoded in a transfer function $T(k)$, which describes the evolution of individual modes as the universe progresses from radiation to matter domination. Although the Boltzmann system is not solvable with purely analytical methods, it allows for quantitative discussions of some asymptotic solutions, e.g. for large, respectively, small values of k . The complete solution for the transfer function requires a numerical treatment. An excellent fit to the numerical result for the transfer function of pressureless, non-relativistic matter is derived in the work of Bardeen, Bond, Kaiser and Szalay (BBKS) [29] and reads

$$T_{\text{BBKS}}(x) = \frac{\log(1 + 0.171x)}{0.171x} (1 + 0.284x + (1.18x)^2 + (0.399x)^3 + (0.49x)^4)^{-1/4}. \quad (2.14)$$

Here $x \equiv k/k_{\text{eq}}$, where k_{eq} is the wavenumber of a fluctuation that entered the comoving Hubble horizon exactly at matter-radiation equality (2.13). The power spectrum for dark matter density fluctuations after matter-radiation equality is thus given by

$$P_{\text{BBKS}}(k) \propto T_{\text{BBKS}}^2(k) P_{(\text{prim.})}(k) \propto T_{\text{BBKS}}^2(k) k^{n_s}. \quad (2.15)$$

It is customary to infer the overall amplitude of the BBKS power spectrum from the quantity⁷ σ_8 , obtained from low redshift observations of large-scale structures. From the Planck data [9] we obtain $\sigma_8 = 0.8102 \pm 0.0060$. Once the amplitude of the BBKS power spectrum is fixed, we can use it as a starting point to derive the late-time power spectrum and, therefore, henceforth refer to it as the initial power spectrum $P_\delta^{(i)}(k)$ for the rest of this work.

⁷ σ_8 is the variance of the density contrast where all structures at length-scales smaller than $8 h^{-1} \text{ Mpc}$ have been smoothed out.

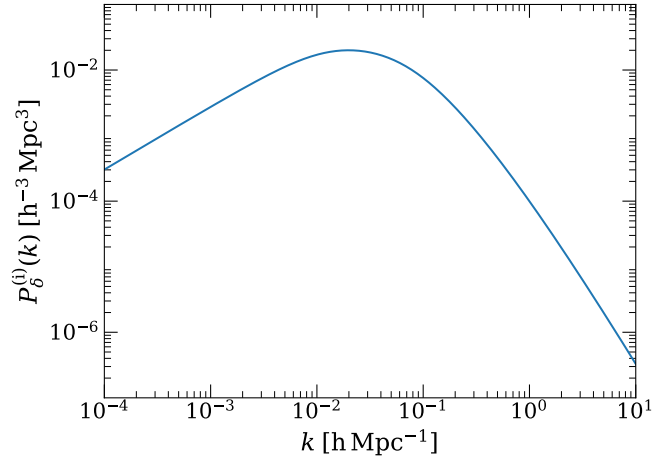


Figure 2.1: The density fluctuation power spectrum resulting from the BBKS transfer function and a primordial power spectrum with spectral index $n_s = 0.965$. Note that we recover the power law behaviour $P_\delta^{(i)}(k) \sim k^{n_s}$ on large scales (small k) and $P_\delta^{(i)}(k) \sim \log^2(k) k^{n_s-4}$ on small scales (large k). The maximum is located around $k_{\text{eq}} \approx 0.015 h \text{ Mpc}^{-1}$. The overall amplitude is inferred from σ_8 and evaluated around recombination $z_{\text{rec}} = 1100$.

2.4 EULERIAN PERTURBATION THEORY

After the transition from radiation to matter domination, density modes continue their evolution according to the Boltzmann equation. As the universe continues to expand, the modes of the density field that make up the universe's large-scale structure become increasingly small relative to the comoving Hubble horizon. As a result, the cosmic structures that interest us today are well inside the Hubble horizon and follow non-relativistic dynamics. When we approach the later stages of cosmic history, the density contrast, which started as a tiny perturbation of the background density, continues to grow. Eulerian perturbation theory attempts to describe the evolution of density fluctuations in terms of fluid dynamics and has been the focus of intense research over the past couple of decades [11, 12, 14, 16, 30]. Here we will briefly introduce the most essential concepts of the ideas of Eulerian perturbation theory.

2.4.1 Equations of motion

Standard Eulerian perturbation theory (SPT) starts from the non-relativistic Vlasov-Poisson system (the collision-less Boltzmann system with a potential that fulfils the Poisson equation) for the one-particle phase-space density and takes moments of this equation w. r. t. the momentum coordinate. In comoving coordinates, this results in the Euler-Poisson system

$$\partial_t \delta + \nabla \cdot [(1 + \delta)\mathbf{v}] = 0 \quad (2.16)$$

$$\partial_t \mathbf{v} + 2H\mathbf{v} + (\mathbf{v} \cdot \nabla)\mathbf{v} = -\frac{1}{a^2} \nabla \Phi \quad (2.17)$$

$$\nabla^2 \Phi = 4\pi G a^2 \bar{\rho}_m \delta, \quad (2.18)$$

where $\delta(\mathbf{q}, t)$ and $\mathbf{v}(\mathbf{q}, t)$ denote the density contrast from (2.8) and the peculiar velocity field, respectively, in terms of the comoving coordinate \mathbf{q} and cosmic time t . Note

that (2.17) should additionally contain a stress-energy tensor σ_{ij} from the second momentum moment of the Vlasov equation. This contribution is neglected in the most basic approach to SPT, thus modelling the matter field as pressure-less dust, which is equivalent to assuming that there is a single-valued velocity field at any moment and therefore called the *single-stream approximation* (SSA). This assumption is far from trivial and significantly limits the usefulness of SPT since the SSA breaks down at scales where gravitationally bound, virialized structures exist. In addition to the SSA, we assume that the peculiar velocity field is curl-free and can therefore be expressed in terms of a velocity potential

$$\mathbf{v}(\mathbf{q}, \tau) = \nabla\psi(\mathbf{q}, \tau). \quad (2.19)$$

A curl-free velocity field is certainly consistent with the SSA since there is no source for vorticity in the Euler-Poisson system, such that any initial vorticity is quickly diluted due to cosmic expansion. As long as perturbations remain small and the SSA is valid, a curl-free velocity field should describe cosmic structures fairly well. However, on length scales where density fluctuations have grown beyond unity, we expect vorticity to build up, and the results of SPT to strongly deviate from reality.

The expressions (2.16)–(2.18) form a non-linear system of partial differential equations and cannot be solved exactly. However, observations confirm that fluctuations around the mean matter density and the cosmic flow are tiny at high redshifts and can be treated perturbatively. SPT is therefore attempting to solve (2.16)–(2.18) by perturbatively expanding around the linearized Euler-Poisson system. Since such an expansion necessarily breaks down for density contrasts that have grown far beyond unity, SPT is mainly valuable for describing cosmic structures in the mildly non-linear regime, where the density contrast is of order unity.

2.4.2 Linear growth

As long as the absolute value of the density contrast is well below unity, its time evolution is dictated by the linearized Euler-Poisson system. This condition is fulfilled only in the large-scale or early-time limit. After linearizing the Euler-Poisson system (2.16)–(2.18), the continuity and the Euler equation can be combined to yield a second-order differential equation for the density contrast. This equation is solved by $\delta^{(1)}(\mathbf{q}, t) = D(t)\delta^{(i)}(\mathbf{q})$, where $D(t)$ fulfills the equation

$$\partial_t^2 D + 2H \partial_t D - 4\pi G \bar{\rho}_m D = 0. \quad (2.20)$$

For special values of the density parameters, this equation can be solved analytically, e. g. for an Einstein-de-Sitter (EdS) universe where $\Omega_m = 1$, we find the two solutions

$$D(t) = \begin{cases} D_+(t) = a(t) & \text{(growing solution)} \\ D_-(t) = a^{-3/2}(t) & \text{(decaying solution)}, \end{cases} \quad (2.21)$$

where the growing solution is usually referred to as the linear growth factor. For the standard Λ CDM cosmology (2.7), however, no analytical solution exists, such that the equation needs to be integrated numerically. Nonetheless, the EdS case is also relevant for Λ CDM, since a large portion of late-time cosmic structure formation takes place during the matter-dominated era, where EdS offers an excellent approximation.

For analytical calculations of cosmic structure formation, using the linear growth factor D_+ to define a new time coordinate often proves useful, leading us to define

$$\tau := \ln \frac{D_+(t)}{D_+(t_i)} \quad (2.22)$$

as our new time parameter. We choose for t_i a moment in cosmic history where the growth of cosmic structures can be described by the non-relativistic, linearized system (2.16)–(2.18). It is sensible to choose this moment to lie around recombination, where $z_i = 1100$. Conveniently, (2.22) defines τ to be zero initially and to increase monotonically, with a final value $\tau_f = \ln(1 + z_i) = 7$ in an EdS and $\tau_f \approx 6.75$ in a Planck cosmology. Switching to τ turns the system of equations (2.16)–(2.18) into

$$\dot{\delta} + \nabla \cdot [(1 + \delta)\mathbf{u}] = 0 \quad (2.23)$$

$$\dot{\mathbf{u}} + \frac{\mu}{2} \mathbf{u} + (\mathbf{u} \cdot \nabla)\mathbf{u} + \nabla\phi = 0 \quad (2.24)$$

$$\nabla^2\phi = (\mu/2 + 1) \delta, \quad (2.25)$$

where we introduced the time-dependent variable $\mu(\tau) = 2\left(\frac{3\Omega_m}{2f^2(\Omega_m)} - 1\right)$ for notational convenience. The steps are detailed in [Appendix A](#), where we also introduce the growth rate $f(\Omega_m) = \frac{d \ln D_+}{d \ln a}$. Here and from now on, a dot signifies a derivative w. r. t. τ . There are a few things to note about these equations, starting with the fact that the entire explicit dependence on the cosmological parameters has been shifted into the function $\mu(\tau)$. It is easy to check that $\mu = 1$ in an EdS cosmology, although this is no longer true once matter ceases to dominate cosmic expansion. In the case of Λ CDM, deviations of up to 20% from unity arise at $z = 0$ due to the increasing dominance of the cosmological constant at low redshifts. Nonetheless, it turns out that cosmic structure formation is extraordinarily well described by fixing μ to one, even when non-relativistic matter no longer dominates the universe's expansion. To understand why, it suffices to re-derive linear growth from (2.23)–(2.25), which is now solved by the Ansatz $\delta(\mathbf{q}, \tau) = e^{\alpha\tau}$, such that

$$\alpha = \begin{cases} 1 & \text{(growing solution)} \\ -\mu/2 - 1 & \text{(decaying solution).} \end{cases} \quad (2.26)$$

The growing solution is thus independent of μ and exactly follows D_+ (as it should) for any cosmology! The second solution $D_+^{-\mu/2-1}$, on the other hand, is only compatible with the decaying solution D_- in the EdS cosmology when $\mu = 1$. Deviations from the EdS result are, therefore, purely contained in the evolution of the subdominant decaying modes.

In the following, we will keep the description in terms of μ general whenever possible, but it should be clear from the previous discussion that restricting μ to be constant at unity is an excellent approximation we will make much use of in later calculations.

2.4.3 Initial conditions and the linear power spectrum

The initial conditions for the density contrast and the peculiar velocity field can be connected by using the linearised continuity equation

$$\dot{\delta} + \nabla \cdot \mathbf{u} = 0. \quad (2.27)$$

For density contrasts that evolve according to the growing solution, it is easy to verify that $\dot{\delta} = \delta$. Making use of the fact that the velocity is initially curl-free, we find

$$\mathbf{u}^{(i)}(\mathbf{q}) = \nabla\psi^{(i)}(\mathbf{q}), \quad \delta^{(i)}(\mathbf{q}) = -\nabla^2\psi^{(i)}(\mathbf{q}), \quad (2.28)$$

where $\psi^{(i)}(\mathbf{q}) = \psi(\mathbf{q}, 0)$ is the velocity potential evaluated at $\tau(t_i) = 0$. From $\delta^{(i)}(\mathbf{k}) = k^2\psi^{(i)}(\mathbf{k})$ the relation between the power spectrum of the velocity potential and the density contrast

$$P_\psi^{(i)}(k) = P_\delta^{(i)}(k) k^{-4} \quad (2.29)$$

follows immediately. Formulating the initial conditions in terms of a velocity potential has the advantage of highlighting the relation between initial density and velocity field. The velocity potential should therefore be viewed as a mere auxiliary field.

The Fourier-space correlation function resulting from the growing solution of linear SPT (2.20) is straightforward to write down since different density modes evolve independently:

$$\langle \delta^{(1)}(\mathbf{k}, \tau) \delta^{(1)}(\mathbf{k}', \tau) \rangle = e^{2\tau} \langle \delta^{(i)}(\mathbf{k}) \delta^{(i)}(\mathbf{k}') \rangle, \quad (2.30)$$

and with the definition (2.22) of the time parameter we find the linear power spectrum

$$P_\delta^{(1)}(k, t) = \left(\frac{D_+(t)}{D_+(t_i)} \right)^2 P_\delta^{(i)}(k). \quad (2.31)$$

Linearly growing density contrasts thus lead to a power spectrum which is a scaled version of the initial power spectrum, with a time-dependent amplitude given by the linear growth factor. Additionally, the Gaussian nature of the density contrast is conserved in this limit. This simple scaling behaviour is lost when higher-order corrections become relevant for the density contrast. Intuitively this can be understood by realising that density modes no longer evolve independently once we leave the linear regime, leading to mode-coupling.

2.4.4 Beyond linear growth

Moving beyond the description of linear growth where density modes evolve independently is most easily done by transferring the system (2.23)–(2.25) to Fourier space, turning it into a coupled system of integral-differential equations [11, 12, 14]. Introducing the velocity divergence $\theta(\mathbf{q}, \tau) = \nabla \cdot \mathbf{u}(\mathbf{q}, \tau)$ and collecting δ and θ in the field tuple $\varphi = (\delta, -\theta)^T$, the system can be compactly written as

$$(\delta_{ab}\partial_\tau + \Omega_{ab})\varphi_b(\mathbf{k}, \tau) = \int_{\mathbf{k}_1, \mathbf{k}_2} \gamma_{abc}(\mathbf{k}, -\mathbf{k}_1, -\mathbf{k}_2)\varphi_b(\mathbf{k}_1, \tau)\varphi_c(\mathbf{k}_2, \tau), \quad (2.32)$$

where we have collected all linear terms on the lhs and the quadratic (mode-coupling) terms on the right. The details of the system are contained in the matrix Ω_{ab} and the vertex tensor $\gamma_{abc}(\mathbf{k}, -\mathbf{k}_1, -\mathbf{k}_2)$, which are given by

$$(\Omega_{ab}) = \begin{pmatrix} 0 & -1 \\ -\frac{\mu}{2} - 1 & \frac{\mu}{2} \end{pmatrix} \stackrel{\mu=1}{=} \begin{pmatrix} 0 & -1 \\ -\frac{3}{2} & \frac{1}{2} \end{pmatrix} \quad (2.33)$$

$$\begin{aligned} \gamma_{\delta\delta\theta}(\mathbf{k}, \mathbf{k}_1, \mathbf{k}_2) &= \gamma_{\delta\theta\delta}(\mathbf{k}, \mathbf{k}_2, \mathbf{k}_1) = (2\pi)^3 \delta_D(\mathbf{k} + \mathbf{k}_1 + \mathbf{k}_2) \frac{(\mathbf{k}_1 + \mathbf{k}_2) \cdot \mathbf{k}_2}{2k_2^2} \\ \gamma_{\theta\theta\theta}(\mathbf{k}, \mathbf{k}_1, \mathbf{k}_2) &= (2\pi)^3 \delta_D(\mathbf{k} + \mathbf{k}_1 + \mathbf{k}_2) \frac{(\mathbf{k}_1 + \mathbf{k}_2)^2 (\mathbf{k}_1 \cdot \mathbf{k}_2)}{k_1^2 k_2^2}. \end{aligned}$$

The common strategy to solve (2.32) is to derive a Green’s function—often called *linear propagator*—for the linear differential operator on the lhs which is then used to derive a formal, self-consistent solution [11, 12, 14]. From the formal solution, explicit expressions for corrections to the linear solution can be found by a series expansion, leading to a perturbative series for the tuple φ_a . To derive results for perturbative spectra, a diagrammatic formulation resembling Feynman diagrams from quantum field theory was introduced [12, 13] such that perturbative corrections to cosmic spectra in SPT are often referred to as loop-corrections. The cosmic power spectrum with second-order cor-

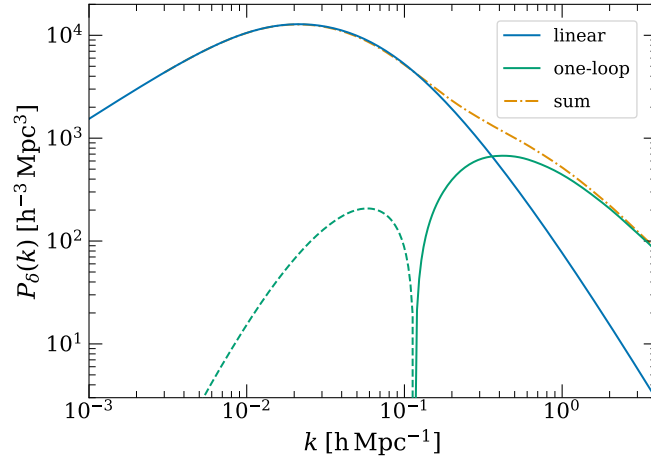


Figure 2.2: A comparison of the linear (2.31) (blue curve) and the one-loop (yellow curve) power spectrum from SPT. The green curve shows the correction, added to the linear spectrum to arrive at the full one-loop result.

rections from SPT, the one-loop power spectrum, is shown in Figure 2.2, together with the linear power spectrum as a reference. The one-loop result was taken from [31]⁸. We can observe the typical mode-coupling behaviour in the green curve, the one-loop correction, which takes negative values on large and positive values on small scales, thus suggesting a power transfer from large- to small-scale structures. The resulting one-loop power spectrum seemingly shows a strong growth of small scale structures, since its amplitude rises sharply on small scales. This, however, is an artefact of the perturbative expansion, and a thorough analysis shows that we cannot trust the values of the power spectrum at these scales.

2.5 LAGRANGIAN PERTURBATION THEORY

As mentioned in the previous section, SPT suffers from a couple of significant drawbacks, most notably that due to the single-stream approximation, it breaks down at stream-crossing and is, therefore, unable to describe cosmic structures in the non-linear regime even in principle. In addition, we need to assume a curl-free velocity field, which is not reflecting the reality of bound structures. Last but not least, it is known that SPT does not converge since the expansion takes place in the density contrast, which can become extremely large. Altogether, these known issues suggest that a description of cosmic structure formation in terms of the Vlasov-Poisson system might not be the most promising approach. Lagrangian perturbation theory (LPT) offers an alternative

⁸ Beware, there is a typo in the self-energy contribution (A21a) to the one-loop correction in this reference. Instead of $\dots \frac{3}{r^2} \dots$ it should read $\dots \frac{3}{r^3} \dots$!

by considering the evolution of particle positions and determining the resulting density contrast [11, 32, 33]. This opens the door to new possibilities since we are not tied to a description of the system in terms of a fluid. Indeed, some basic results from LPT already go beyond the possibilities of SPT and can be used to extend the description of cosmic structures to more non-linear scales [34, 35].

2.5.1 Equations of motion

We need two ingredients to describe cosmic structures in terms of a particle-based approach. First, we need to derive an equation that governs the dynamics of fluid particles, and second, we need to determine how particle positions are related to the density contrast. To derive the equations of motion for particle positions, consider a particle that starts at position $\mathbf{q}^{(i)}$ at t_1 . At any later time t , its position can be written as

$$\mathbf{q}(\mathbf{q}^{(i)}, t) = \mathbf{q}^{(i)} + \mathbf{\Psi}(\mathbf{q}^{(i)}, t), \quad (2.34)$$

where we introduced the displacement field $\mathbf{\Psi}(\mathbf{q}^{(i)}, t)$. We shall refer to \mathbf{q} as the Eulerian, and to $\mathbf{q}^{(i)}$ as the Lagrangian coordinate⁹. Whereas SPT corresponds to the Eulerian picture of fluid dynamics, where we imagine coordinates as a static grid that covers space, LPT takes the Lagrangian perspective (hence the name), where we follow the flow lines of individual fluid elements (or particles). Both points of view can be related by noting that the local velocity field $\mathbf{v}(\mathbf{q}, t)$ in the Eulerian view corresponds to the total time derivative of the fluid element's position $\mathbf{q}(t)$ in the Lagrangian view:

$$\mathbf{v}(\mathbf{q}, t) = \frac{d\mathbf{q}(t)}{dt} = \frac{d\mathbf{\Psi}(t)}{dt}. \quad (2.35)$$

Additionally, the total time derivative is related to the partial time derivative by $\frac{d}{dt} = \partial_t + (\mathbf{v} \cdot \nabla)\mathbf{v}$. This then leads to the equation of motion for the displacement field

$$\frac{d^2\mathbf{\Psi}}{dt^2} + 2H\frac{d\mathbf{\Psi}}{dt} + \frac{1}{a^2}\nabla_{\mathbf{q}}\Phi = 0, \quad (2.36)$$

which follows from the Euler equation (2.17). In LPT, the advection term, which is the source of non-linearity in SPT, is absent since it is absorbed into the total time derivative. The non-linear nature of (2.36) is less evident since it is encoded in the gravitational potential gradient, which is taken w. r. t. the Eulerian position \mathbf{q} . Since the displacement field is a function of the Lagrangian coordinate $\mathbf{q}^{(i)}$, the gradient will give rise to an inverse determinant down the road, as we will see in the following. Regarding the second ingredient, the evolution of the density contrast in terms of the displacement field follows from mass conservation

$$\bar{\rho}(1 + \delta(\mathbf{q}, t))d^3\mathbf{q} = \bar{\rho}(1 + \delta^{(i)})d^3\mathbf{q}^{(i)} \Rightarrow \delta(\mathbf{q}, t) = \left[\det\left(\frac{\partial\mathbf{q}(t)}{\partial\mathbf{q}^{(i)}}\right) \right]^{-1} - 1, \quad (2.37)$$

where we neglected the initial density fluctuations $\delta^{(i)} \ll 1$.

Similar to SPT, we will exclusively consider the evolution of the longitudinal (i. e. curl-free) component of the displacement field by taking the divergence of (2.36) w. r. t. \mathbf{q} .

⁹ Unfortunately, the Eulerian position is usually denoted by \mathbf{x} , and the Lagrangian by \mathbf{q} . Since the variable \mathbf{x} is reserved for the coordinates of a particle in phase-space, we adapted the conventional names for consistency.

Using, in addition, the more convenient time parameter (2.22), the divergence of the displacement field follows

$$\nabla_{\mathbf{q}} \cdot \left(\ddot{\Psi} + \frac{\mu}{2} \dot{\Psi} \right) = (\mu/2 + 1)(1 - J^{-1}), \quad (2.38)$$

where we inserted the Poisson equation (2.25) and replaced the density contrast with the determinant $J = \det \left(\frac{\partial \mathbf{q}(t)}{\partial \mathbf{q}^{(i)}} \right)$. The appearance of the inverse determinant J^{-1} in (2.38) highlights a known deficiency of LPT. Similar to SPT, it leads to the breakdown of the theory once particle streams are crossing since the density diverges at these points.

Example 2.5.1 Consider a simple system of freely streaming particles in one dimension. The initial conditions are chosen such that the Eulerian position of a fluid particle initially located at $q^{(i)}$ is given by

$$q(q^{(i)}, t) = q^{(i)}(1 - t/\tau_c), \quad (2.39)$$

with some parameter τ_c , which will turn out to be the free-streaming time. The initial velocity field is $u(q^{(i)}, 0) = \dot{\Psi}(q^{(i)}, 0) = -q^{(i)}/\tau_c$. The density of such a simple system as a function of time t is given by $\rho(q, t) = (\det(\partial q(t)/\partial q^{(i)}))^{-1} = (\partial q(t)/\partial q^{(i)})^{-1}$. Via the relation (2.34) between the Eulerian and the Lagrangian coordinates q and $q^{(i)}$ we find the time-dependent density field

$$\rho(t) = \frac{1}{(1 - t/\tau_c)}, \quad (2.40)$$

which becomes singular at $t = \tau_c$.

In addition to the appearance of singularities, the naive approach to LPT fails to take into account that multiple initial Lagrangian positions can be mapped to the same Eulerian position after stream-crossing. Unlike the issue with singularities, this can be remedied relatively easily by extending the definition of the density to take multiple particle streams into account.

2.5.2 First-order result and the Zel'dovich approximation

Similar to our analysis of SPT, we are looking to determine the first-order solution of (2.38). In LPT, this requires a tad more work than for the case of SPT since we need to account for the mapping from \mathbf{q} to $\mathbf{q}^{(i)}$ to evaluate $\nabla_{\mathbf{q}}$ and J . We execute these steps in detail in Appendix A, which leads us to

$$\ddot{\Psi}^{(1)} + \frac{\mu}{2} \dot{\Psi}^{(1)} - (\mu/2 + 1)\Psi^{(1)} = 0, \quad (2.41)$$

for a curl-free displacement field $\Psi^{(1)}$. Since this is equivalent to the linear growth equation (2.20) for the density contrast in SPT, the first-order solution for the displacement field is given by

$$\Psi^{(1)}(\mathbf{q}^{(i)}, \tau) = e^{\tau} \Psi^{(i)}(\mathbf{q}^{(i)}) = \frac{D_+(t)}{D_+(t_i)} \Psi^{(i)}(\mathbf{q}^{(i)}). \quad (2.42)$$

From the relation between the Eulerian velocity and the displacement field, it directly follows that

$$\Psi^{(i)}(\mathbf{q}^{(i)}) = \mathbf{u}^{(i)}(\mathbf{q}^{(i)}) = \nabla \psi^{(i)}(\mathbf{q}^{(i)}). \quad (2.43)$$

Extending the first-order result of LPT to calculations of late-time structure formation is known as the *Zel'dovich approximation* (ZA). The peculiar velocity field $\mathbf{u}(\mathbf{q}, \tau)$ can be inferred from (2.41) and comparison to (2.24) shows that

$$\mathbf{u}^{(Z)}(\mathbf{q}, \tau) = -\frac{\nabla\phi(\mathbf{q}, \tau)}{(\mu/2 + 1)}. \quad (2.44)$$

In the Zel'dovich approximation, the peculiar velocity field thus points down the local gravitational well at any given time. It is often stressed that the ZA is a local approximation in that individual fluid elements do not influence each other and evolve independently. Although this is true, one should keep in mind that the trajectories of fluid elements do contain effects of gravity since the third term on the lhs of (2.41) stems from the Poisson equation.

2.5.3 The power spectrum in the Zel'dovich approximation

In [Appendix A](#), we derive the density fluctuation power spectrum in the Zel'dovich approximation and arrive at the result

$$P_{\delta}^{(Z)}(k) = e^{-\sigma_{\Psi}^2 k^2} \int_{\Delta\mathbf{q}^{(i)}} \left(e^{\mathbf{k}^T \mathbf{C}_{\Psi\Psi}(\Delta\mathbf{q}^{(i)}) \mathbf{k}} - 1 \right) e^{-i\mathbf{k} \cdot \Delta\mathbf{q}^{(i)}}, \quad (2.45)$$

where $\mathbf{C}_{\Psi\Psi}(\Delta\mathbf{q}^{(i)})$ is the covariance matrix of the linearly evolved displacement field (2.42) and $\sigma_{\Psi}^2 \mathcal{I}_3 = \mathbf{C}_{\Psi\Psi}(0)$. The power spectrum in the Zel'dovich approximation is quite extraordinary since it results in an expression that contains infinitely many orders of the correlation function $\mathbf{C}_{\Psi\Psi}$. This contrasts the results we expect from SPT, which are ordered in powers of these correlation functions and can be traced back to the non-linear relation between the displacement field and the density contrast (2.37). Expanding (2.45) in terms of $\mathbf{C}_{\Psi\Psi}$ we recover the linear power spectrum from SPT at first-order, plus higher order correction terms. Higher-order perturbations of the displacement field no longer follow a GRF, prohibiting a closed analytical expression for the resulting power spectrum. In [Figure 2.3](#) we show the Zel'dovich power spectrum in green, compared to the linear power spectrum from SPT—which is also the first-order expansion of (2.45)—in blue. Interestingly, the full Zel'dovich result falls below the linear power spectrum on small scales (large k) since particles simply move past each other, washing out structures on small scales. The yellow dashed line shows the expansion of the full Zel'dovich power spectrum (2.45) up to second order in $\mathbf{C}_{\Psi\Psi}$. Although this curve seems to suggest excessive growth of small-scale structures due to the sharp increase in amplitude for large k values, comparison to the full Zel'dovich result shows that it is only a valid approximation of (2.45) until $k \approx 0.2 \text{ h Mpc}^{-1}$. The behaviour at small scales is therefore merely an artifact of the expansion in the correlation function $\mathbf{C}_{\Psi\Psi}$. This clearly shows that the one-loop result in SPT and LPT, which are identical at this order [32] are not to be taken seriously for length scales where $k \approx 0.2 \text{ h Mpc}^{-1}$. The one-loop power spectrum from LPT is shown in the pink dotted line. The derivation of the density power spectrum reveals that we deal with two different series expansions in LPT. On the one hand, the equation of motion for the displacement field (2.38) calls for a perturbative treatment; on the other hand, going beyond the Zel'dovich approximation additionally requires a perturbative treatment of the cumulant expansion (A.15). We encounter the same challenges in Kinetic Field Theory, which, as a particle-based approach to cosmic structure formation, shows a lot of similarity to LPT, but consistently incorporates crossing particle streams.

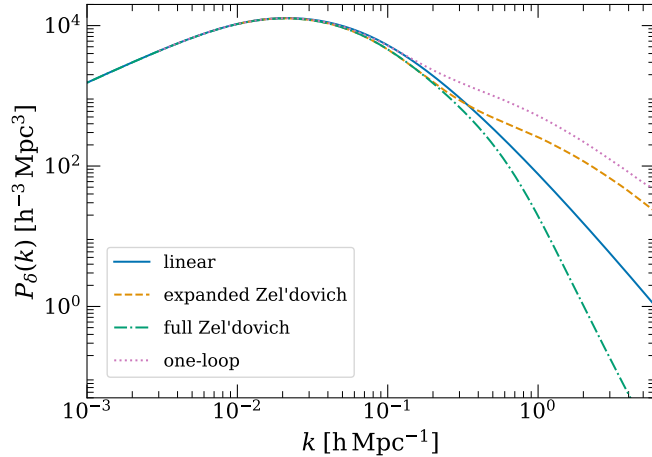


Figure 2.3: A comparison of the linear power spectrum from SPT (2.31) (blue line), the full Zel'dovich power spectrum (2.45) (green line) and the expansion of the Zel'dovich power spectrum up to second order in the initial power spectrum (orange line). The one-loop power spectrum from LPT (identical to the result from SPT) is shown in the pink dotted line.

2.6 SIMULATIONS AND THE HALO MODEL

As we have seen, describing cosmic structure formation in the non-linear regime with either SPT or LPT is fundamentally flawed. In both cases, fundamental assumptions prevent us from successfully describing the system after stream-crossing. To make predictions for the non-linear power spectrum on small scales, where bound objects such as galaxies and galaxy clusters have formed, simulations combined with the halo model are the method of choice. The halo model [36] assumes that all matter in the universe is part of virialised dark matter halos, which can be used to provide estimates for statistical properties of the cosmic matter field. The power spectrum is assumed to consist of a one-halo contribution which dominates on small scales and a two-halo term on large scales. Whereas the small-scale contribution, describing correlations of particles inside a single halo, depends on the density profile of the dark matter halos, the large-scale term describes correlations between the positions of different halos and is often assumed to follow the linear power spectrum. The halo model results in a parametrised description of the dark matter power spectrum and can be used to fit the results of N -body simulations [37, 38]. The non-linear power spectrum thus obtained by Smith et al. [38] is plotted in Figure 2.4. Since simulations can probe much smaller length scales than current analytic methods, the halo model is currently the primary approach to provide non-linear power spectra for wavenumbers $k \gtrsim 10h \text{ Mpc}^{-1}$. Nevertheless, it comes with several severe drawbacks regarding flexibility and interpretability. Since free parameters are fixed with simulation data, the halo model can only provide non-linear power spectra for cosmological models that have been part of a simulation. Since the latter is costly and time-consuming, using the halo model to probe a broad range of cosmological models is impracticable. Although simulations are undoubtedly an immensely useful tool for modern cosmology, they yield little physical insight into the underlying processes. If possible, it is preferable to use analytic methods.

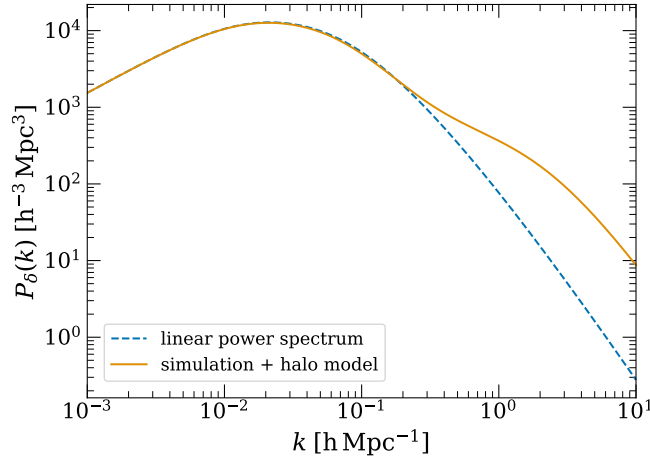


Figure 2.4: The non-linear power spectrum obtained in [38] by fitting the halo model to the result of an N -body dark matter only simulation. On large scales, the fitted non-linear power spectrum coincides with the linear power spectrum by construction (due to finite box sizes, simulations are troubled by boundary effects on these scales, and the linear analytical result is more reliable). Around $k \approx 0.1 h \text{Mpc}^{-1}$, we see small deviations between simulation and linear power spectrum, characterising the mildly non-linear regime. SPT and LPT results are the most useful at these scales since stream-crossing has yet to occur. For larger values of k we enter the non-linear regime, characterised by the presence of bound structures. Currently, simulations are the only method to probe the cosmic density field on these length scales.

2.7 DISCUSSION

We started this chapter by summarising the standard cosmological model and the most recent observational data for the cosmological parameters. We then discussed cosmic structures, giving a glimpse of their formation in the early universe and the derivation of the BBKS transfer function, which sets up the initial conditions for late-time structure formation in the form of an initial power spectrum. We fix the initial time t_i at recombination where $z_i = 1100$, which leaves us with the initial power spectrum displayed in Figure 2.1.

We then proceeded with the discussion by introducing the two most widely spread approaches of late-time structure formation in cosmology. Setting up the system of equations underlying SPT revealed that the hydrodynamical approach requires us to make quite a few assumptions that seriously limit the range of length scales accessible to this method. Most notably, the SSA leads to a breakdown of SPT in the non-linear regime. More recently, approaches based on a hydrodynamical description have emerged that attempt to circumvent the SSA, most notably effective field theory of large-scale structures (EFTofLSS) [39–41]. In a nutshell, EFTofLSS introduces an effective stress-energy tensor for the cosmic fluid, thus avoiding the SSA altogether at the cost of introducing further approximations. Intuitively, the effective stress-energy tensor emerges on large scales by integrating out the shorter (UV) physics. Unfortunately, like all effective field theories, EFTofLSS contains a set of free parameters that need to be fixed, making it rely on simulations for the time being. Since one of the aims of analytical methods for cosmic structure formation is to get a deeper understanding of the underlying physics, this might not be a very satisfying approach. Nevertheless, nowadays, EFTofLSS is among

the most popular approaches to studying structure formation in the mildly non-linear regime.

In addition to SPT, we also had a superficial look at some aspects of LPT, most notably the ZA and the resulting density contrast power spectrum. As we have seen, LPT suffers from the same inconsistencies as SPT once trajectories of fluid elements are crossing. This breakdown can be traced back to the fact that, although LPT is seemingly a particle-based approach, it is based on the continuum ansatz since it assumes a one-to-one mapping of the initial Lagrangian coordinates to the Eulerian coordinates. Stream-crossing can be consistently considered in LPT if we loosen this assumption and treat different particle streams separately. An attempt to make this ansatz work can be found in [35].

In conclusion, SPT and LPT suffer from severe drawbacks in their most basic formulations and do not allow us to describe cosmic structure formation in the non-linear regime. Although there have been valid extensions of both theories to remedy the inconsistencies that have led to exciting developments, some fundamental barriers that are baked into the very assumptions of these descriptions cannot be overcome without a radical change in perspective. Overcoming these fundamental barriers is precisely the aim of Kinetic Field Theory.

3

KINETIC FIELD THEORY

This chapter contains an extensive introduction to KFT in its most general form. Due to the extensive range of systems that can be described in this framework, we keep all considerations as general as possible. Specifications to cosmology will be treated separately in the next chapter.

3.1 GENERAL SETTING AND NOTATION

KFT is a mathematical framework for describing classical many-body systems under general conditions. As such, it offers an alternative to kinetic theory by encoding the system's dynamical evolution, as we will see shortly, in a path integral rather than in a differential equation such as Liouville's equation. Our primary focus will lie in the description of late-time cosmic structure formation, which is a prime example of a classical many-body system far from equilibrium. Nevertheless, it should be stressed that KFT can be applied in a much broader context since it has very few underlying assumptions. In principle, it can treat any system of classical, non-relativistic point particles.

Let us consider the general case of a system of N classical point particles moving in an external potential W and interacting via a two-particle interaction potential $v(|\mathbf{q}_a - \mathbf{q}_b|)$. Such a system is described by the Hamiltonian

$$\mathcal{H} = \sum_{a=1}^N \left\{ \frac{\mathbf{p}_a^2}{2m} + W(\mathbf{q}_a, t) + \sum_{\{b|b<a\}} v(|\mathbf{q}_a - \mathbf{q}_b|) \right\}, \quad (3.1)$$

where t stands for a general time parameter not to be confused with cosmic time. The phase-space dynamics of the particles is described by Hamilton's equations

$$\dot{\mathbf{q}}_a = \frac{\partial \mathcal{H}}{\partial \mathbf{p}_a}, \quad \dot{\mathbf{p}}_a = -\frac{\partial \mathcal{H}}{\partial \mathbf{q}_a} \quad \text{for } a = 1, \dots, N. \quad (3.2)$$

For particle numbers $N > 2$, the equations of motion for non-trivial physical systems cannot be solved exactly. Instead, a statistical approach is chosen, which derives macroscopic quantities, such as overall energy, entropy, pressure, volume etc., from the microscopic phase-space dynamics induced by (3.1). Many systems of interest, such as classical and quantum gases or spin lattices, are studied in situations where they have reached a state close to equilibrium. This assumption greatly simplifies the description of such systems' properties since macroscopic quantities become time-independent, and the ergodic assumption holds.

On the other hand, late-time cosmic structure formation is a process that is far from equilibrium, such that we cannot tackle it with the traditional methods of equilibrium statistical mechanics. Since we have seen previously that a fluid-dynamical approach,

as employed by SPT, comes with its own tight restrictions and is therefore not an option either, a new ansatz is in order. We will explore this in the following section, but before properly introducing KFT, we will have to spend a couple of words on notation.

As we will see in the following, the fundamental fields in KFT are the $6N$ phase-space coordinates of the classical particles of the system under consideration. To abbreviate the equations on the coming pages, we want to introduce a notation that allows us to write them compactly. For each individual particle, we collect the phase-space positions in a single vector $\mathbf{x}_a = (\mathbf{q}_a, \mathbf{p}_a)^\top$, with the particle index $a = 1, \dots, N$. We then define

$$\underline{\mathbf{x}}(t) := \sum_{a=1}^N \mathbf{x}_a(t) \otimes \mathbf{e}_a = \sum_{a=1}^N \begin{pmatrix} \mathbf{q}_a(t) \\ \mathbf{p}_a(t) \end{pmatrix} \otimes \mathbf{e}_a, \quad (3.3)$$

where \mathbf{e}_a is the N -dimensional unit vector pointing in a -direction, such that $(\mathbf{e}_a)_b = \delta_{ab}$. This notation bundles the phase-space coordinates of all the particles of the system into one single tensorial object. We define a scalar product for such tensors $\underline{\mathbf{A}}$ and $\underline{\mathbf{B}}$ by

$$\underline{\mathbf{A}} \cdot \underline{\mathbf{B}} := \sum_{a=1}^N \mathbf{A}_a \cdot \mathbf{B}_a. \quad (3.4)$$

If the tensors are additionally time-dependent we extend the definition of the scalar product to include a time integral

$$\underline{\mathbf{A}} \cdot \underline{\mathbf{B}} := \sum_{a=1}^N \int dt \mathbf{A}_a(t) \cdot \mathbf{B}_a(t). \quad (3.5)$$

Note that in this notation Hamilton's equations (3.2) are compactly expressed as

$$\underline{\mathcal{E}}[\underline{\mathbf{x}}] = \dot{\underline{\mathbf{x}}} - \underline{\mathcal{J}} \nabla_{\underline{\mathbf{x}}} \mathcal{H} = 0, \quad \text{where } \underline{\mathcal{J}} = \begin{pmatrix} 0 & \mathcal{I}_3 \\ -\mathcal{I}_3 & 0 \end{pmatrix} \otimes \mathcal{I}_N. \quad (3.6)$$

3.2 FROM THE PROBABILITY DENSITY TO THE GENERATING FUNCTIONAL

To illustrate the ideas behind KFT, let us consider a many-body system described by the Hamiltonian (3.1). At the initial time t_i , we assume that the particles occupy the infinitesimal phase-space volume around position $\underline{\mathbf{x}}^{(i)}$ with probability $\mathcal{P}(\underline{\mathbf{x}}^{(i)})$. After the initialization, the microscopic degrees of freedom evolve according to the laws of classical mechanics so that the system changes at the macroscopic scale. To calculate the macroscopic properties of such a system, we need a time-dependent phase-space probability density. At some final time t_f the ensemble average of a general observable \mathcal{O} is given by

$$\begin{aligned} \langle \mathcal{O}(t_f) \rangle &= \int \prod_{a=1}^N d^3 p_a d^3 q_a \mathcal{O}(\mathbf{q}_1, \dots, \mathbf{q}_N, \mathbf{p}_1, \dots, \mathbf{p}_N, t_f) \mathcal{P}(\mathbf{q}_1, \dots, \mathbf{q}_N, \mathbf{p}_1, \dots, \mathbf{p}_N, t_f), \\ &=: \int d\underline{\mathbf{x}} \mathcal{O}(\underline{\mathbf{x}}, t_f) \mathcal{P}(\underline{\mathbf{x}}, t_f). \end{aligned} \quad (3.7)$$

In contrast to equilibrium statistical mechanics, the phase-space probability density $\mathcal{P}(\underline{\mathbf{x}}, t_f)$ is time-dependent and needs to be determined by describing the system's evolution from its initial state. From the known initial probability density $\mathcal{P}(\underline{\mathbf{x}}^{(i)})$, we can infer

$$\mathcal{P}(\underline{\mathbf{x}}, t_f) = \int d\underline{\mathbf{x}}^{(i)} \mathcal{P}(\underline{\mathbf{x}}^{(i)}) \mathcal{P}(\underline{\mathbf{x}}, t_f | \underline{\mathbf{x}}^{(i)}), \quad (3.8)$$

where $\mathcal{P}(\underline{\mathbf{x}}, t_f | \underline{\mathbf{x}}^{(i)})$ denotes the transition probability from the initial state $\underline{\mathbf{x}}^{(i)}$ to the final state $\underline{\mathbf{x}}$ at time t_f . Since we are dealing with a classical N -body system, the transition amplitude is non-vanishing only for those phase-space positions $\underline{\mathbf{x}}$ that result from evolving the initial state along its classical trajectory $\tilde{\underline{\mathbf{x}}}(t_f; \underline{\mathbf{x}}^{(i)})$, such that

$$\mathcal{P}(\underline{\mathbf{x}}, t_f | \underline{\mathbf{x}}^{(i)}) = \delta_D(\underline{\mathbf{x}} - \tilde{\underline{\mathbf{x}}}(t_f; \underline{\mathbf{x}}^{(i)})). \quad (3.9)$$

Slicing the classical trajectory into infinitesimal time-steps it can be shown that for each time $t_i < t \leq t_f$ the ensemble average of a general operator \mathcal{O} is given by

$$\langle \mathcal{O}(t) \rangle = \int d\underline{\mathbf{x}}^{(i)} \mathcal{P}(\underline{\mathbf{x}}^{(i)}) \int_{\underline{\mathbf{x}}(t_i)=\underline{\mathbf{x}}^{(i)}} \mathcal{D}\underline{\mathbf{x}}(t) \mathcal{O}(\underline{\mathbf{x}}, t) \delta_D[\underline{\mathbf{x}}(t) - \tilde{\underline{\mathbf{x}}}(t; \underline{\mathbf{x}}^{(i)})]. \quad (3.10)$$

Note that the Dirac delta has become a functional delta distribution under the path integral. For the next step, we note that the expression in the functional delta distribution forces the phase-space coordinates of the system to lie on the classical trajectory at each moment in time. This is equivalent to demanding that Hamilton's equations (3.6) be fulfilled for each time t . The transformation of the phase-space trajectories in the functional delta-distribution to Hamilton's equations of motion involves a functional determinant which is linked to the value of the Heaviside step function at $t = 0$ [42, 43]—naturally, since the Heaviside function is the Green's function of the first-order derivative operator. A common choice in quantum field theory is to set $\theta(0) := \frac{1}{2}$, which preserves time-reversal symmetry at the cost of a non-vanishing functional determinant, thus introducing ghost degrees of freedom into the theory. To avoid the occurrence of ghosts, we choose instead $\theta(0) := 0$, such that the determinant becomes constant and the transformation from particle trajectories to equations of motion can be done without introducing additional dynamical degrees of freedom to the path integral:

$$\delta_D[\underline{\mathbf{x}}(t) - \tilde{\underline{\mathbf{x}}}(t; \underline{\mathbf{x}}^{(i)})] \propto \delta_D[\underline{\mathcal{E}}[\underline{\mathbf{x}}]]. \quad (3.11)$$

This statement holds for general first-order equations of motion, independently of additional assumptions such as a symplectic structure. To arrive at the final expression for the probability density, we represent the functional Dirac delta in Fourier space

$$\delta_D[\underline{\mathcal{E}}[\underline{\mathbf{x}}]] = \int \mathcal{D}\underline{\chi}(t) \exp(i\underline{\chi} \cdot \underline{\mathcal{E}}[\underline{\mathbf{x}}]), \quad (3.12)$$

where $\underline{\chi} = (\chi_q, \chi_p)^T$ is the Fourier conjugate to the equations of motion. Note that the generalized scalar product between $\underline{\chi}$ and the equations of motion

$$\underline{\chi} \cdot \underline{\mathcal{E}}[\underline{\mathbf{x}}] = \int dt \sum_{a=1}^N \chi_a \cdot \mathcal{E}[\mathbf{x}_a] = \int dt \sum_{a=1}^N \begin{pmatrix} \chi_{q_a}(t) \\ \chi_{p_a}(t) \end{pmatrix} \cdot \begin{pmatrix} \dot{\mathbf{q}}_a - \frac{\partial \mathcal{H}}{\partial \mathbf{p}_a} \\ \dot{\mathbf{p}}_a + \frac{\partial \mathcal{H}}{\partial \mathbf{q}_a} \end{pmatrix} \quad (3.13)$$

can be thought of as an action, since $\frac{\delta}{\delta \underline{\chi}}(\underline{\chi} \cdot \underline{\mathcal{E}}[\underline{\mathbf{x}}]) = 0$ generates the classical equations of motion. Introducing the time-dependent source fields $\underline{\mathbf{J}}(t)$ and $\underline{\mathbf{K}}(t)$ for the phase-space coordinates $\underline{\mathbf{x}}(t)$ and the auxiliary field $\underline{\chi}(t)$, respectively, we arrive at the (canonical)¹ generating functional

$$Z[\underline{\mathbf{J}}, \underline{\mathbf{K}}] = \int d\underline{\mathbf{x}}^{(i)} \mathcal{P}(\underline{\mathbf{x}}^{(i)}) \int_{\underline{\mathbf{x}}^{(i)}} \mathcal{D}\underline{\mathbf{x}}(t) \int \mathcal{D}\underline{\chi}(t) \exp\{i\underline{\chi} \cdot \underline{\mathcal{E}}[\underline{\mathbf{x}}] + i\underline{\mathbf{J}} \cdot \underline{\mathbf{x}} + i\underline{\mathbf{K}} \cdot \underline{\chi}\}. \quad (3.14)$$

¹ Canonical refers to the fact that we keep the particle number N constant, in contrast to the grand-canonical formalism introduced in [4].

The lower boundary of the path integral is an abbreviation to remind ourselves that at t_i the initial state $\underline{x}(t_i)$ is fixed at $\underline{x}^{(i)}$. The generating functional (3.14) is the central object in KFT since it allows for a systematic calculation of macroscopic quantities such as correlation functions. Since $Z[\underline{0}, \underline{0}]$ is normalized to unity, the ensemble average of a general observable $\mathcal{O}(\underline{x}, t)$ now takes the form

$$\langle \mathcal{O}(t) \rangle = \hat{\mathcal{O}} \left(\frac{\delta}{i\delta \underline{J}(t)} \right) Z[\underline{J}, \underline{K}] \Big|_{\underline{0}}, \quad (3.15)$$

where $(\dots) \Big|_{\underline{0}}$ implies that the expression is to be evaluated at $\underline{J} = \underline{K} = \underline{0}$. More systematically, we can calculate ensemble averages of a general observable by substituting

$$\underline{x} \rightarrow \hat{\underline{x}} = \frac{\delta}{i\delta \underline{J}} \quad \text{and} \quad \underline{\chi} \rightarrow \hat{\underline{\chi}} = \frac{\delta}{i\delta \underline{K}} \quad (3.16)$$

for its arguments and applying the resulting operator to the generating functional. Observables in operator form are generally marked as such by a hat, e. g. $\hat{\mathcal{O}}(t)$. Note that we do not expect actual physical observables to depend on the auxiliary field $\underline{\chi}$, since it has no direct physical interpretation. Nevertheless, we will see shortly that it plays a vital role in KFT calculations.

3.3 GENERAL PARTICLE TRAJECTORIES AND THE INTERACTION OPERATOR

For most many-body systems of physical interest, e. g. systems with particle interactions, solving the full equations of motion $\underline{\mathcal{E}}[\underline{x}]$ is hopeless. Instead, our strategy will be to split $\underline{\mathcal{E}}[\underline{x}]$ into a simple linear part $\underline{\mathcal{E}}_0[\underline{x}]$ and a non-linear part $\underline{\mathcal{E}}_I[\underline{x}]$ due to interactions. Here linear and non-linear refer to the nature of the resulting differential operator. Note that, in the case of underlying Hamiltonian dynamics, this splitting could be due to a separation of the Hamiltonian $\mathcal{H} = \mathcal{H}_0 + \mathcal{H}_I$, but this does not necessarily have to be the case. For example, we can imagine that we perform a coordinate transform on \underline{x} , which leaves the path integral in (3.14) invariant but destroys the symplectic nature of the equations of motion. We can then still split $\underline{\mathcal{E}}[\underline{x}]$ into two parts, but since it is no longer symplectic, we can not define a split of the underlying Hamiltonian. We will encounter this case when we discuss particle trajectories in an expanding universe.

Performing the separation of the equations of motion and rearranging terms in (3.14) leads to

$$Z[\underline{J}, \underline{K}] = \int d\underline{\Gamma}_i \int_{\underline{x}^{(i)}} \mathcal{D}\underline{x}(t) \int \mathcal{D}\underline{\chi}(t) \exp \left\{ i\underline{\chi} \cdot (\underline{\mathcal{E}}_0[\underline{x}] + \underline{K}) + i\underline{\chi} \cdot \underline{\mathcal{E}}_I[\underline{x}] + i\underline{J} \cdot \underline{x} \right\}, \quad (3.17)$$

where we have additionally introduced the abbreviation $d\underline{\Gamma}_i = d\underline{x}^{(i)} \mathcal{P}(\underline{x}^{(i)})$. We refer to the term containing the non-linear part of the equation of motion as the interaction action S_I . Promoting it to an operator such that

$$iS_I = i\underline{\chi} \cdot \underline{\mathcal{E}}_I[\underline{x}] \quad \rightarrow \quad i\hat{S}_I := i\hat{\underline{\chi}} \cdot \underline{\mathcal{E}}_I[\hat{\underline{x}}] = i \left(\frac{\delta}{i\delta \underline{K}} \cdot \underline{\mathcal{E}}_I \left[\frac{\delta}{i\delta \underline{J}} \right] \right) \quad (3.18)$$

allows us to pull it in front of the path integral. The result is the *interaction operator* \hat{S}_I , which we will spend much time with later. For now, let us focus on the remaining path integral, which we will from now on refer to as the *free generating functional*

$$Z_0[\underline{J}, \underline{K}] = \int d\underline{\Gamma}_i \int_{\underline{x}^{(i)}} \mathcal{D}\underline{x}(t) \int \mathcal{D}\underline{\chi}(t) \exp \left\{ i\underline{\chi} \cdot (\underline{\mathcal{E}}_0[\underline{x}] + \underline{K}) + i\underline{J} \cdot \underline{x} \right\}. \quad (3.19)$$

At this point, we can revert the steps that we have taken previously by recasting the path integral over the auxiliary field $\underline{\chi}$ into a functional delta-distribution

$$Z_0[\underline{J}, \underline{K}] = \int d\underline{\Gamma}_i \int_{\underline{x}^{(i)}} \mathcal{D}\underline{x}(t) \delta_D[\underline{\mathcal{E}}_0[\underline{x}] + \underline{K}] e^{i\underline{J} \cdot \underline{x}}, \quad (3.20)$$

thus enforcing the condition that the particles' motion be dictated by the linear part of the e. o. m. with an inhomogeneity given by the source field \underline{K} . Evaluating the path integral then leads to

$$Z_0[\underline{J}, \underline{K}] = \int d\underline{\Gamma}_i \exp \left\{ i\underline{J} \cdot \tilde{\underline{x}}[\underline{K}] \right\}, \quad (3.21)$$

where $\tilde{\underline{x}}[\underline{K}]$ denotes the \underline{K} -dependent phase-space trajectory which solves the initial value problem $\underline{\mathcal{E}}_0[\underline{x}] + \underline{K} = \underline{0}$, with $\underline{x}(t_i) = \underline{x}^{(i)}$. Since Hamilton's equations are first-order differential equations, and we demand $\underline{\mathcal{E}}_0[\underline{x}]$ to be a linear differential operator, we can write

$$\underline{\mathcal{E}}_0[\underline{x}] + \underline{K} = \dot{\underline{x}} - \underline{\mathcal{M}} \underline{x} + \underline{K} = \underline{0} \quad \underline{x}(t_i) = \underline{x}^{(i)}, \quad (3.22)$$

where the details of the physical system are contained in the matrix $\underline{\mathcal{M}}$. We discuss the solution of this equation in terms of a Green's function in more detail in [Appendix B](#), where we end up with the phase-space trajectory

$$\tilde{\underline{x}}[\underline{K}, t] = \underline{\mathbf{G}}(t, t_i) \underline{x}^{(i)} - \int d\bar{t} \underline{\mathbf{G}}(t, \bar{t}) \underline{K}(\bar{t}) \quad \forall t > t_i. \quad (3.23)$$

Since all particles share the same Green's function, we have $\underline{\mathbf{G}}(t, t') = \underline{\mathbf{G}}(t, t') \otimes \mathcal{I}_N$, where $\underline{\mathbf{G}}(t, t')$ is the single-particle Green's function. Due to the structure of the phase-space coordinates it can be generally written as

$$\underline{\mathbf{G}}(t, t') = \begin{pmatrix} g_{qq}(t, t') \mathcal{I}_3 & g_{qp}(t, t') \mathcal{I}_3 \\ g_{pq}(t, t') \mathcal{I}_3 & g_{pp}(t, t') \mathcal{I}_3 \end{pmatrix} \theta(t - t'), \quad (3.24)$$

but the exact expression for the individual components depends on $\underline{\mathcal{M}}$. A common situation in the application of KFT to cosmic structure formation and beyond is that $p = \dot{q}$ is imposed by the equations of motion². Conditions such as this one are directly translated to the Green's function, such that we would get the relation $g_{p \times}(t, t') = \partial_t g_{q \times}(t, t')$, where \times stands for either q or p . Furthermore, if the linear e. o. m. does not contain any terms that are proportional to the particle position, it follows that $g_{qq}(t, t') = 1$ and $g_{pq}(t, t') = 0$. This situation is quite common in KFT since q -dependent terms tend to be included in the non-linear part of the equations of motion. Under these two conditions, the Green's function retains but a single independent component, $g_{qp}(t, t')$, which we shall refer to as the 'particle propagator'. For all applications of interest in this thesis, the Green's function can therefore be simplified to

$$\underline{\mathbf{G}}(t, t') = \begin{pmatrix} \mathcal{I}_3 & g_{qp}(t, t') \mathcal{I}_3 \\ 0_3 & \dot{g}_{qp}(t, t') \mathcal{I}_3 \end{pmatrix} \theta(t - t'), \quad (3.25)$$

where the dot refers to the derivative w.r.t. the first time argument. Note that the particle propagator $g_{qp}(t, t')$ describes how the position of a particle changes between the times t and t' due to its momentum and, therefore, naturally fulfils $g_{qp}(t, t) = 0$.

² In general, the particle mass should appear in this relation, but we are mostly interested in purely gravitational systems where particle masses cancel out in the e. o. m. .

3.3.1 Free phase-space trajectories

First, let us consider the case where no interaction operator acts on the free generating functional, allowing us to set the source current $\underline{\mathbf{K}}$ to zero. The resulting *free particle trajectory* $\underline{\mathbf{x}}(t)$ is then solely determined by the initial conditions and the Green's function

$$\underline{\mathbf{x}}(t) = \underline{\mathbf{G}}(t, t_i) \underline{\mathbf{x}}^{(i)}. \quad (3.26)$$

Note that free trajectories reflect our choice of the linear part of the equation of motion and do not necessarily correspond to force-free motion in the physical sense. Indeed, it turns out that in cosmological applications incorporating a particular part of particle interactions into the 'free' trajectories can be helpful when doing explicit calculations. Keeping this in the back of our mind, we will mainly glance over this semantic subtlety and refer to the solution to the linear part of the e. o. m. as 'free' trajectories and to the terms inducing deviations therefrom as 'interactions'. For the free phase-space trajectories of individual particles, (3.26) and (3.25) imply that $\forall a = 1, \dots, N$

$$\bar{\mathbf{q}}_a(t) = \mathbf{q}_a^{(i)} + g_{qp}(t, 0) \mathbf{p}_a^{(i)}, \quad (3.27)$$

$$\bar{\mathbf{p}}_a(t) = \dot{g}_{qp}(t, 0) \mathbf{p}_a^{(i)}. \quad (3.28)$$

Recall that, due to the statistical nature of the initial conditions, the free generating functional contains an integral over the initial phase-space density. For particles moving along free trajectories, we can reformulate (3.21) explicitly in terms of the initial phase-space coordinates. Starting from the free generating functional with $\underline{\mathbf{K}} = \underline{\mathbf{0}}$ we define the time-integrated source fields by using the definitions (3.27) and (3.28) for the free phase-space trajectories:

$$\bar{\underline{\mathbf{J}}}_q = \int dt \underline{\mathbf{J}}_q(t) \quad \bar{\underline{\mathbf{J}}}_p = \int dt (g_{qp}(t, 0) \underline{\mathbf{J}}_q(t) + \dot{g}_{qp}(t, 0) \underline{\mathbf{J}}_p(t)). \quad (3.29)$$

As a result, we can rewrite the free generating functional in the particularly simple form

$$Z_0[\underline{\mathbf{J}}, \underline{\mathbf{0}}] = \int d\underline{\Gamma}_i \exp \{ i \bar{\underline{\mathbf{J}}}_q \cdot \underline{\mathbf{q}}^{(i)} + i \bar{\underline{\mathbf{J}}}_p \cdot \underline{\mathbf{p}}^{(i)} \}. \quad (3.30)$$

3.3.2 Fully interacting phase-space trajectories

As a consistency check, it is now instructive to consider the opposite, where we apply the interaction operator in its exponential form to the free generating functional. The fully interacting generating functional is given by

$$Z[\underline{\mathbf{J}}, \underline{\mathbf{K}}] = \exp(i\hat{\mathcal{S}}_I) \int d\underline{\Gamma}_i \exp \{ i \underline{\mathbf{J}} \cdot \underline{\mathbf{x}}[\underline{\mathbf{K}}] \}, \quad (3.31)$$

with the interaction operator defined in (3.18). Applying the functional derivative w. r. t. $\underline{\mathbf{K}}$ introduces a shift, resulting in

$$Z[\underline{\mathbf{J}}, \underline{\mathbf{K}}] = \exp \left\{ i \left(\hat{\underline{\mathcal{E}}}_I \cdot \frac{\delta}{i\delta\underline{\mathbf{K}}} \right) \right\} Z_0[\underline{\mathbf{J}}, \underline{\mathbf{K}}] = Z_0[\underline{\mathbf{J}}, \underline{\mathbf{K}} + \underline{\mathcal{E}}_I] \quad (3.32)$$

in complete analogy to the effect of the translation operator in quantum mechanics $\exp(\mathbf{a} \cdot \nabla) f(\mathbf{x}) = f(\mathbf{x} + \mathbf{a})$. Now that the interaction operator has been applied, there is no further need for the source field $\underline{\mathbf{K}}$, and we may set it to zero, which yields

$$Z[\underline{\mathbf{J}}] = \int d\underline{\Gamma}_i \exp \{ i \underline{\mathbf{J}} \cdot \underline{\mathbf{x}}[\underline{\mathcal{E}}_I[\underline{\mathbf{x}}]] \}, \quad (3.33)$$

$$\text{with } \underline{\mathbf{x}}[\underline{\mathcal{E}}_I[\underline{\mathbf{x}}], t] = \underline{\mathbf{G}}(t, t_i) \underline{\mathbf{x}}^{(i)} - \int d\bar{t} \underline{\mathbf{G}}(t, \bar{t}) \underline{\mathcal{E}}_I[\underline{\mathbf{x}}, \bar{t}]. \quad (3.34)$$

The resulting particle trajectory is thus a self-consistent solution of the full equation of motion $\underline{\mathcal{E}}[\mathbf{x}] = \underline{\mathcal{E}}_0[\mathbf{x}] + \underline{\mathcal{E}}_I[\mathbf{x}]$, illustrating that the interaction operator introduces perturbations into the phase-space trajectory by means of the source field $\underline{\mathbf{K}}$. Of course, as the inhomogeneous part of the trajectory contains the full phase-space trajectory itself, this is a purely formal result, which can lead to a perturbative treatment by iteratively inserting the solution into itself. Whereas the first iteration step corresponds to free trajectories, the second iteration consists of free trajectories perturbed by interacting with all other particles that move along free trajectories themselves, known as Born's approximation.

3.4 ESSENTIAL MACROSCOPIC OPERATORS

So far, we have been laying the groundwork for KFT in constructing the generating functional from the microscopic phase-space dynamics and have kept the discussion of macroscopic observables at an abstract level. Building upon our work in the previous sections, we are now in a position to introduce operator expressions for the physical quantities in which we are interested. It turns out that two fundamental fields naturally enter calculations in KFT, no matter which macroscopic quantities we aim to calculate: the particle density and the so-called response field³. Of course, many more observables of interest can be expressed as operators in KFT, but we will be content with the two mentioned above for our application.

As an aside, let's make a short note on the notation at this point. Since we will continuously work with time-dependent observables in Fourier-space, we should introduce a compact notation for their arguments. For an arbitrary function f in Fourier-space, we therefore define

$$f(1) := f(\mathbf{k}_1, t_1), \quad f(-1) := f(-\mathbf{k}_1, t_1), \quad \int d1 f(1) := \int dt_1 \int_{\mathbf{k}_1} f(\mathbf{k}_1, t_1). \quad (3.35)$$

3.4.1 The density operator

Let us start our discussion of macroscopic observables with the familiar notion of particle density in configuration space. Due to the assumption of classical point-particles, reads

$$\rho(\mathbf{q}, t_1) = \sum_{a=1}^N \delta_D(\mathbf{q} - \mathbf{q}_a(t_1)). \quad (3.36)$$

It is essential to distinguish between the configuration space coordinate \mathbf{q} and particle a 's time-dependent phase-space position $\mathbf{q}_a(t_1)$. Whereas the time-dependent position in phase-space is a particle-bound quantity, the coordinate \mathbf{q} denotes a position in configuration space independent of particles. Due to its distributional nature, it is much more convenient to work with the particle density in Fourier space, where it reads

$$\rho(1) = \rho(\mathbf{k}_1, t_1) = \sum_{a=1}^N \exp(-i\mathbf{k}_1 \cdot \mathbf{q}_a(t_1)). \quad (3.37)$$

³ This is because these two fields are needed to describe the interaction operator for the case of particle interactions that are caused by a two-particle interaction potential. Some applications, such as the resummed version of KFT, require a slight generalisation from the particle density to the total phase-space density, though.

Intuitively, we decompose the density field into its Fourier modes, and each of these modes evolves in time due to its dependence on the spatial trajectories of the microscopic particles of the system. We, therefore, refer to a density mode being *carried by particles*. From (3.37), we derive the density operator by replacing the spatial particle trajectories with functional derivatives w. r. t. the source current $\underline{\mathbf{J}}$

$$\hat{\rho}(1) = \sum_{a=1}^N \exp \left(-i \mathbf{k}_1 \cdot \frac{\delta}{i \delta \mathbf{J}_{q_a}(t_1)} \right) = \sum_{a=1}^N \hat{\rho}_a(1). \quad (3.38)$$

In the last step, we identified the single-particle density operator $\hat{\rho}_a(1)$, which is the operator expression of a density mode being carried by particle a .

To gain some intuition, let us calculate a free (Fourier-space) m -point density correlation function $\bar{G}_{\rho \dots \rho}(1, 2, \dots, m)$ by applying m density operators on the free generating functional. Since density operators in Fourier space (3.4.1) are exponentials of functional derivatives, they generate functional shifts in Z_0 , such that

$$\bar{G}_{\rho \dots \rho}(1, 2, \dots, m) = \sum_{\{a_1 \dots a_m\}}^N \hat{\rho}_{a_1}(1) \hat{\rho}_{a_2}(2) \dots \hat{\rho}_{a_m}(m) Z_0[\underline{\mathbf{J}}, \underline{\mathbf{K}}] \Big|_{\underline{\mathbf{0}}} = \sum_{\{a_1 \dots a_m\}}^N Z_0[\underline{\mathbf{L}}, \underline{\mathbf{0}}], \quad (3.39)$$

$$\text{with} \quad \underline{\mathbf{L}}(t) = \sum_{s=1}^m \begin{pmatrix} -\mathbf{k}_s \\ 0 \end{pmatrix} \delta_D(t - t_s) \otimes \mathbf{e}_{a_s}. \quad (3.40)$$

Note that the shift tensor $\underline{\mathbf{L}}$ implicitly depends on the set of particle indices $\{a_1 \dots a_m\}$. It is enlightening to examine this expression from a different angle by explicitly evaluating the result for Z_0 . After inserting the shift tensor into the definition of the free generating functional (3.21) at vanishing $\underline{\mathbf{K}}$, a quick calculation shows that

$$Z_0[\underline{\mathbf{L}}, \underline{\mathbf{0}}] = \int d\underline{\Gamma}_i \exp \left(- \sum_{s=1}^m i \mathbf{k}_s \cdot \bar{\mathbf{q}}_{a_s}(t_s) \right), \quad (3.41)$$

which integrates the free Fourier-space particle densities over initial conditions. Here $\bar{\mathbf{q}}_{a_s}(t_s)$ denotes the free spatial trajectory of particle a_s at time t_s . We interpret this in a way that a single Fourier mode of the density field evolves in time due to the evolution of particle trajectories, starting from specific initial conditions. In this sense, density modes can thus be thought of as being carried by point particles which govern their evolution via their phase-space dynamics. Correlations between time-evolved particle densities are obtained by propagating the initial correlations between particles forward in time. The expression (3.27) for free spatial trajectories allows us to formulate the integrand explicitly in terms of the initial phase-space positions as in (3.30)

$$Z_0[\underline{\mathbf{L}}, \underline{\mathbf{0}}] = \int d\underline{\Gamma}_i \exp \left(i \bar{\underline{\mathbf{L}}}_q \cdot \underline{\mathbf{q}}^{(i)} + i \bar{\underline{\mathbf{L}}}_p \cdot \underline{\mathbf{p}}^{(i)} \right), \quad (3.42)$$

where we derived the time-integrated position and momentum shift tensor $\bar{\underline{\mathbf{L}}}_q$ and $\bar{\underline{\mathbf{L}}}_p$ from the time-dependent shift tensor (3.40) in analogy to (3.29). To stay consistent with the common notation in KFT, we will drop the bars on these vectors in the following,

$$\bar{\underline{\mathbf{L}}}_q \rightarrow \underline{\mathbf{L}}_q \quad \bar{\underline{\mathbf{L}}}_p \rightarrow \underline{\mathbf{L}}_p, \quad (3.43)$$

always keeping in mind that $\underline{\mathbf{L}}_q$ and $\underline{\mathbf{L}}_p$ are not the p - and q -components of the time-dependent shift tensor! Their definition in terms of the particle indices a_s and the arguments of the density operators is

$$\underline{\mathbf{L}}_q = \sum_{s=1}^m \mathbf{L}_{q_{a_s}} \otimes \mathbf{e}_{a_s} \quad \text{with} \quad \mathbf{L}_{q_{a_s}} = -\mathbf{k}_s, \quad (3.44)$$

$$\underline{\mathbf{L}}_p = \sum_{s=1}^m \mathbf{L}_{p_{a_s}} \otimes \mathbf{e}_{a_s} \quad \text{with} \quad \mathbf{L}_{p_{a_s}} = -g_{qp}(t_s, 0) \mathbf{k}_s. \quad (3.45)$$

Since time has explicitly been integrated out in the definition of the position and momentum shift tensors, they should not be considered as functions but rather as parameters appearing in Z_0 . Additionally, once the source fields $\underline{\mathbf{J}}$ and $\underline{\mathbf{K}}$ are set to zero (3.42) is strictly speaking no longer a generating functional—although it is commonly referred to as the ‘free-generating functional at shift $\underline{\mathbf{L}}$ ’ in KFT literature. To stay somewhat consistent with the standard KFT convention while still recognising these facts, we define the function

$$\mathcal{Z}_0(\underline{\mathbf{L}}_q, \underline{\mathbf{L}}_p) := \int d\Gamma_i \exp(i\underline{\mathbf{L}}_q \cdot \underline{\mathbf{q}}^{(i)} + i\underline{\mathbf{L}}_p \cdot \underline{\mathbf{p}}^{(i)}), \quad (3.46)$$

which, due to (3.39) plays the role of a free m -point correlation function at fixed particle indices in KFT. As we will see in the next chapter, the sums over particle indices in (3.39) turn into trivial prefactors in the continuum limit, such that we can identify $\mathcal{Z}_0(\underline{\mathbf{L}}_q, \underline{\mathbf{L}}_p)$ with a free correlation function up to a constant prefactor.

3.4.2 Interactions and the response field operator

3.4.2.1 The interaction operator

In the previous section, we showed how to calculate free correlation functions. A natural step forward is to ask how interactions can be included—always keeping in mind that free trajectories and interactions are determined by the part of the split equation of motion they stem from—in our considerations. Assuming that $\underline{\mathcal{E}}_I[\underline{\mathbf{x}}]$ contains the interaction potentials from the Hamiltonian (3.1), the interaction action (3.18) and Hamilton’s equations suggest that

$$iS_I = i\underline{\chi}_p \cdot \nabla_{\underline{\mathbf{q}}} V + i\underline{\chi}_p \cdot \nabla_{\underline{\mathbf{q}}} W. \quad (3.47)$$

Here $W(\underline{\mathbf{q}}, t)$ represents a general external potential, whereas particle interactions are encoded in the collective potential

$$V(\underline{\mathbf{q}}, t) = \sum_{a=1}^N v(|\underline{\mathbf{q}} - \underline{\mathbf{q}}_a(t)|) = \int_{\underline{\mathbf{q}}'} v(\underline{\mathbf{q}} - \underline{\mathbf{q}}') \rho(\underline{\mathbf{q}}', t), \quad (3.48)$$

where we relied on the definition (3.36) of the particle density to arrive at the second equality. To clarify the above notation, note that the potentials $W(\underline{\mathbf{q}}, t)$ and $V(\underline{\mathbf{q}}, t)$ are to be understood as functions of the spatial coordinate $\underline{\mathbf{q}}$ and time t , whereas gradients

such as $\nabla_{\underline{\mathbf{q}}} V(t)$ are evaluated at the actual positions of microscopic point-particles at the time t

$$\begin{aligned} \nabla_{\underline{\mathbf{q}}} V(t) &= \sum_{a=1}^N \nabla_{\underline{\mathbf{q}}} V(\underline{\mathbf{q}}, t) \Big|_{\underline{\mathbf{q}}=\underline{\mathbf{q}}_a(t)} \otimes \mathbf{e}_a \\ &= \sum_{a=1}^N \sum_{\{b|b<a\}}^N \nabla_{\underline{\mathbf{q}}} v(|\underline{\mathbf{q}} - \underline{\mathbf{q}}_b(t)|) \Big|_{\underline{\mathbf{q}}=\underline{\mathbf{q}}_a(t)} \otimes \mathbf{e}_a \\ &= \sum_{a=1}^N \int_{\underline{\mathbf{q}}'} \nabla_{\underline{\mathbf{q}}} v(\underline{\mathbf{q}} - \underline{\mathbf{q}}') \rho(\underline{\mathbf{q}}', t) \rho_a(\underline{\mathbf{q}}, t) \otimes \mathbf{e}_a. \end{aligned} \quad (3.49)$$

Once again, we have used (3.36) to derive the last equality. Plugging this into the first term of (3.47) and expanding the generalized scalar product yields

$$i \underline{\chi}_p \cdot \nabla_{\underline{\mathbf{q}}} V = i \int dt' \int_{\underline{\mathbf{q}}', \underline{\mathbf{q}}} \sum_{a=1}^N \chi_{p_a}(t') \cdot \nabla_{\underline{\mathbf{q}}} v(\underline{\mathbf{q}} - \underline{\mathbf{q}}') \rho(\underline{\mathbf{q}}', t') \rho_a(\underline{\mathbf{q}}, t'). \quad (3.50)$$

Transforming to Fourier space once more and shuffling around the resulting terms leaves us with

$$\begin{aligned} i \underline{\chi}_p \cdot \nabla_{\underline{\mathbf{q}}} V &= -i \int dt' \int_{\mathbf{k}'} \left\{ \sum_{a=1}^N (-i \mathbf{k}' \cdot \chi_{p_a}(t')) \rho_a(-\mathbf{k}', t') \right\} v(\mathbf{k}') \rho(\mathbf{k}', t') \\ &= -i \int d1' B(-1') v(1') \rho(1'). \end{aligned} \quad (3.51)$$

In the last step, we identified the term in braces as the response field $B(-1') = B(-\mathbf{k}'_1, t_1)$. Following the same line, the second term in (3.47) gives a similar result but lacks the particle density $\rho(1')$ under the integral. This is, of course, expected since this component represents the particle density that sources the two-particle interaction and should be absent in the case of an external potential.

As we did previously, we can now turn the resulting expressions into operators by employing (3.16). The full expression for the resulting interaction operator thus turns out to be

$$i \hat{S}_I = -i \int d1' \hat{B}(-1') v(1') \hat{\rho}(1') - i \int d1' \hat{B}(-1') W(1'), \quad (3.52)$$

where the two terms are due to particle interactions and the presence of an external potential, respectively.

3.4.2.2 The response field operator

The response field operator $\hat{B}(-1')$ thus appears naturally once we express the interaction operator in terms of macroscopic fields. To understand its role in the evaluation of interactions, we have a closer look at its components. By definition

$$\hat{B}(-1') = \sum_{a=1}^N (-i \mathbf{k}'_1 \cdot \hat{\chi}_{p_a}(t'_1)) \hat{\rho}_a(-1') \equiv \sum_{a=1}^N \hat{b}_a(-1') \hat{\rho}_a(-1'), \quad (3.53)$$

introducing the one-particle response field operator $\hat{b}_a(-1')$ in the second line.

As we show in [Appendix C](#), expressing the effect of response field operators on the free generating functional is a rather messy business. A more elegant description is obtained by interpreting response fields as operators acting on other density operators.

This can then be compactly encoded by considering contractions of response field operators with density operators

$$\overline{\hat{B}(-R)} \hat{\rho}(s) := b(s, -R) \hat{\rho}(s, -R), \quad (3.54)$$

with the response prefactor and the generalized density operator, respectively, defined by

$$b(s, -R) := (-i\mathbf{k}_R \cdot \mathbf{k}_s) g_{qp}(t_s, t_R) \theta(t_s - t_R), \quad (3.55)$$

$$\hat{\rho}(s, -R) := \sum_{a_s=1}^N \hat{\rho}_{a_s}(s) \hat{\rho}_{a_s}(-R). \quad (3.56)$$

Additionally, since response field operators contain one-particle density operators, response fields can contract with other response fields. The result of such a contraction is

$$\overline{\hat{B}(-R)} \hat{B}(-S) = b(-S, -R) \hat{B}(-S, -R), \quad (3.57)$$

$$\text{with } \hat{B}(-S, -R) := \sum_{a_s=1}^N \hat{b}_{a_s}(-S) \hat{\rho}_{a_s}(-S) \hat{\rho}_{a_s}(-R). \quad (3.58)$$

Note that since the prefactor $b(-S, -R)$ contains a particle propagator, contractions are time-directed, leading us to refer to it as a response field ‘targeting’ another operator. We use the convention that response field operators on the left of a contraction are evaluated at an earlier time, allowing response fields to form chains, along which their time and wave-vector arguments are handed down. Causality forbids chains that close in on themselves since such a topology must contain a term with $\theta(t - t')$ where $t' > t$. As a direct consequence, all correlation functions which exclusively contain response fields vanish, such that a chain of response field operators necessarily has to end in a density operator.

The generalized density operators obtained from contractions with response field operators act on the free generating functional to generate density correlation functions such as in (3.46). As an illustration, consider a single response field operator and m density operators acting on the free generating functional. Since contractions have their origin in a functional derivative, they follow a Leibniz rule, such that

$$\begin{aligned} \bar{G}_{B\rho\dots\rho}(-R, 1, \dots, m) &= \overline{\hat{B}(-R)} \hat{\rho}(1) \hat{\rho}(2) \dots \hat{\rho}(m) Z_0[\underline{\mathbf{J}}, \underline{\mathbf{K}}] \Big|_{\underline{\mathbf{0}}} \\ &= \sum_{s=1}^m \overline{\hat{B}(-R) \hat{\rho}(1) \dots \hat{\rho}(s) \dots \hat{\rho}(m)} Z_0[\underline{\mathbf{J}}, \underline{\mathbf{K}}] \Big|_{\underline{\mathbf{0}}} \\ &= \sum_{s=1}^m b(s, -R) \hat{\rho}(1) \dots \hat{\rho}(s, -R) \dots \hat{\rho}(m) Z_0[\underline{\mathbf{J}}, \underline{\mathbf{K}}] \Big|_{\underline{\mathbf{0}}} \\ &=: \sum_{s=1}^m b(s, -R) \sum_{\{a_1, \dots, a_m\}} \mathcal{Z}_0(\underline{\mathbf{L}}_q, \underline{\mathbf{L}}_p). \end{aligned} \quad (3.59)$$

In the last step, we identified the free m -point correlation function $\mathcal{Z}_0(\underline{\mathbf{L}}_q, \underline{\mathbf{L}}_p)$, formally equivalent to (3.46) but contains different shift tensors. From the definition of the generalized density operators (3.56), it follows that the s -components of the shift tensors obtain an additional contribution

$$\mathbf{L}_{q_{a_s}} = -\mathbf{k}_s + \mathbf{k}_R, \quad \mathbf{L}_{p_{a_s}} = -g_{qp}(t_s, 0) \mathbf{k}_s + g_{qp}(t_R, 0) \mathbf{k}_R. \quad (3.60)$$

Informally speaking, we can think of this as the response field handing over its arguments to the density operator with which it contracts. In the most general case where n response field operators and m density operators are applied to the free generating functional, giving us a mixed correlation function of order (n, m)

$$\begin{aligned} & \bar{G}_{B\dots B\rho\dots\rho}(-1', \dots, -n', 1, \dots, m) \\ &= \sum_{\{c_i\} \in \mathcal{C}_n} b(c_1, -1') \dots b(c_n, -n') \sum_{\{a_1, \dots, a_m\}} \mathcal{Z}_0(\underline{\mathbf{L}}_q, \underline{\mathbf{L}}_p), \end{aligned} \quad (3.61)$$

where \mathcal{C}_n is the set of all contractions of the n response fields operators that are allowed by causality. A free mixed correlation function of order (n, m) , i.e. a free correlation function between n response and m density fields, thus generates a sum of terms, each containing a generalized free m -point density function. According to (3.46) each such free correlation function can be assigned a set of shift tensors $(\underline{\mathbf{L}}_q, \underline{\mathbf{L}}_p)$. If no response field operators have been applied, the m components of the shift tensors are directly given by the wave vectors (scaled with particle propagators for the momentum shift vectors) of the density operators that generated the correlation function. Applying response fields, in addition, does not add new components to the shift tensors but instead modifies their existing components by adding arguments of the response fields to them. The modified arguments of the resulting m -point density function take the general form

$$\underline{\mathbf{L}}_q = \sum_{r=1}^m \mathbf{L}_{q_{a_r}} \otimes \mathbf{e}_{a_r} \quad \text{with} \quad \mathbf{L}_{q_{a_r}} = - \sum_{\{i\}} \mathbf{k}_{r_i}, \quad (3.62)$$

$$\underline{\mathbf{L}}_p = \sum_{r=1}^m \mathbf{L}_{p_{a_r}} \otimes \mathbf{e}_{a_r} \quad \text{with} \quad \mathbf{L}_{p_{a_r}} = - \sum_{\{i\}} g_{qp}(t_{r_i}, 0) \mathbf{k}_{r_i}. \quad (3.63)$$

This is a direct generalization of (3.44) and (3.45), in the sense that each component of the shift tensor can now be a linear combination of the arguments of density and response field operators. Note that components of momentum shift vectors are related to those of spatial shift vectors straightforwardly, such that it is sufficient to indicate the spatial shift vectors of a free correlation function.

3.5 CANONICAL PERTURBATION THEORY

We have introduced some basic building blocks at the foundation of KFT, from the canonical generating functional to density and response field operators. Different formulations of KFT can be and have been constructed [4, 22, 44] building upon these foundations. In this section, we introduce the simplest and, in some ways, the most naive formulation, canonical perturbation theory.

We have seen in Section 3.3.2 that we can formally apply the full exponential of the interaction operator to recover fully interacting particle trajectories in the canonical generating functional. However, since these are self-consistent expressions, this approach does not lead us very far in actual calculations. Instead, we evaluate particle interactions by expanding the exponential of the interaction operator in (3.31) in a Taylor series. To this end, consider a system of point particles with particle-particle interactions dictated by the potential $v(|\mathbf{q} - \mathbf{q}'|)$. Additionally, we assume the absence of an external potential, such that the particle interaction operator is given by

$$i\hat{S}_I = -i \int d1' \hat{B}(-1') v(1') \hat{\rho}(1'). \quad (3.64)$$

Intuitively the ingredients of the interaction operator play the following roles: Since $\hat{\rho}(1')$, once it has acted onto the generating functional, represents the entire particle density field, the product $\nu(1')\hat{\rho}(1')$ generates the potential landscape that particles are moving through. The response field operator $\hat{B}(-1')$, by contracting with a density operator, decides which representative particle will be perturbed by the presence of the interaction potential.

Perturbation theory in KFT is an expansion in terms of the interaction potential, which should ideally only lead to minor corrections to the free result. As we will discuss in more detail in our application to cosmology, carefully choosing the splitting of the equations of motion (3.6) can help minimize the impact of the particle interaction operator. For now, let us go ahead with the expansion of the exponential in the generating functional by considering the full m -point density correlation function

$$\begin{aligned} G_{\rho\dots\rho}(1, \dots, m) &= \hat{\rho}(1) \dots \hat{\rho}(m) \exp(i\hat{S}_I) Z_0[\underline{\mathbf{J}}, \underline{\mathbf{K}}] \Big|_{\mathbf{0}} \\ &= \sum_{n=0}^{\infty} \frac{(i\hat{S}_I)^n}{n!} \hat{\rho}(1) \dots \hat{\rho}(m) Z_0[\underline{\mathbf{J}}, \underline{\mathbf{K}}] \Big|_{\mathbf{0}} \\ &=: \sum_{n=0}^{\infty} \delta^{(n)} G_{\rho\dots\rho}(1, \dots, m). \end{aligned} \quad (3.65)$$

In the last line we introduced the notation $\delta^{(n)} G_{\rho\rho}(1, \dots, m)$ for the n -th order correction to a free m -point function. Note that since all operators act on the free generating functional and since functional derivatives commute, operators can be commuted to our liking. If we wish to express the effect of response fields in terms of contractions with other operators, we implicitly impose a natural ordering into our expressions. Response fields can contract with all operators that follow them (on their right) and therefore have to be collected on the left, similar to the normal ordering we encounter in the operator formalism in quantum field theory. As an example, consider the n -th order term in the above expansion

$$\begin{aligned} &\frac{(i\hat{S}_I)^n}{n!} \hat{\rho}(1) \dots \hat{\rho}(m) Z_0[\underline{\mathbf{J}}, \underline{\mathbf{K}}] \Big|_{\mathbf{0}} \\ &= \frac{(-i)^n}{n!} \int d1' \hat{B}(-1') \nu(1') \hat{\rho}(1') \dots \int dn' \hat{B}(-n') \nu(n') \hat{\rho}(n') \hat{\rho}(1) \dots \hat{\rho}(m) Z_0[\underline{\mathbf{J}}, \underline{\mathbf{K}}] \Big|_{\mathbf{0}} \\ &= \frac{1}{n!} \int d1' (-i\nu(1')) \dots \int dn' (-i\nu(n')) \bar{G}_{B\dots B\rho\dots\rho}(-1', \dots, -n', 1', \dots, n', 1, \dots, m) \\ &= \frac{1}{n!} \int d1' \dots \int dn' \sum_{c_n} f(c_1, -1') \dots f(c_n, -n') \sum_{\substack{\{e_1, \dots, e_m\} \\ \{i_1, \dots, i_n\}}} \mathcal{Z}_0(\underline{\mathbf{L}}_{q'}, \underline{\mathbf{L}}_p) \end{aligned} \quad (3.66)$$

In the third line, we identified the free mixed correlation function of order $(n, n+m)$, which we evaluated according to (3.61) to arrive at the final expression. Since their arguments are integrated out, we refer to the n density modes, which act as sources in the interaction operators as *internal density modes*. In contrast, density operators representing the modes of the m -point function are called *external modes*. Whereas internal densities are labelled with the particle indices i_1, \dots, i_n , external density modes carry the indices e_1, \dots, e_m . We additionally collected response field prefactors and interaction potentials in the force prefactors

$$f(c_s, -s') := -i\nu(s') b(c_s, -s') = -\nu(s') (\mathbf{k}_{c_s} \cdot \mathbf{k}_s) g_{qp}(t_{c_s}, t'_s) \theta(t_{c_s} - t'_s). \quad (3.67)$$

As the name suggests, these prefactors contain information on the total deviation of a particle trajectory from inertial motion due to the force caused by a density field. To evaluate perturbative corrections to free correlation functions in KFT, we thus need to evaluate free correlation functions of higher order. In the application to cosmology, most of the complications of the system are contained in these correlation functions, and we will go to great lengths to evaluate them for cosmological initial conditions. But first, to see how these general considerations apply to a concrete situation, let us quickly look at a basic example calculation.

Example 3.5.1 *Consider the simple case of a first-order correction to a two-point density function. We apply two density operators to the free generating functional and follow it up with a particle interaction operator*

$$i\hat{S}_I \hat{\rho}(1) \hat{\rho}(2) Z_0[\underline{\mathbf{J}}, \underline{\mathbf{K}}] \Big|_{\mathbf{0}} = -i \int d1' v(1') \hat{B}(-1') \hat{\rho}(1') \hat{\rho}(1) \hat{\rho}(2) Z_0[\underline{\mathbf{J}}, \underline{\mathbf{K}}] \Big|_{\mathbf{0}}. \quad (3.68)$$

The response field operator has two choices for density operators to contract to since causality forbids it to contract with $\hat{\rho}(1')$. Each of the two contractions gives rise to a free 3-point density function such that

$$\begin{aligned} & i\hat{S}_I \hat{\rho}(1) \hat{\rho}(2) Z_0[\underline{\mathbf{J}}, \underline{\mathbf{K}}] \Big|_{\mathbf{0}} \\ &= \int d1' \hat{\rho}(1') \left\{ f(1, -1') \hat{\rho}(1, -1') \hat{\rho}(2) + f(1, -1') \hat{\rho}(1) \hat{\rho}(2, -1') \right\} Z_0[\underline{\mathbf{J}}, \underline{\mathbf{K}}] \Big|_{\mathbf{0}} \\ &= \sum_{\{e_1, e_2, i_1\}} \int d1' \left\{ f(1, -1') \mathcal{Z}_0(\underline{\mathbf{L}}_q^{(A)}, \underline{\mathbf{L}}_p^{(A)}) + f(2, -1') \mathcal{Z}_0(\underline{\mathbf{L}}_q^{(B)}, \underline{\mathbf{L}}_p^{(B)}) \right\}. \end{aligned} \quad (3.69)$$

The shift tensors that are generated for the two terms each have three components, given by

$$\begin{cases} \mathbf{L}_{qe_1}^{(A)} = -\mathbf{k}_1 + \mathbf{k}'_1 & \mathbf{L}_{pe_1}^{(A)} = -g_{qp}(t_1, 0) \mathbf{k}_1 + g_{qp}(t'_1, 0) \mathbf{k}'_1 \\ \mathbf{L}_{qe_2}^{(A)} = -\mathbf{k}_2 & \mathbf{L}_{pe_2}^{(A)} = -g_{qp}(t_2, 0) \mathbf{k}_2 \\ \mathbf{L}_{qi_1}^{(A)} = -\mathbf{k}'_1 & \mathbf{L}_{pi_1}^{(A)} = -g_{qp}(t'_1, 0) \mathbf{k}'_1 \end{cases} \quad (3.70)$$

$$\begin{cases} \mathbf{L}_{qe_1}^{(B)} = -\mathbf{k}_1 & \mathbf{L}_{pe_1}^{(B)} = -g_{qp}(t_1, 0) \mathbf{k}_1 \\ \mathbf{L}_{qe_2}^{(B)} = -\mathbf{k}_2 + \mathbf{k}'_1 & \mathbf{L}_{pe_2}^{(B)} = -g_{qp}(t_2, 0) \mathbf{k}_2 + g_{qp}(t'_1, 0) \mathbf{k}'_1 \\ \mathbf{L}_{qi_1}^{(B)} = -\mathbf{k}'_1 & \mathbf{L}_{pi_1}^{(B)} = -g_{qp}(t'_1, 0) \mathbf{k}'_1. \end{cases} \quad (3.71)$$

To proceed further in the evaluation, we need more specific knowledge about the initial conditions and the equations of motion of the system at hand, which we postpone to the next chapter. Note that the entire formalism we developed up until this point is completely general and can be applied to arbitrary systems of classical particles. In many cases, systems exhibit additional symmetries that enter the formalism and lead to simplifications. In statistically homogeneous systems like cosmic structures, the two-point correlation function in Fourier space forces the respective wave vectors to be antiparallel since $\langle \rho(\mathbf{k}) \rho(\mathbf{k}') \rangle \propto \delta_D(\mathbf{k} + \mathbf{k}')$. If we additionally consider an equal-time correlation function, contractions of a response field operator with either density operator give the same result. Thus, for a homogeneous system example, 3.5.1 results in one single term with an overall multiplicity factor of 2.

3.6 A TOY MODEL FOR CANONICAL PERTURBATION THEORY

Although KFT merely describes systems following classical dynamics, getting a good intuition for the physical meaning of the perturbative treatment of the interaction operator is quite challenging. Since toy models can hugely benefit our understanding of KFT, it is worth having a deeper look at a specific example.

3.6.1 *Setting*

To illuminate some of the main concepts at the core of canonical perturbation theory, we want to use the simple situation of two interacting particles a and b with equal masses $m_a = m_b = 1$ in a static space-time

$$\mathcal{H} = \frac{\mathbf{p}_a}{2} + \frac{\mathbf{p}_b}{2} + v(|\mathbf{q}_a - \mathbf{q}_b|). \quad (3.72)$$

For now, we keep the interaction potential $v(|\mathbf{q}_a - \mathbf{q}_b|)$ general but assume that it has no explicit time dependence. The Green's function resulting from the free part of Hamilton's equations is given by

$$\mathbf{G}(t_1, t'_1) = \begin{pmatrix} \mathcal{I}_3 & g_{1,1'} \mathcal{I}_3 \\ 0_3 & \dot{g}_{1,1'} \mathcal{I}_3 \end{pmatrix} \theta(t_1 - t'_1) \quad \text{with} \quad g_{1,1'} = t_1 - t'_1. \quad (3.73)$$

To fully concentrate on the effect of particle interactions, we use explicit initial conditions by choosing the initial probability density

$$\mathcal{P}(\underline{\mathbf{x}}^{(i)}) = \delta_D(\mathbf{q}_a^{(i)} - \mathbf{q}_{a,0}) \delta_D(\mathbf{q}_b^{(i)} - \mathbf{q}_{b,0}) \delta_D(\mathbf{p}_a^{(i)} - \mathbf{p}_{a,0}) \delta_D(\mathbf{p}_b^{(i)} - \mathbf{p}_{b,0}), \quad (3.74)$$

where we assume to be in the centre of mass frame of the system such that $\mathbf{q}_{a,0} = -\mathbf{q}_{b,0}$ and $\mathbf{p}_{a,0} = -\mathbf{p}_{b,0}$. The corresponding full generating functional reads

$$Z[\underline{\mathbf{J}}, \underline{\mathbf{K}}] = e^{i\hat{S}_I} \int d\underline{\Gamma}_i e^{i\underline{\mathbf{J}} \cdot \underline{\mathbf{x}}[\underline{\mathbf{K}}]} = e^{i\hat{S}_I} \exp\left(i\underline{\mathbf{J}}_a \cdot \underline{\tilde{\mathbf{x}}}_a[\underline{\mathbf{K}}_a]\right) \exp\left(i\underline{\mathbf{J}}_b \cdot \underline{\tilde{\mathbf{x}}}_b[\underline{\mathbf{K}}_b]\right). \quad (3.75)$$

Since we are interested in the particle density rather than the full phase-space density, the only relevant information lies in the spatial part $\tilde{\mathbf{q}}$ of the phase-space trajectories $\tilde{\mathbf{x}}$. Additionally, we know that response fields only contain functional derivatives w. r. t. $\underline{\mathbf{K}}_p$, such that we set $\underline{\mathbf{K}}_q = \underline{\mathbf{0}}$ right away. The particle trajectory of particle a therefore reads

$$\begin{aligned} \tilde{\mathbf{q}}_a[\underline{\mathbf{K}}_{p_a}, t_1] &= \mathbf{q}_{a,0} + g_{1,0} \mathbf{p}_{a,0} - \int dt'_1 g_{1,1'} \mathbf{K}_{p_a}(t'_1) \\ &= \tilde{\mathbf{q}}_a(t_1) - \int dt'_1 g_{1,1'} \mathbf{K}_{p_a}(t'_1), \end{aligned} \quad (3.76)$$

where we introduced the free spatial trajectory $\tilde{\mathbf{q}}_a(t_1)$ of particle a in the last step. The contribution to the overall free density from particle a can be calculated, as usual, by applying the one-particle density operator to the free generating functional yielding

$$\langle \tilde{\rho}_a(\mathbf{k}_1, t_1) \rangle = \hat{\rho}_a(1) Z_0[\underline{\mathbf{J}}, \underline{\mathbf{K}}] \Big|_{\underline{\mathbf{0}}} = e^{-i\mathbf{k}_1 \cdot \tilde{\mathbf{q}}_a(t_1)}. \quad (3.77)$$

Note that this is technically the ensemble average of the density at the position of particle a , but since we use explicit initial conditions, we simply reproduce the Fourier-space density of a freely evolving particle. For the corresponding density in configuration space, we obtain a delta-peak at the linearly evolving position $\tilde{\mathbf{q}}_a(t_1) = \mathbf{q}_{a,0} + g_{1,0} \mathbf{p}_{a,0}$, and are thus simply describing a point particle moving along a straight line. This exercise aims to derive the full density contribution of particle a from canonical perturbation theory in KFT.

3.6.2 Interactions and diagrams

Doing perturbation theory corresponds to expanding the exponential interaction operator in a Taylor series which is applied order by order. Consider the first-order perturbative correction to the free density of particle a

$$\begin{aligned}
i\hat{S}_I\hat{\rho}_a(1)Z_0[\underline{\mathbf{J}},\underline{\mathbf{K}}]\Big|_{\underline{\mathbf{0}}} &= -i\int d1'\nu(1')\hat{\rho}(1')\overline{\hat{B}(-1')}\hat{\rho}_a(1)Z_0[\underline{\mathbf{J}},\underline{\mathbf{K}}]\Big|_{\underline{\mathbf{0}}} \\
&= -i\int d1'\nu(1')b(1,-1')\hat{\rho}_b(1')\hat{\rho}_a(1,-1')Z_0[\underline{\mathbf{J}},\underline{\mathbf{K}}]\Big|_{\underline{\mathbf{0}}} \\
&= \int_0^{t_1} dt'_1 \int_{\mathbf{k}'_1} g_{1,1'} [(-i\mathbf{k}_1) \cdot (-i\mathbf{k}'_1)] \nu(k'_1) e^{i\mathbf{k}'_1 \cdot \bar{\mathbf{q}}_{ab}(t'_1)} e^{-i\mathbf{k}_1 \cdot \bar{\mathbf{q}}_a(t_1)} \\
&= e^{-i\mathbf{k}_1 \cdot \bar{\mathbf{q}}_a(t_1)} (-i\mathbf{k}_1) \cdot \int_0^{t_1} dt'_1 g_{1,1'} (-\nabla \bar{v}_{ab}(t'_1)). \tag{3.78}
\end{aligned}$$

From the first to the second line, we have evaluated the contraction of the response field with the density and used the fact that there is no self-interaction such that only particle b can be the source of a perturbation to a . In the third line $\bar{\mathbf{q}}_{ab}(t'_1) = \bar{\mathbf{q}}_a(t'_1) - \bar{\mathbf{q}}_b(t'_1)$ is obtained from the \mathbf{k}'_1 -dependent phases of the two density operators. To arrive at the last line, we have performed the internal Fourier integral, yielding the gradient of the interaction potential evaluated at the linearly evolving distance between the two particles

$$-\nabla \bar{v}_{ab}(t'_1) := -\nabla \nu(|\bar{\mathbf{q}}_a(t'_1) - \bar{\mathbf{q}}_b(t'_1)|). \tag{3.79}$$

This expression describes the force acting between particles a and b moving along straight trajectories, i. e. the force between the particles in the Born approximation. We will now introduce a graphical notation to encode contractions of response fields diagrammatically. To this end, we define

$$\circlearrowleft_b \longrightarrow a := -i \int d1'\nu(1')\hat{\rho}(1')\overline{\hat{B}(-1')}\hat{\rho}_a(1)Z_0[\underline{\mathbf{J}},\underline{\mathbf{K}}]\Big|_{\underline{\mathbf{0}}}. \tag{3.80}$$

In this notation, response fields are denoted by empty \circ and (freely evolving) density fields by filled circles \bullet carrying a particle index. Contraction of a response field to another field is indicated by an interaction line \longrightarrow pointing from the response field to its target. Each interaction operator's density and response fields are joined by an undirected edge representing the two-particle interaction potential. In terms of these elements, the distinct contractions of response fields at second-order perturbation theory are given by

$$\frac{1}{2}(i\hat{S}_I)^2\hat{\rho}_a(1)Z_0[\underline{\mathbf{J}},\underline{\mathbf{K}}]\Big|_{\underline{\mathbf{0}}} = \frac{1}{2} \left(2 \begin{array}{c} \circlearrowleft_b \longrightarrow \circlearrowleft_b \longrightarrow a \\ \bullet_b \bullet_b \end{array} + 2 \begin{array}{c} \circlearrowleft_b \longrightarrow a \\ \bullet_a \bullet_b \end{array} + \begin{array}{c} \circlearrowleft_b \longrightarrow a \\ \bullet_b \bullet_b \end{array} \right),$$

(a)
(b)
(c)

where multiplicities follow from permutations of internal arguments among interaction operators that play different roles in the diagram. In the first and second diagrams, both interaction operators play different roles since one contracts with the external density mode and the other with an internal mode. As a result, the two permutations of their

internal arguments contribute to the multiplicity. The same is not the case for the last diagrams since both interaction operators contract to the external density mode and therefore play the same role. In general, the multiplicity of one of these diagrams can be determined by recognising that each interaction operator has a set of internal parameters (\mathbf{k}'_s, t'_s) , which are integrated out. Permuting these arguments among all internal density-response pairs, which play a distinct role in the diagram, gives the multiplicity.

How can we interpret the three diagrams above? The most intuitive diagram seems to be (b) where the trajectory of particle a is perturbed by particle b which moves along a trajectory that was already perturbed by a moving along a free trajectory. Compare this to the physical situation where both particles are moving in each other's total potential, which can be understood as a dynamical process where each particle is perturbed at each instant by the presence of the other particle, which is moving along the fully interacting trajectory. Perturbation theory in KFT corresponds to precisely this idea, except that perturbative corrections of particles to each other's trajectories are truncated at some order. In diagrams (a) and (c), particle a is twice perturbed by a freely evolving particle b . Physically they, therefore, seem to describe the same process, and at this point, it is not yet clear what the difference between both diagrams is. For now, let us evaluate the terms individually, starting with (a):

$$\begin{aligned} (a) &= \frac{1}{2} 2(-i)^2 \int d2' \int d1' v(2') v(1') \overbrace{\hat{\rho}(2') \hat{B}(-2') \hat{\rho}(1') \hat{B}(-1') \hat{\rho}(1)} Z_0[\mathbf{J}, \mathbf{K}] \Big|_0 \\ &= (-i)^2 \int d2' \int d1' v(2') v(1') b(1, -1') b(-1', -2') e^{i\mathbf{k}'_1 \cdot \bar{\mathbf{q}}_{ab}(t'_1)} e^{i\mathbf{k}'_2 \cdot \bar{\mathbf{q}}_{ab}(t'_2)} e^{-i\mathbf{k}_1 \cdot \bar{\mathbf{q}}_a(t_1)} \\ &= e^{-i\mathbf{k}_1 \cdot \bar{\mathbf{q}}_a(t_1)} (-i\mathbf{k}_1) \cdot \int_0^{t_1} dt'_1 \int_0^{t'_1} dt'_2 g_{1,1'} g_{1',2'} (-\nabla \otimes \nabla) \bar{v}_{ab}(t'_1) \cdot (-\nabla \bar{v}_{ab}(t'_2)). \end{aligned}$$

The contribution from the Hessian of the interaction potential $H_{ab}(t'_1) = (\nabla \otimes \nabla) \bar{v}_{ab}(t'_1)$ can be traced back to the intermediate response field operator $\hat{B}(-1')$ which is targeted by $\hat{B}(-2')$. In general, it can be easily checked that each interaction line connecting to an internal response/density contributes an additional spatial derivative to the corresponding two-particle potential.

Diagram (b) is evaluated along the same lines and yields the same result as (a). This equivalence is not valid in general but rather a consequence of the system only consisting of two particles, creating symmetry between perturbing a trajectory twice via response-field contractions and perturbing a particle with a potential sourced by a perturbed trajectory. In the following, we will therefore evaluate all subdiagrams with configurations of the form (a) and (b) by a representative of this group with an increased multiplicity, thus considerably reducing the possible topologies of diagrams that need to be evaluated.

Last but not least, evaluating diagram (c) yields

$$\begin{aligned} (c) &= (-i)^2 \int d2' \int d1' v(2') v(1') \overbrace{\hat{\rho}(2') \hat{B}(-2') \hat{\rho}(1') \hat{B}(-1') \hat{\rho}(1)} Z_0[\mathbf{J}, \mathbf{K}] \Big|_0 \\ &= (-i)^2 \int d2' \int d1' v(2') v(1') b(1, -1') b(1, -2') e^{i\mathbf{k}'_1 \cdot \bar{\mathbf{q}}_{ab}(t'_1)} e^{i\mathbf{k}'_2 \cdot \bar{\mathbf{q}}_{ab}(t'_2)} e^{-i\mathbf{k}_1 \cdot \bar{\mathbf{q}}_a(t_1)} \\ &= e^{-i\mathbf{k}_1 \cdot \bar{\mathbf{q}}_a(t_1)} \left[(-i\mathbf{k}_1) \cdot \int_0^{t_1} dt'_1 g_{1,1'} (-\nabla \bar{v}_{ab}(t'_1)) \right] \\ &\quad \times \left[(-i\mathbf{k}_1) \cdot \int_0^{t_1} dt'_2 g_{1,2'} (-\nabla \bar{v}_{ab}(t'_2)) \right], \quad (3.81) \end{aligned}$$

which can be written as the product of two first-order corrections since the two time integrals are decoupled from one another.

3.6.3 Topologies of diagrams

The total wealth of topologies of diagrams in our toy example is only obtained at third-order perturbation theory. For simplicity, we will drop the particle indices in the coming diagrams and obtain the following diagrams

$$\begin{aligned}
& \frac{1}{3!} (i\hat{S}_I)^3 \hat{\rho}_a(1) Z_0[\underline{\mathbf{J}}, \underline{\mathbf{K}}] \Big|_0 \\
&= \frac{1}{3!} \left\{ 3! \left(\begin{array}{c} \circ \rightarrow \circ \rightarrow \circ \rightarrow \bullet \\ \bullet \quad \bullet \quad \bullet \end{array} + \begin{array}{c} \circ \rightarrow \circ \rightarrow \circ \rightarrow \bullet \\ \bullet \quad \bullet \quad \bullet \end{array} + \begin{array}{c} \circ \rightarrow \circ \rightarrow \circ \rightarrow \bullet \\ \bullet \quad \bullet \quad \bullet \end{array} \right. \\
&+ \begin{array}{c} \circ \rightarrow \circ \rightarrow \circ \rightarrow \bullet \\ \bullet \quad \bullet \quad \bullet \end{array} \left. \right) + 3! \left(\begin{array}{c} \circ \rightarrow \circ \rightarrow \bullet \\ \bullet \quad \bullet \end{array} + \begin{array}{c} \circ \rightarrow \circ \rightarrow \bullet \\ \bullet \quad \bullet \end{array} \right) \\
&+ 3! \left(\begin{array}{c} \circ \rightarrow \circ \rightarrow \bullet \\ \bullet \quad \bullet \end{array} + \begin{array}{c} \circ \rightarrow \circ \rightarrow \bullet \\ \bullet \quad \bullet \end{array} + \begin{array}{c} \circ \rightarrow \circ \rightarrow \bullet \\ \bullet \quad \bullet \end{array} \right) \\
&+ \left. \begin{array}{c} \circ \rightarrow \bullet \\ \bullet \end{array} \right\}. \tag{3.82}
\end{aligned}$$

We want to distinguish between three categories of diagrams here.

1. The first category is the chain diagrams in the first bracket, all of which are all identical in the two-particle case. At n -th order perturbation theory, there will be 2^{n-1} (the number of times we have to choose between connecting an interaction line to an internal density or response field) diagrams with a chain-like topology. We will therefore represent chains of length n by a single diagram

$$\begin{array}{c} 1 \quad 2 \quad \dots \quad n \\ \circ \rightarrow \circ \rightarrow \dots \rightarrow \circ \rightarrow \bullet \\ \bullet \quad \bullet \quad \dots \quad \bullet \end{array} \tag{3.83}$$

with multiplicity $n! 2^{n-1}$.

2. The second category contains all 'branching' topologies, i. e. diagrams where multiple chains connect to the external density mode. This is the case for both diagrams in the second bracket as well as the very last diagram. We will consider these in more detail once we have understood the role of chain diagrams.
3. Diagrams where multiple chains connect to an internal density or response field constitute the third category. Since they contain higher-order derivatives of the interaction potential, these diagrams should be less important in systems where we can assume a relatively smooth potential landscape. Indeed, these diagrams are identically zero for a harmonic two-particle interaction potential.

3.6.4 Special case: harmonic interaction potential

To continue the analysis, we now further narrow down the discussion to a harmonic two-particle interaction potential $v(q) = \frac{1}{2}\omega^2 q^2$ for which gradient and Hessian are given by

$$\nabla \bar{v}_{ab}(t'_1) = \omega^2 \bar{\mathbf{q}}_{ab}(t'_1), \quad H_{ab}(t'_1) = \omega^2 \mathcal{I}_3. \quad (3.84)$$

Since higher-order derivatives vanish, topologies of the third category do not occur in the diagrams, so we are left with chain and branching diagrams. Consider first the contribution from a single chain of length $n > 0$

$$\begin{aligned} & \frac{1}{n!} \begin{array}{c} 1 \quad 2 \quad \dots \quad n \\ \circ \rightarrow \circ \rightarrow \dots \rightarrow \circ \rightarrow \bullet \\ \bullet \quad \bullet \quad \bullet \quad \bullet \end{array} \\ &= \frac{1}{n!} n! 2^{n-1} e^{-i\mathbf{k}_1 \cdot \bar{\mathbf{q}}_a(t_1)} (-i\mathbf{k}_1) \cdot \int_0^{t_1} dt'_1 \dots \int_0^{t'_{n-1}} dt'_n g_{1,1'}(-H_{ab}(t'_1)) \dots \\ & \quad \dots g_{n'-2,n'-1}(-H_{ab}(t'_{n-1})) g_{n'-1,n'}(-\nabla \bar{v}_{ab}(t'_n)) \\ &= \frac{1}{2} (-2)^n e^{-i\mathbf{k}_1 \cdot \bar{\mathbf{q}}_a(t_1)} (-i\mathbf{k}_1) \cdot \int_0^{t_1} dt'_1 g_{1,1'} \dots \int_0^{t'_{n-1}} dt'_n g_{n'-1,n'} \bar{\mathbf{q}}_{ab}(t'_n) \omega^{2n}. \end{aligned} \quad (3.85)$$

Splitting the free trajectories in $\bar{\mathbf{q}}_{ab}(t'_n)$ into the initial position and momentum contributions and using the symmetry between initial conditions in the centre of mass frame, we get $\bar{\mathbf{q}}_{ab}(t'_n) = 2\mathbf{q}_{a,0} + 2g_{n',0}\mathbf{p}_{a,0}$. Reinsertion into the above equation, we obtain the sum of two contributions

$$\begin{aligned} & \frac{1}{n!} \begin{array}{c} 1 \quad 2 \quad \dots \quad n \\ \circ \rightarrow \circ \rightarrow \dots \rightarrow \circ \rightarrow \bullet \\ \bullet \quad \bullet \quad \bullet \quad \bullet \end{array} = (-1)^n (\sqrt{2}\omega)^{2n} e^{-i\mathbf{k}_1 \cdot \bar{\mathbf{q}}_a(t_1)} (-i\mathbf{k}_1) \\ & \quad \cdot \left[\mathcal{C}_q^{(n)}(t_1) \mathbf{q}_{a,0} + \mathcal{C}_p^{(n)}(t_1) \mathbf{p}_{a,0} \right], \end{aligned} \quad (3.86)$$

where the time integrals are contained in the factors $\mathcal{C}_q^{(n)}(t_1)$ and $\mathcal{C}_p^{(n)}(t_1)$, respectively given by

$$\mathcal{C}_q^{(n)}(t_1) = \int_0^{t_1} dt'_1 g_{1,1'} \dots \int_0^{t'_{n-1}} dt'_n g_{n'-1,n'} = \frac{t_1^{2n}}{2n!} \quad (3.87)$$

$$\mathcal{C}_p^{(n)}(t_1) = \int_0^{t_1} dt'_1 g_{1,1'} \dots \int_0^{t'_{n-1}} dt'_n g_{n'-1,n'} g_{n',0} = \frac{t_1^{2n+1}}{(2n+1)!}. \quad (3.88)$$

The last equalities follow by specifying $g_{1,1'} = t_1 - t'_1$ and solving the nested time integrals analytically. From this, we can already guess that summing up chains of all lengths will result in the sine and cosine contributions we expect for a harmonic oscillator. In this simple toy example, the contributions from chains of interaction lines are exactly reproducing the Taylor series of the sine and cosine functions. Doing the calculation, we obtain the full contribution to the one-particle density from chain diagrams

$$\left\langle \rho_a(\mathbf{k}_1, t_1) \right\rangle_{\text{chains}} = e^{-i\mathbf{k}_1 \cdot \bar{\mathbf{q}}_a(t_1)} \left[1 - i\mathbf{k}_1 \cdot \left(\tilde{\mathbf{q}}_a(t_1) - \bar{\mathbf{q}}_a(t_1) \right) \right], \quad (3.89)$$

where the full trajectory is given by

$$\tilde{\mathbf{q}}_a(t_1) = \mathbf{q}_{a,0} \cos \sqrt{2}\omega t_1 + \frac{\mathbf{p}_{a,0}}{\sqrt{2}\omega} \sin \sqrt{2}\omega t_1. \quad (3.90)$$

Thus summing up all chain diagrams recovers the full particle trajectories. However, we do not recover the full particle density but merely the first-order Taylor expansion of the full Fourier factor. At this point, the branching diagrams come into play. Recall from the diagram (c) in second-order perturbation theory that two interaction lines connecting to the external particle density result in the product of two time integrals. The same behaviour continues for chains of increasing length connecting to the external modes, such that we can again sum up contributions from all chain lengths individually and attach an increasing number of them to the external density. For example, the diagrams where two chains connect to the external density can be resummed to

$$\sum_{n_1, n_2=1}^{\infty} \begin{array}{c} \begin{array}{c} 1 \quad 2 \quad \dots \quad n_1 \\ \circ \rightarrow \circ \rightarrow \dots \rightarrow \circ \\ \bullet \quad \bullet \quad \dots \quad \bullet \end{array} \\ \begin{array}{c} \circ \rightarrow \circ \rightarrow \dots \rightarrow \circ \\ \bullet \quad \bullet \quad \dots \quad \bullet \end{array} \\ \begin{array}{c} 1 \quad 2 \quad \dots \quad n_2 \end{array} \end{array} \rightarrow \bullet = \left[(-i\mathbf{k}_1) \cdot (\tilde{\mathbf{q}}_a(t_1) - \bar{\mathbf{q}}_a(t_1)) \right]^2. \quad (3.91)$$

Summing over all numbers of resummed branches recovers the full Taylor series of the exponential, such that we end up with the final result

$$\langle \rho_a(\mathbf{k}_1, t_1) \rangle = e^{-i\mathbf{k}_1 \cdot \bar{\mathbf{q}}_a(t_1)} \sum_{n=0}^{\infty} \frac{1}{n!} \left[-i\mathbf{k}_1 \cdot (\tilde{\mathbf{q}}_a(t_1) - \bar{\mathbf{q}}_a(t_1)) \right]^n = e^{-i\mathbf{k}_1 \cdot \tilde{\mathbf{q}}_a(t_1)}. \quad (3.92)$$

The factor $\frac{1}{n!}$ is obtained by correcting for the fact that we overcount the multiplicity of each diagram by the number of permutations of chains. By a careful resummation of different groups of diagrams, we have thus obtained the final result for the density due to particle a , which in configuration space reads

$$\langle \rho_a(\mathbf{q}_1, t_1) \rangle = \delta_D \left(\mathbf{q}_1 - \mathbf{q}_{a,0} \cos \sqrt{2}\omega t_1 - \frac{\mathbf{P}_{a,0}}{\sqrt{2}\omega} \sin \sqrt{2}\omega t_1 \right). \quad (3.93)$$

Notwithstanding that this result could have been derived in a couple of lines by straightforwardly integrating Hamilton's equations, we can draw some important conclusions from it:

- Diagrams of different topologies in canonical perturbation theory can be interpreted in terms of the physical process they represent, as well as the kind of resummation they lead to.
- Chains of interaction lines lead to a resummation of the perturbative expansion of particle trajectories, whereas multiple chains targeting the same external density mode result in the resummation of the density itself.
- Internal modes that are targeted multiple times lead to higher-order derivatives of the interaction potential. This insight could be helpful considering the potential dominance or subdominance of certain diagram classes since we expect higher-order derivatives to play a secondary role if the potential landscape is sufficiently smooth. This situation is similar to the idea behind the derivative expansion employed in specific applications of the functional renormalization group [45].

In general, a closer understanding of certain diagrams' role in the perturbative expansion of the interaction operator in KFT is helpful since it might allow to partially resum particular classes of diagrams also in more general systems of interest. We will see that this is indeed the case for cosmic structure formation, where linear growth follows from precisely the kind of resummation we have explored here.

3.7 DISCUSSION

This chapter was dedicated to constructing KFT for general non-equilibrium classical particle systems. Starting with a generic Hamiltonian (3.1) we showed how to construct a generating functional (3.14) that allows for the calculation of statistical quantities. Specification for actual physical systems occurs by fixing two principal ingredients: the initial probability distribution $\mathcal{P}(\underline{\mathbf{x}}^{(i)})$ and the equations of motion $\underline{\mathcal{E}}[\underline{\mathbf{x}}]$. In the general case where the equations of motion are not exactly solvable, we split them into a free (linear) part and a non-linear part used to construct the interaction operator. Again, we should stress that the split $\underline{\mathcal{E}}[\underline{\mathbf{x}}] = \underline{\mathcal{E}}_0[\underline{\mathbf{x}}] + \underline{\mathcal{E}}_I[\underline{\mathbf{x}}]$ is not unique and can be chosen in such a way as to improve the convergence of the perturbative expansion of the interaction operator. This ambiguity can be illustrated by considering a single particle in an external potential

$$\mathcal{H} = \frac{\mathbf{p}^2}{2m} + \frac{m\omega^2}{2}\mathbf{q}^2 + \lambda\mathbf{q}^4, \quad (3.94)$$

where λ is a small (coupling) constant. Physically, we would interpret the \mathbf{q}^2 -term as an interaction potential (as we did in our toy model) and attribute it to the interaction operator together with the \mathbf{q}^4 -term. However, both the first and second terms lead to a linear differential operator in Hamilton's equations, allowing us to consider the simple harmonic oscillator as our system's 'free' trajectory and only include the \mathbf{q}^4 -term perturbatively. Both splitting choices are allowed and would lead to the same result if we evaluate infinitely many perturbation orders. Practically, however, including the harmonic potential into the free trajectories would be preferred since it already captures the essential nature of the motion (an ellipse in phase-space) with small perturbation due to the quartic potential. We will encounter a similar, albeit more subtle, situation in the application to cosmology.

Calculating ensemble averages of macroscopic quantities requires introducing operators for the particle density (3.4.1) and the response field (3.53) which act on the free generating functional. Whereas density operators generate freely evolving density modes with explicit initial conditions (3.46), response field operators have a less straightforward effect on Z_0 . This circumstance inspired us to interpret them as operators targeting other density modes, instead resulting in the combined correlation function (3.61).

With our understanding of density and response field operators, we can evaluate the effect of the interaction operator on free correlation functions (3.66). In 3.5.1, we calculate the concrete example of a first-order perturbation of a two-point function, which results in an integral over a free three-point function. This relation hints towards the deeper connection of KFT to the Boltzmann equation and the BBGKY hierarchy, which was discussed in detail in [46].

The canonical perturbation theory introduced in this chapter is the most straightforward but certainly not the only way to approach interactions in KFT. So far, two alternative formulations of KFT exist, leading to different perturbation theories. One such reformulation leads to the *grand-canonical ensemble* by summing over the number of particles N that contribute to the macroscopic system [4]. In a physical system with correlated initial conditions, this leads to a set of self-consistent equations for the macroscopic cumulants, which are challenging to solve. Perturbation theory corresponds to an ambiguous truncation of these self-consistent equations, which poses significant conceptual challenges. Structurally the grand-canonical formulation of KFT closely follows the original works of Das and Mazenko [20, 21], by which KFT was initially inspired. Yet, it turns out that the description of systems with initial phase-space correlations (evalu-

ated by employing a Mayer-cluster expansion) adds considerable complications to their formalism, e. g. the ambiguity of the perturbative expansion.

A different approach is taken by *resummed KFT* (rKFT) [22, 47], which reformulates the canonical generating functional in terms of macroscopic fields. This method leads to a path integral formulation of the generating functional for the macroscopic density and response fields, where the action contains infinitely many non-local vertices. This formulation allows for a diagrammatic formulation à la Feynman, and the resulting perturbation theory consists of a consistent loop expansion of the involved diagrams. Due to its structural similarities to path integrals in quantum field theory, it can additionally be used as the starting point for applications of non-perturbative methods.

Both of the above approaches have in common that they implement infinite resummations of terms that arise in canonical perturbation theory, which requires a great deal of effort. Additionally, the effects from initial correlations and particle interactions are not separable in either of these formulations⁴. Canonical perturbation theory, on the other hand, is more straightforward and offers similar rewards to grand-canonical and resummed KFT with comparably little effort. Furthermore, particle interactions and initial correlations are cleanly separated in the canonical generating functional (3.31), circumventing the ambiguity that currently plagues both of the latter reformulations. We will investigate the relationship between the canonical, grand-canonical and resummed KFT in more detail in Chapter 5, where it will turn out that a clever choice of particle trajectories allows us to mimic the results of macroscopic resummations with the simple canonical formalism.

With the preliminary work behind us, we can now apply KFT to arbitrary systems of classical particles. The specifications to the central situation of interest, cosmic structure formation, are given in the following chapter and consist of a discussion of the initial conditions, the trajectories of classical point particles in an expanding space-time, and a diagrammatic language for KFT perturbation theory.

⁴ However, it was recently shown that rKFT could be obtained from canonical KFT via a Hubbard-Stratonovich transformation. In this derivation, particle interactions and initial correlations become perfectly separable, making it a promising direction for further investigations.

KINETIC FIELD THEORY FOR COSMIC STRUCTURE FORMATION

4.1 THE CONTINUUM LIMIT

Before we get into the mathematical details of the initial phase-space density and particle trajectories in cosmology, we should discuss the continuum limit in KFT. Until this point, we were careful to formulate our expressions so that they describe systems with an arbitrary (small or large) number of particles. Indeed, although our main focus lies in describing many-body systems, considerations and calculations of single or two-particle systems in the form of toy models can yield surprising insights into the mechanics of, e. g. perturbation theory in KFT. This being said, we now turn to the proper application of KFT to cosmology, where the number of point particles in any volume of interest can be assumed to be extremely large. Indeed, even assuming the most massive dark matter candidate, PBHs, the number of particles within a volume relevant for large-scale structure formation is gigantic, allowing us to formally consider the continuum limit $N \rightarrow \infty$ in our calculations. This consideration directly affects our calculations; since particles are indistinguishable, indices in the sums over particles in correlation functions such as (3.46) can be fixed, and the sum replaced by a factor N for each index. Thus, an m -point function scales like N^m to the leading order in the particle number, which is obtained by choosing a distinct representative particle for each density mode. The sum over all particle indices in (3.46) also leads to terms where particle indices are equal and which thus scale with lower powers of N . These terms, which are subdominant in systems with large particle numbers and are formally vanishing in the continuum limit, are referred to as *shot-noise*. In the application of KFT to cosmology, we neglect all shot-noise contributions, enabling us to express the correlation function (3.46) by

$$\bar{G}_{\rho\dots\rho}(1, 2, \dots, m) = N^m \int d\underline{\Gamma}_i \exp(i\underline{\mathbf{L}}_q \cdot \underline{\mathbf{q}}^{(i)} + i\underline{\mathbf{L}}_p \cdot \underline{\mathbf{p}}^{(i)}) = N^m \mathcal{Z}_0(\underline{\mathbf{L}}_q, \underline{\mathbf{L}}_p), \quad (4.1)$$

where the indices of the m components $\{e_1, e_2, \dots, e_m\}$ of the shift tensors (3.44) and (3.45) are now fixed, distinct labels for representative particles. Due to this one-to-one correspondence we refer to both $\mathcal{Z}_0(\underline{\mathbf{L}}_q, \underline{\mathbf{L}}_p)$ and $\bar{G}_{\rho\dots\rho}(1, 2, \dots, m)$ as free correlation functions.

4.2 INITIAL CONDITIONS

In the previous chapter, we have seen that the central object to evaluate in KFT, be it to calculate free correlation functions or contributions from the perturbative expansion of the interaction operator, is the free correlation function $\mathcal{Z}_0(\underline{\mathbf{L}}_q, \underline{\mathbf{L}}_p)$. The main challenge this poses for cosmological applications lies in the initial probability distribution, which will be treated in this section. Due to the technical and lengthy nature of the calculations

ahead, some steps will be skipped; for a complete derivation and thorough discussion of the initial phase-space density, we refer the reader to chapter 3 of [4].

4.2.1 Probability density

In Section 2.4, we have seen that the initial conditions for the density and velocity fields in cosmology can both be related to the initial velocity potential by

$$\delta^{(i)}(\mathbf{q}) = -\nabla^2\psi^{(i)}(\mathbf{q}), \quad \mathbf{u}^{(i)}(\mathbf{q}) = \nabla\psi^{(i)}(\mathbf{q}), \quad (4.2)$$

and follow a GRF. These initial fields can be used to derive a probability density for the initial phase-space coordinates by Poisson sampling. The idea is the following: For fixed initial density and velocity fields, each of the N particles of our system is assigned a phase-space position with probability $d\mathbf{x}^{(i)} \mathcal{P}(\mathbf{x}^{(i)}|\delta^{(i)}, \mathbf{u}^{(i)})$, which is then weighted with the probability density for the initial fields and integrated over the realisations of $\delta^{(i)}$ and $\mathbf{u}^{(i)}$. The conditional probability for a particle to be placed in a small volume around phase-space position $\mathbf{x}^{(i)}$ is independent of other particles and depends locally on the initial fields, i. e.

$$\mathcal{P}(\mathbf{x}^{(i)}|\delta^{(i)}, \mathbf{u}^{(i)}) = \prod_{a=1}^N \mathcal{P}(\mathbf{x}_a^{(i)}|\delta^{(i)}(\mathbf{q}_a^{(i)}), \mathbf{u}^{(i)}(\mathbf{q}_a^{(i)})). \quad (4.3)$$

To allow for a more condensed notation, we define

$$\underline{\mathbf{d}} = \sum_{a=1}^N \mathbf{d}_a \otimes \mathbf{e}_a, \quad \mathbf{d}_a = \begin{pmatrix} \delta_a^{(i)} \\ \mathbf{u}_a^{(i)} \end{pmatrix} := \begin{pmatrix} \delta^{(i)}(\mathbf{q}_a^{(i)}) \\ \mathbf{u}^{(i)}(\mathbf{q}_a^{(i)}) \end{pmatrix}, \quad (4.4)$$

bundling the initial density and velocity fields evaluated at the initial particle positions in the data tensor $\underline{\mathbf{d}}$. With this notation, the initial phase-space density reads

$$\mathcal{P}(\mathbf{x}^{(i)}) = \int d\underline{\mathbf{d}} \mathcal{P}(\mathbf{x}^{(i)}|\underline{\mathbf{d}}) \mathcal{P}(\underline{\mathbf{d}}). \quad (4.5)$$

The conditional probability density for an initial phase-space position $\mathbf{x}^{(i)}$ given the data tensor $\underline{\mathbf{d}}$ factorises into one part for initial particle positions and another for particle momenta, respectively, given by

$$\mathcal{P}(\mathbf{q}_a^{(i)}|\delta_a^{(i)}) = \frac{1}{N}\bar{\rho}(1 + \delta_a^{(i)}) \quad \mathcal{P}(\mathbf{p}_a^{(i)}|\mathbf{u}_a^{(i)}) = \delta_D(\mathbf{p}_a^{(i)} - \mathbf{u}_a^{(i)}). \quad (4.6)$$

The probability of finding a particle in a small volume around $\mathbf{q}^{(i)}$ is directly proportional to the fraction of particles in that volume, i. e. the local particle density. On the other hand, initial momenta are sampled by simply assigning particles the local value of the velocity field. As a result, integrating out the initial velocity field simply replaces $\mathbf{u}_a^{(i)}$ with $\mathbf{p}_a^{(i)}$ in $\mathcal{P}(\underline{\mathbf{d}})$.

Initial covariance matrix

Since the initial particle density and velocity fields follow a GRF, the probability density for the initial data reads

$$\mathcal{P}(\underline{\mathbf{d}}) = \frac{1}{\sqrt{\det(2\pi\mathbf{C})}} \exp\left(-\frac{1}{2} \sum_{a,b} \mathbf{d}_a^T \mathbf{C}_{ab}^{-1} \mathbf{d}_b\right), \quad (4.7)$$

with the data covariance matrix

$$\mathbf{C}_{ab} = \begin{pmatrix} \langle \delta_a^{(i)} \delta_b^{(i)} \rangle & \langle \delta_a^{(i)} \mathbf{p}_b^{(i)} \rangle^T \\ \langle \mathbf{p}_a^{(i)} \delta_b^{(i)} \rangle & \langle \mathbf{p}_a^{(i)} \otimes \mathbf{p}_b^{(i)} \rangle \end{pmatrix} =: \begin{pmatrix} \mathbf{C}_{ab}^{\delta\delta} & (\mathbf{C}_{ab}^{\delta p})^T \\ \mathbf{C}_{ab}^{p\delta} & \mathbf{C}_{ab}^{pp} \end{pmatrix}. \quad (4.8)$$

By (4.2) and the relation (2.29) between the density and velocity potential power spectra, all elements of the initial covariance matrix can be expressed as integrals over the initial density fluctuation power spectrum. Specifically, we find

$$\mathbf{C}_{ab}^{\delta\delta} = \int_{\mathbf{k}} P_\delta^{(i)}(k) e^{i\mathbf{k} \cdot \mathbf{q}_{ab}^{(i)}} \quad (4.9)$$

$$\mathbf{C}_{ab}^{\delta p} = -i \int_{\mathbf{k}} \frac{\mathbf{k}}{k^2} P_\delta^{(i)}(k) e^{i\mathbf{k} \cdot \mathbf{q}_{ab}^{(i)}} \quad (4.10)$$

$$\mathbf{C}_{ab}^{pp} = \int_{\mathbf{k}} \frac{\mathbf{k} \otimes \mathbf{k}}{k^4} P_\delta^{(i)}(k) e^{i\mathbf{k} \cdot \mathbf{q}_{ab}^{(i)}}, \quad (4.11)$$

where we defined $\mathbf{q}_{ab}^{(i)} := \mathbf{q}_a^{(i)} - \mathbf{q}_b^{(i)}$. Note that density-momentum correlation $\mathbf{C}_{ab}^{\delta p}$ is a vector pointing in $\mathbf{q}_{ab}^{(i)}$ -direction such that $\mathbf{C}_{ab}^{\delta p} = -\mathbf{C}_{ba}^{\delta p} = -\mathbf{C}_{ab}^{p\delta}$, and consequently $\mathbf{C}_{aa}^{\delta p} = \mathbf{0}$. The momentum-momentum correlation \mathbf{C}^{pp} is a 3×3 matrix and defines the momentum variance σ_p^2 via its trace

$$\sigma_p^2 = \frac{1}{3} \int_{\mathbf{k}} \frac{P_\delta^{(i)}(k)}{k^2} = \frac{1}{3} \text{Tr} \mathbf{C}_{aa}^{pp}. \quad (4.12)$$

Taking the initial power spectrum from the BBKS transfer function (2.15) we find $\sigma_p^2 = 3.639 \cdot 10^{-5}$, which gives a typical order of magnitude for initial momentum correlations.

Resulting phase-space density

Using the GRF (4.7) and integrating out the initial density and velocity fields—a lengthy and tedious calculation—eventually leads to the final expression for the initial probability density

$$\mathcal{P}(\underline{\mathbf{x}}^{(i)}) = \frac{1}{V^N \sqrt{\det(2\pi \underline{\mathbf{C}}^{pp})}} \mathcal{C} \left(\frac{\partial}{i\partial \underline{\mathbf{p}}^{(i)}} \right) \exp \left(-\frac{1}{2} \sum_{a,b=1}^N \mathbf{p}_a^{(i)T} (\mathbf{C}^{pp})_{ab}^{-1} \mathbf{p}_b^{(i)} \right), \quad (4.13)$$

where we introduced the straightforward generalisation of the momentum-momentum correlation elements to a tensorial object $\underline{\mathbf{C}}^{pp} = \sum_{a,b} \mathbf{C}_{ab}^{pp} \otimes (\mathbf{e}_a \otimes \mathbf{e}_b)$. Density-density and density-momentum correlations are contained in the operator

$$\begin{aligned} \mathcal{C} \left(\frac{\partial}{i\partial \underline{\mathbf{p}}^{(i)}} \right) &= \prod_{a=1}^N \left(1 - \sum_{\substack{b=1 \\ b \neq a}}^N i \mathbf{C}_{ab}^{\delta p} \cdot \frac{\partial}{i\partial \mathbf{p}_b^{(i)}} \right) + \sum_{\{a,b\}} \mathbf{C}_{ab}^{\delta\delta} \prod_{\substack{c=1 \\ c \neq a,b}}^N \left(1 - \sum_{\substack{d=1 \\ d \neq c}}^N i \mathbf{C}_{cd}^{\delta p} \cdot \frac{\partial}{i\partial \mathbf{p}_d^{(i)}} \right) \\ &+ \sum_{\{\{a,b\}, \{c,d\}\}} \mathbf{C}_{ab}^{\delta\delta} \mathbf{C}_{cd}^{\delta\delta} \prod_{\substack{e=1 \\ e \neq a,b,c,d}}^N \left(1 - \sum_{\substack{f=1 \\ f \neq e}}^N i \mathbf{C}_{ef}^{\delta p} \cdot \frac{\partial}{i\partial \mathbf{p}_f^{(i)}} \right) + \dots, \end{aligned} \quad (4.14)$$

whose form is a direct consequence of the sampling procedure of initial phase-space positions according to the density field. The sums over indices of density-density correlations go over distinct pairs of particles a and b , indicated by the notation $\{a, b\}$; e.g. $\{1, 2\}$ and $\{2, 1\}$ are not distinct and count only once. $\{\{a, b\}, \{c, d\}\}$ is a distinct

tuple of two distinct pairs of particles; as such $\{\{1,3\}, \{2,4\}\}$ and $\{\{4,2\}, \{1,3\}\}$ are two identical configurations and thus only counted once. In particular, note that pairs of indices belonging to initial densities can never be equal, which can be traced back to $\mathcal{P}(\mathbf{q}_a^{(i)}|\delta_a^{(i)}) \propto 1 + \delta_a^{(i)}$. Likewise, indices on density-momentum correlation lines cannot be equal due to homogeneity. The next term in the series in (4.14) will contain three density-density correlation functions but is structurally equivalent to the ones shown, and the total number of terms is $\lfloor N/2 \rfloor$. The restrictions on the allowed index configurations in (4.14) will become clearer with the graphical representation we introduce for initial correlations in the next section.

4.2.2 KFT correlation functions with cosmological initial conditions

Consider the case of an arbitrary correlation function with an m -component shift tensor. This can be either a free m -point density correlation function or a mixed density-response field correlation function, the difference being encoded in the definition of the shift tensors $\underline{\mathbf{L}}_q$ and $\underline{\mathbf{L}}_p$. No matter the exact definition of the shift tensors, we need to evaluate the expression

$$\begin{aligned} \mathcal{Z}_0(\underline{\mathbf{L}}_q, \underline{\mathbf{L}}_p) &= \int d\mathbf{x}^{(i)} \mathcal{P}(\mathbf{x}^{(i)}) \exp(\mathbf{i}\underline{\mathbf{L}}_q \cdot \mathbf{q}^{(i)} + \mathbf{i}\underline{\mathbf{L}}_p \cdot \mathbf{p}^{(i)}) \\ &= \int \frac{d\mathbf{q}_1^{(i)}}{V} \dots \frac{d\mathbf{q}_m^{(i)}}{V} \mathcal{C}(-\underline{\mathbf{L}}_p) \exp\left(-\frac{1}{2} \sum_{a,b=1}^m \mathbf{L}_{p_a}^T \mathbf{C}_{ab}^{pp} \mathbf{L}_{p_b}\right) \exp(\mathbf{i}\underline{\mathbf{L}}_q \cdot \mathbf{q}^{(i)}), \end{aligned} \quad (4.15)$$

where the second line follows from inserting (4.13) for the initial probability density, applying partial integration for the $\mathbf{p}^{(i)}$ -derivatives in \mathcal{C} and solving the Gaussian integral over the initial momenta. Since position and momentum shift tensors have only m non-vanishing components, sums over particle indices in the initial conditions now run up to m . The $N - m$ trivial position integrals were solved to yield a factor V^{N-m} , partly cancelling the prefactor. The main challenge is posed by the remaining integral over initial particle positions since the initial probability density depends on these in a highly non-trivial manner. To take full advantage of the symmetries of the system, i.e. that correlations only depend on distances between particles, we cast the components of the initial probability density in (4.15) into a graphical representation.

Density-density and density-momentum correlation lines

First, consider the polynomial (4.14) of initial density-density and density-momentum correlations. In the context of cosmology, initial correlations are characterized by the amplitude of initial density and velocity fluctuations w.r.t. the background, raising the hope that terms of higher order in initial correlations are less important than the lower order terms. We, hence, order the polynomial (4.14) in powers of initial correlations

$$\begin{aligned} \mathcal{C}(-\underline{\mathbf{L}}_p) &= 1 + \sum_{a \neq b}^m \mathbf{i}\mathbf{C}_{ab}^{\delta p} \cdot \mathbf{L}_{p_b} + \sum_{\{a,b\}}^m \mathbf{C}_{ab}^{\delta\delta} + \sum_{\substack{a \neq b, c \neq d \\ a \neq c}}^m (\mathbf{i}\mathbf{C}_{ab}^{\delta p} \cdot \mathbf{L}_{p_b}) (\mathbf{i}\mathbf{C}_{cd}^{\delta p} \cdot \mathbf{L}_{p_d}) \\ &\quad + \sum_{\substack{\{a,b\}, c \neq d \\ c \neq a, b}}^m \mathbf{C}_{ab}^{\delta\delta} (\mathbf{i}\mathbf{C}_{cd}^{\delta p} \cdot \mathbf{L}_{p_d}) + \sum_{\{\{a,b\}, \{c,d\}\}}^m \mathbf{C}_{ab}^{\delta\delta} \mathbf{C}_{cd}^{\delta\delta} + \dots, \end{aligned} \quad (4.16)$$

where all remaining contributions are of third and higher order in $\mathbf{C}^{\delta\delta}$ and $\mathbf{C}^{\delta p}$. For a more intuitive understanding of which index combinations are allowed to occur in

(4.16) we follow [4] and introduce a graphical notation, representing density-density and density-momentum correlations by

$$C_{ab}^{\delta\delta} =: \overset{\bullet}{a} \text{---} \overset{\bullet}{b}, \quad iC_{ab}^{\delta p} \cdot \mathbf{L}_{p_b} =: \overset{\bullet}{a} \text{---} \overset{\bullet}{b}. \quad (4.17)$$

Initial particle positions are represented by vertices endowed with a particle index, whereas the corresponding lines depict correlations between particles. Note that the density-momentum correlation line is a directed edge in the sense that one end corresponds to a density (solid), whereas the other end corresponds to momentum (dashed). As such, permuting its indices results in a different line, unlike the symmetric density-density lines. Representing initial correlations in terms of the lines (4.17) allows for an intuitive graphical representation of the sums in (4.16) if we adhere to the following rule:

δ -rule No two delta line-ends are allowed to meet at the same vertex. This includes both ends of the density-density correlation line and the density-end of the density-momentum correlation line.

The δ -rule is an elegant way to encode the restrictions on the sums over particle indices in (4.16), both for density-density and density-momentum correlations. In terms of the correlation lines (4.17) and under consideration of the δ -rule, expression (4.16) turns into

$$\begin{aligned} C(-\mathbf{L}_p) = 1 + \sum_{\{a,b\}}^m & \left[\overset{\bullet}{a} \text{---} \overset{\bullet}{b} + \left(\overset{\bullet}{a} \text{---} \overset{\bullet}{b} + \overset{\bullet}{a} \text{---} \overset{\bullet}{b} \right) + \overset{\bullet}{a} \text{---} \overset{\bullet}{b} \right] \\ & + \sum_{\{\{a,b\},\{b,c\}\}}^m \left[\overset{\bullet}{a} \text{---} \overset{\bullet}{b} \text{---} \overset{\bullet}{c} + \overset{\bullet}{a} \text{---} \overset{\bullet}{b} \text{---} \overset{\bullet}{c} + \overset{\bullet}{a} \text{---} \overset{\bullet}{b} \text{---} \overset{\bullet}{c} \right] \\ & + \sum_{\{\{a,b\},\{c,d\}\}}^m \left[\left(\overset{\bullet}{a} \text{---} \overset{\bullet}{b} + \overset{\bullet}{a} \text{---} \overset{\bullet}{b} + \overset{\bullet}{a} \text{---} \overset{\bullet}{b} \right) \right. \\ & \quad \left. \times \left(\overset{\bullet}{c} \text{---} \overset{\bullet}{d} + \overset{\bullet}{c} \text{---} \overset{\bullet}{d} + \overset{\bullet}{d} \text{---} \overset{\bullet}{c} \right) \right] + \dots, \end{aligned} \quad (4.18)$$

where the first line contains all contributions with two, the second with three and the third with four distinct particle indices. Attaching two correlation lines, such as for the three-particle case, corresponds to multiplying the two corresponding correlations with a shared particle index, e. g.

$$\overset{\bullet}{a} \text{---} \overset{\bullet}{b} \text{---} \overset{\bullet}{c} = \overset{\bullet}{a} \text{---} \overset{\bullet}{b} \times \overset{\bullet}{b} \text{---} \overset{\bullet}{c} = C_{ab}^{\delta\delta} (iC_{cb}^{\delta p} \cdot \mathbf{L}_{p_b}). \quad (4.19)$$

To get the full sum in the second line for m particles, we have to go through all the combinations of drawing three out of m representative indices. With the three indices fixed at $(1,2,3)$, the distinct configurations represented by $\{\{a,b\},\{b,c\}\}$ are $\{\{1,2\},\{2,3\}\}$, $\{\{1,3\},\{3,2\}\}$ and $\{\{3,1\},\{1,2\}\}$. Similarly, for the four representative indices $(1,2,3,4)$, the configurations prescribed by the sum in the third line are $\{\{1,2\},\{3,4\}\}$, $\{\{1,3\},\{2,4\}\}$ and $\{\{1,4\},\{2,3\}\}$. Although tedious, pushing to higher orders in the initial correlation lines is straightforwardly done by drawing all graphs with three, four, etc. edges that are allowed by the δ -rule.

Momentum correlation lines

Similarly, we assign a correlation line to the momentum correlation term in (4.15) by first splitting off the diagonal term

$$\begin{aligned} \exp\left(-\frac{1}{2}\sum_{a,b=1}^m \mathbf{L}_{p_a}^T \mathbf{C}_{ab}^{pp} \mathbf{L}_{p_b}\right) &= \exp\left(-\frac{\sigma_p^2}{2}\sum_{a=1}^m L_{p_a}^2\right) \exp\left(-\sum_{\{a,b\}} \mathbf{L}_{p_a}^T \mathbf{C}_{ab}^{pp} \mathbf{L}_{p_b}\right) \\ &= e^{-Q_D} \prod_{\{a,b\}} \exp\left(-\mathbf{L}_{p_a}^T \mathbf{C}_{ab}^{pp} \mathbf{L}_{p_b}\right), \end{aligned} \quad (4.20)$$

where, in the first line, the second sum on the right goes over *distinct* pairs of particles, thus cancelling the factor $\frac{1}{2}$. In the second line, we have identified the damping factor

$$Q_D := \frac{\sigma_p^2}{2} \sum_{a=1}^m L_{p_a}^2, \quad (4.21)$$

which arises due to momentum auto-correlation and thus describes diffusion caused by statistical momentum uncertainty. The remaining non-diagonal part of \mathbf{C}^{pp} quantifies correlations between the initial momenta of distinct particles, although a trivial uncorrelated part is still retained by $\prod_{\{a,b\}} \exp\left(-\mathbf{L}_{p_a}^T \mathbf{C}_{ab}^{pp} \mathbf{L}_{p_b}\right)$, since $\exp(x) = 1 + \mathcal{O}(x)$. To ensure that the momentum correlation line exclusively quantifies correlations between the momenta of different particles, we subtract the trivial background contribution by defining

$$\exp\left(-\mathbf{L}_{p_a}^T \mathbf{C}_{ab}^{pp} \mathbf{L}_{p_b}\right) - 1 =: \overset{\bullet}{a} \text{---} \overset{\bullet}{b}. \quad (4.22)$$

The treatment of initial momentum correlations thus closely follows the Mayer cluster expansion [48], which is used in equilibrium statistical mechanics to calculate perturbative corrections to the canonical partition function, e. g. of an ideal gas, due to two-particle interactions. Although, in our case, the interest lies in corrections due to initial momentum correlations, the treatment is equivalent and relies on the fact that perturbations depend only on the absolute distance between pairs of particles. Due to the subtraction of the factor unity, the momentum correlation line is at least of first order in the initial momentum correlation \mathbf{C}^{pp} . For the Gaussian in (4.20) this yields

$$\begin{aligned} &\prod_{\{a,b\}} \exp\left(-\mathbf{L}_{p_a}^T \mathbf{C}_{ab}^{pp} \mathbf{L}_{p_b}\right) \\ &= 1 + \sum_{\{a,b\}} \overset{\bullet}{a} \text{---} \overset{\bullet}{b} + \sum_{\{\{a,b\},\{b,c\}\}} \overset{\bullet}{a} \text{---} \overset{\bullet}{b} \text{---} \overset{\bullet}{c} + \sum_{\{\{a,b\},\{c,d\}\}} \overset{\bullet}{a} \text{---} \overset{\bullet}{b} \text{---} \overset{\bullet}{c} \text{---} \overset{\bullet}{d} + \dots, \end{aligned} \quad (4.23)$$

where we have again ordered the resulting terms in powers of the correlation line and included all distinct two-, three-, four- etc. particle contributions, as for density-density and density-momentum correlations. Note that, since the product in (4.20) only includes distinct particle pairs, graphs or subgraphs with topology $\overset{\bullet}{a} \text{---} \overset{\bullet}{b} \text{---} \overset{\bullet}{c}$ do not occur.

Combined correlation lines

The expressions we have derived for the initial probability density in terms of correlation lines allowed us to arrange contributions from density-density, density-momentum as

well as momentum-momentum correlations in terms of clusters of particles. Integration over the initial probability density leads to a product of $\mathcal{C}(-\underline{\mathbf{L}}_p)$, containing density-density and density-momentum lines and the Gaussian factor encoding momentum-momentum correlations. The result will therefore contain all allowed combinations of correlation lines. Consider the contribution of up to two-particle clusters between a fixed pair of particles

$$\begin{aligned}
& \left\{ 1 + \left[\overset{\bullet}{a} \text{---} \overset{\bullet}{b} + \left(\overset{\bullet}{a} \text{---} \overset{\bullet}{b} + \overset{\bullet}{a} \text{---} \overset{\bullet}{b} \right) + \overset{\bullet}{a} \text{---} \overset{\bullet}{b} \right] \right\} \left\{ 1 + \overset{\bullet}{a} \text{---} \overset{\bullet}{b} \right\} \\
&= 1 + \left[\overset{\bullet}{a} \text{---} \overset{\bullet}{b} + \overset{\bullet}{a} \text{---} \overset{\bullet}{b} + \overset{\bullet}{a} \text{---} \overset{\bullet}{b} + \overset{\bullet}{a} \text{---} \overset{\bullet}{b} \right] \\
&\quad + \overset{\bullet}{a} \text{---} \overset{\bullet}{b} \\
&=: 1 + \overset{\bullet}{a} \text{---} \overset{\bullet}{b}, \tag{4.24}
\end{aligned}$$

where the first equality follows by simply multiplying out all the terms. In the last line, we have defined the combined correlation line, collecting all allowed combinations of lines for two-particle clusters. The combined correlation line can now be used as the fundamental building block to formulate the initial probability density in terms of clusters of particles:

$$\begin{aligned}
& \mathcal{C}(-\underline{\mathbf{L}}_p) \prod_{\{a,b\}}^m \exp \left(-\underline{\mathbf{L}}_{p_a}^T \mathbf{C}_{ab}^{pp} \underline{\mathbf{L}}_{p_b} \right) \\
&= 1 + \sum_{\{a,b\}}^m \overset{\bullet}{a} \text{---} \overset{\bullet}{b} + \sum_{\{\{a,b\},\{b,c\}\}}^m \overset{\bullet}{a} \text{---} \overset{\bullet}{b} \text{---} \overset{\bullet}{c} + \sum_{\{\{a,b\},\{c,d\}\}}^m \overset{\bullet}{c} \text{---} \overset{\bullet}{d} \text{---} \overset{\bullet}{a} \text{---} \overset{\bullet}{b} + \dots, \tag{4.25}
\end{aligned}$$

where terms with a larger number of distinct indices need to be constructed under adherence to the δ -rule. We have thus managed to order the initial probability density for correlated phase-space positions in such a way that each term exclusively depends on a fixed number of initial positions, and inserting (4.25) into (4.15) yields

$$\begin{aligned}
\mathcal{Z}_0(\underline{\mathbf{L}}_q, \underline{\mathbf{L}}_p) &= e^{-Q_D} \int \frac{d\mathbf{q}_1^{(i)}}{V} \dots \frac{d\mathbf{q}_m^{(i)}}{V} \exp \left(i\underline{\mathbf{L}}_q \cdot \underline{\mathbf{q}}^{(i)} \right) \left(1 + \sum_{\{a,b\}}^m \overset{\bullet}{a} \text{---} \overset{\bullet}{b} \right. \\
&\quad \left. + \sum_{\{\{a,b\},\{b,c\}\}}^m \overset{\bullet}{a} \text{---} \overset{\bullet}{b} \text{---} \overset{\bullet}{c} + \sum_{\{\{a,b\},\{c,d\}\}}^m \overset{\bullet}{c} \text{---} \overset{\bullet}{d} \text{---} \overset{\bullet}{a} \text{---} \overset{\bullet}{b} + \dots \right). \tag{4.26}
\end{aligned}$$

With the initial conditions in this form, the integration over initial positions can now be performed for each term individually. The first term in brackets represents the uncorrelated background

$$e^{-Q_D} \int \frac{d\mathbf{q}_1^{(i)}}{V} \dots \frac{d\mathbf{q}_m^{(i)}}{V} \exp \left(i\underline{\mathbf{L}}_q \cdot \underline{\mathbf{q}}^{(i)} \right) = \prod_{a=1}^m (2\pi)^3 \delta_D(\underline{\mathbf{L}}_{q_a}), \tag{4.27}$$

and is a direct consequence of particle positions being sampled not according to the density contrast δ but to the overall density ρ , which has a non-zero mean. Since the

natural quantity to work with in KFT is the particle density rather than the density contrast, we inevitably obtain such trivial background contributions. Comparing, for example, the relation between density and density fluctuation two-point functions using (2.8) we find

$$G_{\delta\delta}(1,2) = \bar{\rho}^{-2} G_{\rho\rho}(1,2) - (2\pi)^6 \delta_D(\mathbf{k}_1) \delta_D(\mathbf{k}_2). \quad (4.28)$$

The second term on the rhs stemming from the homogeneous background density $\bar{\rho}$ exactly corresponds to, and thus cancels, the constant in the initial conditions. Keeping this in mind, we will henceforth discard the constant part, thus ignoring the contribution of the homogeneous background.

The first non-trivial term in (4.25) quantifies initial correlations of pairs of particles and reads

$$\begin{aligned} & V^{-m} \sum_{\{a,b\}}^m e^{-Q_D} \int d\mathbf{q}_1^{(i)} \cdots d\mathbf{q}_m^{(i)} \overset{a}{\longleftarrow} \overset{b}{\longrightarrow} \exp(i\mathbf{L}_q \cdot \mathbf{q}^{(i)}) \\ &= V^{-m} \sum_{\{a,b\}}^m \left[\prod_{\substack{c=1 \\ c \neq a,b}}^m (2\pi)^3 \delta_D(\mathbf{L}_{q_c}) \right] (2\pi)^3 \delta_D(\mathbf{L}_{q_a} + \mathbf{L}_{q_b}) e^{-Q_D} \int_{\mathbf{q}_{ab}^{(i)}} \overset{a}{\longleftarrow} \overset{b}{\longrightarrow} e^{i\mathbf{L}_{q_a} \cdot \mathbf{q}_{ab}^{(i)}} \\ &= V^{-m} \sum_{\{a,b\}}^m \Delta_{\not{a}\not{b}} (2\pi)^3 \delta_D(\mathbf{L}_{q_a} + \mathbf{L}_{q_b}) e^{-Q_D} \tilde{\mathcal{P}}_{ab}(\mathbf{L}_{q_a}). \end{aligned} \quad (4.29)$$

In the step from the first to the second line, the integrals over all initial positions except for $\mathbf{q}_a^{(i)}$ and $\mathbf{q}_b^{(i)}$ lead to Dirac-delta distributions for the respective spatial shift vectors. The coordinate transform $(\mathbf{q}_a^{(i)}, \mathbf{q}_b^{(i)}) \rightarrow (\mathbf{q}_a^{(i)} - \mathbf{q}_b^{(i)}, \mathbf{q}_b^{(i)})$ and subsequent integration over $\mathbf{q}_b^{(i)}$ result in $(2\pi)^3 \delta_D(\mathbf{L}_{q_a} + \mathbf{L}_{q_b})$. In the last line, we have defined $\Delta_{\not{a}\not{b}}$ and the Fourier-space combined correlation line

$$\tilde{\mathcal{P}}_{ab}(\mathbf{L}_{q_a}) := \int_{\mathbf{q}_{ab}^{(i)}} \overset{a}{\longleftarrow} \overset{b}{\longrightarrow} e^{i\mathbf{L}_{q_a} \cdot \mathbf{q}_{ab}^{(i)}}, \quad \Delta_{\not{a}\not{b}} := \prod_{\substack{c=1 \\ c \neq a,b}}^m (2\pi)^3 \delta_D(\mathbf{L}_{q_c}). \quad (4.30)$$

The product over Dirac deltas $\Delta_{\not{a}\not{b}}$ arises due to all particles of the system, which represent a density mode and are not initially correlated to any other particle. If we think of uncorrelated particles as isolated one-particle clusters, the Dirac-delta distributions for the spatial shift vectors occurring in the initial conditions enforce spatial homogeneity for each cluster.

Integration over initial particle positions for three- and four-particle clusters is performed analogously to (4.29), leading to the final expression of the free correlation function

$$\begin{aligned} \mathcal{Z}_0(\mathbf{L}_{q_r}, \mathbf{L}_p) &= V^{-m} e^{-Q_D} \left\{ \sum_{\{a,b\}}^m \Delta_{\not{a}\not{b}} (2\pi)^3 \delta_D(\mathbf{L}_{q_a} + \mathbf{L}_{q_b}) \tilde{\mathcal{P}}_{ab}(\mathbf{L}_{q_a}) \right. \\ &+ \sum_{\{\{a,b\}, \{b,c\}\}}^m \Delta_{\not{a}\not{b}\not{c}} (2\pi)^3 \delta_D(\mathbf{L}_{q_a} + \mathbf{L}_{q_b} + \mathbf{L}_{q_c}) \tilde{\mathcal{P}}_{ab}(\mathbf{L}_{q_a}) \tilde{\mathcal{P}}_{cb}(\mathbf{L}_{q_c}) \\ &+ \sum_{\{\{a,b\}, \{b,c\}\}}^m \Delta_{\not{a}\not{b}\not{c}\not{d}} (2\pi)^6 \delta_D(\mathbf{L}_{q_a} + \mathbf{L}_{q_b}) \delta_D(\mathbf{L}_{q_c} + \mathbf{L}_{q_d}) \tilde{\mathcal{P}}_{ab}(\mathbf{L}_{q_a}) \tilde{\mathcal{P}}_{cd}(\mathbf{L}_{q_c}) \\ &+ \dots \left. \right\}, \end{aligned} \quad (4.31)$$

where $\Delta_{\not{a}\not{b}\not{c}}$ and $\Delta_{\not{a}\not{b}\not{c}\not{d}}$ are products of Dirac-deltas of shift vectors excluding those with indices (a, b, c) and (a, b, c, d) respectively. When evaluating three-particle contributions, special care must be taken since the δ -rule must be applied correctly. Additionally, note that the ordering of the two indices of the Fourier-space correlation lines in relation to the index of the spatial shift vector is crucial since density-momentum lines are not symmetric. As a consequence, $\tilde{\mathcal{P}}_{ab}(\mathbf{L}_{q_a}) \neq \tilde{\mathcal{P}}_{ba}(\mathbf{L}_{q_a})!$ As a rule of thumb, the spatial shift vector in the argument of a correlation line should always carry the first index of the pair of the line. For correlation lines that share a particle index like the second line in (4.31), the spatial shift-vector arguments always carry the index which is not shared.

Although we have truncated the series at quadratic combined correlation lines, the logic that we applied to derive (4.31) extends straight to higher orders. Were we inclined to include all cubic terms, we would get (a lot of) additional contributions containing three, four, five and six particles, respectively. For example, the cubic contribution from initial correlations between three particles a, b, c would read

$$\int d\mathbf{q}^{(i)} \begin{array}{c} b \\ \triangle \\ a \quad c \end{array} e^{i\mathbf{L}_q \cdot \mathbf{q}^{(i)}} \\ = \Delta_{\not{a}\not{b}\not{c}} (2\pi)^3 \delta_D(\mathbf{L}_{q_a} + \mathbf{L}_{q_b} + \mathbf{L}_{q_c}) \int_{\mathbf{k}} \tilde{\mathcal{P}}_{ab}(\mathbf{L}_{q_a} - \mathbf{k}) \tilde{\mathcal{P}}_{cb}(\mathbf{L}_{q_c} + \mathbf{k}) \tilde{\mathcal{P}}_{ac}(\mathbf{k}). \quad (4.32)$$

4.2.3 Expanding in the initial power spectrum

The proper evaluation of the initial correlation lines and, most notably, the momentum correlation line poses a significant challenge for KFT calculations from a numerical point of view. The Fourier-space momentum correlation line is traditionally denoted by \mathcal{P} and reads

$$\mathcal{P}_{ab}(\mathbf{L}_{q_a}) = \int_{\mathbf{q}_{ab}^{(i)}} \begin{array}{c} \bullet \\ \text{---} \\ a \quad b \end{array} e^{i\mathbf{L}_{q_a} \cdot \mathbf{q}_{ab}^{(i)}} = \int_{\mathbf{q}_{ab}^{(i)}} \left\{ \exp(-\mathbf{L}_{p_a} \mathbf{C}_{ab}^{pp} \mathbf{L}_{p_b}) - 1 \right\} e^{i\mathbf{L}_{q_a} \cdot \mathbf{q}_{ab}^{(i)}}. \quad (4.33)$$

This is a notoriously difficult integral to solve numerically since the Fourier phase oscillates rapidly for intermediate to large particle separations. In the last step of our analysis of correlation functions of cosmic structures, we will therefore be forced to introduce one further approximation by expanding the momentum correlation line in orders of initial momentum correlations

$$\mathcal{P}_{ab}(\mathbf{L}_{q_a}) = \int_{\mathbf{q}_{ab}^{(i)}} \left\{ -\mathbf{L}_{p_a} \mathbf{C}_{ab}^{pp} \mathbf{L}_{p_b} + \frac{1}{2} (\mathbf{L}_{p_a} \mathbf{C}_{ab}^{pp} \mathbf{L}_{p_b}) (\mathbf{L}_{p_a} \mathbf{C}_{ab}^{pp} \mathbf{L}_{p_b}) + \dots \right\} e^{i\mathbf{L}_{q_a} \cdot \mathbf{q}_{ab}^{(i)}} \\ =: \int_{\mathbf{q}_{ab}^{(i)}} \left(\begin{array}{c} \bullet \\ \text{---}^{(1)} \\ a \quad b \end{array} + \frac{1}{2} \begin{array}{c} \bullet \\ \text{---}^{(2)} \\ a \quad b \end{array} + \dots \right) e^{i\mathbf{L}_{q_a} \cdot \mathbf{q}_{ab}^{(i)}}, \quad (4.34)$$

thus defining the respective first- and second-order expanded momentum correlation lines $\begin{array}{c} \bullet \\ \text{---}^{(1)} \\ a \quad b \end{array}$ and $\begin{array}{c} \bullet \\ \text{---}^{(2)} \\ a \quad b \end{array}$. Since all initial correlations $C^{\delta\delta}$, $\mathbf{C}^{\delta p}$ and $C^{\delta\delta}$ are integrals over the initial power spectrum (4.9)–(4.11), expanding the momentum correlation lines up to a fixed order in \mathbf{C}^{pp} and truncating the initial conditions at the same order in terms of the correlation lines, we obtain expressions for correlation functions in KFT at a fixed maximum order in the initial power spectrum $P_\delta^{(i)}(k)$. Note that the Gaussian damping due to momentum auto-correlations (4.21) should be part of such an expansion since σ_p^2 is an integral over the initial power spectrum itself.

When evaluating correlation functions in KFT, we thus have to refer to two different expansions. The first expansion, taking place in the interaction operator, is intrinsic to the basic formalism of KFT, and we will generally refer to it as the n -th order perturbative expansion, or S_I -expansion. The second expansion, namely the expansion of correlation lines in terms of the initial power spectrum, is not a fundamental feature of KFT but rather an unfortunate practical necessity. To avoid confusion as far as possible, we will refer to it as the linear or quadratic expansion in terms of $P_\delta^{(i)}$, or $P_\delta^{(i)}$ -expansion.

Consistent expansion of free correlation functions

To perform the $P_\delta^{(i)}$ -expansion of the free correlation function (4.31), all its components are expanded in the initial power spectrum. To include all terms up to quadratic order in $P_\delta^{(i)}$, the Gaussian damping factor must be included up to linear order. In the expansion, all the contributions from the combined correlation line that are of the same order in the initial power spectrum need to be collected, such that

$$\begin{aligned}
\overline{a \text{---} b} &= \overline{a \text{---} b} + \overline{a \text{---} b} + \overline{a \text{---} b} + \overline{a \text{---} b}^{(1)} \\
&\quad + \frac{1}{2} \overline{a \text{---} b}^{(2)} + \overline{a \text{---} b}^{(1)} + \overline{a \text{---} b}^{(1)} + \overline{a \text{---} b}^{(1)} + \overline{a \text{---} b}^{(1)} + \dots \\
&=: \overline{a \text{---} b}^{(1)} + \overline{a \text{---} b}^{(2)} + \dots
\end{aligned} \tag{4.35}$$

All the terms on the rhs of the first line are linear in the initial power spectrum and are collected in $\overline{a \text{---} b}^{(1)}$, whereas the second line contains quadratic contributions which make up $\overline{a \text{---} b}^{(2)}$. The linear and quadratic contributions of a consistent expansion of the free correlation function (4.31) then read

$$\mathcal{Z}_0^{(1)}(\mathbf{L}_q, \mathbf{L}_p) = V^{-m} \sum_{\{a,b\}}^m \Delta_{\not{a}\not{b}} (2\pi)^3 \delta_D(\mathbf{L}_{q_a} + \mathbf{L}_{q_b}) \tilde{\mathcal{P}}_{ab}^{(1)}(\mathbf{L}_{q_a}) \tag{4.36}$$

$$\begin{aligned}
\mathcal{Z}_0^{(2)}(\mathbf{L}_q, \mathbf{L}_p) &= V^{-m} \left\{ \sum_{\{a,b\}}^m \Delta_{\not{a}\not{b}} (2\pi)^3 \delta_D(\mathbf{L}_{q_a} + \mathbf{L}_{q_b}) \left[-Q_D \tilde{\mathcal{P}}_{ab}^{(1)}(\mathbf{L}_{q_a}) + \tilde{\mathcal{P}}_{ab}^{(2)}(\mathbf{L}_{q_a}) \right] \right. \\
&\quad + \sum_{\{\{a,b\},\{b,c\}\}}^m \Delta_{\not{a}\not{b}\not{c}} (2\pi)^3 \delta_D(\mathbf{L}_{q_a} + \mathbf{L}_{q_b} + \mathbf{L}_{q_c}) \tilde{\mathcal{P}}_{ab}^{(1)}(\mathbf{L}_{q_a}) \tilde{\mathcal{P}}_{cb}^{(1)}(\mathbf{L}_{q_c}) \\
&\quad \left. + \sum_{\{\{a,b\},\{b,c\}\}}^m \Delta_{\not{a}\not{b}\not{c}\not{d}} (2\pi)^6 \delta_D(\mathbf{L}_{q_a} + \mathbf{L}_{q_b}) \delta_D(\mathbf{L}_{q_c} + \mathbf{L}_{q_d}) \tilde{\mathcal{P}}_{ab}^{(1)}(\mathbf{L}_{q_a}) \tilde{\mathcal{P}}_{cd}^{(1)}(\mathbf{L}_{q_c}) \right\},
\end{aligned} \tag{4.37}$$

where $\tilde{\mathcal{P}}_{ab}^{(1)}$ and $\tilde{\mathcal{P}}_{ab}^{(2)}$ are defined in terms of the linear and quadratic correlation lines via (4.30). The full m -point correlation function expanded in the initial power spectrum reads

$$G_{\rho\dots\rho}(1, \dots, m) = G_{\rho\dots\rho}^{(1)}(1, \dots, m) + G_{\rho\dots\rho}^{(2)}(1, \dots, m) + \dots, \tag{4.38}$$

where we will reserve the notation $(\dots)^{(1)}$ for the $P_\delta^{(i)}$ -expansion. Formally $G_{\rho\dots\rho}^{(1)}(1, \dots, m)$ thus contains the full information on particle interactions, but all expressions are evaluated at linear order in $P_\delta^{(i)}$.

Example 4.2.1 *As an instructive and important example, consider the calculation of the free two-point function at linear order in $P_\delta^{(i)}$*

$$\bar{G}_{\rho\rho}^{(1)}(1,2) = \left[\hat{\rho}(1)\hat{\rho}(2) Z_0[\underline{\mathbf{J}}, \underline{\mathbf{K}}] \Big|_{\underline{\mathbf{0}}} \right]^{(1)} = N^2 \mathcal{Z}_0^{(1)}(\underline{\mathbf{L}}_q, \underline{\mathbf{L}}_p), \quad (4.39)$$

$$\text{with} \quad \begin{cases} \mathbf{L}_{q_{e_1}} = -\mathbf{k}_1 & \mathbf{L}_{p_{e_1}} = -g_{qp}(\tau_1, 0)\mathbf{k}_1 \\ \mathbf{L}_{q_{e_2}} = -\mathbf{k}_2 & \mathbf{L}_{p_{e_2}} = -g_{qp}(\tau_2, 0)\mathbf{k}_2. \end{cases} \quad (4.40)$$

Since there are only two spatial shift vectors (4.36) reduces to

$$\mathcal{Z}_0^{(1)}(\underline{\mathbf{L}}_q, \underline{\mathbf{L}}_p) = V^{-2} \delta_D(\mathbf{L}_{q_{e_1}} + \mathbf{L}_{q_{e_2}}) \tilde{\mathcal{P}}_{e_1 e_2}^{(1)}(\mathbf{L}_{q_{e_1}}), \quad (4.41)$$

where the combined linearized Fourier-space correlation line evaluates to

$$\begin{aligned} \tilde{\mathcal{P}}_{e_1 e_2}^{(1)}(\mathbf{L}_{q_{e_1}}) &= \int_{\mathbf{q}_{12}^{(i)}} \left(\overset{\bullet}{e_1} \text{---} \overset{\bullet}{e_2} + \overset{\bullet}{e_1} \text{---} \overset{\bullet}{e_2} + \overset{\bullet}{e_1} \text{---} \overset{\bullet}{e_2} + \overset{\bullet}{e_1} \overset{(1)}{\text{---}} \overset{\bullet}{e_2} \right) e^{i\mathbf{L}_{q_1} \cdot \mathbf{q}_{12}^{(i)}} \\ &= \int_{\mathbf{q}_{12}^{(i)}} \left(\mathbf{C}_{e_1 e_2}^{\delta\delta} + i\mathbf{C}_{e_1 e_2}^{\delta p} \cdot \mathbf{L}_{p_{e_2}} + i\mathbf{C}_{e_2 e_1}^{\delta p} \cdot \mathbf{L}_{p_{e_1}} - \mathbf{L}_{p_{e_1}} \cdot \mathbf{C}_{e_1 e_2}^{pp} \cdot \mathbf{L}_{p_{e_2}} \right) e^{i\mathbf{L}_{q_{e_1}} \cdot \mathbf{q}_{12}^{(i)}} \\ &= \left(1 - \frac{\mathbf{L}_{q_{e_1}} \cdot \mathbf{L}_{p_{e_2}}}{L_{q_{e_1}}^2} + \frac{\mathbf{L}_{q_{e_1}} \cdot \mathbf{L}_{p_{e_1}}}{L_{q_{e_1}}^2} - \frac{(\mathbf{L}_{q_{e_1}} \cdot \mathbf{L}_{p_{e_1}})(\mathbf{L}_{q_{e_1}} \cdot \mathbf{L}_{p_{e_2}})}{L_{q_{e_1}}^4} \right) P_\delta^{(i)}(\mathbf{L}_{q_{e_1}}). \end{aligned} \quad (4.42)$$

Due to the presence of the Dirac-delta in $\mathcal{Z}_0^{(1)}(\underline{\mathbf{L}}_q, \underline{\mathbf{L}}_p)$, the shift vectors are antiparallel, and the final expression for the free two-point correlation function becomes

$$\bar{G}_{\rho\rho}^{(1)}(1,2) = \bar{\rho}^2 \delta_D(\mathbf{k}_1 + \mathbf{k}_2) (1 + g_{qp}(t_1, 0)) (1 + g_{qp}(t_2, 0)) P_\delta^{(i)}(k_1). \quad (4.43)$$

4.3 DIAGRAMMATIC APPROACH TO CANONICAL PERTURBATION THEORY

4.3.1 Motivation

As is the case for most field theories, a diagrammatic language is helpful in KFT to keep track of the large number of terms arising due to the perturbative expansion of the interaction operator. Since diagrams represent applications of the interaction operator to the free generating functional, their topological properties are a direct consequence of the structural details of the interaction operator. As an illustration, consider ϕ^4 theory with the generating functional

$$Z[J] = \int \mathcal{D}\phi e^{iS[\phi] + i \int_x J(x)\phi(x)}, \quad (4.44)$$

$$\text{where} \quad S[\phi] = \int_x \left(\phi(x) \frac{1}{2} (\nabla^2 + m^2) \phi(x) + \frac{\lambda}{4!} \phi^4(x) \right). \quad (4.45)$$

To evaluate correlation functions perturbatively, we split the action into a free quadratic part for which the path integral can be solved directly, resulting in the Feynman propagator $G(x, x')$ fulfilling $\frac{1}{2}(\nabla^2 + m^2)G(x, x') = (2\pi^4)\delta_D(x - x')$, and an interaction operator representing the ϕ^4 term:

$$Z[J] = e^{i\hat{S}_I} e^{-\frac{1}{2} \int_{x,x'} J(x)G(x,x')J(x')} \quad \text{with} \quad \hat{S}_I = \frac{\lambda}{4!} \int_y \left(\frac{\delta}{i\delta J(y)} \right)^4. \quad (4.46)$$

Whereas the Feynman propagator quantifies ‘free correlations’ of the field ϕ between two space-time points, the interaction operator describes a local self-interaction of the field, which is represented as a four-vertex in the resulting Feynman diagrams. Diagrams in ϕ^4 -theory are thus constructed from lines which represent the Feynman propagator and vertices which always connect four edges. This simple structure is shared by many field theories where interactions are simple monomials of degree n in the fundamental field ϕ of the theory.

In contrast, the interaction operator in the canonical formulation of KFT shows a fundamentally different structure, most notably since density and response field operators are related to the microscopic phase-space coordinates—which are the fundamental dynamical degrees of freedom, playing the role of ϕ in KFT—in a highly non-linear way. Furthermore, KFT needs to deal with an additional component absent in equilibrium field theories, namely non-Gaussian initial conditions, which we want to include in the diagrammatic formulation. Therefore, it should be no surprise that diagrams for canonical perturbation theory in KFT are pretty different from the well-known Feynman diagrams. Nonetheless, expressing canonical perturbation theory in terms of diagrams holds the same advantages as in other field theories; it allows for a compact and intuitive notation for the perturbative inclusion of interactions into calculating statistical quantities. This section will construct such an approach, starting with the rules for applying the interaction operator to the free generating functional. Once we have understood these rules, the evaluation of the initial probability density in terms of correlation lines is included in the diagrams.

4.3.2 Density operators

The dynamics of macroscopic quantities in KFT occur at the microscopic level, where classical point particles with correlated initial conditions evolve along their Hamiltonian trajectories. We, therefore, choose to describe perturbation theory in terms of microscopic particles as well. From this point of view, each density operator is represented by a particle label and the time evolution of the corresponding particle density is caused purely by the correlations and interactions between particles. Furthermore, since shot-noise terms are neglected, only contributions where different density operators are represented by distinct microscopic particles are relevant, such that we can attribute a distinct particle label to each density operator. Microscopic particles with their respective labels form the first ingredient for the diagrams of canonical perturbation theory in KFT. We draw a node with a particle label for each density operator applied to the free generating functional. By convention external density modes are labelled with e_1, \dots, e_m , whereas internal densities carry indices i_1, \dots, i_n :

$$\sum_{\substack{\{i_1, \dots, i_n\} \\ \{e_1, \dots, e_m\}}} \hat{\rho}_{i_1}(1') \dots \hat{\rho}_{i_n}(n') \hat{\rho}_{e_1}(1) \dots \hat{\rho}_{e_m}(m) Z_0[\underline{\mathbf{J}}, \underline{\mathbf{K}}] \Big|_{\mathbf{0}} \cong \sum_{\substack{\{i_1, \dots, i_n\} \\ \{e_1, \dots, e_m\}}} \begin{array}{ccc} e_1 & e_2 & e_m \\ \bullet & \bullet \dots \bullet & \bullet \\ \bullet & \bullet \dots \bullet & \bullet \\ i_1 & i_2 & i_n \end{array} . \quad (4.47)$$

Since we are considering the continuum limit, the sum over particle indices evaluates to N^{n+m} , and the indices turn into fixed particle labels as described in [Section 4.1](#). Henceforth, we will therefore discard the sum but retain the particle indices for bookkeeping, assigning the arguments (\mathbf{k}'_s, t'_s) to internal i_s and (\mathbf{k}_r, t_r) to external e_s particle labels.

4.3.3 Response field contractions

Each internal particle represents a density contained in an interaction operator. Consider the interaction operator due to the presence of a two-particle potential in KFT in terms of density and response fields

$$\hat{S}_I = - \int d1' \nu(1') \hat{\rho}(1') \hat{B}(-1'), \quad (4.48)$$

where we recall that the effect of response fields can be interpreted in terms of contractions with other operators. Response fields that contract to density modes identify their own particle label to that of their target, thus handing over their arguments to the particle representing the targeted density mode. In the interaction operator, a response field is paired with a density and a two-particle interaction potential, jointly representing a potential landscape that causes a deviation to the particle trajectory targeted by the response field. We thus define the interaction line

$$\begin{aligned} \overset{\bullet}{i_1} \longrightarrow \overset{\bullet}{e_1} &\cong -i \int d1' \nu(1') \hat{\rho}_{i_1}(1') \overbrace{\hat{B}(-1')} \hat{\rho}_{e_1}(1) Z_0[\underline{\mathbf{J}}, \underline{\mathbf{K}}] \Big|_0 \\ &= \int d1' f(1, -1') \hat{\rho}_{i_1}(1') \hat{\rho}_{e_1}(1, -1') Z_0[\underline{\mathbf{J}}, \underline{\mathbf{K}}] \Big|_0, \end{aligned} \quad (4.49)$$

to encode the perturbation of a density represented by e_1 . Recall that particle labels denote sums over all particles, such that the above expression represents a perturbation of all particles' trajectories due to interactions with all other particles which move along free trajectories. Therefore, the internal particle i_1 represents the entire freely evolving potential landscape that particle e_1 is moving through. Although the above example shows an external particle e_1 being targeted, targeting internal particles works in the same way.

Since contractions of response field operators follow a Leibniz rule, we need to represent the distinct contractions of all response field operators with internal and external density operators and other response field operators. In the two-particle toy model in Section 3.6, response fields were represented with empty circles, and their contractions were taken into account separately. We found that diagrams consisting of chains of response field operators and those where multiple interaction lines target the same external density lead to the respective resummation of the particle trajectory and the density.

Unlike in the toy model, the primary motivation for diagrams in cosmology lies in the need for an efficient way of encoding the perturbative corrections due to particle interactions. We would like to reduce the number of possible topologies as much as possible by collecting contributions from different contractions in a single class of diagrams. The question that poses itself is, which contributions should be collected together? To answer this question, we note that the shift tensors generated by a chain of response fields acting on a density field are identical to those where all the response fields of the chain directly contract to the density mode. Consider, for example, a chain of two response field operators acting on a density operator

$$\overbrace{\hat{B}(-1') \hat{B}(-2')} \hat{\rho}_{e_1}(1) Z_0[\underline{\mathbf{J}}, \underline{\mathbf{K}}] \Big|_0 = b(-2', -1') b(1, -2') \mathcal{Z}_0(\underline{\mathbf{L}}_q, \underline{\mathbf{L}}_p) \quad (4.50)$$

with $\underline{\mathbf{L}}_{q_{e_1}} = -\mathbf{k}_1 + \mathbf{k}'_1 + \mathbf{k}'_2$.

The momentum shift vector of particle e_1 follows directly from $\mathbf{L}_{q_{e_1}}$ by attaching particle propagators with the corresponding time argument to each wave vector. The shift vectors $\mathbf{L}_{q_{e_1}}$ and $\mathbf{L}_{p_{e_1}}$ have exactly the same components as those of the contraction

$$\overbrace{\hat{B}(-1')\hat{B}(-2')\hat{\rho}_{e_1}(1)Z_0[\mathbf{J}, \mathbf{K}]|_0} = b(1, -1')b(1, -2')\mathcal{Z}_0(\mathbf{L}_q, \mathbf{L}_p), \quad (4.51)$$

and thus, the only difference between both contributions lies in the response field prefactors. This leads us to define subdiagrams where two internal particles i_1, i_2 target the same particle e_1 by summing up both contributions (4.50) and (4.51)

$$\begin{array}{c} i_1 \\ \searrow \\ \bullet \\ \nearrow \\ i_2 \end{array} e_1 \cong \int d1' \int d2' [f(1, -1') + f(-2', -1')] [f(1, -2') + f(-1', -2')] \mathcal{Z}_0(\mathbf{L}_q, \mathbf{L}_p),$$

$$\text{with } \mathbf{L}_{q_{e_1}} = -\mathbf{k}_1 + \mathbf{k}'_1 + \mathbf{k}'_2, \quad \mathbf{L}_{q_{i_1}} = -\mathbf{k}'_1, \quad \mathbf{L}_{q_{i_2}} = -\mathbf{k}'_2. \quad (4.52)$$

Multiplying the two sums of force prefactors will result in three non-vanishing contributions, two of which correspond to chains of response field operators (4.50) and one to both response fields targeting the density operator (4.51). The product of the force prefactors $f(-2', -1')f(-1', -2') \propto \theta(t'_1 - t'_2)\theta(t'_2 - t'_1)$, corresponding to a closed chain of response field operators, vanishes due to causality. The same logic applies for a larger number of particles targeting e_1 , e. g.

$$\begin{array}{c} i_1 \\ \searrow \\ \bullet \\ \nearrow \\ i_2 \\ \nearrow \\ i_3 \end{array} e_1 = \int d1' \int d2' \int d3' [f(1, -1') + f(-2', -1') + f(-3', -1')] \\ \times [f(1, -2') + f(-1', -2') + f(-3', -2')] \\ \times [f(1, -3') + f(-1', -3') + f(-2', -3')] \\ \times \mathcal{Z}_0(\mathbf{L}_q, \mathbf{L}_p). \quad (4.53)$$

Identifying the contractions of response fields to other response fields with those between response fields and the target of other response fields has the significant advantage that the evaluation of both topologies in terms of initial correlations is identical. Additionally, the number of distinct diagram topologies reduces dramatically in this approach, making the evaluation much more efficient and less computationally intensive. As we will see in [Chapter 6](#), the number of terms that need to be evaluated at a given order in canonical perturbation theory is quite considerable and poses one of the main computational bottlenecks.

Notwithstanding the complications of contractions between response fields, the physical interpretation of interaction lines between particle nodes should be intuitively clear. The source node stands for a particle representing the density field which causes a potential that influences the trajectory of the target particle. Thus, each node represents the trajectory of a particle which is perturbed by interactions with other particles depending on how many interaction lines end in the respective node.

4.3.4 Rules for the construction and evaluation of diagrams

Construction

Diagrams corresponding to n -th order perturbation theory of an m -th order density correlation function are constructed by following a simple recipe

- Draw m nodes corresponding to external particles and label them with the external labels e_1, \dots, e_m . The arguments of the density modes being carried by the external particles are $(\mathbf{k}_1, t_1), \dots, (\mathbf{k}_m, t_m)$, respectively.
- Draw n nodes corresponding to internal particles and label them with the internal labels i_1, \dots, i_n . Thus, one internal node is drawn for each interaction operator. The arguments of the density modes carried by the internal particles are named $(\mathbf{k}'_1, t'_1), \dots, (\mathbf{k}'_m, t'_m)$, respectively. Due to the definition of the interaction operator, these arguments are integrated over.
- Response field contractions are marked by interaction lines pointing away from internal particles. Whereas each internal particle is the origin of precisely one interaction line, there is no limit on the number of interaction lines that can end in a node. All distinct configurations of interaction lines need to be drawn, giving rise to an increasing number of diagrams for higher orders in perturbation theory.
- Determine the multiplicity of the diagram. Multiplicities are constant numerical prefactors of diagrams reflecting that several interaction line configurations are equivalent. Since the arguments of internal nodes are integrated out, they are not distinguishable, and permutations among internal particle labels have to be considered for the multiplicity. If external modes are evaluated at the same time parameter, they are indistinguishable as well, and their permutations contribute to the multiplicity. However, if we do not consider synchronous correlation functions, targeting different external modes is not equivalent, and each configuration requires a distinct diagram. The multiplicity of a diagram corresponding to a perturbative correction to a synchronous correlation function is obtained by counting all permutations among internal as well as among external particle labels that lead to distinct graphs. For example, the multiplicities of the three diagrams in (4.55) are 2, 4 and 2, respectively. In the first diagram, swapping the two external indices leads to a distinct configuration, giving a factor 2. However, since the two internal indices play the same role (they both target the same node), permuting them results in the exact same graph and therefore does not increase the multiplicity. For the second diagram, both internal and external label permutations yield a factor 2, resulting in an overall multiplicity of 4. Permuting internal and external labels in the third diagram is equivalent, such that only one permutation counts, yielding an overall multiplicity of 2.

As a result of these rules, diagrams for the n -th order corrections of an m -point density functions are graphs with $n + m$ vertices and n directed edges. In terms of these diagrams, the first- and second-order corrections to a synchronous two-point function are

$$\delta^{(1)}G_{\rho\rho}(1,2) = 2N^3 \begin{array}{c} e_1 \quad e_2 \\ \diagdown \quad \cdot \\ \cdot \\ i_1 \end{array} \quad (4.54)$$

$$\delta^{(2)}G_{\rho\rho}(1,2) = N^4 \left(\begin{array}{c} e_1 \quad e_2 \\ \cdot \quad \cdot \\ \uparrow \quad \diagdown \\ i_1 \quad i_2 \end{array} + \begin{array}{c} e_1 \quad e_2 \\ \cdot \quad \cdot \\ \uparrow \quad \leftarrow \\ i_1 \quad i_2 \end{array} + \begin{array}{c} e_1 \quad e_2 \\ \cdot \quad \cdot \\ \uparrow \quad \uparrow \\ i_1 \quad i_2 \end{array} \right). \quad (4.55)$$

4.3.5 Including initial correlations

One of the primary motivations for the approach we followed when constructing our diagrams is to create a graphical language that can simultaneously represent the effect of initial correlations and particle interactions. The main underlying challenge comes from the fact that initial correlations naturally lead to a description in terms of microscopic particles, whereas the interaction operator is defined in terms of macroscopic quantities. We choose to work in a diagrammatic language that uses point particles as its fundamental building blocks, which comes at the cost of having a less straightforward representation of contractions among response fields. Initial correlations, on the other hand, can be included straightforwardly by drawing correlation lines between particle nodes. Since free correlation functions are naturally ordered in clusters of particles (4.31), diagrams are evaluated by drawing all configurations of initial correlation lines between particles up to a given number of lines. For example, at linear order in correlation lines (not in the initial power spectrum!), the first-order correction to a two-point function (4.54) formally has three contributions

$$\delta^{(1)}G_{\rho\rho}(1,2)\Big|_{1\text{-line}} = 2N^3 \left(\begin{array}{c} e_1 \quad e_2 \\ \diagdown \quad \diagup \\ i_1 \end{array} + \begin{array}{c} e_1 \quad e_2 \\ \diagdown \quad \diagup \\ i_1 \end{array} + \begin{array}{c} e_1 \quad e_2 \\ \text{---} \\ i_1 \end{array} \right). \quad (4.61)$$

The true power of the diagrammatic approach comes from the observations that (i) in a homogeneous system, the spatial shift vector of every particle which is not connected to other particles by a correlation line is set to zero, and that (ii) the spatial shift vector of every particle s which is not targeted by an interaction line contains only a single element $\mathbf{L}_{q_s} = -\mathbf{k}_s$. Consequently, *if a node is neither connected to a correlation line nor targeted by an interaction line, its corresponding wave-vector is set to zero, leading to a vanishing contribution to the correlation function*. In other words, diagrams are only non-vanishing if all particle nodes are either targeted by an interaction line or connected to a correlation line. As a consequence, among the three diagrams in (4.61), only the second one is non-vanishing and evaluates to

$$\begin{aligned} \delta^{(1)}G_{\rho\rho}(1,2)\Big|_{1\text{-line}} &= 2N^3 \begin{array}{c} e_1 \quad e_2 \\ \diagdown \quad \diagup \\ i_1 \end{array} \\ &= 2N^3 \int d\mathbf{l}' f(1, -1') (2\pi)^6 \delta_D(\mathbf{L}_{q_{e_1}}) \delta_D(\mathbf{L}_{q_{i_1}} + \mathbf{L}_{q_{e_2}}) \tilde{\mathcal{P}}_{i_1 e_2}(\mathbf{L}_{q_{i_1}}). \end{aligned} \quad (4.62)$$

Note that the presence of only connected nodes is a necessary but not a sufficient requirement for non-vanishing diagrams, i. e. there are configurations of correlation and interaction lines that lead to vanishing contributions even though they contain no isolated particle nodes. Nonetheless, we will make ample use of this fact to reduce the number of possible topologies of diagrams at a given order in perturbation theory and in correlation lines.

As a last remark for this section, the number of interaction arrows in a diagram directly corresponds to the number of time integrals in the resulting expression. The same is not valid for (non-trivial) wave-vector integrals since initial correlations provide Dirac-delta functions that trivially solve some integrals over wave vectors. Since correlation lines additionally provide \mathbf{k} -space integrals if evaluated beyond linear order in $P_\delta^{(i)}$, the

number of non-trivial wave-vector integrals depends on the order in the initial power spectrum at which the diagram is evaluated. For example, evaluating perturbations to a two-point function at quadratic order in $P_\delta^{(i)}$ will leave us with a single non-trivial \mathbf{k} -space integral at any order in the interaction.

4.4 PHASE-SPACE TRAJECTORIES IN AN EXPANDING UNIVERSE

4.4.1 *The Lagrangian of a particle in expanding space-time*

The dynamics of classical point particles in an expanding space-time with small scalar perturbations can be derived directly from general relativity. Although straightforward, the calculation is technical and rather lengthy, such that we shall state the result here and refer the interested reader to [Appendix F](#) for a detailed derivation. The final result is the Lagrangian of a point-particle in a gravitational potential

$$\mathcal{L}_t\left(\mathbf{q}, \frac{d\mathbf{q}}{dt}, t\right) = \frac{a^2}{2} \left(\frac{d\mathbf{q}}{dt}\right)^2 - \Phi(\mathbf{q}, t), \quad (4.63)$$

and a Poisson equation for the gravitational potential itself

$$\nabla^2 \Phi = 4\pi G a^2 \bar{\rho}_m \delta, \quad (4.64)$$

which is a valid, effective description for small gravitational potentials $\Phi/c^2 \ll 1$ at length scales far inside the Hubble horizon. Note that the mass of individual particles does not influence the overall dynamics of the system since particles only interact gravitationally.

For calculations of cosmic structure formation with SPT and LPT it proved helpful in [Section 2.4](#) to introduce a new time parameter in terms of the linear growth factor (2.22). We will perform the same transformation from cosmic time to $\tau = \ln D_+ / D_+^{(i)}$ in KFT for two reasons: (i) Using the approximation $\Omega_m / f^2 = 1$ we get a straightforward form for the particle propagator and (ii) we identified initial momentum $\mathbf{p}_a^{(i)}$ of particle a with the velocity field $\mathbf{u}(\mathbf{q}_a^{(i)}, \tau)$ in (4.6). This identity is only valid for the momentum \mathbf{p} that we will define in the next steps with the time coordinate τ . Invariance of the action under the transformation of the new time parameter τ results in the new Lagrangian

$$\mathcal{L}(\mathbf{q}, \dot{\mathbf{q}}, \tau) = \frac{a^2 H f}{2} \dot{\mathbf{q}}^2 - \frac{\Phi(\mathbf{q}, \tau)}{H f}, \quad (4.65)$$

where dots denote derivatives w. r. t. the time parameter τ and f is the growth rate.

4.4.2 *Hamiltonian and equations of motion*

Since KFT is formulated in phase-space we need a description of particle dynamics in terms of Hamilton's equations. A Legendre transform leads from (4.65) straight to the corresponding Hamiltonian

$$\mathcal{H}(\mathbf{q}, \mathbf{P}, \tau) = \dot{\mathbf{q}}(\mathbf{P}) \cdot \mathbf{P} - \mathcal{L}(\mathbf{q}, \dot{\mathbf{q}}(\mathbf{P}), \tau) = \frac{\mathbf{P}^2}{2a^2 H f} + \frac{\Phi(\mathbf{q}, \tau)}{H f}. \quad (4.66)$$

The resulting equations of motion in terms of the canonical momentum \mathbf{P}

$$\dot{\mathbf{q}} = \frac{\mathbf{P}}{a^2 H f} \quad (4.67)$$

$$\dot{\mathbf{P}} = -\frac{1}{H f} \nabla \Phi(\mathbf{q}, \eta), \quad (4.68)$$

pose an inconvenience due to the time-dependent factors appearing in the relation between the time derivative of the comoving coordinate \mathbf{q} and the canonical momentum. We, therefore, introduce the new momentum coordinate

$$\mathbf{p} := \frac{\mathbf{P}}{a^2 H f}. \quad (4.69)$$

Note that since this is not a canonical transformation, the resulting system of equations is no longer symplectic and cannot be traced back to a Hamiltonian $\mathcal{H}(\mathbf{q}, \mathbf{p})$. However, it can be shown that transforming from the canonical momentum \mathbf{P} to the new momentum \mathbf{p} in (4.67) leaves the path-integral measure in the generating functional (3.14) invariant, and therefore does not change the results, e. g. for density correlators, obtained in the framework of KFT. The e. o. m. for the new momentum variable can be derived from (4.68) in analogy to the calculation for the velocity field in Appendix A and reads

$$\dot{\mathbf{p}} = -\left(\frac{3}{2} \frac{\Omega_m}{f^2} - 1\right) \mathbf{p} - \frac{1}{a^2 H^2 f^2} \nabla \Phi(\mathbf{q}, \tau) = -\frac{\mu}{2} \mathbf{p} - \nabla \phi(\mathbf{q}, \tau), \quad (4.70)$$

where the potential $\phi(\mathbf{q}, \tau)$ fulfills the Poisson equation (2.25). The resulting equations of motion for a single particle in terms of the new momentum coordinate suggest a straightforward splitting into a free, linear part and an interacting, non-linear part:

$$\mathcal{E}_0[\mathbf{x}] = \begin{pmatrix} \dot{\mathbf{q}} \\ \dot{\mathbf{p}} \end{pmatrix} - \begin{pmatrix} 0_3 & \mathcal{I}_3 \\ 0_3 & -\frac{\mu}{2} \mathcal{I}_3 \end{pmatrix} \begin{pmatrix} \mathbf{q} \\ \mathbf{p} \end{pmatrix}, \quad \mathcal{E}_I[\mathbf{x}] = \begin{pmatrix} \mathbf{0} \\ \nabla \phi(\mathbf{q}, \tau) \end{pmatrix}. \quad (4.71)$$

Interestingly, due to space-time expansion, the free e. o. m. is equivalent to a particle moving against a time-dependent friction force (Hubble friction). In the second section of Appendix B we show that the Green's function solving (4.71) for $\mu = 1$ reads

$$\mathbf{G}(\tau, \tau') = \begin{pmatrix} \mathcal{I}_3 & g_{qp}(\tau, \tau') \mathcal{I}_3 \\ 0_3 & \dot{g}_{qp}(\tau, \tau') \mathcal{I}_3 \end{pmatrix} \theta(\tau - \tau'), \quad (4.72)$$

$$\text{with } g_{qp}(\tau, \tau') = 2(1 - e^{-\frac{1}{2}(\tau - \tau')}). \quad (4.73)$$

We will refer to the phase-space trajectories defined in terms of the particle propagator (4.73) as *Newtonian trajectories*.

For the interaction operator resulting from the non-linear e. o. m. in (4.71), the Fourier-space representation of the two-particle interaction potential arising from the collective potential $\phi(\mathbf{q}, \tau)$ needs to be determined. Since the collective potential fulfills the Poisson equation

$$\nabla^2 \phi(\mathbf{q}, \tau) = \frac{3}{2} \delta(\mathbf{q}, \tau), \quad (4.74)$$

going to Fourier space and inserting the definition of the density contrast in terms of the full density leads to

$$-k^2 \phi(\mathbf{k}, \tau) = \frac{3}{2\bar{\rho}} (\rho(\mathbf{k}, \tau) - \bar{\rho}). \quad (4.75)$$

The last term is proportional to the mean particle density and does not lead to a net force on phase-space trajectories in a homogeneous matter distribution. We can therefore drop it, finally arriving at

$$\phi(\mathbf{k}, \tau) = v(k)\rho(\mathbf{k}, \tau) \quad \text{with} \quad v(k) = -\frac{3}{2\bar{\rho}} \frac{1}{k^2}. \quad (4.76)$$

The inverse mean density in the two-particle potential appears because the actual source of gravity, the density contrast, is expressed in terms of the full particle density to incorporate the two-particle potential into the KFT interaction operator (3.64). As a consequence, applying an interaction operator increases the number of particles in the correlation function by one (best seen in the example 3.5.1), leading to an additional factor $\bar{\rho}$. This factor is exactly cancelled by the inverse mean density in the two-particle interaction potential, such that all perturbative corrections to an m -point function scale with $\bar{\rho}^m$.

4.4.3 Zel'dovich trajectories

Motivation: Free-streaming growth

Using the Green's function (4.72) and the knowledge from the previous section allows us to determine the free-streaming power spectrum in KFT

$$P_\delta(k_1, \tau_1) = \bar{\rho}^{-2} \int_{\mathbf{k}_2} \bar{G}_{\rho\rho}(1, 2) \Big|_{\tau_1=\tau_2}. \quad (4.77)$$

For now, let us consider the large-scale limit, where different density modes evolve independently, which is obtained by expanding the free two-point correlation function to linear order in $P_\delta^{(i)}$. Setting $\tau_1 = \tau_2$ in the free linearized two-point function (4.43) we obtain the free linear power spectrum

$$P_\delta^{(\text{LS, free})}(k_1, \tau_1) = (1 + g_{qp}(\tau_1, 0))^2 P_\delta^{(i)}(k_1). \quad (4.78)$$

Due to Hubble friction the particle propagator (4.73) is bounded from above by 2. As a consequence, the free-streaming amplitude of the power spectrum stays small for arbitrary times τ , in contrast to the expectation of large-scale linear growth from SPT and LPT, which scales like $e^{2\tau}$ in both the former and the latter. Unlike theories built upon hydrodynamics, KFT is seemingly incapable of reproducing linear growth without considerable effort. Using (4.73) as the particle propagator in KFT, it will turn out that we formally need an infinite resummation of interactions to reproduce the correct large-scale behaviour of the power spectrum. Considering the equations of motion (4.71), this apparent shortcoming of KFT should not come as a surprise since particle interactions due to gravity are entirely contained in the non-linear equations of motion while Hubble friction slows down the free motion of particles. This is in contrast to the solution of first-order LPT (2.41), which contains a contribution from the interaction potential, which is linear in the displacement field.

Equations of motion and particle propagator

The lack of large-scale growth in the free-streaming solution is not a problem of KFT itself but rather shows that we might not be working with the best possible splitting of the equations of motion. Luckily, as we have stressed previously, the splitting of $\underline{\mathcal{E}}[\mathbf{x}]$ is

largely arbitrary and can be chosen such as to fit our needs best. To find the splitting that will reproduce the correct large-scale growth of structures at the level of free-streaming we take a page out of the LPT book. In the first-order equation for the displacement field (2.41), the term stemming from the gravitational potential fulfills (for $\mu = 1$)

$$\nabla^2 \phi^{(Z)}(\mathbf{q}, \tau) = \frac{3}{2} e^{\tau} \delta^{(i)}(\mathbf{q}). \quad (4.79)$$

We will refer to this as the Zel'dovich potential henceforth. It follows from the definition of the linear displacement field in terms of the initial velocity potential (A.16) and the relation between initial density and initial velocity potential (2.28). Note that the conceptual similarity of KFT and LPT allows us to transfer quantities from one to the other straightforwardly; e. g. initial particle positions in KFT correspond directly to the Lagrangian coordinates of LPT. Using this knowledge, we rewrite the equations of motion to

$$\mathcal{E}_0^{(Z)}[\mathbf{x}] = \begin{pmatrix} \dot{\mathbf{q}} \\ \dot{\mathbf{p}} \end{pmatrix} - \begin{pmatrix} 0_3 & \mathcal{I}_3 \\ 0_3 & -\frac{\mu}{2} \mathcal{I}_3 \end{pmatrix} \begin{pmatrix} \mathbf{q} \\ \mathbf{p} \end{pmatrix} + \begin{pmatrix} \mathbf{0} \\ \nabla \phi^{(Z)}(\mathbf{q}^{(i)}, \tau) \end{pmatrix}, \quad (4.80)$$

$$\mathcal{E}_I^{(Z)}[\mathbf{x}] = \begin{pmatrix} \mathbf{0} \\ \nabla \phi(\mathbf{q}, \tau) - \nabla \phi^{(Z)}(\mathbf{q}^{(i)}, \tau) \end{pmatrix}, \quad (4.81)$$

where $\mathbf{q}^{(i)}$ is the initial position of the phase-space trajectory $\mathbf{x}(\tau)$. $\nabla \phi^{(Z)}(\mathbf{q}^{(i)}, \tau)$ is to be understood as a shorthand notation for taking the gradient of the scalar field $\phi^{(Z)}$ and evaluating it at the initial position of the trajectory $\mathbf{x}(\tau)$. Notwithstanding that the first-order LPT solution suggests the choice of the Zel'dovich potential, it might seem unusual to add an inhomogeneity to a differential equation defined in terms of the initial conditions we impose on the solution. Indeed, this rather awkward form of the free equations of motion is reminiscent of the fact that Zel'dovich trajectories do not come naturally to KFT and that introducing them by hand is connected to a loss of intuition about the physical meaning of free trajectories and deviations from them. This will also be reflected in the rather peculiar expression for the operator, which compensates for the effect of imposing free Zel'dovich motion. Nonetheless, from a mathematical point of view, pulling the Zel'dovich potential into the free equation of motion (4.80) is perfectly legitimate, as it merely corresponds to a time-dependent inhomogeneity in the momentum equation. Although we refer to it as such, the Zel'dovich potential is not a potential in the usual sense of particle interactions but rather represents a local, single-particle effect, in exactly the same way as the Zel'dovich approximation in LPT being a local approximation. For want of a clear physical interpretation at the level of individual particles, Zel'dovich trajectories in KFT should therefore be regarded mainly as a mathematical trick that leans on physical intuition from a different theory (LPT) and, as we will show in Chapter 6, improves the convergence of perturbation theory.

In the third part of Appendix B we show that including the Zel'dovich potential into the free trajectories results in

$$\mathbf{x}[\mathbf{K}, \tau] = \mathbf{G}^{(Z)}(\tau, 0) \mathbf{x}^{(i)} - \int d\bar{\tau} \mathbf{G}(\tau, \bar{\tau}) \mathbf{K}(\bar{\tau}). \quad (4.82)$$

Whereas the inhomogeneous term still contains the Green's function (4.72), the free evolution of the initial conditions is governed by

$$\mathbf{G}^{(Z)}(\tau, 0) = \begin{pmatrix} \mathcal{I}_3 & g_{qp}^{(Z)}(\tau, 0) \mathcal{I}_3 \\ 0_3 & \dot{g}_{qp}^{(Z)}(\tau, 0) \mathcal{I}_3 \end{pmatrix}, \quad \text{with} \quad g_{qp}^{(Z)}(\tau, 0) = e^{\tau} - 1. \quad (4.83)$$

The free part of (4.82) defines what we will refer to as *Zel'dovich trajectories*. As expected, using free Zel'dovich trajectories in the generating functional to calculate a free two-point function results in the correct large-scale growth behaviour of the power spectrum since

$$P_{\delta}^{(\text{LS, free, Z})}(k_1, \tau_1) = (1 + g_{qp}^{(Z)}(\tau_1, 0))^2 P_{\delta}^{(i)}(k_1) = D_+^2(t_1) P_{\delta}^{(i)}(k_1). \quad (4.84)$$

The non-linear part of the e. o. m. (4.81), which will give rise to the interaction operator, describes deviations of the gravitational potential from the Zel'dovich potential. Since the latter is an excellent approximation for particle interactions evaluated on large scales, we should expect deviations from it to lead to smaller corrections than the original gravitational potential. In this sense, we expect KFT perturbation theory to converge more quickly when employing Zel'dovich trajectories than Newtonian trajectories.

We achieved this at the price of dealing with an additional component in the non-linear part of the e. o. m. (4.81). Currently, there are two approaches one can follow to evaluate the resulting interaction operator:

- One can attempt to approximate the two-particle interaction potential corresponding to $\phi(\mathbf{q}, \tau) - \phi^{(Z)}(\mathbf{q}^{(i)}, \tau)$. Such a construction proves tricky since both potentials are evaluated at different positions and because the transition from the collective potential $\phi(\mathbf{q}, \tau) - \phi^{(Z)}(\mathbf{q}^{(i)}, \tau)$ to the corresponding two-particle potential is not straightforward. On top of that, we have noted that the Zel'dovich potential is not a particle interaction potential in the usual sense. However, intuitive reasoning suggests that the resulting two-particle potential should roughly follow a Yukawa-like shape

$$v(1') \approx -\frac{3}{2\bar{\rho}} \frac{1}{k_1'^2 + k_0^2(\tau_1')}. \quad (4.85)$$

As of now, there is no mathematically rigorous derivation of this statement, however. Although the description of interactions between particles moving along Zel'dovich trajectories has already been successfully applied to KFT in the context of mean-field theory [49], many open questions remain in this approach. In particular, the derivation of the Yukawa cutoff $k_0^2(au_1)$ from fundamental principles has yet to be achieved. The Yukawa cutoff can, therefore, either be regarded as a free parameter of the theory or one can attempt to determine it in a self-consistent, iterative way from KFT itself such as in [49, 50]. Since the final aim of KFT is to provide a parameter-free description of cosmic structure formation from first principles, more work is needed to better understand this ansatz.

- A different approach is to evaluate both potentials in (4.81) as two separate interaction operators, thus staying closer to the initial formalism of KFT where perturbations to particle trajectories are applied to the free generating functional in operator form. The two resulting operators show a very different structure and collude in surprising ways, e. g. to guarantee the correct linear growth of the power spectrum. As we will see, however, a downside of this approach is that the operator resulting from the Zel'dovich potential allows for little physical insight.

Compensating for Zel'dovich trajectories: the counter-operator

If we want to follow the second approach, we need to derive an expression for the operator that the Zel'dovich potential gives rise to in (4.81). The full interaction operator perturbing particles which move along free Zel'dovich trajectories is

$$i\Delta\hat{S}_I = \left(i\hat{\chi}_p \cdot \nabla \hat{\phi} \right) - \left(i\hat{\chi}_p \cdot \nabla \hat{\phi}^{(Z)} \Big|_{\mathbf{q}^{(i)}} \right) =: i\hat{S}_I + i\hat{S}_C, \quad (4.86)$$

where we identified the unchanged particle interaction operator \hat{S}_I (3.18) and the *counter* operator \hat{S}_C . Using the relation between initial density, initial momentum and the velocity potential (4.2) allows us to express the gradient of the Zel'dovich potential in terms of the initial momentum of the corresponding phase-space trajectory:

$$\nabla \phi^{(Z)}(\mathbf{q}^{(i)}, \tau) = -\frac{3}{2} e^\tau \nabla \psi^{(i)}(\mathbf{q}^{(i)}) = -\frac{3}{2} e^\tau \mathbf{p}^{(i)}. \quad (4.87)$$

This identity leads to the expression for the counter-operator

$$i\hat{S}_C = i \frac{3}{2} \int d\tau'_1 e^{\tau'_1} \sum_{a=1}^N \left(\frac{\delta}{i\delta \mathbf{K}_{p_a}(\tau'_1)} \cdot \hat{\mathbf{p}}_a^{(i)} \right), \quad (4.88)$$

where $\hat{\mathbf{p}}_a^{(i)}$ is the operator that extracts the initial momentum of particle a from the generating functional. In Appendix E, it is shown that the counter-operator can be formulated simply as a sum of derivatives acting on the free correlation function

$$i\hat{S}_C Z_0[\underline{\mathbf{J}} + \underline{\mathbf{L}}, \underline{\mathbf{K}}] \Big|_{\mathbf{0}} = \left(\Delta \underline{\mathbf{L}}_p \cdot \frac{\partial}{\partial \underline{\mathbf{L}}_p^{(Z)}} \right) \mathcal{Z}_0(\underline{\mathbf{L}}_{q'}, \underline{\mathbf{L}}_p^{(Z)}), \quad (4.89)$$

$$\text{where} \quad \Delta \underline{\mathbf{L}}_p = \underline{\mathbf{L}}_p^{(N)} - \underline{\mathbf{L}}_p^{(Z)}. \quad (4.90)$$

For clarity, we have explicitly marked the momentum shift tensors $\underline{\mathbf{L}}_p^{(N)}$ and $\underline{\mathbf{L}}_p^{(Z)}$ which are defined with Newtonian and Zel'dovich particle propagators, respectively. To understand what this operator is doing, consider the full generating functional for particles moving along free Zel'dovich trajectories. The interaction operator compensating for the free particle motion is then given by (4.86), such that

$$Z[\underline{\mathbf{J}}, \underline{\mathbf{K}}] = e^{i\Delta\hat{S}_I} Z_0[\underline{\mathbf{J}}, \underline{\mathbf{K}}] = e^{i\hat{S}_C} e^{i\hat{S}_I} Z_0[\underline{\mathbf{J}}, \underline{\mathbf{K}}]. \quad (4.91)$$

Note that, although we do not mark it explicitly, the free generating functionals with Newtonian and Zel'dovich trajectories are different from each other since they contain distinct definitions of inertial motion. Let us now set the physical interaction potential contained in \hat{S}_I to zero to calculate a free m -point function

$$\begin{aligned} \hat{\rho}(1) \dots \hat{\rho}(m) e^{i\hat{S}_C} Z_0[\underline{\mathbf{J}}, \underline{\mathbf{K}}] \Big|_{\mathbf{0}} &= \exp \left(\Delta \underline{\mathbf{L}}_p \cdot \frac{\partial}{\partial \underline{\mathbf{L}}_p^{(Z)}} \right) \mathcal{Z}_0(\underline{\mathbf{L}}_{q'}, \underline{\mathbf{L}}_p^{(Z)}) \\ &= \mathcal{Z}_0(\underline{\mathbf{L}}_{q'}, \underline{\mathbf{L}}_p^{(Z)} + \Delta \underline{\mathbf{L}}_p) \\ &= \mathcal{Z}_0(\underline{\mathbf{L}}_{q'}, \underline{\mathbf{L}}_p^{(N)}). \end{aligned} \quad (4.92)$$

As expected, the exponential of the counter-operator thus replaces all Zel'dovich particle propagators in the momentum shift vectors by Newtonian particle propagators. Applying the full exponential form of \hat{S}_C thus brings us exactly back to where we started,

namely to free Newtonian particle trajectories. When we calculate perturbative corrections to correlation functions with Zel'dovich trajectories, we expand the full interaction operator $i\Delta\hat{S}_I$, which will contain contributions from particle interactions and the counter-operator. For a fixed order n in perturbation theory, we thus need to evaluate terms of the form

$$\sum_{r=1}^n \frac{1}{r!} (i\hat{S}_C)^r \frac{1}{(n-r)!} (i\hat{S}_I)^{n-r} Z_0[\underline{\mathbf{J}}, \underline{\mathbf{K}}], \quad (4.93)$$

which is allowed since the counter-operator (4.88) and the particle interaction operator commute. Practically, we, hence, evaluate the full interaction operator by first applying the particle interaction operators to the free generating functional, setting the source fields $\underline{\mathbf{J}}$ and $\underline{\mathbf{K}}$ to zero and applying the counter-operator in the form of (4.89) to the resulting free correlation function.

4.5 THE KFT POWER SPECTRUM IN THE ZEL'DOVICH APPROXIMATION

To wrap up the discussion on evaluating cosmic correlation functions with KFT, let us compute the free two-point function in the Zel'dovich approximation. We have shown in example 4.2.1 that the large-scale growth of a free two-point function is given by

$$\bar{G}_{\rho\rho}^{(1)}(1, 2) = \bar{\rho}^2 \delta_D(\mathbf{k}_1 + \mathbf{k}_2) (1 + g_{qp}(\tau_1, 0)) (1 + g_{qp}(\tau_2, 0)) P_\delta^{(i)}(k_1), \quad (4.94)$$

which is obtained by applying two density operators to the free generating functional and expanding the resulting initial correlation lines to linear order in the initial power spectrum. Evaluating the amplitude at $\tau_1 = \tau_2 = \tau_{\text{today}}$ and assuming Zel'dovich propagators, $g_{qp}(\tau_{\text{today}}, 0) \approx 850$ such that we can safely approximate

$$(1 + g_{qp}(\tau_{\text{today}}, 0))^2 \approx g_{qp}^2(\tau_{\text{today}}, 0). \quad (4.95)$$

This approximation is equivalent to neglecting all but momentum correlation lines when deriving the large-scale limit of the two-point function; since momentum correlations evolve with the square of the particle propagator, they quickly dominate over the other initial correlations for unbounded motion, such as Zel'dovich trajectories. In terms of the full momentum correlation line, the synchronous two-point function at time τ reads

$$\begin{aligned} \bar{G}_{\rho\rho}^{(Z)}(\mathbf{k}, \tau) \Big|_{p\text{-line only}} &= \bar{\rho}^2 \delta_D(\mathbf{k} + \mathbf{k}') e^{Q_D} \int_{\Delta\mathbf{q}^{(i)}} \left(e^{T^2 \mathbf{k}^T \mathbf{C}^{pp}(\Delta\mathbf{q}^{(i)}) \mathbf{k}} - 1 \right) e^{-i\mathbf{k} \cdot \Delta\mathbf{q}^{(i)}} \\ &=: \bar{\rho}^2 \delta_D(\mathbf{k} + \mathbf{k}') P_\delta^{(Z, \text{KFT})}(k, \tau), \end{aligned} \quad (4.96)$$

where we introduced the abbreviation $T := g_{qp}^{(Z)}(\tau, 0) = D_+ - 1$. The resulting power spectrum is formally identical to the expression that is obtained from the first-order solution of LPT

$$P_\delta^{(Z, \text{LPT})}(k) = e^{-\sigma_\Psi^2 k^2} \int_{\Delta\mathbf{q}^{(i)}} \left(e^{\mathbf{k}^T \mathbf{C}_{\Psi\Psi}(\Delta\mathbf{q}^{(i)}) \mathbf{k}} - 1 \right) e^{-i\mathbf{k} \cdot \Delta\mathbf{q}^{(i)}} \quad (4.97)$$

$$\text{with} \quad \mathbf{C}_{\Psi\Psi}(\Delta\mathbf{q}^{(i)}) = D_+^2 \int_{\mathbf{k}'} \frac{\mathbf{k}' \otimes \mathbf{k}'}{k'^4} P_\delta^{(i)}(k') e^{i\mathbf{k}' \cdot \Delta\mathbf{q}^{(i)}}, \quad (4.98)$$

except for the factor 1, which is missing in the time-evolution in the exponent. We recall that KFT gives formal expressions for perturbative corrections to the power spectrum in terms of correlation lines which contain the full hierarchy of initial correlations. On

the other hand, LPT can express the power spectrum in terms of this hierarchy only in the Zel'dovich approximation, whereas the evaluation of higher-order corrections to the displacement field requires a perturbative expansion of (A.15). In this sense, KFT can be considered a systematic extension of LPT that achieves the calculation of density spectra with perturbed particle trajectories without expanding the initial power spectrum, at least at the formal level. Unfortunately, the resulting expressions in terms of the full correlation lines are tough to evaluate numerically since the kernels of the resulting integrals are rapidly oscillating. These computational challenges render a systematic evaluation of correlation functions in KFT extremely problematic. Although the similarity between both expressions for the power spectrum is a nice illustration of the parallels between KFT and LPT, it does leave some open questions. Whereas the correct linear growth behaviour is obtained straightforwardly in the large-scale limit by accounting for all initial correlations between phase-space positions, it is yet to be clarified how the full expression of the free-streaming KFT power spectrum is related to the first-order LPT result. Although the momentum correlation line is extremely close to the LPT result, both results are not precisely equal, and so far, it was not possible to show whether including density-density and density-momentum correlation lines leads to $D_+ - 1 \rightarrow D_+$ beyond the large-scale limit.

4.6 DISCUSSION

The initial conditions and particle trajectories are the two primary components that we need to specify to apply KFT to cosmic structure formation. The probability density of the initial phase-space positions can be derived via Poisson sampling from the density and velocity fields, which follow Gaussian statistics initially. The resulting probability density is expressed in initial density-density, density-momentum, and momentum-momentum correlations between pairs of initial positions. Representing initial correlations graphically in terms of correlation lines, we then derived an expression for the initial probability density that we explicitly ordered in the number of correlation lines. For practical reasons, we limit our discussion to quadratic contributions in the correlation lines. However, it is formally clear how to generalize to higher orders—although evaluating KFT correlation functions at cubic or higher order in the initial correlation lines is an entirely different story. Since each line connects two initial particle positions, going up to quadratic order in the correlation lines results in expression with two-, three- and four-particle contributions (single particle contributions leading to trivial Dirac-deltas), as illustrated in (4.25). Note that, unlike m -point cumulants, which exclusively contain connected contributions from initial correlations between m particle positions, correlation functions in KFT contain sums of all contributions from initial correlations between up to m particles. Canonical perturbation theory is therefore not ordered in initial correlations (unlike perturbation theory in rKFT where one-loop corrections contain all terms with two initial correlation lines), so every order in the S_I -expansion contains quadratic contributions in $P_\delta^{(i)}$. Since we cannot numerically evaluate the full correlation line (4.30) yet, we are forced to expand KFT correlation functions in orders of the initial power spectrum if we wish to arrive at quantitative results. In (4.36) and (4.37), we have summarized the expressions for a general KFT correlation function at linear and quadratic order in $P_\delta^{(i)}$.

To specify particle trajectories in an expanding universe, we started with the Lagrangian of a single particle in comoving coordinates, which can be straightforwardly

obtained from the weak-field limit of a relativistic action. Changing the time parameter to τ (2.22) and introducing a new momentum¹ variable then leads us to Hamilton's equations (4.71) which define the Green's function for Newtonian trajectories. Since cosmic expansion leads to an effective friction term in the equations of motion, the particle propagator $g_{qp}(\tau, \tau')$ is bounded from above, and consequently, the large-scale growth of the dark matter power spectrum from free particle trajectories is much smaller than the expected result. Effectively, this suggests that microscopic particle interactions play a vital role in structure growth even on large scales, where the evolution of density modes follows the linearized hydrodynamical equations. Consequently, a perturbative expansion of the interaction operator should not be expected to converge quickly toward the physical result. If we wish to stick to canonical perturbation theory, this is a solid argument to consider modifications of particle trajectories to force KFT to produce the correct linear growth behaviour already at the level of free-streaming. Drawing inspiration from LPT, we introduce the Zel'dovich potential (4.79) to alter the splitting of the equations of motion (4.80) and (4.81). As a result, the interaction operator gains an additional term, which we refer to as the counter-operator (4.88). Perturbation theory now consists in a consistent expansion of the full interaction operator $i\Delta\hat{S}_I = i\hat{S}_I + i\hat{S}_C$ which is small at least on intermediate if not small scales by construction. There is no straightforward physical interpretation of the counter-operator in terms of particle-based quantities. The fact that large-scale growth of cosmic structures is not automatically built into the free theory as for SPT and LPT is an interesting feature of KFT. Indeed, attempting to derive a formulation of LPT that does not break down at stream-crossing automatically results in equations of motion for the displacement field that show the same peculiarity, and one is forced to introduce the correct linear growth behaviour by hand [35].

¹ The new momentum coordinate \mathbf{p} is defined analogously to the velocity field $\mathbf{u}(\mathbf{q}, \tau)$ in SPT which, in hindsight, motivates the assumption that initial momenta are sampled by precisely tracing the initial velocity field from SPT.

Part II

RESULTS

ANALYTICAL RESULTS FOR THE TWO-POINT FUNCTION

5.1 LINEAR GROWTH FROM NEWTONIAN TRAJECTORIES

Whereas in SPT and LPT, the large-scale behaviour of the power spectrum (linear growth) is entirely contained in the first-order solution to the respective equations of motion, the derivation of linear growth from microscopic KFT requires more work. Since the Newtonian particle propagator is bounded from above, the large-scale result of KFT from free particle trajectories shows a much smaller amplitude than expected for linear growth. To obtain the correct large-scale amplitude of the power spectrum from Newtonian particle trajectories, we do need to consider particle interactions, but we do not need to evaluate the KFT two-point function $G_{\rho\rho}(1,2)$ in its full glory. Rather the two-point function is evaluated at linear order in the initial power spectrum

$$G_{\rho\rho}^{(N,1)}(1,2) = \sum_{n=0}^{\infty} \left[\frac{1}{n!} (i\hat{S}_I)^n \hat{\rho}(1)\hat{\rho}(2) Z_0[\underline{\mathbf{J}}, \underline{\mathbf{K}}] \Big|_0 \right]^{(1)} = \sum_{n=0}^{\infty} \delta^{(n)} G_{\rho\rho}^{(N,1)}(1,2). \quad (5.1)$$

Here $[\dots]^{(1)}$ signifies that the contained expression is to be evaluated only up to order one in $P_\delta^{(i)}$, and we used the notation $\delta^{(n)} G_{\rho\rho}^{(N,1)}(1,2)$ for the n -th order correction to the free two-point function evaluated at linear order in the initial power spectrum. Since the complicated initial conditions pose the biggest challenge in KFT, discarding order two and higher terms in the initial power spectrum is an enormous simplification. To keep the discussion as general as possible, we do not restrict ourselves to the case of synchronous two-point functions but rather keep τ_1 and τ_2 independent.

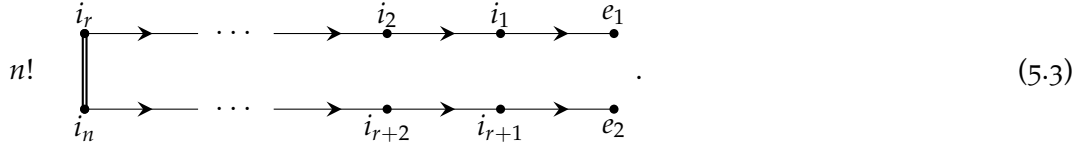
5.1.1 Non-vanishing diagrams

To evaluate the linearized two-point function, we will derive an expression for the n -th order term in the perturbative expansion of (5.1)

$$\delta^{(n)} G_{\rho\rho}^{(N,1)}(1,2) = \frac{1}{n!} \sum_{\text{diagr.}} \int d1' \dots \int dn' f(c_1, -1') \dots f(c_n, -n') N^{n+2} \mathcal{Z}_0^{(1)}(\underline{\mathbf{L}}_q, \underline{\mathbf{L}}_p), \quad (5.2)$$

where $\mathcal{Z}_0^{(1)}(\underline{\mathbf{L}}_q, \underline{\mathbf{L}}_p)$ is the general correlation function evaluated at linear order in $P_\delta^{(i)}$. Formally, the sum runs over all diagrams generated for n -th order perturbation theory, i. e. all contractions of response fields. Since we are interested in linear growth, however, we only have a single correlation line at our disposal in the diagrams. Recalling that diagrams containing particle nodes that are neither targeted by interaction lines nor part of a correlation line are vanishing, the presence of only a single correlation line

drastically reduces the number of relevant diagrams at linear order in $P_\delta^{(i)}$. Diagrams corresponding to n -th order corrections to a two-point function contain $n + 2$ nodes (n internal and 2 external) and n interaction lines. For a diagram to result in a non-vanishing configuration, each interaction line, therefore, has to connect to a different node, leaving two untargeted particle nodes, which then have to be connected by a correlation line. As a result, interaction lines form chains of length r and $n - r$, where $r \in \{0, \dots, n\}$, which end in the two external nodes. These arguments yield a single allowed topology for non-vanishing diagrams, parametrized by the length r of the chain connecting to particle e_1 :



The multiplicity of the diagram is $n!$, corresponding to the number of distinct permutations among internal labels. Since both external nodes can carry different time parameters τ_1 and τ_2 , we treat them as distinguishable nodes. For the particular values $r = 0, n$ where one of the chains has length zero, the external node that is not targeted must be correlated with the first internal node of the chain i_n . The free correlation function corresponding to (5.3) reads

$$\mathcal{Z}_0^{(1)}(\underline{\mathbf{L}}_q, \underline{\mathbf{L}}_p) = V^{-n-2} \Delta_{i_r i_n} (2\pi)^3 \delta_D(\mathbf{L}_{q_{i_r}} + \mathbf{L}_{q_{i_n}}) \tilde{\mathcal{P}}_{i_r i_n}^{(1)}(\mathbf{L}_{q_{i_r}}), \quad (5.4)$$

where we recall that $\Delta_{i_r i_n}$ is a product of Dirac-deltas of all spatial shift-vectors except for $\mathbf{L}_{q_{i_r}}$ and $\mathbf{L}_{q_{i_n}}$. For the linearized two-point function (5.1), the n -th order perturbative correction is found by summing (5.3) over all chain lengths r resulting in

$$\begin{aligned} \delta^{(n)} G_{\rho\rho}^{(N,1)}(1, 2) &= \sum_{r=0}^n \int d1' \dots \int dn' f(1, -1') f(1', -2') \dots f((r-1)', -r') \\ &\quad \times f(2, -(r+1)') f((r+1)', -(r+2)') \dots f((n-1)', -n') \quad (5.5) \\ &\quad \times N^{n+2} \mathcal{Z}_0^{(1)}(\underline{\mathbf{L}}_q, \underline{\mathbf{L}}_p), \end{aligned}$$

where the multiplicity $n!$ of each diagram exactly cancelled the prefactor from the exponential series. The first and second lines contain the force prefactors that form the chain to the external nodes e_1 and e_2 , respectively, whereas the third line contains the information on particle correlations. The physical interpretation of (5.3) is quite straightforward: We start with two initially correlated (representative) particles, each of which evolves along a free phase-space trajectory and perturbs the trajectory of another particle. This particle then propagates on its perturbed trajectory and perturbs another particle, and so on, until the chain reaches the two particles which represent the external density modes. This process imprints the initial phase-space correlations between the two particles at the chain's origin onto the external particles. Interestingly, due to the extremely restricted topology of diagrams with a single correlation line, initial correlations between the two external particles play no role at this order in the initial power spectrum.

5.1.2 Evaluation of non-vanishing diagrams

The key to evaluating (5.5) is the free correlation function $\mathcal{Z}_0^{(1)}(\underline{\mathbf{L}}_q, \underline{\mathbf{L}}_p)$, whose spatial shift vectors can be read off the diagram in (5.3):

$$\begin{aligned}
 \mathbf{L}_{qe_1} &= -\mathbf{k}_1 + \mathbf{k}'_1 & \mathbf{L}_{qe_2} &= -\mathbf{k}_2 + \mathbf{k}'_{r+1} \\
 \mathbf{L}_{qi_1} &= -\mathbf{k}'_1 + \mathbf{k}'_2 & \mathbf{L}_{qi_{r+1}} &= -\mathbf{k}'_{r+1} + \mathbf{k}'_{r+2} \\
 \mathbf{L}_{qi_2} &= -\mathbf{k}'_2 + \mathbf{k}'_3 & \mathbf{L}_{qi_{r+2}} &= -\mathbf{k}'_{r+2} + \mathbf{k}'_{r+3} \\
 &\vdots & &\vdots \\
 \mathbf{L}_{qi_{r-1}} &= -\mathbf{k}'_{r-1} + \mathbf{k}'_r & \mathbf{L}_{qi_{n-1}} &= -\mathbf{k}'_{n-1} + \mathbf{k}'_n \\
 \mathbf{L}_{qi_r} &= -\mathbf{k}'_r & \mathbf{L}_{qi_n} &= -\mathbf{k}'_n.
 \end{aligned} \tag{5.6}$$

These identities turn the product of the Dirac-deltas of spatial shift vectors in (5.4) into the following

$$\begin{aligned}
 \mathcal{Z}_0^{(1)}(\underline{\mathbf{L}}_q, \underline{\mathbf{L}}_p) &= \frac{(2\pi)^{3n}}{V^{n+2}} \left[\delta_D(\mathbf{k}_1 - \mathbf{k}'_1) \dots \delta_D(\mathbf{k}'_{r-1} - \mathbf{k}'_r) \right] \\
 &\quad \cdot \left[\delta_D(\mathbf{k}_2 - \mathbf{k}'_{r+1}) \dots \delta_D(\mathbf{k}'_{n-1} - \mathbf{k}'_n) \right] (2\pi)^3 \delta_D(\mathbf{k}'_r + \mathbf{k}'_n) \tilde{\mathcal{P}}_{i_r i_n}^{(1)}(\mathbf{L}_{q_{i_r}}),
 \end{aligned} \tag{5.7}$$

where the Dirac-delta distributions were ordered into the two chains, respectively ending in the nodes e_1 carrying the wave-vector \mathbf{k}_1 and e_2 carrying \mathbf{k}_2 . The integration over internal wave-vectors in (5.5) then trivially results in setting all wave-vectors belonging to the first chain to \mathbf{k}_1 and those belonging to the second chain to \mathbf{k}_2 . In particular, this means that $\mathbf{k}'_r = \mathbf{k}_1$ and $\mathbf{k}'_n = \mathbf{k}_2$, and with the Dirac-delta in the second line forcing both external wave vectors to be antiparallel, the correlation lines evaluate to

$$\tilde{\mathcal{P}}_{i_r i_n}^{(1)}(\mathbf{L}_{q_{i_r}}) = (1 + g_{r'}) (1 + g_{n'}) P_\delta^{(i)}(k_1), \tag{5.8}$$

where we have introduced the shorthand notation $g_{r'} := g_{qp}(\tau'_r, 0)$. Recall that force prefactors in (5.5) read

$$f(c, -d) = -\frac{3}{2\bar{\rho}} \frac{(-\mathbf{k}_c \cdot \mathbf{k}_d)}{k_d^2} g_{qp}(\tau_c, \tau_d) \theta(\tau_c - \tau_d), \tag{5.9}$$

By construction, their wave-vector arguments coincide with those of the pairs of wave-vectors that the Dirac-deltas identify in (5.7), such that upon integration over the wave-vectors each force prefactor becomes

$$f(c, -d) = \frac{3}{2\bar{\rho}} g_{c,d} \theta(\tau_c - \tau_d) =: \frac{1}{\bar{\rho}} \theta(\tau_c - \tau_d) f_{c,d}, \tag{5.10}$$

where we have collected the constant amplitude of the two-particle interaction potential and the time-dependent particle propagator in $f_{c,d}$. Now that the internal wave vectors in (5.5) have been integrated out, we are left with n time integrals, which organize into two independent chains of nested integrals. We define the chain of length r by collecting all time-dependent functions

$$C_r(\tau_1) := \int_0^{\tau_1} d\tau'_1 f_{1,1'} \int_0^{\tau'_1} d\tau'_2 f_{1',2'} \dots \int_0^{\tau'_{r-1}} d\tau'_r f_{(r-1)',r'} (1 + g_{r'}), \tag{5.11}$$

$$C_0(\tau_1) := (1 + g_1), \tag{5.12}$$

where the integration bounds follow from the time-dependent step functions in the force prefactors (5.10). In this case, the expression for the chain of length zero only contains the contribution from the correlation line, which attaches to the external particle. The product of particle densities in the denominator of (5.10) results in an overall factor $\bar{\rho}^{-n}$, which is cancelled by the combined volume and particle number factors from the free correlation function. The overall result thus scales with $\bar{\rho}^2$ for each perturbation order n . Collecting all the results yields the final expression for the n -th order correction of the linearized two-point function (5.5), expressed in terms of the nested time integrals (5.11)

$$\delta^{(n)} G_{\rho\rho}^{(N,1)}(1,2) = \bar{\rho}^2 (2\pi)^3 \delta_D(\mathbf{k}_1 + \mathbf{k}_2) \left(\sum_{r=0}^n C_r(\tau_1) C_{n-r}(\tau_2) \right) P_\delta^{(i)}(k_1). \quad (5.13)$$

As expected, perturbations amount to a time-dependent scaling of the initial power spectrum. This result emphasizes that particle interactions in KFT do not inherently lead to mode-coupling; rather, the transfer of power between different scales is obtained at every order in perturbation theory by considering contribution from higher orders in the initial power spectrum $P_\delta^{(i)}$. To obtain the final result for the two-point function, we sum up all perturbation orders, resulting in an overall time-dependent amplitude

$$\begin{aligned} G_{\rho\rho}^{(N,1)}(1,2) &= \bar{\rho}^2 (2\pi)^3 \delta_D(\mathbf{k}_1 + \mathbf{k}_2) \left(\sum_{n=0}^{\infty} \sum_{r=0}^n C_r(\tau_1) C_{n-r}(\tau_2) \right) P_\delta^{(i)}(k_1) \\ &= \bar{\rho}^2 (2\pi)^3 \delta_D(\mathbf{k}_1 + \mathbf{k}_2) A(\tau_1, \tau_2) P_\delta^{(i)}(k_1). \end{aligned} \quad (5.14)$$

The infinite sum in the resulting amplitude leads to a decoupling of the two chains of particle interaction operators, allowing us to express the amplitude of the two-point function as

$$A(\tau_1, \tau_2) = \left(\sum_{n_1=0}^{\infty} C_{n_1}(\tau_1) \right) \left(\sum_{n_2=0}^{\infty} C_{n_2}(\tau_2) \right). \quad (5.15)$$

We will see in the next section how to evaluate the infinite sums of chains of integrals, but before we move on, let us consider the steps that brought us to this result. Although we focused our discussion purely on expanding the initial conditions in terms of the initial power spectrum, the main simplification in the above derivation came from considering the contributions of only a single correlation line. Even though we chose to expand this line to linear order in $P_\delta^{(i)}$, which simplifies the result, this step is not strictly necessary. Without the $P_\delta^{(i)}$ -expansion, additional exponential damping factors due to initial momentum dispersion would appear, and the correlation line would have to be evaluated numerically, leading straight to the resummed propagator discussed in [22].

5.1.3 Formal resummation

To evaluate the infinite sums in (5.15) analytically first note that time-integral chains defined in (5.11) contain elements of different physical origins. On the one hand, we have the factors f_c, d encoding perturbations to particle trajectories due to gravitational interactions; on the other hand, each chain starts with a freely propagating correlation line $(1 + g_{r'})$. We separate both contributions by rewriting the infinite sum over the chains as

$$\sum_{n=0}^{\infty} C_n(\tau_1) = \int_0^{\tau_1} d\tau_2 \Delta_R(\tau_1, \tau_2) (1 + g_2). \quad (5.16)$$

Here we introduced Δ_R , which exclusively represents particle interactions and can be interpreted as an effective propagator for a density fluctuation. Comparison between (5.16) and (5.11) suggests that

$$\begin{aligned} \Delta_R(\tau_1, \tau_2) &= \delta_D(\tau_1 - \tau_2) + \tilde{\Delta}_R(\tau_1, \tau_2), \\ \text{with } \tilde{\Delta}_R(\tau_1, \tau_2) &= f_{1,2} + \int_{\tau_2}^{\tau_1} d\tau_3 f_{1,3} f_{3,2} + \int_{\tau_2}^{\tau_1} d\tau_3 f_{1,3} \int_{\tau_2}^{\tau_3} d\tau_4 f_{3,4} f_{4,2} + \dots \\ &= f_{1,2} + \int_{\tau_2}^{\tau_1} d\tau_3 f_{1,3} \tilde{\Delta}_R(\tau_3, \tau_2), \end{aligned} \quad (5.17)$$

where we used the integrals' recursive nature in the second line to formulate the self-consistent relation for $\tilde{\Delta}_R$ in the last line. Under the condition that all the components in (5.17) depend only on the difference of their time arguments, i. e. $\tilde{\Delta}_R(\tau_1, \tau_2) = \tilde{\Delta}_R(\tau_1 - \tau_2)$ and $f_{1,3} = f(\tau_1 - \tau_3)$ the self-consistent equation (5.17) can be solved for $\tilde{\Delta}_R$ by using a Laplace transform [4, 22]. Since Newtonian particle propagators depend on the difference between their two time arguments, the same should follow for the resummed propagator. Then, by the convolution theorem of the Laplace transform, we get

$$\tilde{\Delta}_R(\tau, 0) = \mathcal{L}_{\tau \leftarrow s}^{-1} \left[\frac{\mathcal{L}_{\tau \rightarrow s}[f(\tau, 0)]}{1 - \mathcal{L}_{\tau \rightarrow s}[f(\tau, 0)]} \right] = \frac{3}{5} (e^\tau - e^{-\frac{3}{2}\tau}), \quad (5.18)$$

which is a result that was already derived both in the grand-canonical [4] as well as the resummed [22] formulation of KFT. For completeness, the derivation can also be found in Appendix G with a very brief discussion of Laplace transforms. Reinserting this expression into (5.16) and evaluating the integral recovers the linear growth factor from SPT

$$\sum_{n=0}^{\infty} C_n(\tau_1) = e^{\tau_1} = D_+(t_1). \quad (5.19)$$

Thus, we have managed to derive the linear growth of the two-point function in the microscopic description of KFT by explicitly resumming all the diagrams with non-vanishing linear contributions in $P_\delta^{(i)}$. Note that analytically resumming the chains of time integrals relies on the expression of the Newtonian particle propagator

$$g_{qp}(\tau, \tau') = 2(1 - e^{\frac{1}{2}(\tau - \tau')}) \quad (5.20)$$

and leads to the correct large-scale growth behaviour of the power spectrum for arbitrary cosmic parameters. This result might seem surprising since we used the approximation $\frac{\Omega_m}{f^2} = 1$ in the derivation of the particle propagator. In our discussion of SPT in Section 2.4, we have stressed that deviations from the actual growth behaviour due to this approximation are contained exclusively in the decaying mode. This behaviour seems to carry over to KFT, although it is less obvious that the correct large-scale growth should be reproduced in our calculations since we had to evaluate integrations over time, where the decaying mode usually becomes relevant in SPT. This highlights the quite non-trivial connection between both approaches.

5.1.4 Truncation at a finite order

Although we managed to recover the correct linear growth behaviour from Newtonian particle dynamics with the naive perturbation theory in KFT, one cannot help but notice

that it took quite a considerable effort to derive this basic result. Indeed, attempting a similar resummation by hand for mode-coupling contributions, e. g. at quadratic order in $P_\delta^{(i)}$, seems ludicrous. If finding an analytical scheme to resum all diagrams that contribute at a given order in $P_\delta^{(i)}$ is not possible, the alternative in canonical perturbation theory is to truncate the Taylor expansion of the interaction operator at some highest achievable order M and evaluate the resulting non-vanishing diagrams. Doing this for the linear evolution of the power spectrum by calculating

$$A_M(\tau_1, \tau_2) = \sum_{n=0}^M \sum_{r=0}^n C_r(\tau_1) C_{n-r}(\tau_2), \quad (5.21)$$

provides an intuition for the impact of particle interactions on structure formation. This calculation was done in a slightly different KFT formalism in [44]. Figure 5.1 shows

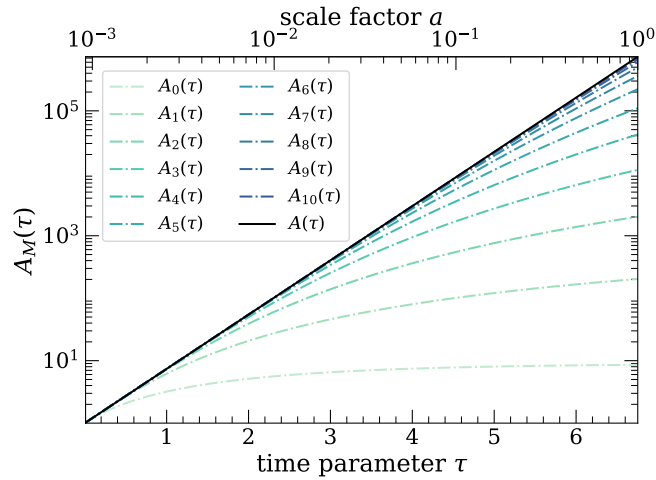


Figure 5.1: The linear amplitudes for the first ten orders of perturbation theory in KFT (blue dashed-dotted), as well as the fully resummed result from (5.19) (solid black line) as a function of τ and the scale factor a . As we go towards higher orders, the blue lines continue to follow the true amplitude until later times. Only for orders ten and beyond do we start to get a reasonable approximation of the true linear growth.

the time-dependence of the amplitude of a synchronous linearized two-point correlation function for different orders in perturbation theory. The solid black line forming the diagonal of the plot is the fully resummed result $e^{2\tau} = D_+^2$. Starting from the free-streaming amplitude $A_0(\tau)$, which falls below $A(\tau)$ very early on, the darker blue curves, which correspond to increasing orders in the interaction operator, continue to follow the full results up to increasingly late times until they eventually fall below the black curve for scale factors close to unity.

The amplitude that each perturbative correction contributes individually is plotted for the first fourteen orders in the left panel of Figure 5.2. Unlike what is usually expected in a perturbative expansion, corrections to the linear amplitude become increasingly larger, reach a maximum around order eight and start decreasing after that. The right panel demonstrates that to achieve a reasonable accuracy for linear growth at $a = a_0$, we need to include perturbative corrections due to gravity of order thirteen and beyond. Although achievable for the linearized two-point function, aiming to include quadratic or even higher contributions in the initial power spectrum is daunting. This result already hints at the fact that canonical perturbation theory with Newtonian trajectories in KFT is probably not the smartest choice if one is aiming for high-precision results

for the non-linear power spectrum. In the next chapter, we will confirm this suspicion when we evaluate perturbation theory at quadratic order in the initial power spectrum.

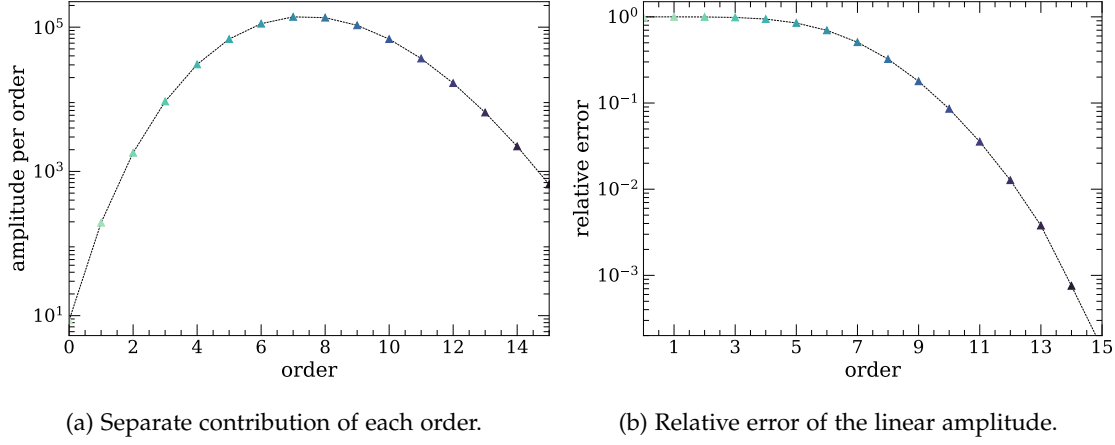


Figure 5.2: The individual amplitudes of each order (a) and the relative error of the linear amplitude (b) from Newtonian trajectories, both at $a = a_0$ plotted against the order of perturbation theory. For low orders, the amplitude of each contribution rises with increasing order in the interaction and reaches its maximum around order 8. The perturbation order, which provides the largest contribution to the linear amplitude, increases with time. As pointed out in [44], we reach percent-level accuracy for the overall linear amplitude only around the thirteenth order in the interaction operator as shown in (b).

5.2 LINEAR GROWTH FROM ZEL'DOVICH TRAJECTORIES

The infinite resummation of diagrams needed in canonical perturbation theory to describe large-scale growth of the dark matter power spectrum from Newtonian trajectories can be circumvented by forcing particles onto free Zel'dovich trajectories. As shown in Section 4.4, free Zel'dovich trajectories by construction reproduce linear growth of the two-point function and, therefore, represent an intelligent choice for KFT calculations in cosmology. Since the full linear growth is contained in the free-streaming solution, corrections to the two-point function due to particle interactions must have a vanishing linear contribution. If this wasn't the case, KFT would lead to inconsistent predictions for large-scale growth. In this section, we will show that perturbative corrections to free Zel'dovich trajectories have no linear contributions in the initial power spectrum.

The splitting (4.80) and (4.81) of the equations of motion leads to the total interaction operator $i\Delta\hat{S}_I$ and to a free generating functional whose evolution is governed by Zel'dovich particle propagators. As a result, the linearized two-point function reads

$$\begin{aligned}
 G_{\rho\rho}^{(Z,1)}(1,2) &= \sum_{n=0}^{\infty} \left[\frac{1}{n!} (i\Delta\hat{S}_I)^n \hat{\rho}(1)\hat{\rho}(2) Z_0[\underline{\mathbf{J}}, \underline{\mathbf{K}}] \Big|_{\underline{\mathbf{0}}} \right]^{(1)} \\
 &= \sum_{n=0}^{\infty} \left[\sum_{s=0}^n \frac{1}{s!} (i\hat{S}_C)^s \frac{1}{(n-s)!} (i\hat{S}_I)^{n-s} \hat{\rho}(1)\hat{\rho}(2) Z_0[\underline{\mathbf{J}}, \underline{\mathbf{K}}] \Big|_{\underline{\mathbf{0}}} \right]^{(1)} \\
 &= \sum_{n=0}^{\infty} \sum_{s=0}^n \frac{1}{s!} (i\hat{S}_C)^s \left[\delta^{(n-s)} G_{\rho\rho}^{(Z,1)}(1,2) \right]. \tag{5.22}
 \end{aligned}$$

In the last line, we have isolated the expression for the $(n-r)$ -th order perturbation theory evaluated at linear order in the initial power spectrum $\delta^{(n-s)}G_{\rho\rho}^{(Z,1)}(1,2)$ evaluated with free Zel'dovich trajectories. Since the counter-operator can be expressed as a derivative w. r. t. the momentum shift tensor, the source fields in the free generating functional are no longer needed once all other operators have been applied. This formulation allows us to separately evaluate the term in brackets in the last line and apply the counter-operator only at the end. Since the two-particle interaction potential is unchanged when transitioning from Newtonian to Zel'dovich trajectories, the particle interaction operator \hat{S}_I is identical to the Newtonian case in the previous section, such that

$$\delta^{(n-s)}G_{\rho\rho}^{(Z,1)}(1,2) = \bar{\rho}^2 (2\pi)^3 \delta_D(\mathbf{k}_1 + \mathbf{k}_2) \left(\sum_{r=0}^{n-s} C_r^{(Z)}(\tau_1) C_{n-s-r}^{(Z)}(\tau_2) \right) P_\delta^{(i)}(k_1). \quad (5.23)$$

Although structurally identical to the Newtonian results, the free propagation of the initial correlation lines appearing in the chains of time integrals is defined in terms of the Zel'dovich particle propagator

$$C_r^{(Z)}(\tau_1) := \int_0^{\tau_1} d\tau'_1 f_{1,1'} \int_0^{\tau'_1} d\tau'_2 f_{1',2'} \dots \int_0^{\tau'_{r-1}} d\tau'_r f_{(r-1)',r'} (1 + T_{r'}), \quad (5.24)$$

where we defined $T_{r'} := g_{qp}^{(Z)}(t'_{r'}, 0)$ for compactness. $f_{a,b}$ is unchanged w. r. t. the previous section. To evaluate applications of the counter-operator to this expression, recall that momentum shift vectors are contained in the free correlation line. With the only two momentum shift vectors that occur in the linearized correlation line being

$$\mathbf{L}_{p_{i_r}}^{(Z)} = -T_{r'} \mathbf{k}'_r \quad \mathbf{L}_{p_{i_n}}^{(Z)} = -T_{n'} \mathbf{k}'_{n'}, \quad (5.25)$$

the correlation line evaluates to

$$\begin{aligned} & (2\pi)^3 \delta_D(\mathbf{k}'_r + \mathbf{k}'_{n'}) \overset{(1)}{\bullet} \xrightarrow{i_r} \overset{(1)}{\bullet} \xrightarrow{i_n} \\ & = \left[1 - \frac{\mathbf{L}_{q_{i_r}} \cdot \mathbf{L}_{p_{i_n}}^{(Z)}}{L_{q_{i_r}}^2} + \frac{\mathbf{L}_{q_{i_r}} \cdot \mathbf{L}_{p_{i_r}}^{(Z)}}{L_{q_{i_r}}^2} - \frac{(\mathbf{L}_{q_{i_r}} \cdot \mathbf{L}_{p_{i_r}}^{(Z)})(\mathbf{L}_{q_{i_r}} \cdot \mathbf{L}_{p_{i_n}}^{(Z)})}{L_{q_{i_r}}^4} \right]_{\mathbf{k}'_r = -\mathbf{k}'_{n'}} \\ & = (1 + T_{r'})(1 + T_{n'}). \end{aligned} \quad (5.26)$$

This simplification has two important consequences for the counter-operator. First, the derivative w. r. t. the full momentum shift tensor reduces to the two non-vanishing components and can be rewritten in terms of derivatives w. r. t. Zel'dovich particle propagators

$$\left(\Delta \underline{\mathbf{L}}_p \cdot \frac{\partial}{\partial \underline{\mathbf{L}}_p^{(Z)}} \right) \overset{(1)}{\bullet} \xrightarrow{i_r} \overset{(1)}{\bullet} \xrightarrow{i_n} = \left[(g_{r'} - T_{r'}) \frac{\partial}{\partial T_{r'}} + (g_{n'} - T_{n'}) \frac{\partial}{\partial T_{n'}} \right] \overset{(1)}{\bullet} \xrightarrow{i_r} \overset{(1)}{\bullet} \xrightarrow{i_n}. \quad (5.27)$$

As a result applying the counter-operator to the chain $C_r^{(Z)}(\tau_1)$ replaces the free-streaming correlation line $(1 + T)$ by $(g - T)$:

$$\begin{aligned} i\hat{S}_C C_r^{(Z)}(\tau_1) &= \int_0^{\tau_1} d\tau'_1 f_{1,1'} \int_0^{\tau'_1} d\tau'_2 f_{1',2'} \dots \int_0^{\tau'_{r-1}} d\tau'_r f_{(r-1)',r'} (g_{r'} - T_{r'}) \\ &=: \delta C_r^{(Z)}(\tau_1). \end{aligned} \quad (5.28)$$

Second, since the amplitude in (5.23) is linear in both $T_{r'}$ and $T_{n'}$ (5.25) all contributions containing more than two counter-operators ($s > 2$ in (5.22)) are zero. The full expression that needs to be evaluated for n -th order perturbation theory at linear order in $P_\delta^{(i)}$ with Zel'dovich particle trajectories, therefore, reduces to three non-vanishing terms

$$\left[\frac{1}{n!} (i\Delta\hat{S}_I)^n \hat{\rho}(1)\hat{\rho}(2)Z_0[\underline{\mathbf{J}}, \underline{\mathbf{K}}] \Big|_0 \right]^{(1)} = \delta^{(n)} G_{\rho\rho}^{(Z,1)}(1,2) + (i\hat{S}_C) \left[\delta^{(n-1)} G_{\rho\rho}^{(Z,1)}(1,2) \right] + \frac{1}{2} (i\hat{S}_C)^2 \left[\delta^{(n-2)} G_{\rho\rho}^{(Z,1)}(1,2) \right]. \quad (5.29)$$

Evaluating the three terms on the rhs according to (5.23) yields the three time-dependent amplitudes:

$$\sum_{r=0}^n C_r^{(Z)}(\tau_1) C_{n-r}^{(Z)}(\tau_2) + (i\hat{S}_C) \sum_{r=0}^{n-1} C_r^{(Z)}(\tau_1) C_{n-1-r}^{(Z)}(\tau_2) + \frac{1}{2} (i\hat{S}_C)^2 \sum_{r=0}^{n-2} C_r^{(Z)}(\tau_1) C_{n-2-r}^{(Z)}(\tau_2). \quad (5.30)$$

We will now show that these three contributions exactly cancel each other, which relies on the following relation between chains of length r and $r-1$:

$$C_r^{(Z)}(\tau) = -\delta C_{r-1}^{(Z)}(\tau) \quad \forall \quad r > 0. \quad (5.31)$$

This identity can be shown by explicitly performing the first integral in the chain (5.24) and comparing the result to (5.28). Note that (5.31) relies on the specific expression for the free particle propagator and only holds for Zel'dovich trajectories. Splitting off the terms with chains of zero length in the first term of (5.30) (the $s=0$ term) and using (5.31) we obtain

$$\sum_{r=0}^n C_r^{(Z)}(\tau_1) C_{n-r}^{(Z)}(\tau_2) = -C_0^{(Z)}(\tau_1) \delta C_{n-1}^{(Z)}(\tau_2) - \delta C_{n-1}^{(Z)}(\tau_1) C_0^{(Z)}(\tau_2) - \sum_{r=0}^{n-2} \delta C_r^{(Z)}(\tau_1) C_{n-1-r}^{(Z)}(\tau_2). \quad (5.32)$$

In the last ($s=2$) term in (5.30) the square of the counter-operator is applied to the product of the two chains of time integrals. Since each chain is linear in the Zel'dovich particle propagator applying the counter-operator twice to a single chain gives a vanishing contribution such that

$$\frac{1}{2} (i\hat{S}_C)^2 \sum_{r=0}^{n-2} C_r^{(Z)}(\tau_1) C_{n-2-r}^{(Z)}(\tau_2) = \sum_{r=0}^{n-2} \delta C_r^{(Z)}(\tau_1) \delta C_{n-2-r}^{(Z)}(\tau_2). \quad (5.33)$$

For the second ($s=1$) term in (5.30) we first apply the counter-operator using (5.28) and split off chains of zero length to find

$$(i\hat{S}_C) \sum_{r=0}^{n-1} C_r^{(Z)}(\tau_1) C_{n-1-r}^{(Z)}(\tau_2) = \sum_{r=0}^{n-2} \delta C_r^{(Z)}(\tau_1) C_{n-1-r}^{(Z)}(\tau_2) + \delta C_{n-1}^{(Z)}(\tau_1) C_0^{(Z)}(\tau_2) + C_0^{(Z)}(\tau_1) \delta C_{n-1}^{(Z)}(\tau_2) + \sum_{r=1}^{n-1} C_r^{(Z)}(\tau_1) \delta C_{n-1-r}^{(Z)}(\tau_2). \quad (5.34)$$

The first three terms cancel the $s = 0$ contribution, whereas the remaining term, upon using (5.31), cancels the $s = 2$ contribution. Thus, the three contributions conspire in such a way as to cancel exactly for all orders in perturbation theory $n > 0$. Consequently, the free-streaming amplitude of the power spectrum from Zel'dovich trajectories is exact, and perturbations to this result only occur at higher orders in the initial power spectrum. This outcome is extremely reassuring, as it shows that Zel'dovich trajectories, in conjunction with the counter-operator, lead to exact results in KFT. Compared to the Newtonian case, where each increasing order in the interaction operator needs to be considered to reproduce the correct linear growth, interactions play no role in the linear evolution in the Zel'dovich approximation. Zel'dovich trajectories, hence, represent a quantitative example of a suitable choice for particle trajectories to minimize the impact of the interaction operator.

5.3 DISCUSSION

As formulations of KFT go, canonical perturbation theory has comparably little theoretical overhead. Calculating perturbative corrections to the free two-point functions is done by naively applying the interaction operator to the free generating functional. Focussing on the calculation of linear growth for a two-point function by applying two external density operators on the generating functional and expanding the correlation lines in the resulting free correlation functions to linear order in the initial power spectrum, we were able to formally resum the entire perturbation series for Newtonian trajectories (see (5.19)) to arrive at the expected linear growth behaviour. For the formal resummation, we took inspiration from rKFT where the retarded propagator results from the same chain of time integrals (5.16) and can be calculated via Laplace transforms. An almost identical result was obtained in earlier works with the grand-canonical ensemble (section 4.3 of [4]). One notable difference between canonical perturbation theory and its grand-canonical/resummed counterparts is that the former is formulated in terms of correlation functions, while both of the latter work with cumulants. While using correlation functions appears natural for canonical perturbation theory, it also tends to obscure some underlying structures and relations. Only the comparison to grand-canonical KFT reveals that the infinite chains of time integrals that make up linear growth are chains of density-response field cumulants $\bar{G}_{B\rho}$, giving these quantities the interpretation of a statistical propagator. What the resummation (5.1) is then effectively doing is to create two infinite chains of statistical propagators, each of which hands down its arguments to its neighbour in a 'bucket brigade' process until they reach the external modes at τ_1 and τ_2 . Nonetheless, calculations of the large-scale amplitude of the power spectrum for a finite order in canonical perturbation theory are interesting in their own right.

On the other hand, working with alternative splittings of the particle's equations of motion is most easily done in canonical perturbation theory. Zel'dovich trajectories are a natural choice for cosmic structure formation and can be consistently introduced as free particle motion. A counter term, which effectively pushes particles back on their physical trajectories, occurs in the interaction operator to obtain the same complete particle trajectories. Since Zel'dovich particle propagators lead to the correct linear growth behaviour of the power spectrum at the level of free-streaming, perturbative corrections due to the interaction operator should not contain contributions that are linear in the initial power spectrum. Indeed, using approximation methods to include the Zel'dovich potential into the KFT interaction operator, e.g. by introducing an effective Yukawa potential [49] leads to an inconsistent linear growth behaviour in canonical perturbation

theory since such an interaction potential will fail to cancel unphysical contributions to the linear amplitude. However, we were able to show in this section that a consistent treatment of the Zel'dovich potential as an independent operator leads to an exact cancellation of terms at linear order in $P_\delta^{(i)}$ for each order in perturbation theory. At the level of linear growth, canonical perturbation theory can thus reproduce the predictions of other perturbative approaches to cosmic structure formation, either by an infinite resummation of diagrams for Newtonian trajectories or from free motion in the case of Zel'dovich trajectories.

As a final note on linear growth, comparing the results of SPT to canonical KFT with Newtonian trajectories in the linear regime could be a good playground for more systematic comparisons between both theories. Like KFT, SPT can be formulated in terms of a generating functional building on the path integral formulation of classical mechanics by Martin, Siggia, and Rose [14, 19, 51]. Gravitational interactions are entirely contained in the linear e. o. m. , namely in the $\delta\theta$ -component of the matrix (2.33). For a systematic comparison between SPT and canonical KFT, one could imagine extracting the contribution of the gravitational potential from the free equation of motion [51] and formulate it as an independent interaction operator. Structurally, the resulting interaction operator has much in common with the particle interaction operator in KFT since both are quadratic in macroscopic fields. The perturbative expansion of this operator in SPT leads to the *exact same* result for the linear amplitude of the density power spectrum (5.15) as for Newtonian trajectories in KFT. Additionally, it was shown in [47] that one-loop rKFT at quadratic order in the initial power spectrum reproduces one-loop SPT. A better understanding of this result could help find promising pathways to move beyond SPT.

GOING BEYOND LINEAR GROWTH

Although useful to deepen our understanding of canonical perturbation theory, the linear growth behaviour of the dark matter power spectrum is not what KFT was developed to calculate. Indeed, both SPT and LPT do a perfectly fine job in this regime at a much lower computational effort. KFT's true strength lies in describing the non-linear regime where other perturbation theories break down. Formally, to obtain results for the evolution of non-linear structures, we have to consider the complete hierarchy of initial correlations between particles. Although KFT, unlike other theories of cosmic structure formation, has access to this information in principle, the numerical evaluation of correlation lines is exceptionally challenging. To evaluate expressions in canonical perturbation theory in KFT beyond linear growth, we are forced to expand the correlation lines in the initial power spectrum up to quadratic order. This chapter discusses how the results of canonical perturbation theory can be derived consistently at this order. Throughout the chapter, we narrow the discussion to evaluating synchronous two-point functions. Since the final expressions are all derived by using a symbolic code, we will refrain from showing calculations in complete detail and instead focus on highlighting the essential ideas at play.

6.1 RESULTS FOR NEWTONIAN TRAJECTORIES

Since evaluating perturbative corrections to free correlation functions in KFT at quadratic order in the initial power spectrum involves treating an increasing number of terms, going beyond second-order perturbation theory is best done by implementing a symbolic code. But before we discuss the mechanics and logic behind the symbolic evaluation of perturbation theory, we want to build some intuition for the diagrammatic language introduced in [Section 4.3](#) by revisiting the evaluation of first and second-order diagrams. Consider the two-point function evaluated with the Newtonian splitting of the equations of motion

$$\begin{aligned}
G_{\rho\rho}^{(N)}(1,2) &= G_{\rho\rho}^{(N,1)}(1,2) + G_{\rho\rho}^{(N,2)}(1,2) + \dots \\
&= \left[\bar{G}_{\rho\rho}^{(N,1)}(1,2) + \delta^{(1)} G_{\rho\rho}^{(N,1)}(1,2) + \delta^{(2)} G_{\rho\rho}^{(N,1)}(1,2) + \dots \right] \\
&\quad + \left[\bar{G}_{\rho\rho}^{(N,2)}(1,2) + \delta^{(1)} G_{\rho\rho}^{(N,2)}(1,2) + \delta^{(2)} G_{\rho\rho}^{(N,2)}(1,2) + \dots \right] + \dots,
\end{aligned} \tag{6.1}$$

which we first separated into contributions in increasing orders of the expansion in the initial power spectrum in the first line. Each order in the $P_\delta^{(i)}$ -expansion is then split into the free-streaming contribution and perturbative corrections of the latter. Whereas the previous chapter was treating perturbative corrections, which are linear in the initial power spectrum (line 2 in (6.1)), the last line of (6.1) is what we will be discussing in this chapter.

6.1.1 First and second-order perturbative corrections

First-order corrections

Although the first-order correction to the dark matter power spectrum in canonical perturbation theory has been studied previously [1, 50], we will provide an overview of the calculations here to get acquainted with the basic ideas underlying the evaluation of canonical perturbation theory. Also note that our analysis is slightly more general than that in previous works since we consider all initial correlation lines, as opposed to [1, 50] where both density-density and density-momentum lines were neglected. For a synchronous two-point function, we obtain a single distinct diagram

$$\begin{aligned} \delta^{(1)}G_{\rho\rho}^{(N,2)}(1,2) &= \left[i\hat{S}_1\hat{\rho}(1)\hat{\rho}(2)Z_0[\underline{\mathbf{J}},\underline{\mathbf{K}}] \Big|_{\underline{\mathbf{0}}} \right]^{(2)} = 2N^3 \begin{array}{c} e_1 \quad e_2 \\ \swarrow \quad \cdot \\ \quad \quad \quad \downarrow \\ \quad \quad \quad \text{quad} \\ i_1 \end{array} \quad (6.2) \\ &= 2N^3 \int d1' f(1,-1') \mathcal{Z}_0^{(2)}(\underline{\mathbf{L}}_{q'}, \underline{\mathbf{L}}_p), \end{aligned}$$

where it is understood that particle indices are fixed labels which mark the components of the shift tensors in $\mathcal{Z}_0^{(2)}(\underline{\mathbf{L}}_{q'}, \underline{\mathbf{L}}_p)$ in the last line. The spatial shift tensor components, which directly follow from the configuration of interaction lines, read

$$\mathbf{L}_{q_{e_1}} = -\mathbf{k}_1 + \mathbf{k}'_1 \quad \mathbf{L}_{q_{e_2}} = -\mathbf{k}_2 \quad \mathbf{L}_{q_{i_1}} = -\mathbf{k}'_1, \quad (6.3)$$

and the momentum shift vectors follow from it in the usual way. The evaluation of the diagram in terms of initial phase-space correlations is obtained by drawing all non-vanishing configurations of up to two correlation lines into the diagram and expanding the overall expression to quadratic order in the initial power spectrum

$$\begin{aligned} & 2N^3 \begin{array}{c} e_1 \quad e_2 \\ \swarrow \quad \cdot \\ \quad \quad \quad \downarrow \\ \quad \quad \quad \text{quad} \\ i_1 \end{array} \\ &= 2N^3 \left(\begin{array}{c} e_1 \quad e_2 \\ \swarrow \quad \searrow \\ \quad \quad \quad \downarrow \\ \quad \quad \quad \text{(2)} \\ i_1 \end{array} + \begin{array}{c} e_1 \quad \text{(1)} \quad e_2 \\ \swarrow \quad \downarrow \quad \searrow \\ \quad \quad \quad \downarrow \\ \quad \quad \quad \text{(1)} \\ i_1 \end{array} + \begin{array}{c} e_1 \quad e_2 \\ \swarrow \quad \downarrow \quad \searrow \\ \quad \quad \quad \downarrow \\ \quad \quad \quad \text{(1)} \\ i_1 \end{array} + \begin{array}{c} e_1 \quad \text{(1)} \quad e_2 \\ \swarrow \quad \downarrow \quad \searrow \\ \quad \quad \quad \downarrow \\ \quad \quad \quad \text{(1)} \\ i_1 \end{array} \right) \quad (6.4) \\ &= (2\pi)^3 \delta_D(\mathbf{k}_1 + \mathbf{k}_2) 2\bar{\rho}^3 \int d1' f(1,-1') \left[(2\pi)^3 \delta_D(\mathbf{L}_{q_{e_1}}) (-Q_D \tilde{\mathcal{P}}_{e_2 i_1}^{(1)}(\mathbf{L}_{q_{e_2}}) + \tilde{\mathcal{P}}_{e_2 i_1}^{(2)}(\mathbf{L}_{q_{e_2}})) \right. \\ & \quad \left. + \tilde{\mathcal{P}}_{e_1 e_2}^{(1)}(\mathbf{L}_{q_{e_1}}) \tilde{\mathcal{P}}_{i_1 e_2}^{(1)}(\mathbf{L}_{q_{i_1}}) + \tilde{\mathcal{P}}_{e_2 i_1}^{(1)}(\mathbf{L}_{q_{e_2}}) \tilde{\mathcal{P}}_{e_1 i_1}^{(1)}(\mathbf{L}_{q_{e_1}}) + \tilde{\mathcal{P}}_{e_2 e_1}^{(1)}(\mathbf{L}_{q_{e_2}}) \tilde{\mathcal{P}}_{i_1 e_1}^{(1)}(\mathbf{L}_{q_{i_1}}) \right], \end{aligned}$$

where $\bar{\rho}^3$ is obtained from the inverse volume factors in the free correlation function and N^3 from the sum over particle labels. The next steps in the evaluation consist in expressing the expanded correlations in terms of the initial power spectrum and wave-vector-dependent factors, which follow directly from the definitions of initial correlations (4.9)–(4.11) and the shift vector configuration (6.3). As was noted at the end of Section 4.2, care needs to be taken when evaluating the correlation lines in three-particle

clusters since the δ -rule prohibits two delta-ends to meet at a particle node. For example $\tilde{\mathcal{P}}_{e_1 e_2}^{(1)}(\mathbf{L}_{q_{e_1}})\tilde{\mathcal{P}}_{i_1 e_2}^{(1)}(\mathbf{L}_{q_{i_1}})$ is obtained from

$$\begin{aligned}
& \begin{array}{cccccc}
\begin{array}{c} e_2 \\ \bullet \\ / \quad \backslash \\ e_1 \quad i_1 \end{array} & + & \begin{array}{c} e_2 \\ \bullet \\ / \quad \backslash \\ e_1 \quad i_1 \end{array} & + & \begin{array}{c} e_2 \\ \bullet \\ / \quad \backslash \\ e_1 \quad i_1 \end{array} & + & \begin{array}{c} e_2 \\ \bullet \\ / \quad \backslash \\ e_1 \quad i_1 \end{array} & + & \begin{array}{c} e_2 \\ \bullet \\ / \quad \backslash \\ e_1 \quad i_1 \end{array} & + & \begin{array}{c} e_2 \\ \bullet \\ / \quad \backslash \\ e_1 \quad i_1 \end{array} & + & \begin{array}{c} e_2 \\ \bullet \\ / \quad \backslash \\ e_1 \quad i_1 \end{array} \\
& + & \begin{array}{c} e_2 \\ \bullet \\ / \quad \backslash \\ e_1 \quad i_1 \end{array} & + & \begin{array}{c} e_2 \\ \bullet \\ / \quad \backslash \\ e_1 \quad i_1 \end{array} & + & \begin{array}{c} e_2 \\ \bullet \\ / \quad \backslash \\ e_1 \quad i_1 \end{array} & + & \begin{array}{c} e_2 \\ \bullet \\ / \quad \backslash \\ e_1 \quad i_1 \end{array} & + & \begin{array}{c} e_2 \\ \bullet \\ / \quad \backslash \\ e_1 \quad i_1 \end{array} & + & \begin{array}{c} e_2 \\ \bullet \\ / \quad \backslash \\ e_1 \quad i_1 \end{array} \\
& = \left(\begin{array}{c} \bullet \quad \bullet \\ e_1 \quad e_2 \end{array} + \begin{array}{c} \bullet \quad \bullet \\ e_1 \quad e_2 \end{array} \right) \left(\begin{array}{c} \bullet \quad \bullet \\ e_2 \quad i_1 \end{array} + \begin{array}{c} \bullet \quad \bullet \\ e_2 \quad i_1 \end{array} \right) \\
& \quad + \left(\begin{array}{c} \bullet \quad \bullet \\ e_1 \quad e_2 \end{array} + \begin{array}{c} \bullet \quad \bullet \\ e_1 \quad e_2 \end{array} \right) \left(\begin{array}{c} \bullet \quad \bullet \\ e_2 \quad i_1 \end{array} + \begin{array}{c} \bullet \quad \bullet \\ e_2 \quad i_1 \end{array} + \begin{array}{c} \bullet \quad \bullet \\ e_2 \quad i_1 \end{array} + \begin{array}{c} \bullet \quad \bullet \\ e_2 \quad i_1 \end{array} \right).
\end{aligned} \tag{6.5}$$

The evaluation of the resulting expression is then obtained by Fourier-transforming the individual correlation lines. As usual, care must be taken when evaluating the density-momentum correlation lines since they are not symmetric under the exchange of indices. As a final expression, we get

$$\begin{aligned}
\tilde{\mathcal{P}}_{e_1 e_2}^{(1)}(\mathbf{L}_{q_{e_1}})\tilde{\mathcal{P}}_{i_1 e_2}^{(1)}(\mathbf{L}_{q_{i_1}}) &= \left(Q_{e_1 e_2}^{\delta\delta} + Q_{e_1 e_2}^{p\delta} \right) \left(Q_{i_1 e_2}^{pp} + Q_{i_1 e_2}^{\delta p} \right) \\
& \quad + \left(Q_{e_1 e_2}^{pp} + Q_{e_1 e_2}^{\delta p} \right) \left(Q_{i_1 e_2}^{\delta\delta} + Q_{i_1 e_2}^{pp} + Q_{i_1 e_2}^{(\delta p)} \right),
\end{aligned} \tag{6.6}$$

where we encoded the Fourier-space correlation lines in the factors

$$\begin{aligned}
Q_{ab}^{\delta\delta} &:= P_{\delta}^{(i)}(|\mathbf{L}_{q_a}|) & Q_{ab}^{pp} &:= -\frac{(\mathbf{L}_{p_a} \cdot \mathbf{L}_{q_a})(\mathbf{L}_{p_b} \cdot \mathbf{L}_{q_a})}{L_{q_a}^4} P_{\delta}^{(i)}(|\mathbf{L}_{q_a}|) \\
Q_{ab}^{\delta p} &:= \frac{\mathbf{L}_{p_b} \cdot \mathbf{L}_{q_a}}{L_{q_a}^2} P_{\delta}^{(i)}(|\mathbf{L}_{q_a}|) & Q_{ab}^{p\delta} &:= -\frac{\mathbf{L}_{p_a} \cdot \mathbf{L}_{q_a}}{L_{q_a}^2} P_{\delta}^{(i)}(|\mathbf{L}_{q_a}|) \\
Q_{ab}^{(\delta p)} &:= \frac{(\mathbf{L}_{p_b} - \mathbf{L}_{p_a}) \cdot \mathbf{L}_{q_a}}{L_{q_a}^2} P_{\delta}^{(i)}(|\mathbf{L}_{q_a}|).
\end{aligned} \tag{6.7}$$

The other correlation line configurations in (6.4) need to be evaluated following the same procedure. In contrast to the products of two linearized Fourier-space correlation lines, the quadratic contribution from the single correlation line is not a simple product of Fourier-space correlation lines but a convolution:

$$\tilde{\mathcal{P}}_{e_2 i_1}^{(2)}(\mathbf{L}_{q_{e_2}}) = \left[Q_{e_2 i_1}^{pp} * \left(Q_{e_2 i_1}^{\delta\delta} + Q_{e_2 i_1}^{(\delta p)} + \frac{1}{2} Q_{e_2 i_1}^{pp} \right) \right] (\mathbf{L}_{q_{e_2}}) + \left(Q_{e_2 i_1}^{\delta p} * Q_{e_2 i_1}^{p\delta} \right) (\mathbf{L}_{q_{e_2}}). \tag{6.8}$$

Expanding individual correlation lines to quadratic order in the initial power spectrum thus results in an additional \mathbf{k} -space integral. However, we also see in (6.4) that contributions from single correlation lines obtain an additional Dirac-delta due to the uncorrelated particle e_1 . This behaviour is systematically continued for higher-order perturbation theory and ensures that a single \mathbf{k} -space integral remains for all corrections to a

two-point function at quadratic order in $P_\delta^{(i)}$ except for those terms that contain the expanded Gaussian damping. We refer to those contributions which retain an integration over an internal wave-vector as *mode-coupling* terms, whereas negative contributions due to the damping are usually called *self-energy* terms.

Second-order corrections

At second-order in the interaction operator, evaluating the initial conditions at quadratic order in the initial power spectrum already gives rise to quite a number of terms. Three distinct topologies are possible for the interaction lines and result in the diagrams

$$\delta^{(2)} G_{\rho\rho}^{(N,2)}(1,2) = N^4 \left(\begin{array}{c} e_1 \quad e_2 \\ \uparrow \quad \uparrow \\ i_1 \quad i_2 \\ \uparrow \quad \swarrow \\ i_1 \quad i_2 \end{array} + \begin{array}{c} e_1 \quad e_2 \\ \uparrow \quad \uparrow \\ i_1 \quad i_2 \\ \leftarrow \quad \leftarrow \\ i_1 \quad i_2 \end{array} + \begin{array}{c} e_1 \quad e_2 \\ \uparrow \quad \uparrow \\ i_1 \quad i_2 \\ \uparrow \quad \uparrow \\ i_1 \quad i_2 \end{array} \right)_{\text{quad}}. \quad (6.9)$$

Although the approach to evaluating these diagrams is identical to the first-order correction, the number of configurations of correlation lines is significantly larger. At second-order in the initial power spectrum, we obtain 24 non-vanishing terms: 6 from the first diagram in (6.9), and 9 from both the second and the third.

Once the trivial \mathbf{k} -space integral has been solved, we are left with two integrals over time and one over an internal wave vector, which can not be solved analytically. We, therefore, collect all the remaining terms in a single integrand $I(\mathbf{k}_1, \tau_1; \mathbf{k}'_1, \tau'_1, \tau'_2)$ and use numerical Monte Carlo integration to obtain the final correction to the two-point function at different values for the external wave-vector \mathbf{k}_1 .

6.1.2 Evaluation of higher orders

Although the 24 terms from second-order perturbation theory are still manageable and can be implemented by hand, third-order perturbation theory contains 83 distinct terms, all of which need to be evaluated analytically and implemented in a code to obtain the final result. The quickly growing number of non-vanishing terms per interaction order plotted in Figure 6.1 indicates that going beyond second or (for the brave) third-order perturbation theory is unfeasible without relying on a symbolic evaluation of the resulting terms. The general procedure that we followed to systematically generate contributions from n -th order perturbation theory and evaluate them at quadratic order in the initial power spectrum consists of the following steps:

1. Generate all non-vanishing diagrams and calculate their multiplicities.
2. Determine the shift tensors and force prefactors corresponding to each diagram.
3. Determine and evaluate the non-vanishing correlation configurations for each diagram.
4. Expand all correlation lines and the Gaussian damping factor consistently to second-order in the initial power spectrum.
5. Solve the trivial \mathbf{k} -space integrals, leaving one single Fourier integral for terms without damping. These terms will lead to mode-coupling effects. Those terms that contain the expanded Gaussian damping factor are left with no \mathbf{k} -space integral.

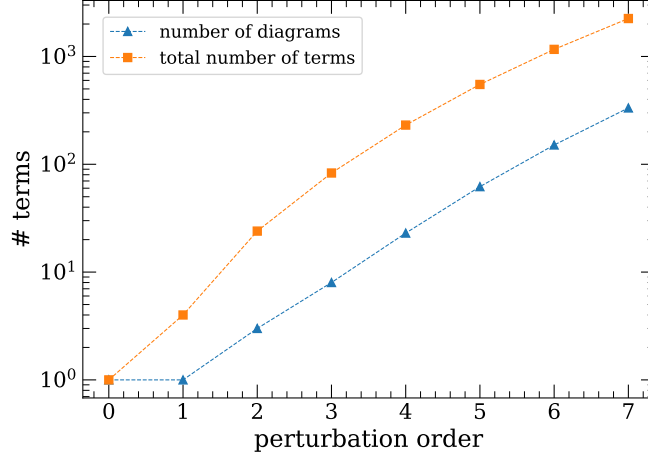


Figure 6.1: The number of non-vanishing terms (orange squares) as well as the number of diagrams (blue triangles). Since we only consider correlations between up to four particles, the average number of terms per diagram, i. e. the offset between the two curves, is more or less constant.

6. Collect all mode-coupling and damping terms in two separate functions

$$I_{\text{MC}}(\mathbf{k}_1, \tau_1; \mathbf{l}, \tau'_1, \dots, \tau'_n) = \sum_{\text{diagr.}} \sum_{\text{line configs.}} (\text{prefactors}) \times (\text{correlation lines}) \quad (6.10)$$

$$I_{\text{D}}(\mathbf{k}_1, \tau_1; \tau'_1, \dots, \tau'_n) = \sum_{\text{diagr. MC-line configs.}} (\text{prefactors}) \times (\text{correlation lines}), \quad (6.11)$$

where \mathbf{l} denotes the remaining internal integration variable in the mode-coupling contributions.

7. Perform the $(n+2)$ -dimensional integration of the function $I_{\text{MC}}(\mathbf{k}_1, \tau_1; \mathbf{l}, \tau'_1, \dots, \tau'_n)$ (mode-coupling) and the n -dimensional time integration of $I_{\text{D}}(\mathbf{k}_1, \tau_1; \tau'_1, \dots, \tau'_n)$ (self-energy) using Monte Carlo integration.

While steps 2.–5. are merely the generalization of the calculation sketched above for first-order perturbation theory, and 6.–7. a simple matter of numerics, the first step deserves more attention. To cast the diagrams of canonical perturbation theory into a shape that can easily be implemented numerically, note that their actual content is the information on which internal particle perturbs which other particle. Since each internal particle can act on exactly one target particle (by a contraction of the corresponding response field operator), we can therefore represent an n -th order diagram as a list of n labels denoting the targets of the interaction lines. This list can be generated iteratively, starting with a single entry for first-order perturbation theory and adding a free slot filled by all possible target labels for each order.

Similar to the linear case, there are restrictions to the allowed topologies of diagrams if we allow for a maximum of two correlation lines since only those configurations where all particles are either targets of interaction lines or part of a correlated cluster are non-vanishing. In general, if we allow for the presence of a maximum of n_C correlation lines, giving us a contribution of order n_C or higher in the initial power spectrum, non-

vanishing n -th order corrections to a free m -point function need to contain n_t targeted particles where

$$n_t \stackrel{!}{\geq} n + m - 2n_C. \quad (6.12)$$

The rhs counts the minimum number of particles not connected to other particles with an initial correlation line. For a non-vanishing diagram, these uncorrelated particles need to be targeted by interaction lines, which can only be ensured if (6.12) holds. We can make use of this knowledge to find restrictions on the possible topologies of non-vanishing diagrams at a given order in the initial power spectrum by asking ‘‘What is the maximum number X of times a single particle can be targeted and still leave enough interaction lines to fulfil (6.12)?’’ A quick calculation shows that X needs to fulfill

$$X \stackrel{!}{\leq} 2n_C - m + 1. \quad (6.13)$$

Consequently, only topologies where nodes are targeted up to three times by interaction lines need to be considered in the diagrammatic evaluation of perturbations to a two-point function evaluated at quadratic order in the initial power spectrum.

6.1.3 Results for the dark matter power spectrum

The results for perturbative contributions to the dark matter power spectrum due to free-streaming and the first eight orders in perturbation theory with Newtonian trajectories at quadratic order in the initial power spectrum are shown in [Figure 6.2a](#). We recognize the typical mode-transport behaviour in each order, where large scales (small wavenumbers) obtain negative and small scales positive contributions from quadratic corrections. Thus, power is transported from large to small scales, indicating growth in small-scale structures.

The transition scale between positive and negative contributions shows an interesting behaviour, moving towards larger scales as we increase the perturbation order from zero to three and then turning around to move towards smaller scales after that. It is not completely clear what causes this non-monotonous behaviour, but one possible explanation is that there is a shift in the balance between the self-energy (damping) contribution, which is overall negative, and the mode-coupling contributions. Due to the expansion up to the second order in the initial power spectrum, the self-energy contribution is exclusively contained in two-particle correlations. Since there are no three- or four-particle clusters in the free-streaming solution, the relative importance of the self-energy compared to the mode-coupling term should be pretty large at the level of free-streaming, leading to the dominance of the negative self-energy contribution up to comparatively large k (lightest curve in [Figure 6.2a](#)). Adding an internal particle by doing first-order perturbation theory and thus allowing the occurrence of three-particle correlations tips the balance between mode-coupling and self-energy in favour of the positive mode-coupling terms. This mechanism could explain the shift of the transition scale towards smaller k -values when comparing low orders in perturbation theory. Once we proceed beyond second-order perturbation theory, no qualitatively new correlation contributions arise by adding more internal particles, resulting in a slow monotonous rise of the zero-crossing beyond the third order.

Unlike what is commonly observed for perturbation theories, the maximum amplitude of quadratic corrections to the power spectrum increases as we crank up the order

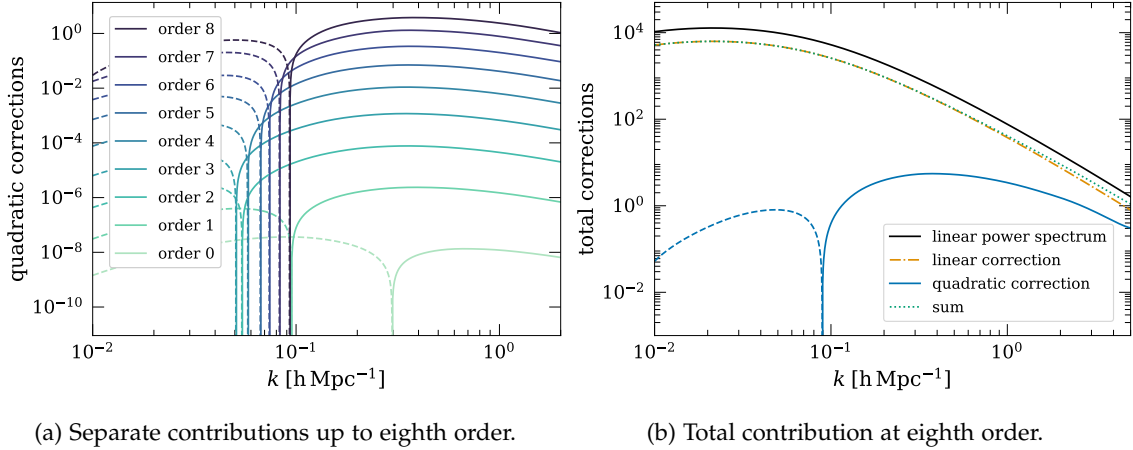


Figure 6.2: Contributions from free-streaming (order 0) up to perturbations of order 8 to the dark matter power spectrum evaluated at quadratic order in the initial power spectrum. The individual contributions from each order are shown in (a), whereas their sum is plotted in (b), together with the corrections linear in the initial power spectrum. Adding up quadratic and linear contributions (green dotted curve) yields the total result for the ‘non-linear’ power spectrum for a given order in perturbation theory. The black curve shows the correct amplitude to which linear corrections should eventually converge. (b) illustrates that perturbations of this order are insufficient to describe the correct power spectrum at any scale.

in perturbation theory. This can be considered troublesome for two reasons: (i) it suggests that the perturbative series might be divergent, and (ii) if it does converge, going to eighth-order perturbation theory is insufficient to obtain a reasonable estimate for the result. Considering (i), we do not need to worry too much since the results from linear growth show the same behaviour; the overall time-dependent amplitude increases for each order until it reaches a maximum and starts to decrease—cf. Figure 5.2. We can expect the same behaviour from quadratic corrections since we expect that perturbations in the interaction operator are agnostic about the expansion in the initial power spectrum. As for (ii), better methods for evaluating perturbation theory are needed to investigate how many perturbation orders are required until the maximum amplitude is reached and corrections start to decline. Unfortunately, with the current approach of using Monte Carlo methods to integrate over the $n + 2$ arguments of the time and wave-vector integral at n -th order perturbation theory, obtaining results beyond $n = 8$ is not attainable. Nonetheless, comparing the amplitudes of individual contributions for different orders in perturbation theory can provide us with a rough understanding of the behaviour of perturbative corrections at quadratic order in the initial power spectrum.

In Figure 6.3, we plotted the amplitude of individual perturbative corrections, both linear and quadratic in the initial power spectrum at $k = 1 \text{ h Mpc}^{-1}$. Note that the exact value of k is unimportant here since our main interest lies in the relative amplitude of different contributions. Most notably, we should point out that while the corrections linear in $P_\delta^{(i)}$ seem to reach their maximum amplitude around the eighth order, the same can not be said for the quadratic contributions. Although the curve flattens for increasing orders in the interaction, it does so at a considerably lower rate than in the linear case, suggesting that convergence will happen only later. We expect convergence to happen much slower at quadratic order in the initial power spectrum, forcing us to go to extraordinarily high orders in the interaction operator until contributions become negligible. This trend most certainly continues if we go to cubic order in $P_\delta^{(i)}$ for the

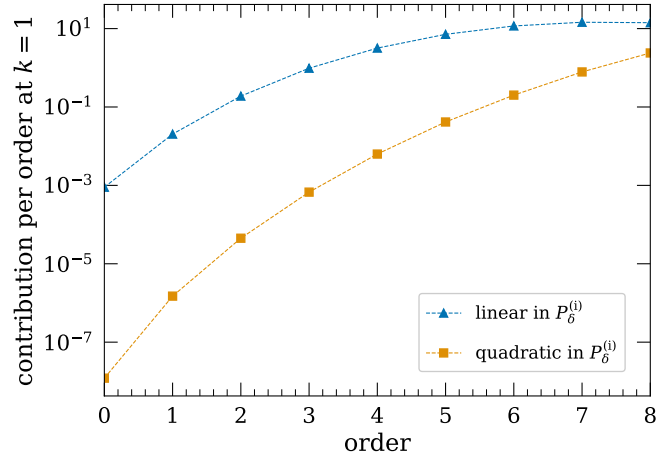


Figure 6.3: Comparison of the amplitude of linear and quadratic corrections at $k = 1 h\text{Mpc}^{-1}$. On the left panel, the amplitude of individual corrections is plotted as a function of their order. Whereas linear corrections (blue triangles) attain their maximum amplitude at order 8 and start to decrease after that—as illustrated in Figure 5.2—the curve corresponding to the corrections that are quadratic in the initial power spectrum (orange squares) suggests that these contributions reach this turning point only at a higher perturbation order.

following reason: From the linear calculation in Section 5.1, we have understood that summing up the diagrams contributing to linear growth can essentially be understood as replacing Newtonian particle trajectories, which propagate the initial correlation lines, by Zel’dovich trajectories. For linear growth, a single linearized correlation line needs to be propagated, requiring the resummation of two particle propagators. At quadratic order in the initial power spectrum, each term consists of two correlation lines, joining up to four particles. Each of these particle trajectories is then perturbed, and a subclass of diagrams contributes to the resummation of its propagator, meaning that, naively, we need twice as many orders in the interaction operator to achieve the same convergence as for linear growth. Intuitively, it makes sense that more interactions are needed for higher orders in the initial power spectrum.

Adding up all quadratic contributions from Figure 6.2a, we obtain the total quadratic correction to the dark matter power spectrum up to the eighth order in canonical perturbation theory. This result is plotted in Figure 6.2b, together with the total linear correction of the same order and the expected linear power spectrum. Although it is technically possible to go beyond the results of this work by an improvement of the numerical evaluation, our results suggest that an alternative approach, such as a resummation scheme [22] or a change to a more suitable definition of free motion—which will be investigated in the next section—might be more fruitful.

6.2 RESULTS FOR ZEL’DOVICH TRAJECTORIES

If we wish to proceed beyond the results of Newtonian trajectories in canonical perturbation theory, Zel’dovich trajectories are a promising candidate. As we have seen in the previous chapter, they reproduce the correct large-scale growth of the cosmic power spectrum at the level of free-streaming, and one can analytically show that all linear corrections to this result cancel exactly. At least for linear growth, they can be considered as a resummed result of Newtonian trajectories. To proceed beyond the discussion of

linear growth for Zel'dovich trajectories, we consider the perturbative corrections of the interaction operator to a free two-point function

$$\begin{aligned} G_{\rho\rho}^{(Z)}(1,2) &= G_{\rho\rho}^{(Z,1)}(1,2) + G_{\rho\rho}^{(Z,2)}(1,2) + \dots \\ &= \left[\bar{G}_{\rho\rho}^{(Z,1)}(1,2) + \Delta^{(1)} G_{\rho\rho}^{(Z,1)}(1,2) + \Delta^{(2)} G_{\rho\rho}^{(Z,1)}(1,2) + \dots \right] \\ &\quad + \left[\bar{G}_{\rho\rho}^{(Z,2)}(1,2) + \Delta^{(1)} G_{\rho\rho}^{(Z,2)}(1,2) + \Delta^{(2)} G_{\rho\rho}^{(Z,2)}(1,2) + \dots \right] + \dots \end{aligned} \quad (6.14)$$

In the first line, we expanded the fully interacting two-point function in orders of the initial power spectrum, each of which is then evaluated perturbatively. n -th order perturbative corrections at a given order o in the initial power spectrum are defined with the full interaction operator

$$\Delta^{(n)} G_{\rho\rho}^{(Z,o)}(1,2) := \frac{1}{n!} \left[(i\Delta\hat{S}_I)^n \hat{\rho}(1)\hat{\rho}(2) Z_0[\mathbf{J}, \mathbf{K}] \Big|_{\mathbf{0}} \right]^{(o)}, \quad (6.15)$$

and we have shown in the previous chapter that all corrections at linear order ($o = 1$) are identically zero, leaving nothing but the free-streaming solution. To evaluate the quadratic contributions, we split the full interaction operator into particle interactions and contributions from the counter-operator such that

$$\begin{aligned} \Delta^{(n)} G_{\rho\rho}^{(Z,2)}(1,2) &:= \left[(i\Delta\hat{S}_I)^n \hat{\rho}(1)\hat{\rho}(2) Z_0[\mathbf{J}, \mathbf{K}] \Big|_{\mathbf{0}} \right]^{(2)} \\ &= \sum_{s=0}^n \frac{1}{s!} (i\hat{S}_C)^s \left[\frac{1}{(n-s)!} (i\hat{S}_I)^{(n-s)} \hat{\rho}(1)\hat{\rho}(2) Z_0[\mathbf{J}, \mathbf{K}] \Big|_{\mathbf{0}} \right]^{(2)} \\ &= \sum_{s=0}^n \frac{1}{s!} (i\hat{S}_C)^s \left[\delta^{(n-s)} G_{\rho\rho}^{(Z,2)}(1,2) \right]. \end{aligned} \quad (6.16)$$

In the last step, we identified perturbations of the two-point function evolving along Zel'dovich trajectories due to particle interactions $\delta^{(n-s)} G_{\rho\rho}^{(Z,2)}(1,2)$.

6.2.1 Evaluation of particle interactions

As we have stressed before, the perturbations in $\delta^{(n-s)} G_{\rho\rho}^{(Z,2)}(1,2)$ are caused by the same particle interaction operator \hat{S}_I as in the Newtonian case, the only difference being that correlation lines are evolved with Zel'dovich instead of Newtonian particle propagators. Consequently, the same diagrammatic representation applies to determine these perturbations as in the previous section. For example, the first-order perturbation due to particle interactions,

$$\delta^{(1)} G_{\rho\rho}^{(Z,2)}(1,2) = 2N^3 \int d1' f(1, -1') \mathcal{Z}_0^{(2)}(\mathbf{L}_{q'}, \mathbf{L}_p^{(Z)}), \quad (6.17)$$

is identical to (6.2) if we replace the propagators in the momentum shift tensor with Zel'dovich particle propagators. This result holds true for all orders in the particle interaction operator, such that

$$\delta^{(n)} G_{\rho\rho}^{(Z,2)}(1,2) = \delta^{(n)} G_{\rho\rho}^{(N,2)}(1,2) \Big|_{\mathbf{L}_p = \mathbf{L}_p^{(Z)}}. \quad (6.18)$$

6.2.2 Evaluation of the counter-operator

The real difference between Zel'dovich and Newtonian trajectories lies in the additional application of the counter-operator

$$i\hat{S}_C \delta^{(n)} G_{\rho\rho}^{(Z,2)}(1,2) = \left(\Delta \underline{\mathbf{L}}_p \cdot \frac{\partial}{\partial \underline{\mathbf{L}}_p^{(Z)}} \right) \delta^{(n)} G_{\rho\rho}^{(Z,2)}(1,2). \quad (6.19)$$

Recall that the dependence of $\delta^{(n)} G_{\rho\rho}^{(Z,2)}(1,2)$ on the momentum shift tensor lies entirely in the correlation lines, such that applying the counter-operator comes down to taking derivatives of the Fourier-space correlation lines w.r.t. the momentum shift tensor. Schematically, corrections due to particle interactions are of the form

$$\delta^{(n)} G_{\rho\rho}^{(Z,2)}(1,2) = \sum_{\text{diagr.}} \int d\mathbf{l}' \dots \int d\mathbf{n}' (\text{prefactor}) \times \left\{ \sum_{\{a,b\}} \left[-Q_D^{(Z)} \tilde{\mathcal{P}}_{ab}^{(Z,1)} + \tilde{\mathcal{P}}_{ab}^{(Z,2)} \right] \right. \\ \left. \sum_{\{a,b,c\}} \tilde{\mathcal{P}}_{ab}^{(Z,1)} \tilde{\mathcal{P}}_{cb}^{(Z,1)} + \sum_{\{a,b,c,d\}} \tilde{\mathcal{P}}_{ab}^{(Z,1)} \tilde{\mathcal{P}}_{cd}^{(Z,1)} \right\}, \quad (6.20)$$

where we assume that all details about each term, such as the correct prefactors and the non-vanishing index configurations on the Fourier-space correlation lines, are known. Once again, correlation lines and the Gaussian damping term were explicitly marked with a (Z) to remind us that their momentum shift vectors contain the Zel'dovich particle propagator. Note that each correlation line expanded to linear order in the initial power spectrum $\tilde{\mathcal{P}}^{(Z,1)}$ is at most quadratic in $\underline{\mathbf{L}}_p^{(Z)}$, while $\tilde{\mathcal{P}}^{(Z,2)}$ contains up to four orders of the momentum shift tensor components. Thus, each term in (6.20) is of fourth order in momentum shift vectors, such that applying up to four powers of the counter-operator results in non-vanishing contributions. For the application of the counter-operator, we abbreviate $i\hat{S}_C \equiv \partial$ and first consider its effect on individual linearized correlation lines and on the Gaussian damping as the fundamental building blocks of our expressions:

$$\begin{aligned} \partial Q_{ab}^{pp} &= - \left\{ \frac{(\Delta \underline{\mathbf{L}}_{p_a} \cdot \underline{\mathbf{L}}_{q_a})(\underline{\mathbf{L}}_{p_b} \cdot \underline{\mathbf{L}}_{q_a})}{L_{q_a}^4} + \frac{(\underline{\mathbf{L}}_{p_a} \cdot \underline{\mathbf{L}}_{q_a})(\Delta \underline{\mathbf{L}}_{p_b} \cdot \underline{\mathbf{L}}_{q_a})}{L_{q_a}^4} \right\} P_\delta^{(i)}(|\underline{\mathbf{L}}_{q_a}|) \\ \partial^2 Q_{ab}^{pp} &= - \frac{(\Delta \underline{\mathbf{L}}_{p_a} \cdot \underline{\mathbf{L}}_{q_a})(\Delta \underline{\mathbf{L}}_{p_b} \cdot \underline{\mathbf{L}}_{q_a})}{L_{q_a}^4} P_\delta^{(i)}(|\underline{\mathbf{L}}_{q_a}|) \\ \partial Q_{ab}^{\delta p} &= \frac{\Delta \underline{\mathbf{L}}_{p_b} \cdot \underline{\mathbf{L}}_{q_a}}{L_{q_a}^2} P_\delta^{(i)}(|\underline{\mathbf{L}}_{q_a}|) & \partial Q_{ab}^{p\delta} &= - \frac{\Delta \underline{\mathbf{L}}_{p_a} \cdot \underline{\mathbf{L}}_{q_a}}{L_{q_a}^2} P_\delta^{(i)}(|\underline{\mathbf{L}}_{q_a}|) \\ \partial Q_{ab}^{(\delta p)} &= \frac{(\Delta \underline{\mathbf{L}}_{p_b} - \Delta \underline{\mathbf{L}}_{p_a}) \cdot \underline{\mathbf{L}}_{q_a}}{L_{q_a}^2} P_\delta^{(i)}(|\underline{\mathbf{L}}_{q_a}|) \\ \partial Q_D^{(Z)} &= \sigma_p^2 \Delta \underline{\mathbf{L}}_p \cdot \underline{\mathbf{L}}_p^{(Z)} & \partial^2 Q_D^{(Z)} &= \sigma_p^2 \Delta \underline{\mathbf{L}}_p \cdot \Delta \underline{\mathbf{L}}_p. \end{aligned} \quad (6.21)$$

The result of applying the counter-operator to a perturbation of the two-point function due to particle interactions reads

$$\begin{aligned} i\hat{S}_C \delta^{(n)} G_{\rho\rho}^{(Z,2)}(1,2) &= \int \sum_{\substack{\text{diagr.} \\ \text{indices}}} \left(-\partial Q_D^{(Z)} \tilde{\mathcal{P}}_{ab}^{(Z,1)} - Q_D^{(Z)} \partial \tilde{\mathcal{P}}_{ab}^{(Z,1)} + \partial \tilde{\mathcal{P}}_{ab}^{(Z,2)} \right. \\ &\quad \left. + \partial \tilde{\mathcal{P}}_{ab}^{(Z,1)} \tilde{\mathcal{P}}_{cb}^{(Z,1)} + \tilde{\mathcal{P}}_{ab}^{(Z,1)} \partial \tilde{\mathcal{P}}_{cb}^{(Z,1)} + \partial \tilde{\mathcal{P}}_{ab}^{(Z,1)} \tilde{\mathcal{P}}_{cd}^{(Z,1)} + \tilde{\mathcal{P}}_{ab}^{(Z,1)} \partial \tilde{\mathcal{P}}_{cd}^{(Z,1)} \right), \end{aligned} \quad (6.22)$$

where derivatives of combined correlation lines $\tilde{\mathcal{P}}_{ab}$ are evaluated by expressing them in terms of individual linearized lines $Q^{\delta\delta}$, $Q^{\delta p}$ and Q^{pp} and applying Leibniz' rule. These terms need to be evaluated for up to four powers of the counter-operator, such that at n -th order perturbation theory, where $n \geq 4$ we get

$$\begin{aligned} \Delta^{(n)} G_{\rho\rho}^{(Z,2)}(1,2) &= \delta^{(n)} G_{\rho\rho}^{(Z,2)}(1,2) + i\hat{S}_C \delta^{(n-1)} G_{\rho\rho}^{(Z,2)}(1,2) + \frac{1}{2} (i\hat{S}_C)^2 \delta^{(n-2)} G_{\rho\rho}^{(Z,2)}(1,2) \\ &+ \frac{1}{3!} (i\hat{S}_C)^3 \delta^{(n-3)} G_{\rho\rho}^{(Z,2)}(1,2) + \frac{1}{4!} (i\hat{S}_C)^4 \delta^{(n-4)} G_{\rho\rho}^{(Z,2)}(1,2). \end{aligned} \quad (6.23)$$

As was the case for Newtonian trajectories, manually evaluating perturbation theory beyond the first order with Zel'dovich trajectories is extremely lengthy and most certainly fails due to inevitable arithmetic mistakes. Instead, diagrams are evaluated symbolically with the same algorithm as for Newtonian perturbation theory, and applications of the counter-operator are implemented on top of these results.

6.2.3 Results for the dark matter power spectrum

The corrections to the dark matter power spectrum with Zel'dovich trajectories at linear and quadratic order in the initial power spectrum are plotted in [Figure 6.4a](#). As was

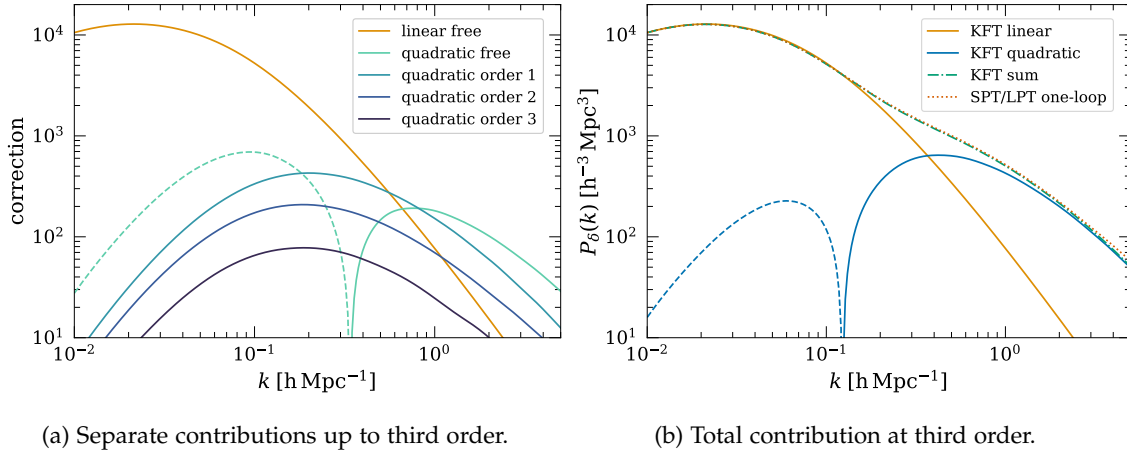


Figure 6.4: Contributions to the dark matter power spectrum linear and quadratic in the initial power spectrum. Whereas the blue curves in (a) show corrections to the power spectrum at quadratic order in the initial power spectrum, the linear order is shown in orange. Quadratic corrections decrease in overall amplitude with increasing order, showing a nice convergent behaviour. Only the quadratic free-streaming term leads to negative contributions (marked by a dashed line) on large scales. In (b), the overall quadratic correction, as well as the full power spectrum at quadratic order in $P_{\delta}^{(i)}$ are shown. Comparison with one-loop SPT shows that both results coincide with great accuracy. Including even higher order corrections (in the interaction operator) in KFT, we expect to converge exactly towards the SPT result.

stressed previously, the only contribution at linear order is the linear power spectrum with the correct large-scale amplitude. Quadratic corrections are displayed up to third order and show a different behaviour from the Newtonian case. Where corrections due to particle interactions were increasing in amplitude up to extremely high orders for Newtonian trajectories, we observe a monotonous decrease in their overall amplitude

for Zel'dovich trajectories. Additionally, perturbations due to the interaction operator show an overall positive contribution on all length scales; negative contributions on large scales are entirely due to free-streaming. From this point of view, we can confirm that Zel'dovich trajectories are much better suited for a perturbative treatment of canonical perturbation theory in cosmic structure formation than their Newtonian counterpart.

Higher-order corrections become increasingly smaller, and going beyond third-order perturbation theory will only lead to tiny corrections compared to the third-order result. Adding up all quadratic contributions to the third order in the interaction operator results in the blue curve in [Figure 6.4b](#). Interestingly, comparing the final result of the power spectrum to one-loop SPT/first-order LPT shows that both curves match almost perfectly. Indeed, were we to include corrections of even higher order, we expect that the result would converge precisely towards the one-loop power spectrum. This outcome is quite unfortunate since SPT results are notoriously unstable and not to be trusted beyond mildly non-linear scales, suggesting that the same must be true for KFT. The fact that KFT and SPT yield the same result comes as a surprise, since there is no apparent reason for KFT to break down after stream-crossing has happened. On the other hand, we did need to expand the initial conditions up to quadratic order in the initial power spectrum. Although it is not evident that this expansion inevitably leads to an inconsistent theory on small scales, expanding the correlation lines in $P_\delta^{(i)}$ seems to be equivalent to doing a loop-expansion in SPT. It, hence, becomes clear that the full power of KFT can only be harnessed by evaluating correlation lines without the need for an expansion in the initial power spectrum. The advantage of KFT compared to SPT of LPT is that, although computationally challenging, circumventing a power series in the linear/initial power spectrum is possible, at least in principle. There is, therefore, a clear, albeit tedious path ahead for canonical perturbation theory in KFT.

6.2.4 Remarks on the evaluation

Cancellations between different terms

Before concluding the section on the Zel'dovich power spectrum, let us point out that the current evaluation of corrections to the power spectrum is problematic from a numerical point of view. It is a known issue in SPT that mode-coupling and self-energy contributions lead to significant cancellations on small scales, which require enormously accurate integration techniques. As we can observe in [Figure 6.5](#), the same is true even more in KFT with Zel'dovich trajectories. The curves shown in the figure represent the individual terms in first-order perturbation theory, which can be sketched as

$$\begin{aligned} \Delta^{(1)} G_{\rho\rho}^{(Z,2)}(1,2) = & \left[(i\hat{S}_C)\hat{\rho}(1)\hat{\rho}(2)Z_0[\underline{\mathbf{J}},\underline{\mathbf{K}}] \right]_{\text{SE}}^{(2)} + \left[(i\hat{S}_C)\hat{\rho}(1)\hat{\rho}(2)Z_0[\underline{\mathbf{J}},\underline{\mathbf{K}}] \right]_{\text{MC}}^{(2)} \\ & + \left[(i\hat{S}_I)\hat{\rho}(1)\hat{\rho}(2)Z_0[\underline{\mathbf{J}},\underline{\mathbf{K}}] \right]_{\text{SE}}^{(2)} + \left[(i\hat{S}_I)\hat{\rho}(1)\hat{\rho}(2)Z_0[\underline{\mathbf{J}},\underline{\mathbf{K}}] \right]_{\text{MC}}^{(2)}, \end{aligned} \quad (6.24)$$

where self-energy and mode-coupling contributions are split up and marked with a SE and MC, respectively. There is a quite precise cancellation both between damping and mode-coupling terms for counter and particle interaction individually and again between both results. As a result, cancellations of up to two orders of magnitude are necessary to arrive from the results of the numerical integration to the final expression. These large cancellations severely limit the precision of our results since they worsen—the amplitude of individual contributions rising and that of the final result decreasing—for

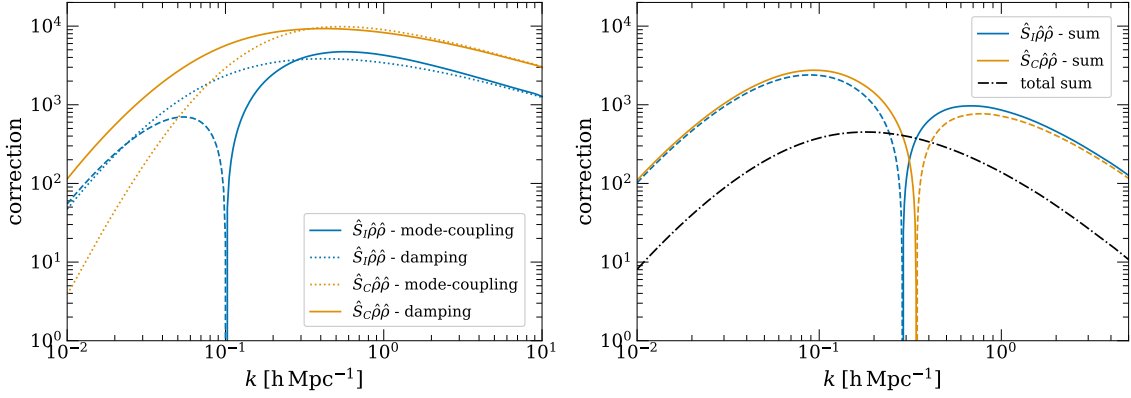


Figure 6.5: Illustration of the large cancellations that occur when evaluating KFT with Zel’dovich trajectories. In the left panel, the blue curves represent the negative damping (dotted) and mode-coupling (full, dashed where negative) contributions from the term that stems from applying the particle interaction operator to the two-point function. Orange curves represent the same contributions for the counter-operator. Note that the counter-operator switches the signs of the contributions, leading to a positive damping (full line) and a negative mode-coupling term. In the right panel, the sum of damping and mode-coupling contributions are shown for the counter-operator (orange) and the particle interaction (blue) terms. Dashed lines indicate negative terms. The final result, i. e. the sum of both contributions, is the black dashed-dotted line.

increasing orders in perturbation theory, prohibiting us from reliably calculating corrections beyond the third order with our current numerical methods. If we could evaluate correlation lines without an expansion in the initial power spectrum, cancellations between mode-coupling and damping terms would be eliminated, but those caused by the counter-operator would persist.

The relevance of all correlation lines

We have seen in [Section 4.5](#) that momentum correlation lines completely dominate the free-streaming power spectrum in KFT if we use Zel’dovich trajectories. This dominance can be traced back to the fact that the other lines come with smaller powers of the particle propagator and therefore become irrelevant as the latter grows larger. In earlier works on KFT, this was used as a motivation to neglect all but momentum correlation lines, even in perturbative calculations with Zel’dovich trajectories. Here we compare the results of neglecting density-density and density-momentum correlations with those where all correlation lines are evaluated for different perturbation orders. [Figure 6.6](#) shows that neglecting certain correlation lines for calculations of corrections to the dark matter power spectrum leads to considerable errors in the resulting terms. The underlying reason is two-fold:

1. Perturbative corrections in KFT integrate the effect of particle interactions over time, such that contributions from early times, where all correlation lines are equally important, become relevant. This argument is similar to SPT, where linear growth is entirely dominated by the growing solution for the density contrast such that the decaying solution plays no role in the tree-level amplitude. When calculating loop corrections, however, results are obtained by integrating over time, such that both the growing and the decaying modes need to be taken into account to recover the correct one-loop result.

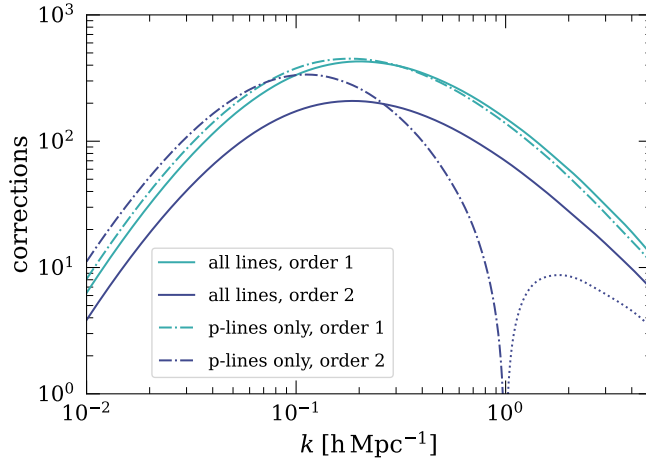


Figure 6.6: Comparison of first (teal) and second (dark blue) order corrections to the power spectrum at quadratic order in the initial power spectrum. Results, where all correlation lines were considered, are represented by full lines. The dashed-dotted lines, on the other hand, show the results if only momentum correlations are taken into account. In first-order perturbation theory, the difference is noticeable but small, whereas the second-order result deviates considerably from the correct curve and even becomes negative (dotted line) on small scales.

2. Due to the substantial cancellations between counter- and particle interaction terms, small contributions to the resulting terms become essential and cannot simply be neglected.

Figure 6.6 nicely illustrates that the difference between results with only momentum correlation lines and those with all correlation lines considered becomes larger for increasing order in perturbation theory. The upshot is that, even when working with Zel’dovich trajectories in KFT, all correlation lines need to be taken into account.

6.3 DISCUSSION

This chapter introduced a systematic approach to derive expressions in canonical KFT perturbation theory for Newtonian and Zel’dovich trajectories. Whereas we put the focus on calculating the synchronous two-point function at quadratic order in the initial power spectrum, the methods and ideas we introduced extend to higher-order spectra. The basis of the derivation of the final results is a symbolic code that allows for the systematic calculation of perturbative corrections, in theory, up to arbitrary order in perturbation theory. However, we encounter limitations in the symbolic evaluation of diagrams due to the sheer number of terms that need to be calculated and in the numerical stability of the integration of the result due to the increasingly large number of time integrals.

For Newtonian trajectories, perturbations up to the eighth order were calculated, plotted, and discussed, the upshot being that canonical perturbation theory, in combination with Newtonian particle propagators, is seemingly not well suited for precision calculations in cosmology. Indeed, the convergence of corrections at quadratic order in $P_\delta^{(i)}$ seems to proceed considerably slower than for the linear calculation. Although we were unable to calculate corrections reliably beyond order 8 in the interaction operator, ex-

trapolating our results suggests that considerably higher orders would be needed to observe convergence towards SPT.

Perturbative corrections to the two-point function with Zel'dovich trajectories, however, seem well-behaved and show a decreasing amplitude with increasing perturbation order. Already at third-order perturbation theory, we observe a convergence toward the one-loop SPT result, which is both reassuring and concerning at the same time. On the one hand, it shows that Zel'dovich trajectories, although seemingly unnatural to KFT, result in a perturbation series that converges very quickly. On the other hand, it is mildly surprising that KFT converges toward the result of a theory, which we know to be inconsistent in the non-linear regime. This is a non-trivial result in that we start with a theory that should be well-behaved even in the multi-streaming regime and end up with the same result as SPT, which manifestly breaks down at stream-crossing. The most likely explanation for this behaviour is that KFT loses its conceptual edge once we expand correlation lines in the initial power spectrum. It is unclear how, but this approximation appears to reintroduce the single-stream approximation that KFT tries to circumvent. This result suggests that the most promising path forward for KFT is to try at all costs to circumvent the expansion of correlation lines.

 CONCLUSION

We started this work with a condensed introduction into cosmic structures and their formal description, giving brief overviews of the basics of two well-established analytical approaches to cosmic structure formation. Both these approaches, namely Standard (Eulerian) Perturbation Theory (SPT) and Lagrangian Perturbation Theory (LPT), are based on the assumption that the content of the Universe can be treated as a collisionless fluid, restricting their range of applicability to relatively large scales and only mildly non-linear structures. Although various extensions of SPT and LPT, trying to tackle their fundamental restrictions from different angles, exist, we proposed to drop the hydrodynamic description altogether by working with Kinetic Field Theory (KFT), a particle-based approach.

KFT is a path-integral approach to statistical non-equilibrium systems whose evolution is governed by the phase-space dynamics of classical particles. In our thorough introduction to KFT, we derived the generating functional, emphasising the perturbative treatment of particle interactions and their interpretation. Over the years, various reformulations of KFT have emerged from the need to cast the theory into a shape that is more akin to the path integral formalism of quantum field theory (QFT). While we believe these to be promising paths to strike, we were curious to examine how far the most basic approach, i. e. canonical KFT, can take us in the description of cosmic structures. The extreme flexibility of the theory allowed us to use a simple toy model, far removed from the complexity of cosmic structure formation, to gain some intuition about the physical role and the mathematical description of the perturbative treatment of the interaction operator. Building on these ideas, we developed a new diagrammatic language for canonical perturbation theory, putting the particle nature of the underlying dynamics into the spotlight. The main challenge in describing cosmic structures lies in the initial conditions obtained via Poisson sampling of the particles' initial phase-space coordinates from the underlying Gaussian density and velocity field. We ordered these initial conditions in the number of correlation lines connecting increasingly large particle clusters. The main advantage of our diagrammatic approach is that it allows us to treat both particle interactions and correlations in the same graphical description.

Besides the complicated initial conditions, particle trajectories are a crucial point of discussion for the description of cosmic structures with canonical KFT. We have highlighted that Newtonian particle trajectories cannot reproduce the correct linear growth behaviour at the level of free-streaming, prompting us to impose Zel'dovich trajectories for the free motion of microscopic particles. Unlike previous works, we imposed this alternative definition of free particle trajectories at the level of the equations of motion by pulling the expression for the interaction potential of first-order LPT into the free e. o. m. $\mathcal{E}[\mathbf{x}]$. This choice naturally leads to an additional component, the counter-operator \hat{S}_C in the interaction operator, which, as we could show, restores the correct particle trajectories. For particles on Zel'dovich trajectories, the interaction operator thus

turned into a sum of two operators, one encoding particle interactions due to gravity and the other compensating for the unbounded free motion described by the Zel'dovich particle propagator.

We then moved on to proper applications of canonical KFT, notably calculating the dark matter power spectrum, starting with the linear-growth behaviour. Since the dynamics of macroscopic quantities, such as the particle density, do not trivially follow from that of the microscopic degrees of freedom, describing linear growth from canonical KFT alone requires a considerable amount of effort. We showed how the inclusion of correlation lines in our diagrammatic approach could be used to derive the topology of diagrams contributing to linear structure formation and evaluated the resulting expressions. Leaning on previous results from resummed and grand-canonical KFT, we were able to analytically perform the resummation of the entire class of diagrams to exactly recover the large-scale linear growth of the dark matter power spectrum from Newtonian phase-space dynamics. On the one hand, this result is a significant step in clarifying the relation between the different approaches to KFT and can be built upon to deepen our intuition of more abstract macroscopic reformulations of KFT. On the other hand, it highlights the challenges facing canonical KFT when applied to cosmic structure formation with simple Newtonian trajectories. Indeed, truncating the perturbative expansion of the interaction operator shows that we converge towards the correct linear growth behaviour at the percent level only after thirteen orders in the expansion.

Zel'dovich trajectories, on the other hand, are known to reproduce the correct linear growth behaviour of the dark matter power spectrum at the free-streaming level. However, since a systematic treatment of the interaction operator in KFT with Zel'dovich trajectories has not been analysed systematically until this point, it was unclear whether corrections due to the interaction operator would add further unphysical, large-scale growth. Using the expression of the interaction operator in terms of the counter-operator, we could show for the first time that this is not the case. At linear order in the initial power spectrum, the counter-operator leads to an exact cancellation of terms at each perturbation order individually, such that there are no corrections to the free linear Zel'dovich solution. This result puts Zel'dovich trajectories in canonical KFT on a solid foundation, at least at the mathematical level.

With the description of linear structure formation in the framework of canonical KFT clarified, we then moved on to the more interesting case of higher-order corrections in the initial power spectrum. Specifically, we restricted ourselves to quadratic contributions in the initial power spectrum. Immediately we are confronted with significantly more challenging calculations since both the diversity of diagram topologies and the number of configurations of initial correlations dramatically increase if we allow for the occurrence of two correlation lines. Most of the analysis was therefore performed with a symbolic code, and the final results were obtained by numerically integrating the automatically generated expressions.

For Newtonian particle trajectories, we obtained results up to eighth order in the interaction operator and concluded that a far higher order is needed until the series converges. Indeed, the behaviour of the resulting corrections suggests that we need considerably higher orders in the interaction operator at quadratic order compared to linear order in $P_\delta^{(i)}$, which is problematic for two reasons:

- The vastly higher number and increased variety of terms at quadratic order in $P_\delta^{(i)}$ compared to the linear result makes an evaluation of high order corrections, at

the level of both the symbolic generation of terms and their numerical integration, much more costly.

- As we will see, results from Zel'dovich trajectories suggest that the result does indeed converge towards one-loop SPT, which is known to be untrustworthy at non-linear scales.

It is questionable whether canonical perturbation theory with Newtonian particle trajectories is a good way to move forward if we are interested in a precise and efficient description of non-linear structure formation.

Our results for Zel'dovich trajectories, on the other hand, look more promising. In the analysis of perturbation theory, both the particle interaction operator and the counter-operator need to be evaluated consistently. Since \hat{S}_C acts on free correlation lines, at most, four powers of the counter-operator need to be taken into account at quadratic order in $P_\delta^{(i)}$. The numerical evaluation of the resulting corrections to the power spectrum looks promising; unlike for Newtonian trajectories, perturbative corrections systematically decrease in amplitude as we proceed to higher orders. As a result, we observe a quick convergence of the series, suggesting that corrections beyond third order play little to no role in our analysis. As we pointed out, consistent treatment of Zel'dovich trajectories and the corresponding interaction operator requires information on all the initial correlations. The final result for the power spectrum at quadratic order in the initial power spectrum converges towards the one-loop SPT result. Since the basic assumptions of KFT are much less restrictive than those of SPT, and there is no apparent reason why KFT should not be able to describe non-linear structure formation if evaluated exactly, we conclude that the expansion of initial correlation lines in the initial power spectrum is responsible for this correspondence. A more systematic comparison between KFT and SPT would help us understand this result better. For now, the results suggest that an expansion in terms of the initial power spectrum robs KFT of its conceptual edge and pulls it back to the same level as hydrodynamic descriptions. However, unlike the hydrodynamic descriptions of cosmic structure formation, KFT does not rely on such an expansion. Indeed, we can derive expressions for perturbations of the power spectrum due to particle interactions that include the complete hierarchy of initial correlations. If we wish to harness the full power of KFT, the proper evaluation of correlation lines can and should not be circumvented and should occupy the top spot in the list of priorities for the future developments of KFT.

Part III

APPENDIX

A

DETAILED CALCULATIONS FOR EULERIAN AND LAGRANGIAN PERTURBATION THEORY

A.1 TRANSFORMING THE TIME COORDINATE IN THE EULER-POISSON SYSTEM

To rewrite (2.16)–(2.18) in terms τ from (2.22), first note that $\frac{d\tau}{dt} = f(\Omega_m)H$, where $f(\Omega_m) = \frac{d \ln D_+}{d \ln a}$ is the growth rate of cosmic structures. The continuity equation (2.16) in terms of the new time coordinate reads

$$\dot{\delta} + \nabla \cdot [(1 + \delta)\mathbf{u}] = 0, \quad (\text{A.1})$$

where we redefined the velocity field $\mathbf{u}(\mathbf{q}, \tau) = \frac{\mathbf{v}(\mathbf{q}, t(\tau))}{Hf}$. Additionally, we defined the dot to represent derivatives w. r. t. the new time coordinate τ for a more compact notation. The time-derivative of the velocity field in the Euler equation thus turns into

$$\partial_t \mathbf{v}(\mathbf{q}, t) = \partial_t(Hf)\mathbf{u}(\mathbf{q}, \tau) + Hf \frac{d\tau}{dt} \dot{\mathbf{u}}(\mathbf{q}, \tau). \quad (\text{A.2})$$

The prefactor of the second term is simply $H^2 f^2$. Using that $Hf = \partial_t D_+ / D_+$ the prefactor of the first term evaluates to

$$\partial_t(Hf) = \frac{\partial_t^2 D_+}{D_+} - \left(\frac{\partial_t D_+}{D_+} \right)^2 = \frac{3}{2} H^2 \Omega_m - 2H^2 f - H^2 f^2, \quad (\text{A.3})$$

where we used (2.20) to get rid of the second order time derivative and re-expressed the derivative of the growth factor in terms of f and H . Reinsertion into the Euler equation shows that the new velocity field $\mathbf{u}(\mathbf{q}, \tau)$ satisfies

$$\dot{\mathbf{u}} + \left(\frac{3\Omega_m}{2f^2} - 1 \right) \mathbf{u} + (\mathbf{u} \cdot \nabla) \mathbf{u} + \frac{1}{a^2 H^2 f^2} \nabla \Phi = 0, \quad (\text{A.4})$$

which in turn suggests a redefinition of the gravitational potential. In fact, absorbing the arising pre-factor results in a new potential $\phi(\mathbf{q}, \tau)$ which satisfies the Poisson equation

$$\nabla^2 \phi = \frac{4\pi G}{a^2 H^2 f^2} a^2 \bar{\rho}_m \delta = \frac{3\Omega_m}{2f^2} \delta, \quad (\text{A.5})$$

where we used the definition of the mean mass density in terms of the critical density (2.4) and the density parameter Ω_m in the last step. In summary, after performing the transformation to the new time coordinate τ , the Euler-Poisson system (2.16)–(2.18) turns into

$$\dot{\delta} + \nabla \cdot [(1 + \delta)\mathbf{u}] = 0 \quad (\text{A.6})$$

$$\dot{\mathbf{u}} + \frac{\mu}{2} \mathbf{u} + (\mathbf{u} \cdot \nabla) \mathbf{u} + \nabla \phi = 0 \quad (\text{A.7})$$

$$\nabla^2 \phi = (\mu/2 + 1) \delta, \quad (\text{A.8})$$

where we introduced the time-dependent variable $\mu(\tau) = 2\left(\frac{3\Omega_m}{2f^2} - 1\right)$ for notational convenience.

A.2 FIRST ORDER LPT SOLUTION EQUATION

To derive the first order e. o. m. for the displacement field in LPT we need to perform a coordinate transform from the Eulerian coordinate \mathbf{q} to the Lagrangian coordinate $\mathbf{q}^{(i)}$ for $\nabla_{\mathbf{q}}$ and expand both $\nabla_{\mathbf{q}}$ and the determinant J to first order in the displacement field. First, note that $\nabla_{\mathbf{q}} = (\partial\mathbf{q}/\partial\mathbf{q}^{(i)})^{-1}\nabla_{\mathbf{q}^{(i)}} = \nabla_{\mathbf{q}^{(i)}} + \mathcal{O}(\Psi)$, allowing us to simply replace the gradient in (2.38) by $\nabla_{\mathbf{q}^{(i)}}$ at lowest order. For small values of the displacement field the argument of the determinant

$$J = \det\left(\mathcal{I}_3 + \frac{\partial\Psi}{\partial\mathbf{q}^{(i)}}\right) \quad (\text{A.9})$$

can be viewed as a first order expansion of a matrix exponential. Using $\det e^A = e^{\text{Tr}A}$ and re-expanding the exponential of the trace, we find

$$J^{-1} = 1 - \text{Tr}\left(\frac{\partial\Psi}{\partial\mathbf{q}^{(i)}}\right) + \mathcal{O}(\Psi^2) = 1 - \nabla_{\mathbf{q}^{(i)}} \cdot \Psi + \mathcal{O}(\Psi^2). \quad (\text{A.10})$$

Introducing the index notation $\Psi_{i,i} := \nabla_{\mathbf{q}^{(i)}} \cdot \Psi$ for the divergence of the displacement field turns (2.38) at first order into

$$\ddot{\Psi}_{i,i}^{(1)} + \frac{\mu}{2} \dot{\Psi}_{i,i}^{(1)} - (\mu/2 + 1)\Psi_{i,i}^{(1)} = 0, \quad (\text{A.11})$$

which is exactly the linear growth equation from SPT and therefore solved by

$$\Psi_{i,i}^{(1)}(\mathbf{q}^{(i)}, \tau) = e^{\tau} \Psi_{i,i}^{(i)}(\mathbf{q}^{(i)}). \quad (\text{A.12})$$

Since the equation of motion is valid for the divergence of Ψ it also holds for Ψ itself if the field is curl-free.

A.3 DERIVATION OF THE POWER SPECTRUM IN THE ZEL'DOVICH APPROXIMATION

Using mass conservation (2.37) and neglecting initial density fluctuations we can derive the relation between the Fourier-space density contrast and the displacement field

$$\delta(\mathbf{k}, \tau) = \int_{\mathbf{q}^{(i)}} e^{-i\mathbf{k}\cdot\mathbf{q}^{(i)}} (e^{-i\mathbf{k}\cdot\Psi(\mathbf{q}^{(i)}, \tau)} - 1). \quad (\text{A.13})$$

The density power spectrum therefore reads

$$P_{\delta}(k) = \int_{\mathbf{k}'} \langle \delta(\mathbf{k}, \tau) \delta(\mathbf{k}', \tau) \rangle = \int_{\Delta\mathbf{q}^{(i)}} e^{-i\mathbf{k}\cdot\Delta\mathbf{q}^{(i)}} (\langle e^{-i\mathbf{k}\cdot\Delta\Psi} \rangle - 1), \quad (\text{A.14})$$

where we defined $\Delta\Psi = \Psi(\mathbf{q}^{(i)}) - \Psi(\mathbf{q}^{(i)} + \Delta\mathbf{q}^{(i)})$ whose expectation value is independent of $\mathbf{q}^{(i)}$ due to homogeneity. The expectation value of a Fourier-phase can be expressed by a cumulant expansion

$$\langle e^{-i\mathbf{k}\cdot\Delta\Psi} \rangle = \exp\left\{ \sum_{n=1}^{\infty} \frac{(-i)^n}{n!} \langle (\mathbf{k} \cdot \Delta\Psi)^n \rangle_c \right\}, \quad (\text{A.15})$$

where the n -th order cumulants of shifts in the displacement fields $\langle (\mathbf{k} \cdot \Delta\Psi)^n \rangle_c$ are non-vanishing for all even n in general. In the case of non-vanishing higher order cumulants ($n > 2$), we again have to resort to a perturbative expansion of (A.15), which is the

usual approach of LPT. The ZA, on the other hand, is a special case that allows for an exact evaluation of (A.15). Here, the displacement field which, expressed in terms of the initial velocity potential, reads

$$\Psi^{(1)}(\mathbf{q}^{(i)}, \tau) = e^\tau \nabla \psi^{(i)}(\mathbf{q}^{(i)}), \quad (\text{A.16})$$

follows a GRF for which all cumulants beyond second order are vanishing. The sum in expression (A.15) then collapses and, the only remaining term being the quadratic one, turns into a Gaussian for the second cumulant. The latter splits into two parts

$$\begin{aligned} \langle (\mathbf{k} \cdot \Delta \Psi^{(1)})^2 \rangle_c &= 2\mathbf{k} \cdot \langle \Psi^{(1)}(\mathbf{q}^{(i)}) \otimes \Psi^{(1)}(\mathbf{q}^{(i)}) \rangle_c \cdot \mathbf{k} \\ &\quad - 2\mathbf{k} \cdot \langle \Psi^{(1)}(\mathbf{q}^{(i)}) \otimes \Psi^{(1)}(\mathbf{q}^{(i)} + \Delta \mathbf{q}^{(i)}) \rangle_c \cdot \mathbf{k}, \end{aligned} \quad (\text{A.17})$$

which can be evaluated in terms of the velocity potential power spectrum by employing (A.16) and going to Fourier-space. Using (2.29) to replace the power spectrum with the density fluctuation power spectrum, we get

$$\begin{aligned} \langle \Psi^{(1)}(\mathbf{q}^{(i)}) \otimes \Psi^{(1)}(\mathbf{q}^{(i)} + \Delta \mathbf{q}^{(i)}) \rangle_c &= e^{2\tau} \int_{\mathbf{k}'} \frac{\mathbf{k}' \otimes \mathbf{k}'}{k'^4} P_\delta^{(i)}(k') e^{i\mathbf{k}' \cdot \Delta \mathbf{q}^{(i)}} \\ &=: \mathbf{C}_{\Psi\Psi}(\Delta \mathbf{q}^{(i)}). \end{aligned} \quad (\text{A.18})$$

Altogether, the resulting power spectrum in the Zel'dovich approximation thus turns out to be

$$P_\delta^{(Z)}(k) = e^{-\sigma_\Psi^2 k^2} \int_{\Delta \mathbf{q}^{(i)}} \left(e^{\mathbf{k}^\top \mathbf{C}_{\Psi\Psi}(\Delta \mathbf{q}^{(i)}) \mathbf{k}} - 1 \right) e^{-i\mathbf{k} \cdot \Delta \mathbf{q}^{(i)}}, \quad (\text{A.19})$$

where we defined the variance of the displacement field via the matrix evaluated at zero distance $-\sigma_\Psi^2 \mathcal{I}_3 := \mathbf{C}_{\Psi\Psi}(0)$.

B

PARTICLE TRAJECTORIES

B.1 DERIVATION OF GENERAL PARTICLE TRAJECTORIES

Particle trajectories in the KFT generating functional are derived from the initial value problem

$$\mathcal{E}_0[\underline{x}] + \underline{K} = \dot{\underline{x}} - \mathcal{M} \underline{x} + \underline{K} = \underline{0} \quad \underline{x}(t_i) = \underline{x}^{(i)}. \quad (\text{B.1})$$

Here we will show how to solve this first order linear inhomogeneous differential equation in general to derive (3.23). To this end, we express the equations of motion for single particles

$$\dot{\mathbf{x}}_a(t) - \mathcal{M}(t) \mathbf{x}_a(t) = -\mathbf{K}_a(t) \quad \mathbf{x}_a(t_i) = \mathbf{x}_a^{(i)} \quad \forall a = 1, \dots, N. \quad (\text{B.2})$$

In the most general case, $\mathcal{M}(t)$ is a time-dependent matrix which does not commute with itself at different times. First we solve the homogeneous equation which results in

$$\begin{aligned} \mathbf{x}_a^{(\text{hom.})}(t) &= \mathcal{G}(t, t_i) \mathbf{x}_a^{(i)} \\ \text{with } \mathcal{G}(t, t_i) &= \mathcal{I}_6 + \sum_{n=1}^{\infty} \int_{t_i}^t dt_1 \cdots \int_{t_i}^{t_{n-1}} dt_n \mathcal{M}(t_1) \cdots \mathcal{M}(t_n). \end{aligned} \quad (\text{B.3})$$

For the special case where the matrix $\mathcal{M}(t)$ is self-commuting at different times, the above series expression simplifies to a matrix exponential

$$\mathcal{G}(t, t_i) = \exp\left(\int_{t_i}^t d\bar{t} \mathcal{M}(\bar{t})\right). \quad (\text{B.4})$$

To solve the inhomogeneous equation we derive the Green's function $\mathbf{G}(t, t')$ which, by definition, solves the differential equation

$$(\mathcal{I}_6 \partial_t - \mathcal{M}(t)) \mathbf{G}(t, t') = \mathcal{I}_6 \delta_D(t - t'). \quad (\text{B.5})$$

This can be solved by using the Ansatz $\mathbf{G}(t, t') = \mathbf{F}(t, t') \theta(t - t')$, with the Heaviside step function $\theta(t - t')$. Inserting this into (B.5), we find that the matrix $\mathbf{F}(t, t')$ has to satisfy the homogeneous equation and that $\mathbf{F}(t, t) = \mathcal{I}_6$. The solution to the inhomogeneous equation is thus given by

$$\mathbf{x}_a^{(\text{inhom.})}(t) = - \int d\bar{t} \mathbf{G}(t, \bar{t}) \mathbf{K}_a(\bar{t}) \quad \text{with } \mathbf{G}(t, \bar{t}) = \mathcal{G}(t, \bar{t}) \theta(t - \bar{t}). \quad (\text{B.6})$$

Note that the Green's function is simply the product of the matrix that solves the homogeneous equations evaluated at t and \bar{t} , and the Heaviside function. The final particle trajectory is the sum of both solutions and can therefore be written as

$$\tilde{\mathbf{x}}_a[\mathbf{K}_a, t] = \mathbf{G}(t, t_i) \mathbf{x}_a^{(i)} - \int d\bar{t} \mathbf{G}(t, \bar{t}) \mathbf{K}_a(\bar{t}). \quad (\text{B.7})$$

For simplicity, we refer to the time-dependent factors in both the homogeneous and the inhomogeneous solutions as the Green's function $\mathbf{G}(t, \bar{t})$, keeping in mind that the homogeneous solution is defined without a step function. Returning to the tensor notation, the full bundle of phase-space trajectories is given by

$$\tilde{\mathbf{x}}[\mathbf{K}, t] = \underline{\mathbf{G}}(t, t_i) \mathbf{x}^{(i)} - \int d\bar{t} \underline{\mathbf{G}}(t, \bar{t}) \mathbf{K}(\bar{t}). \quad (\text{B.8})$$

B.2 PHASE-SPACE TRAJECTORIES IN COSMOLOGY - NEWTONIAN TRAJECTORIES

For phase-space trajectories on an expanding background with the time parameter τ from (2.22) the free equations of motion read

$$\underline{\mathcal{E}}_0[\mathbf{x}] = \dot{\mathbf{x}} - \mathcal{M}\mathbf{x} \quad \text{with} \quad \mathcal{M} = \begin{pmatrix} 0_3 & \mathcal{I}_3 \\ 0_3 & -\frac{\mu}{2} \mathcal{I}_3 \end{pmatrix}. \quad (\text{B.9})$$

Note that we omitted particle indices here, but it should be clear that $\mathbf{x}(\tau)$ is the phase-space trajectory of a single particle with initial conditions $\mathbf{x}^{(i)}$. Since \mathcal{M} is not self-commuting at different times, we employ (B.3). Straightforward matrix multiplication yields

$$\mathcal{M}(\tau_1) \cdots \mathcal{M}(\tau_n) = \begin{pmatrix} \mathcal{I}_3 & (-1)^{n-1} \frac{\mu_2}{2} \cdots \frac{\mu_n}{2} \mathcal{I}_3 \\ 0_3 & (-1)^n \frac{\mu_1}{2} \cdots \frac{\mu_n}{2} \mathcal{I}_3 \end{pmatrix}, \quad (\text{B.10})$$

where we abbreviated $\mu(\tau_i) \equiv \mu_i$, allowing us to identify the particle propagator as

$$g_{qp}(\tau, \tau') = \sum_{n=1}^{\infty} \int_{\tau'}^{\tau} d\tau_1 \int_{\tau'}^{\tau_1} d\tau_2 \cdots \int_{\tau'}^{\tau_{n-1}} d\tau_n (-1)^{n-1} \frac{\mu_2}{2} \cdots \frac{\mu_n}{2}. \quad (\text{B.11})$$

The integrand in the nested integral is no-longer matrix-valued, such that the individual terms commute, and we get

$$\int_{\tau'}^{\tau_1} d\tau_2 \cdots \int_{\tau'}^{\tau_{n-1}} d\tau_n (-1)^{n-1} \frac{\mu_2}{2} \cdots \frac{\mu_n}{2} = \frac{(-1)^{n-1}}{(n-1)!} \frac{1}{2^{n-1}} \left(\int_{\tau'}^{\tau_1} d\bar{\tau} \mu(\bar{\tau}) \right)^{n-1}. \quad (\text{B.12})$$

The series therefore takes the form of an exponential series, yielding the final result

$$g_{qp}(\tau, \tau') = \int_{\tau'}^{\tau} d\tau_1 \exp\left(-\frac{1}{2} \int_{\tau'}^{\tau_1} d\bar{\tau} \mu(\bar{\tau})\right). \quad (\text{B.13})$$

The pp -component is derived analogously from the resummation of a series or by using the fact that the equations of motion impose that it is given by a derivative of the particle propagator w. r. t. time τ . As a result, we recover the Green's function

$$\mathbf{G}(\tau, \tau') = \begin{pmatrix} \mathcal{I}_3 & g_{qp}(\tau, \tau') \mathcal{I}_3 \\ 0_3 & \dot{g}_{qp}(\tau, \tau') \mathcal{I}_3 \end{pmatrix} \theta(\tau - \tau'), \quad (\text{B.14})$$

$$\text{with} \quad g_{qp}(\tau, \tau') = \int_{\tau'}^{\tau} d\tau_1 \exp\left(-\frac{1}{2} \int_{\tau'}^{\tau_1} d\bar{\tau} \mu(\bar{\tau})\right). \quad (\text{B.15})$$

As we have shown in Section 2.4, approximating μ by one, although a seemingly crude approximation, yields highly accurate results when we calculate cosmic structure formation, since it is only an approximation for decaying modes in SPT. Setting $\mu = 1$, the integrals in the particle propagator analytically evaluate to

$$g_{qp}(\tau, \tau') = 2(1 - e^{-\frac{1}{2}(\tau - \tau')}). \quad (\text{B.16})$$

B.3 PHASE-SPACE TRAJECTORIES IN COSMOLOGY - ZEL'DOVICH TRAJECTORIES

To include the Zel'dovich potential in the equations of motion we solve

$$\mathcal{E}_0^{(Z)}[\mathbf{x}] + \mathbf{K} = \mathbf{0}, \quad (\text{B.17})$$

where the free e. o. m. $\mathcal{E}_0^{(Z)}[\mathbf{x}]$ defined in (4.80) is the sum of the free e. o. m. for Newtonian trajectories and the Zel'dovich potential. As in the previous section, we omitted particle indices here, but it should be clear that $\mathbf{x}(\tau)$ is the phase-space trajectory of a single particle with initial conditions $\mathbf{x}^{(i)}$. Pulling the Zel'dovich potential into the inhomogeneity by rearranging the e. o. m. to

$$\begin{pmatrix} \dot{\mathbf{q}} \\ \dot{\mathbf{p}} \end{pmatrix} - \begin{pmatrix} 0_3 & \mathcal{I}_3 \\ 0_3 & -\frac{\mu}{2} \mathcal{I}_3 \end{pmatrix} \begin{pmatrix} \mathbf{q} \\ \mathbf{p} \end{pmatrix} = - \begin{pmatrix} \mathbf{K}_q \\ \mathbf{K}_p \end{pmatrix} - \begin{pmatrix} \mathbf{0} \\ \nabla \phi^{(Z)}(\mathbf{q}^{(i)}, \tau) \end{pmatrix}, \quad (\text{B.18})$$

permits us to write down the solution in terms of the Newtonian particle propagator from the previous section. The full phase-space trajectory therefore reads

$$\mathbf{x}[\mathbf{K}, \tau] = \mathbf{G}(\tau, 0) \mathbf{x}^{(i)} - \int d\bar{\tau} \mathbf{G}(\tau, \bar{\tau}) (\mathbf{0}, \nabla \phi^{(Z)}(\mathbf{q}^{(i)}, \bar{\tau}))^T - \int d\bar{\tau} \mathbf{G}(\tau, \bar{\tau}) \mathbf{K}(\bar{\tau}). \quad (\text{B.19})$$

Since $\mathbf{p} = \dot{\mathbf{q}}$, we will focus on the spatial trajectory for the rest; the momentum trajectory can be derived from it by a simple derivative. Ignoring \mathbf{K} for the moment the spatial trajectory reads

$$\mathbf{q}(\tau) = \mathbf{q}^{(i)} + g_{qp}(\tau, 0) \mathbf{p}^{(i)} - \int d\bar{\tau} g_{qp}(\tau, \bar{\tau}) \nabla \phi^{(Z)}(\mathbf{q}^{(i)}, \bar{\tau}). \quad (\text{B.20})$$

Using the initial conditions enables us to evaluate the gradient of the Zel'dovich potential by relating initial density and momenta via the velocity potential:

$$\nabla^2 \phi^{(Z)}(\mathbf{q}^{(i)}, \tau) = \frac{3}{2} e^\tau \delta^{(i)}(\mathbf{q}^{(i)}) = -\frac{3}{2} e^\tau \nabla^2 \psi^{(i)}(\mathbf{q}^{(i)}) \quad (\text{B.21})$$

$$\Rightarrow \nabla \phi^{(Z)}(\mathbf{q}^{(i)}, \tau) = -\frac{3}{2} e^\tau \nabla \psi^{(i)}(\mathbf{q}^{(i)}) = -\frac{3}{2} e^\tau \mathbf{p}^{(i)}. \quad (\text{B.22})$$

This is consistent with the intuition from LPT that particle momenta point into the local gravity well. Inserting the Zel'dovich potential and the definition of the particle propagator (B.16) into the particle trajectory (B.20) results in the time integral

$$\frac{3}{2} \int_0^\tau d\bar{\tau} 2(1 - e^{-\frac{1}{2}(\tau - \bar{\tau})}) e^{\bar{\tau}} = (e^\tau - 1) - 2(1 - e^{-\frac{1}{2}\tau}) \quad (\text{B.23})$$

$$=: g_{qp}^{(Z)}(\tau, 0) - g_{qp}(\tau, 0). \quad (\text{B.24})$$

The Newtonian particle propagator cancels the particle propagator of the homogeneous part in (B.20), effectively replacing $g_{qp}(\tau, 0)$ by $g_{qp}^{(Z)}(\tau, 0)$. Reinstalling the source field \mathbf{K} , we recover the full phase-space trajectories

$$\mathbf{x}[\mathbf{K}, \tau] = \mathbf{G}^{(Z)}(\tau, 0) \mathbf{x}^{(i)} - \int d\bar{\tau} \mathbf{G}(\tau, \bar{\tau}) \mathbf{K}(\bar{\tau}), \quad (\text{B.25})$$

with the Zel'dovich Green's function

$$\mathbf{G}^{(Z)}(\tau, 0) = \begin{pmatrix} \mathcal{I}_3 & g_{qp}^{(Z)}(\tau, 0) \mathcal{I}_3 \\ 0_3 & g_{qp}^{(Z)}(\tau, 0) \mathcal{I}_3 \end{pmatrix}, \quad \text{with } g_{qp}^{(Z)}(\tau, 0) = e^\tau - 1. \quad (\text{B.26})$$

EFFECT OF RESPONSE FIELD OPERATORS

To investigate the effect of response field operators on the generating functional consider applying a single operator $\hat{B}(-R) = \hat{B}(-\mathbf{k}_R, t_R)$ in addition to n density operators to the free generating functional. This gives us the mixed correlation function

$$\begin{aligned}
 & \bar{G}_{B\rho\dots\rho}(-R, 1, \dots, n) \\
 &= \hat{B}(-R) \hat{\rho}(1) \hat{\rho}(2) \dots \hat{\rho}(n) Z_0[\underline{\mathbf{J}}, \underline{\mathbf{K}}] \Big|_{\mathbf{0}} \\
 &= \sum_{\{a_R, a_1 \dots a_n\}}^N \hat{b}_{a_R}(-R) \hat{\rho}_{a_R}(-R) \hat{\rho}_{a_1}(1) \hat{\rho}_{a_2}(2) \dots \hat{\rho}_{a_n}(n) Z_0[\underline{\mathbf{J}}, \underline{\mathbf{K}}] \Big|_{\mathbf{0}} \\
 &= \sum_{\{a_R \dots a_n\}}^N \int d\underline{\Gamma}_i \hat{b}_{a_R}(-R) \exp\left(-\sum_{s=1}^n i\mathbf{k}_s \cdot \bar{\mathbf{q}}_{a_s}[\mathbf{K}_{a_s}, t_s]\right) \exp\left(-i\mathbf{k}_R \cdot \bar{\mathbf{q}}_{a_R}[\mathbf{K}_{a_R}, t_R]\right) \Big|_{\underline{\mathbf{K}}=\mathbf{0}}.
 \end{aligned} \tag{C.1}$$

The one-particle density operator that is part of the response field operator simply adds another one-particle density mode to the free generating functional. In addition, we now have to evaluate the effect of the one-particle response field operator on the density modes. Since it contains a derivative w. r. t. the p -component of the $\underline{\mathbf{K}}$ source field, the one-particle response field operator acts on the inhomogeneous part of the particle trajectories. Recalling that the trajectories read

$$\tilde{\mathbf{q}}_{a_s}[\underline{\mathbf{K}}, t_s] = \mathbf{q}_{a_s}^{(i)} + g_{qp}(t_s, 0) \mathbf{p}_{a_s}^{(i)} - \int_{t_i}^{t_s} d\bar{t} (g_{qp}(t_s, \bar{t}) \mathbf{K}_{p_{a_s}}(\bar{t}) + \mathbf{K}_{q_{a_s}}(\bar{t})) \tag{C.2}$$

and employing the chain rule, we recover the density modes, multiplied by the factor

$$\begin{aligned}
 & \left\{ \hat{b}_{a_R}(-R) \left(-\sum_{s=1}^n i\mathbf{k}_s \cdot \bar{\mathbf{q}}_{a_s}[\mathbf{K}_{a_s}, t_s] \right) \right\}_{\underline{\mathbf{K}}=\mathbf{0}} \\
 &= \left\{ \left(-i\mathbf{k}_R \cdot \frac{\delta}{i\delta\mathbf{K}_{p_{a_R}}(t_R)} \right) \left(-\sum_{s=1}^n i\mathbf{k}_s \cdot \bar{\mathbf{q}}_{a_s}[\mathbf{K}_{a_s}, t_s] \right) \right\}_{\underline{\mathbf{K}}=\mathbf{0}} \\
 &= \sum_{s=1}^n (-i\mathbf{k}_R \cdot \mathbf{k}_s) g_{qp}(t_s, t_R) \delta_{a_R a_s}.
 \end{aligned} \tag{C.3}$$

Due to the property $g_{qp}(t, t) = 0$ of the particle propagator—a direct consequence of causality—the contribution of one-particle response fields acting on density modes at equal time is vanishing. It will turn out that this is equivalent to the statement that particles do not perturb their own trajectories, i. e. there is no self-interaction. To get to the last line we used $\frac{\delta}{i\delta\mathbf{K}_{p_{a_R}}(t_R)} \mathbf{K}_{p_{a_s}}(\bar{t}) = \delta_D(t_R - \bar{t}) \delta_{a_R a_s}$. Now that the dust is slowly

settling, let us collect the emerging terms and make sense of the result. First we note that the one-particle response field operator has left us with a bunch of pre-factors which we collect and refer to as the response-field pre-factor

$$b(s, -R) := (-i\mathbf{k}_R \cdot \mathbf{k}_s) g_{qp}(t_s, t_R). \quad (\text{C.4})$$

Next we scrape together all the other remaining terms

$$\sum_{s=1}^n b(s, -R) \sum_{\{a_R, a_1, \dots, a_n\}}^N \delta_{a_R a_s} \int d\Gamma_{\mathbf{i}} \exp\left(-\sum_{s=1}^n i\mathbf{k}_s \cdot \bar{\mathbf{q}}_{a_s}(t_s)\right) \exp\left(-i\mathbf{k}_R \cdot \bar{\mathbf{q}}_{a_R}(t_R)\right), \quad (\text{C.5})$$

and allow ourselves a closer look at the effect of the Kronecker-delta $\delta_{a_R a_s}$. It identifies the particle indices a_R and a_s , which entails that the wave-vector \mathbf{k}_R will be attributed to position of particle a_s at time t_R . Since each particle index can be attributed to one density operator, identifying the index of the response field with that of a particle representing another density mode can be interpreted as the response field operator contracting with a density operator. With this interpretation, we introduce the notation

$$\begin{aligned} \bar{G}_{B\rho\dots\rho}(-R, 1, \dots, n) &= \hat{B}(-R) \hat{\rho}(1) \hat{\rho}(2) \dots \hat{\rho}(n) Z_0[\underline{\mathbf{J}}, \underline{\mathbf{K}}] \Big|_{\mathbf{0}} \\ &= \sum_{s=1}^n \overbrace{\hat{B}(-R) \hat{\rho}(1) \dots \hat{\rho}(s) \dots \hat{\rho}(n)} \Big|_{\mathbf{0}} Z_0[\underline{\mathbf{J}}, \underline{\mathbf{K}}] \Big|_{\mathbf{0}}, \end{aligned} \quad (\text{C.6})$$

where the contraction of a response field operator with a density operator is defined such that

$$\begin{aligned} \overbrace{\hat{B}(-R) \hat{\rho}(s)} &:= b(s, -R) \sum_{a_s=1}^N \exp\left(-i\mathbf{k}_s \cdot \hat{\mathbf{q}}_{a_s}(t_s) + i\mathbf{k}_R \cdot \hat{\mathbf{q}}_{a_s}(t_R)\right) \\ &\equiv b(s, -R) \hat{\rho}(s, -R). \end{aligned} \quad (\text{C.7})$$

The result of this contraction can again be interpreted as a density operator $\hat{\rho}(s, -R)$ evaluated at two different wave-vectors at different times. Like a usual density operator it acts on the generating functional to generate density modes that are to be integrated over the initial conditions. Informally speaking, we can think of this as the response fields operator ‘handing over its arguments’ to the density operator it contracts with.

Since response field operators contain one-particle density operators themselves, response fields may contract with other response fields, such that

$$\begin{aligned} \overbrace{\hat{B}(-R) \hat{B}(-S)} &= b(-S, -R) \sum_{a_S=1}^N \exp\left(i\mathbf{k}_S \cdot \hat{\mathbf{q}}_{a_S}(t_S) + i\mathbf{k}_R \cdot \hat{\mathbf{q}}_{a_S}(t_R)\right) \hat{b}_{a_S}(t_S) \\ &\equiv b(-S, -R) \hat{B}(-S, -R). \end{aligned} \quad (\text{C.8})$$

The remaining response field operator is free to target further density or response field operators. This allows response fields to form chains, along which their time and wave-vector arguments are handed down. Causality forbids chains that close in on themselves, since such a topology necessarily has to contain a particle propagator $g_{qp}(t, t')$ with $t' > t$ and thus vanishes. As a direct consequence all correlation functions which exclusively contain response fields have to vanish. In other words, a chain of response

field operators necessarily has to end in a density operator. We may write the resulting correlation function

$$\begin{aligned}\bar{G}_{B\rho\dots\rho}(-R, 1, \dots, n) &= \sum_{s=1}^n b(-R, s) \hat{\rho}(1) \dots \hat{\rho}(s-R) \dots \hat{\rho}(n) \mathcal{Z}_0[\underline{\mathbf{J}}, \underline{\mathbf{K}}]_{\underline{\mathbf{0}}} \\ &= \sum_{s=1}^n b(-R, s) \sum_{\{a_1, \dots, a_n\}} \mathcal{Z}_0(\underline{\mathbf{L}}_q, \underline{\mathbf{L}}_p),\end{aligned}\quad (\text{C.9})$$

where the free n -point function in the last line is defined such that the shift vectors belonging to the targeted particle a_s are given by

$$\underline{\mathbf{L}}_{q_{a_s}} = -\mathbf{k}_s + \mathbf{k}_R \quad \underline{\mathbf{L}}_{p_{a_s}} = -g_{qp}(t_s, 0) \mathbf{k}_s + g_{qp}(t_R, 0) \mathbf{k}_R. \quad (\text{C.10})$$

In the most general case where m response field operators and n density operators are applied to the free generating functional, the result is

$$\bar{G}_{B\dots B\rho\dots\rho}(-1', \dots, -m', 1, \dots, n) = \sum_{\{s'_1, \dots, s'_m\}} b(s'_1, -1') \dots b(s'_m, -m') \sum_{\{a_1, \dots, a_n\}} \mathcal{Z}_0(\underline{\mathbf{L}}_q, \underline{\mathbf{L}}_p), \quad (\text{C.11})$$

where $\{s'_1, \dots, s'_m\}$ is the set of all indices of targeted modes that are allowed by causality and the components of the shift tensors $\underline{\mathbf{L}}_q$ and $\underline{\mathbf{L}}_p$ are determined by the contractions of response fields and take the general form

$$\underline{\mathbf{L}}_q = \sum_{r=1}^n \underline{\mathbf{L}}_{q_r} \otimes \mathbf{e}_{a_r} \quad \text{with} \quad \underline{\mathbf{L}}_{q_r} = - \sum_{\{i\}} \mathbf{k}_{r_i}, \quad (\text{C.12})$$

$$\underline{\mathbf{L}}_p = \sum_{r=1}^n \underline{\mathbf{L}}_{p_r} \otimes \mathbf{e}_{a_r} \quad \text{with} \quad \underline{\mathbf{L}}_{p_r} = - \sum_{\{i\}} g_{qp}(t_{r_i}, 0) \mathbf{k}_{r_i}. \quad (\text{C.13})$$

The exact allocation of the wave-vectors and time arguments to the different particle indices depends on the configuration of response field contractions.

D

TRADITIONAL DIAGRAMS OF CANONICAL PERTURBATION THEORY

In the main body of this thesis [Section 4.3](#) a diagrammatic language was introduced for the treatment of perturbative corrections in canonical KFT. The emphasis was put on the particle nature of KFT, allowing us to accommodate both particle interactions and correlations in the same graphical representation. We should, however, mention that a different diagrammatic language had already been developed previously for KFT [2]. Nevertheless, we opted for a different approach to the graphical representation of perturbation theory for the following reasons:

1. The emphasis in [2] is put on density and response field operators, which are macroscopic quantities. However, evaluating the initial conditions in KFT naturally leads to the picture of clusters of point particles. The fact that these point particles are the carriers of the modes of macroscopic fields, and that microscopic interactions between their trajectories are the physical source of perturbations in KFT, is obscured in the traditional diagrams.
2. There is no straightforward or intuitive way to include the discussion of initial correlations in the diagrams of [2]. Since initial correlations are the main crux in the evaluation of perturbative corrections in KFT it would be highly desirable to include them into the diagrams in a straightforward manner.
3. As soon as we go beyond second order perturbation theory, drawing all diagrams that contribute at a given order becomes quite cumbersome and yields little to no physical insight.

Nonetheless, for completeness we want to briefly introduce the traditional diagrammatic language of KFT.

D.1 CONSTRUCTION OF DIAGRAMS

What we wish to represent diagrammatically is the application of density and particle interaction operators on the free generating functional. As we have discussed at length in [Section 3.4.1](#) applying density operators to the free generating functional generates density modes with fixed initial conditions that are then integrated over. Response field operators act on these density modes by updating the shift vectors corresponding to the representative particle of said mode. Since particle interaction operators contain an interaction potential, a density and a response field operator, each evaluated at the same arguments, this results in the following algorithm to construct a diagrammatic language for canonical perturbation theory:

1. The free generating functional Z_0 is represented by a circle. All operators act on Z_0 and therefore need to be attached to this circle.
2. For each density operator that is applied to the generating functional an arrow pointing radially away from the center is attached to the circle. This arrow represents the wave-vector of the density mode. The position where the arrow is attached represents the time argument of the density operator, increasing in counter-clockwise direction. By convention, density operators that are not part of an interaction operator are attached around the 12 o'clock position. We shall refer to these as *external density modes*, since they represent modes that explicitly appear in the final correlation function.
3. Particle interaction operators are represented by two arrows that are attached at the same point, representing the response field and the density operator attributed to the interaction. Both of these arrows are connected by line, representing the interaction potential ν . By convention, we attach these arrows around the bottom of the diagram and refer to the densities as *internal density modes*, as they are integrated out and hence do not appear explicitly in the final result.
4. Since response field operators act on other operators, a dashed arrow is drawn from the mode of each response field to connect to another mode. Due to causality these arrows have to point counter-clockwise.

Since each configuration of response field contractions is represented by one diagram, we have to account for and sum up all distinct diagrams for a given order. With distinct diagrams we mean diagrams that result in non-identical expressions.

Let us consider, once more, a first order correction to a two-point function as in example 3.5.1, evaluated at equal time. In a homogeneous system, the only distinct diagram at this order is shown in Figure D.1, where we chose the response field to contract with the external density mode carrying the wave-vector \mathbf{k}_1 by connecting the wave-vector of the response field to \mathbf{k}_1 . Connection with the wave-vector \mathbf{k}_2 is equally possible and yields the same expression, such that we attribute to this diagram a multiplicity of 2. We can proceed towards higher order corrections in the diagrammatic language by attaching further pairs of wave-vectors corresponding to particle interaction operators. With each additional pair attached, the number of configurations grows, and it becomes increasingly difficult to identify distinct diagrams. The second order correction to an equal-time two-point function in homogeneous system gives rise to four distinct diagrams, shown in Figure D.2. Note that, for all four diagrams the first response field connects to the external density mode \mathbf{k}_1 , which is a convention that we adopt for all higher orders. The remaining response field operator is allowed to connect to each of the modes that are positioned in the counter-clockwise direction, leaving it with four choices, each of which results in a distinct contribution. What is left to determine is the multiplicity of each diagram in Figure D.2, which is most easily done by keeping the arrows of the diagram fixed, and considering the possible permutations of the wave-vectors of external and internal modes. In the upper left diagram, permuting the internal wave-vector pairs $(\mathbf{k}'_1, -\mathbf{k}'_1)$ and $(\mathbf{k}'_2, -\mathbf{k}'_2)$ results in the exact same diagram, since both internal pairs connect to the same external mode anyway. On the other hand, exchanging the external wave-vectors results in a different, but equivalent configuration, adding a factor 2 to the multiplicity. Overall, the multiplicity of this diagram is therefore 2. The upper right diagram has a multiplicity of 2 as well; permuting the external wave-vectors results in two different configurations, whereas exchanging the internal wave-vectors is exactly

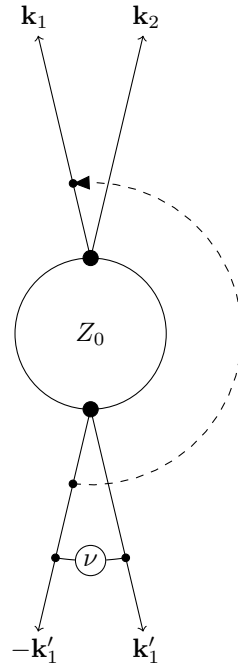


Figure D.1: The only distinct diagram that contributes to first order corrections of an equal-time two-point function in a statistically homogeneous system. The multiplicity attributed to this diagram is 2, since it represents the two identical contributions where we either connect to the external mode \mathbf{k}_1 or \mathbf{k}_2 .

equivalent to exchanging the external ones and therefore adds nothing further to the multiplicity. On the lower row, exchanging both internal and external indices result in 4 distinct configurations, and we therefore recover an overall multiplicity of 4 for both diagrams.

For higher order corrections, the construction continues along the same lines, yielding an increasing number of distinct diagrams. Although we have focused on diagrams for equal-time two-point functions in a homogeneous system, it should be evident that the diagrammatic language we have introduced can be applied to all correlation functions and systems that allow for a description in terms of KFT. The number of external modes and the notion of distinct diagrams then has to be adapted.

D.2 EVALUATION OF DIAGRAMS

Now that we know how to construct KFT diagrams in general, the next step is to make use of them for an efficient evaluation of the resulting expressions. There are two main elements that determine the result of a term in KFT perturbation theory (3.66), namely the overall prefactor and shift tensors in the free correlation function. Both the prefactor and the shift tensors are a direct consequence of the contraction configuration of the response fields and can therefore be read off a diagram.

Example D.2.1 Consider the lower left diagram in Figure D.2, which corresponds to a contraction of a response field with the external density mode, and another response field with an internal

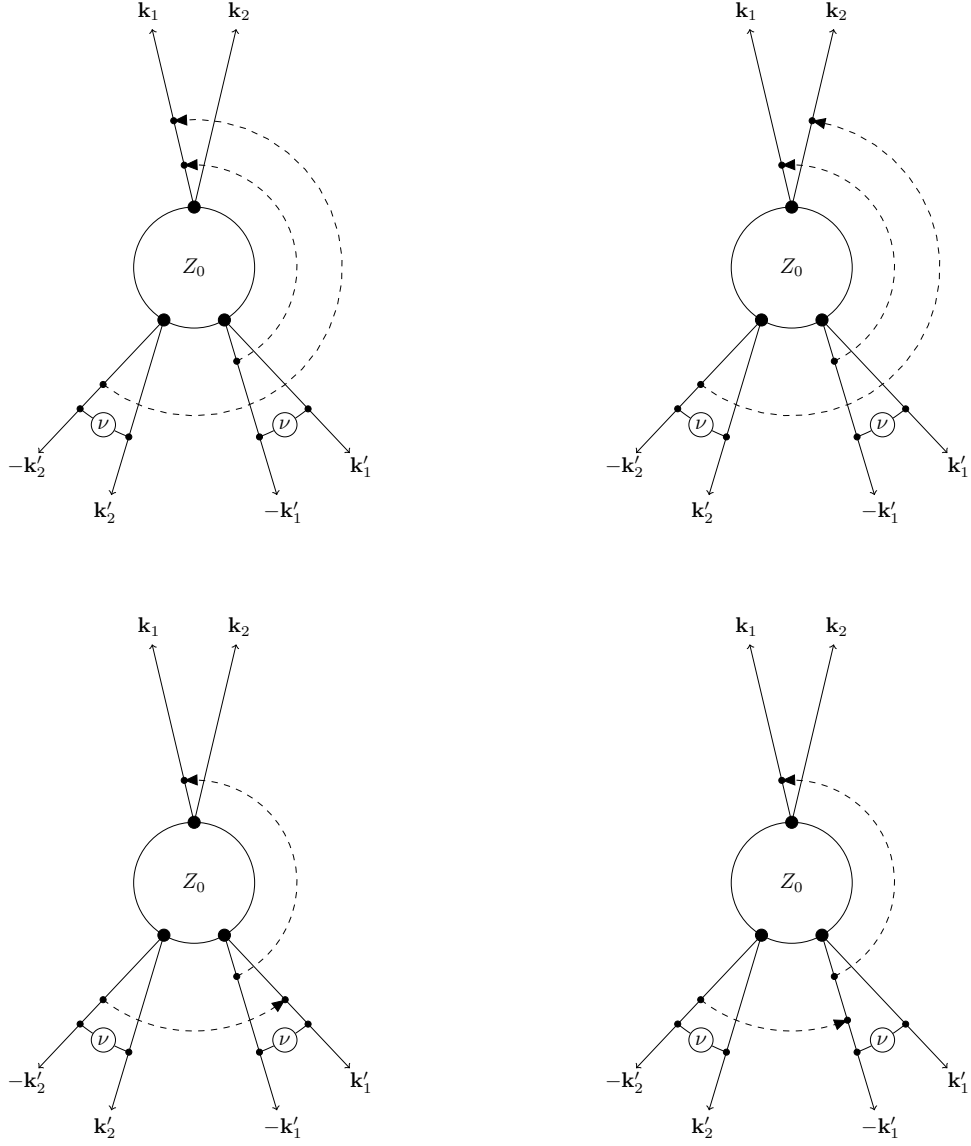


Figure D.2: The only distinct diagram that contributes to first order corrections of an equal-time two-point function in a statistically homogeneous system. The multiplicity attributed to this diagram is 2, since it represents two identical contributions.

density mode. The fact that there are two response fields tells us that we are considering a second order correction to a two-point function that reads

$$\frac{4}{2!} \int d1' \int d2' f(1, -1') f(1', -2') N^4 Z_0(\mathbf{L}_q, \mathbf{L}_p) \quad (\text{D.1})$$

$$\text{with } \begin{cases} \mathbf{L}_{q_1} = -\mathbf{k}_1 + \mathbf{k}'_1 & \mathbf{L}_{p_1} = -g_{qp}(t_1, 0) \mathbf{k}_1 + g_{qp}(t'_1, 0) \mathbf{k}'_1 \\ \mathbf{L}_{q_2} = -\mathbf{k}_2 & \mathbf{L}_{p_2} = -g_{qp}(t_2, 0) \mathbf{k}_2 \\ \mathbf{L}_{q_3} = -\mathbf{k}'_1 + \mathbf{k}'_2 & \mathbf{L}_{p_3} = -g_{qp}(t'_1, 0) \mathbf{k}'_1 + g_{qp}(t'_2, 0) \mathbf{k}'_2 \\ \mathbf{L}_{q_4} = -\mathbf{k}'_2 & \mathbf{L}_{p_4} = -g_{qp}(t'_2, 0) \mathbf{k}'_2. \end{cases} \quad (\text{D.2})$$

There are four shift-vectors, two from the external density operators and one for each interaction operator. This is all the information we need to evaluate the diagram for specified particle dynamics and initial conditions.

Generalizing this to arbitrary diagrams is straightforward and leads to the following recipe to determine the force prefactor $f(\cdot, \cdot)$ and the shift tensors $\underline{\mathbf{L}}_q, \underline{\mathbf{L}}_p$ for a perturbative correction to an m -point density function:

- (i) **Prefactor:** Each interaction operator generates exactly one force prefactor $f(s, -r)$ defined by (3.67) whose first argument s belongs to the mode the response field connects to, and whose second argument to the response field itself $-r$.
- (ii) **Shift tensors:** The total number of components of the shift tensors is given by the sum of the number of external modes and the number of particle interaction operators (i. e. pairs of internal wave-vectors.). The components are assigned clockwise, starting with the pair $(\mathbf{L}_{q_1}, \mathbf{L}_{p_1})$ assigned to the left-most external mode. In addition to the wave-vector of the base mode that the shift-vectors are assigned to we add all the response fields wave-vectors connecting to the base mode to the according shift-vector as illustrated in D.2.1. Chains of response fields transfer the arguments of each component to the density mode that is targeted by the final response field in the chain.

Once we have understood these rules, we can essentially forget about all the complicated properties of density and response field operators. Nonetheless, bluntly applying a recipe that hides the many layers of steps contained in KFT is not satisfactory and leads to little physical understanding.

Note that an alternative diagrammatic approach to canonical perturbation theory in KFT was proposed in [44], where diagrams are essentially graphs with directed edges representing the targeting of a mode and vertices represent density modes or interaction operators. Although both approaches lead to the same final expressions, there is one significant difference between the diagrams from [2], which were presented in this section, and [44] in that the latter do not distinguish between a response field acting on the response field or the density field belonging to the same interaction operator. As we will see later on, targeting a response field or an internal density operator have vastly different consequences for the resulting correlation function, such that one should consider them as distinct targets.

DERIVATION OF THE COUNTER-OPERATOR

To derive the result of applications of the counter-operator

$$i\hat{S}_C = i \frac{3}{2} \int d\tau'_1 e^{\tau'_1} \sum_{a=1}^N \left(\frac{\delta}{i\delta\mathbf{K}_{p_a}(\tau'_1)} \cdot \hat{\mathbf{p}}_a^{(i)} \right) \quad (\text{E.1})$$

onto the free generating functional, consider the case where m density and n response field operators have been applied to Z_0 . As we know, density operators generate the time-dependent shift tensor $\underline{\mathbf{L}}$ (3.40), in this case with n components. In a system where the particle number is sent to infinity, only such terms where each component of the shift tensor is assigned to a different particle are non-negligible. Our generating functional will therefore contain n different particle indices, each of which can formally take integer values between 0 and N . Since all particles are identical, we choose one representative particle for each index and multiply the generating functional by a factor N for each particle index. Response fields, on the other hand, do not add any new particle indices to the shift-tensor, but add modes to already existing particles. In fact, each response field operator that is applied to the generating functional will generate a sum of contributions, one for each particle index that its mode can be added to. This creates a large amount of configurations of the shift tensor, which are represented by the diagrams of KFT perturbation theory. Let us now assume that we are dealing with one specific configuration of the shift tensor (i. e. one specific diagram)

$$\underline{\mathbf{L}}(\tau) = \sum_{a=1}^n \begin{pmatrix} L_{q_a}(\tau) \\ 0 \end{pmatrix} \otimes \hat{e}_a \quad \text{with} \quad L_{q_a}(\tau) = - \sum_{\{i\}} \mathbf{k}_{a_i} \delta_D(\tau - \tau_{a_i}), \quad (\text{E.2})$$

where the indices a represent the different particle indices. Due to the effect of response fields, the component of the shift tensor corresponding to particle index r may depend on different wave-vectors and times, which are indexed with r_i . The number of modes for each particle index depends on the specific diagram. Before applying any counter-operators, the free generating functional therefore reads

$$Z_0[\underline{\mathbf{J}} + \underline{\mathbf{L}}, \underline{\mathbf{K}}] = \int d\underline{\Gamma}_i e^{i(\underline{\mathbf{J}} + \underline{\mathbf{L}}) \cdot \underline{\tilde{\mathbf{x}}}[\underline{\mathbf{K}}]}. \quad (\text{E.3})$$

First, applying the initial momentum operator in (E.1) simply generated initial momenta under the integral. Once this has been accomplished, no further functional derivatives w. r. t. the source field $\underline{\mathbf{J}}$ remain such that it can be set to zero, which leaves us with

$$\begin{aligned} i\hat{S}_C Z_0[\underline{\mathbf{J}} + \underline{\mathbf{L}}, \underline{\mathbf{K}}] \Big|_0 &= i \sum_{a=1}^N \frac{3}{2} \int d\tau'_1 e^{\tau'_1} \int d\underline{\Gamma}_i \left(\mathbf{p}_a^{(i)} \cdot \frac{\delta}{i\delta\mathbf{K}_{p_a}(\tau'_1)} \right) e^{i(\underline{\mathbf{L}} \cdot \underline{\tilde{\mathbf{x}}})[\underline{\mathbf{K}}]} \Big|_{\underline{\mathbf{K}}=0} \\ &= i \sum_{a=1}^N \frac{3}{2} \int d\tau'_1 e^{\tau'_1} \int d\underline{\Gamma}_i e^{i(\underline{\mathbf{L}} \cdot \underline{\tilde{\mathbf{x}}})[\underline{\mathbf{K}}]} \left[\mathbf{p}_a^{(i)} \cdot \left(\frac{\delta}{\delta\mathbf{K}_{p_a}(\tau'_1)} (\underline{\mathbf{L}} \cdot \underline{\tilde{\mathbf{x}}})[\underline{\mathbf{K}}] \right) \right] \Big|_{\underline{\mathbf{K}}=0}. \end{aligned} \quad (\text{E.4})$$

To evaluate the functional derivative, we first expand the generalized scalar product

$$\begin{aligned} (\underline{\mathbf{L}} \cdot \underline{\tilde{\mathbf{x}}})[\underline{\mathbf{K}}] &= \sum_{b=1}^n \int d\tau \mathbf{L}_{q_b}(\tau) \cdot \tilde{\mathbf{q}}_b[\mathbf{K}_{p_b}, \tau] \\ &= \sum_{b=1}^n \int d\tau \mathbf{L}_{q_b}(\tau) \cdot \left(\mathbf{q}_b^{(i)} + g_{qp}^{(Z)}(\tau, 0) \mathbf{p}_b^{(i)} - \int_0^\tau d\tau' g_{qp}(\tau, \tau') \mathbf{K}_{p_a}(\tau') \right), \end{aligned} \quad (\text{E.5})$$

where we have already set the q -component of \mathbf{K} to zero, since it is not involved in any functional derivatives. Recall that the inhomogeneous part of the spatial trajectories contains the Newtonian particle propagator $g_{qp}(\tau, \tau')$ even for free Zel'dovich motion. With this, the functional derivative in (E.4) evaluates to

$$\frac{\delta}{\delta \mathbf{K}_{p_a}(\tau'_1)} (\underline{\mathbf{L}} \cdot \underline{\tilde{\mathbf{x}}})[\underline{\mathbf{K}}] = - \int d\tau \mathbf{L}_{q_a}(\tau) g_{qp}(\tau, \tau'_1). \quad (\text{E.6})$$

Note that the particle index on the time-dependent shift vector has been identified with one of the particle indices a . The sum over all particles in (E.4) thus turns into a sum over all representative particles that have a non-vanishing shift vector assigned to them. We can collect these results to find

$$i\hat{S}_C Z_0[\underline{\mathbf{J}} + \underline{\mathbf{L}}, \underline{\mathbf{K}}] \Big|_0 = i \sum_{a=1}^n \frac{3}{2} \int d\tau'_1 e^{\tau'_1} \left(- \int d\tau \mathbf{L}_{q_a}(\tau) g_{qp}(\tau, \tau'_1) \right) \cdot \int d\underline{\Gamma}_i \mathbf{p}_a^{(i)} e^{i\underline{\mathbf{L}} \cdot \underline{\tilde{\mathbf{x}}}}. \quad (\text{E.7})$$

There are two individual components to this expression that we want to analyze separately, starting with the initial phase-space integral

$$\int d\underline{\Gamma}_i \mathbf{p}_a^{(i)} e^{i\underline{\mathbf{L}} \cdot \underline{\tilde{\mathbf{x}}}}, \quad (\text{E.8})$$

where we can rewrite the phase factor in terms of the initial positions and momenta of the n representative particles:

$$i\underline{\mathbf{L}} \cdot \underline{\tilde{\mathbf{x}}} = i\underline{\mathbf{L}}_q \cdot \underline{\mathbf{q}}^{(i)} + i\underline{\mathbf{L}}_p^{(Z)} \cdot \underline{\mathbf{p}}^{(i)}. \quad (\text{E.9})$$

Here we have again identified the effectively time-independent (the time parameter τ being integrated out) shift tensors

$$\underline{\mathbf{L}}_q = \sum_{a=1}^n \underline{\mathbf{L}}_{q_a} \otimes \mathbf{e}_a, \quad \underline{\mathbf{L}}_p^{(Z)} = \sum_{a=1}^n \underline{\mathbf{L}}_{p_a}^{(Z)} \otimes \mathbf{e}_a. \quad (\text{E.10})$$

Using the general form of the time-dependent shift-tensor in (E.2) we find for the components of the time independent shift vectors

$$\underline{\mathbf{L}}_{q_a} = - \sum_{\{i\}} \mathbf{k}_{a_i}, \quad \underline{\mathbf{L}}_{p_a}^{(Z)} = - \sum_{\{i\}} g_{qp}^{(Z)}(\tau_{a_i}, 0) \mathbf{k}_{a_i}, \quad (\text{E.11})$$

where, again, the exact constellation of wave-vectors is determined by the diagram we consider. Note that we have explicitly marked the momentum-shift tensor/vectors with a '(Z)' to indicate that they are defined with a Zel'dovich particle propagator. Having reformulated the phase of our initial expression (E.8) in this way, we can now pull the initial momentum factor in front of the integral by converting it to a partial derivative, resulting in

$$\int d\underline{\Gamma}_i \mathbf{p}_a^{(i)} e^{i\underline{\mathbf{L}} \cdot \underline{\tilde{\mathbf{x}}}} = \frac{\partial}{i\partial \underline{\mathbf{L}}_{p_a}^{(Z)}} \int d\underline{\Gamma}_i e^{i\underline{\mathbf{L}}_q \cdot \underline{\mathbf{q}}^{(i)}} e^{i\underline{\mathbf{L}}_{p_a}^{(Z)} \cdot \underline{\mathbf{p}}^{(i)}}. \quad (\text{E.12})$$

The second step is to inspect the time-integral in the pre-factor more thoroughly. Once more the general form of the time-dependent shift-tensor (E.2) lets us rewrite the time integral

$$\int d\tau \mathbf{L}_{q_a}(\tau) g_{qp}(\tau, \tau'_1) = - \sum_{\{i\}} g_{qp}(\tau_{s_i}, \tau'_1) k_{s_i}, \quad (\text{E.13})$$

which in turn allows us to solve the τ'_1 -integral

$$\begin{aligned} & i \sum_{a=1}^n \frac{3}{2} \int d\tau'_1 e^{\tau'_1} \left(- \int d\tau \mathbf{L}_{q_a}(\tau) g_{qp}(\tau, \tau'_1) \right) \\ &= -i \sum_{a=1}^n \sum_{\{i\}} \left(- \frac{3}{2} \int d\tau'_1 e^{\tau'_1} g_{qp}(\tau_{a_i}, \tau'_1) \right) \mathbf{k}_{a_i}, \end{aligned} \quad (\text{E.14})$$

where we can, once again, recognize the same integral as in (B.23). Inserting the solution from Appendix B the expression turns into

$$-i \sum_{a=1}^n \left(- \sum_{\{i\}} \left(g_{qp}^{(Z)}(\tau_{a_i}, 0) - g_{qp}(\tau_{a_i}, 0) \right) \mathbf{k}_{a_i} \right) = i \sum_{a=1}^n \left(\mathbf{L}_{p_a}^{(N)} - \mathbf{L}_{p_a}^{(Z)} \right) =: i \sum_{a=1}^n \Delta \mathbf{L}_{p_a}, \quad (\text{E.15})$$

where we identified the momentum shift-vectors with two different particle propagators, namely

$$\mathbf{L}_{p_a}^{(Z)} = - \sum_{\{i\}} g_{qp}^{(Z)}(\tau_{a_i}, 0) \mathbf{k}_{a_i} \quad \text{and} \quad \mathbf{L}_{p_a}^{(N)} = - \sum_{\{i\}} g_{qp}(\tau_{a_i}, 0) \mathbf{k}_{a_i} \quad (\text{E.16})$$

After these rather painful steps, we can now collect the results from the two components to arrive at the final, simple form of the counter-operator

$$i \hat{S}_C Z_0[\underline{\mathbf{J}} + \underline{\mathbf{L}}, \underline{\mathbf{K}}] \Big|_0 = \sum_{a=1}^n \left(\Delta \mathbf{L}_{p_a} \cdot \frac{\partial}{\partial \mathbf{L}_{p_a}^{(Z)}} \right) Z_0(\underline{\mathbf{L}}_q, \underline{\mathbf{L}}_p^{(Z)}) = \left(\Delta \mathbf{L}_p \cdot \frac{\partial}{\partial \mathbf{L}_p^{(Z)}} \right) Z_0(\underline{\mathbf{L}}_q, \underline{\mathbf{L}}_p^{(Z)}). \quad (\text{E.17})$$

In the end the counter-operator can be rewritten in such a way that it needs no functional derivatives w. r. t. to either source field $\underline{\mathbf{K}}$ and $\underline{\mathbf{J}}$, allowing us to apply it after setting all the source fields to zero.

 DERIVATION OF PARTICLE DYNAMICS IN COSMOLOGY FROM
 GENERAL RELATIVITY

In KFT calculations we describe particle trajectories using Newtonian dynamics, but we know that a precise description of an ensemble of particles in an expanding space-time has to have its roots in General Relativity (GR). In this section we want to use the formalism of GR in its full glory to derive the expressions describing the dynamics of the metric and of individual freely-falling particles. This will confirm our intuition about the limits we have to take in order to recover the Newtonian result. Additionally, it is a nice practical application of Einstein's field equations and a lot of fun.

A note on notation: Throughout the main text of this thesis, we were cautious to use the dot-notation only for derivative w. r. t. the time parameter τ defined in (2.22). For ease of notation, we will drop this restriction here, such that derivatives w. r. t. coordinate time t are written as dots.

F.1 INGREDIENTS

First, let's summarize the ingredients that we are going to need to describe the dynamics of particles in an expanding universe.

- Of course, the fundamental equation describing the evolution of space-time itself is Einstein's field equation for the metric

$$G_{\mu\nu} + \Lambda g_{\mu\nu} = \frac{8\pi G}{c^4} T_{\mu\nu}. \quad (\text{F.1})$$

It connects the dynamics of the metric $g_{\mu\nu}$ (lhs) to the energy contained in a space-time region (rhs).

- Furthermore, we want to describe individual freely-falling particles moving on our space-time manifold. Their motion is described by the relativistic Euler-Lagrange equations, which can be derived from the action

$$S = -mc^2 \int d\tau = -mc \int \sqrt{-g_{\mu\nu} dx^\mu dx^\nu}. \quad (\text{F.2})$$

Here τ is the particle's proper time (not to be confused with the time parameter (2.22)) and the only Lorentz scalar we have at our disposal to construct an action. The prefactor is constructed such that the action yields the correct non-relativistic limit.

To solve Einstein's equations (F.1) we further need to specify the metric and the energy momentum tensor for the situation we are interested in. From our standard cosmology

lectures we remember that the Ansatz for the line element of a spatially flat (we assume this here in advance to make the calculations simpler) homogeneous and isotropic universe is

$$ds^2 = -c^2 dt^2 + a^2(t) \delta_{ij} dq^i dq^j. \quad (\text{F.3})$$

With regard to the final application to KFT we call the spatial, comoving coordinates q^i . We need to go one step further here and consider a universe that contains small scalar perturbation in the metric. Introducing these perturbations into the metric is not unique due to gauge invariance. For cosmic structure formation it has proved very convenient to work in the Newtonian gauge, where the perturbed metric becomes

$$ds^2 = -c^2 \left(1 + \frac{2\Phi}{c^2}\right) dt^2 + a^2(t) \left(1 - \frac{2\Phi}{c^2}\right) \delta_{ij} dq^i dq^j. \quad (\text{F.4})$$

Here, Φ is for the moment just a scalar perturbation that we introduced, but it will turn out to correspond exactly to the Newtonian potential in the non-relativistic limit. In the most general case the Newtonian gauge should actually contain two scalar potentials Φ and Ψ , but they are equivalent to each other unless we are in the presence of anisotropic stress. Since this is not the case we start with the single potential Φ . Note that we assume that $\frac{\Phi}{c^2} \ll 1$ and therefore discard any higher order contributions of this quantity. Practically this means that we will frequently use relations like

$$\begin{aligned} \frac{1}{1 - \frac{2\Phi}{c^2}} &= 1 + \frac{2\Phi}{c^2} + \mathcal{O}\left(\frac{\Phi^2}{c^4}\right) \\ \sqrt{1 + \frac{2\Phi}{c^2}} &= 1 + \frac{\Phi}{c^2} + \mathcal{O}\left(\frac{\Phi^2}{c^4}\right) \end{aligned} \quad (\text{F.5})$$

without bothering to write that this only holds to first order.

Last but not least, since we are mostly interested in structure formation due to cold dark matter particles (whatever they may be) we define the energy content of our universe as a pressure-less fluid

$$T_{\mu\nu} = \rho_m(\mathbf{q}, t) u_\mu u_\nu, \quad (\text{F.6})$$

where u_μ is the 4-velocity field of the fluid and fulfills $u_\mu u^\mu = -c^2$. The mass density $\rho_m(q, t)$ is not completely uniform, but contains small fluctuations itself

$$\rho_m(\mathbf{q}, t) = \bar{\rho}_m(t) (1 + \delta(\mathbf{q}, t)). \quad (\text{F.7})$$

F.2 THE DYNAMICS OF THE METRIC

Having all the necessary ingredients at hand we simply have to insert them into Einstein's equations and calculate. Since the metric only contains a single potential Φ , a single one of the Einstein equations is sufficient to describe its evolution. We therefore focus on calculating the 00 component, i.e.

$$G_0^0 + \Lambda = \frac{8\pi G}{c^4} T_0^0. \quad (\text{F.8})$$

As a reminder, these are the definitions of all the objects we are going to need:

$$G_{\mu\nu} = R_{\mu\nu} - \frac{1}{2}Rg_{\mu\nu} \quad (\text{F.9})$$

$$R = g^{\mu\nu}R_{\mu\nu} \quad (\text{F.10})$$

$$R_{\mu\nu} = R^\rho{}_{\mu\rho\nu} = \partial_\rho\Gamma_{\mu\nu}^\rho - \partial_\nu\Gamma_{\rho\mu}^\rho + \Gamma_{\rho\lambda}^\rho\Gamma_{\mu\nu}^\lambda - \Gamma_{\nu\lambda}^\rho\Gamma_{\mu\rho}^\lambda \quad (\text{F.11})$$

$$\Gamma_{\mu\nu}^\lambda = \frac{1}{2}g^{\lambda\rho}(\partial_\mu g_{\rho\nu} + \partial_\nu g_{\rho\mu} + \partial_\rho g_{\mu\nu}). \quad (\text{F.12})$$

What we need to calculate in order to evaluate (F.8) is

$$G_0^0 = g^{00}R_{00} - \frac{1}{2}R. \quad (\text{F.13})$$

For the Ricci scalar R we need the spatial components R_{ij} as well as R_{00} . In order to find these we start by inserting the components of our perturbed FLRW metric

$$\begin{aligned} g_{00} &= -c^2 \left(1 + \frac{2\Phi}{c^2}\right) & g^{00} &= -c^{-2} \left(1 - \frac{2\Phi}{c^2}\right) \\ g_{ij} &= a^2 \left(1 - \frac{2\Phi}{c^2}\right) \delta_{ij} & g^{ij} &= a^{-2} \left(1 + \frac{2\Phi}{c^2}\right) \delta^{ij} \end{aligned} \quad (\text{F.14})$$

into (F.12). The resulting entries of the Christoffel symbols are

$$\begin{aligned} \Gamma_{00}^0 &= \frac{1}{c^2}\dot{\Phi} & \Gamma_{0i}^0 &= \frac{1}{c^2}\partial_i\Phi \\ \Gamma_{ij}^0 &= \frac{a^2}{c^2}\delta_{ij}\left(H - 4H\frac{\Phi}{c^2} - \frac{\dot{\Phi}}{c^2}\right) & \Gamma_{00}^i &= \frac{1}{a^2}\partial_i\Phi \\ \Gamma_{0j}^i &= \delta_{ij}\left(H - \frac{\dot{\Phi}}{c^2}\right) & \Gamma_{jk}^i &= \frac{1}{c^2}(-\delta_{ik}\partial_j\Phi - \delta_{ij}\partial_k\Phi + \delta_{jk}\partial_i\Phi), \end{aligned} \quad (\text{F.15})$$

where derivatives w.r.t. the coordinate time t are denoted with a dot and we defined the Hubble function $H = \frac{\dot{a}}{a}$. Until now we have refrained from making the usual simplification of setting $c = 1$ as it might be confusing at times to figure out where the c 's belong in the final expression. To make the notation more compact however, we are now going to make the following replacements

$$\frac{\Phi}{c^2} \rightarrow \Phi \quad \frac{a^2}{c^2} \rightarrow a^2. \quad (\text{F.16})$$

At the end of the calculation we can then reverse these identifications to recover the correct factors of c . Working our way through the equations towards the components of the Ricci tensor is tedious but simple. After a couple of pages of algebra we should arrive at the following expressions

$$R_{00} = \frac{1}{a^2}\nabla^2\Phi - 3\frac{\ddot{a}}{a} + 2\ddot{\Phi} + 9H\dot{\Phi} \quad (\text{F.17})$$

$$R_{ij} = \delta_{ij}\left[(2a^2H^2 + \ddot{a}a)(1 - 4\Phi) - 7a^2H\dot{\Phi} - a^2\ddot{\Phi} + \nabla^2\Phi\right] \quad (\text{F.18})$$

$$R = \frac{1}{c^2}\left[6\left(H^2 + \frac{\ddot{a}}{a}\right)(1 - 2\Phi) + \frac{2}{a^2}\nabla^2\Phi - 30H\dot{\Phi} - 6\ddot{\Phi},\right] \quad (\text{F.19})$$

which altogether result in the following expression for the lhs of (F.8):

$$G_0^0 + \Lambda = -\frac{1}{c^2}\left[\frac{2}{a^2}\nabla^2\Phi - 6H(\dot{\Phi} + H\Phi) + 3H^2 - \Lambda c^2\right]. \quad (\text{F.20})$$

The rhs of (F.8) is quickly evaluated by assuming the fluid to be at rest w. r. t. the expansion of the universe. Since in this case $u_\mu u^\mu = u_0 u^0 = -c^2$ we simply get

$$T_0^0 = \rho_m(\mathbf{q}, t) u_0 u^0 = -c^2 \bar{\rho}_m(t) (1 + \delta(\mathbf{q}, t)), \quad (\text{F.21})$$

the final result for the Einstein equation reads

$$\underbrace{(3H^2 - \Lambda c^2)}_{\mathcal{O}(0)} + \underbrace{\left[\frac{2}{a^2} \nabla^2 \Phi - 6H(\dot{\Phi} + H\Phi) \right]}_{\mathcal{O}(1)} = \underbrace{8\pi G \bar{\rho}_m(t)}_{\mathcal{O}(0)} + \underbrace{8\pi G \bar{\rho}_m(t) \delta(\mathbf{q}, t)}_{\mathcal{O}(1)}. \quad (\text{F.22})$$

Here we have highlighted the parts that are of zeroth and first order in the perturbations Φ and δ . Unsurprisingly the zeroth order is simply the first Friedmann equation for a flat universe containing non-relativistic (cold) dark matter. The first order describes the dynamics of the scalar perturbation that was introduced into the metric

$$\nabla^2 \Phi - 3aH(a\dot{\Phi} + aH\Phi) = 4\pi G a^2 \bar{\rho}_m(t) \delta(\mathbf{q}, t). \quad (\text{F.23})$$

This looks suspiciously like the Poisson equation we are used to from Newtonian gravity. To make the similarity complete, let us have a closer look at the left-hand side. Going to Fourier space and reinstalling the factors of c contained in the definitions of Φ and a , we obtain

$$-\frac{k^2}{c^2} \left[\Phi + 3 \frac{a^2 H^2}{k^2 c^2} \left(\frac{1}{H} \dot{\Phi} + \Phi \right) \right]. \quad (\text{F.24})$$

The factor $\frac{a^2 H^2}{c^2}$ corresponds to the inverse comoving Hubble radius. What this expression tells us is that the first term dominates the rest for modes of the gravitational potential that fulfill

$$\frac{k^2 c^2}{a^2 H^2} \gg 1. \quad (\text{F.25})$$

In other words, for modes that are far smaller than the comoving Hubble radius we can neglect the second and the third term in (F.23), yielding

$$\nabla^2 \Phi(\mathbf{q}, t) = 4\pi G a^2 \bar{\rho}_m(t) \delta(\mathbf{q}, t). \quad (\text{F.26})$$

These are in fact the modes that we are interested in when we calculate late-time structure formation. With this calculation we have thus shown that the scalar perturbation we introduced into the metric fulfills the non-relativistic Poisson equation if we restrict ourselves to scales that are far below the Hubble radius. Therefore, we have every right to interpret this potential as the Newtonian gravitational potential. We will see in the following that it also appears in the non-relativistic equations of motion of freely falling particles in exactly the way we would expect from the Newtonian potential.

F.3 PARTICLE DYNAMICS

In KFT we imagine the universe being filled with an ensemble of particles with equal mass m_0 , moving on the manifold described by the perturbed background metric (F.4). We assume these particles to be freely falling, i.e. they interact with each other only due

to gravity. The trajectory of a single particle of the ensemble minimizes the relativistic action

$$\begin{aligned}
 S &= -m_0 c \int dt \sqrt{-g_{\mu\nu} \frac{dx^\mu}{dt} \frac{dx^\nu}{dt}} dt \\
 &= -m_0 c \int dt \sqrt{-g_{00} - g_{ij} \dot{q}^i \dot{q}^j} \\
 &= -m_0 c \int dt \sqrt{c^2(1 + 2\Phi/c^2) - a^2(1 - 2\Phi/c^2) \dot{q}^2} \\
 &= -m_0 c^2 \int dt (1 + \Phi/c^2) \sqrt{1 - a^2(1 - 4\Phi/c^2) \frac{\dot{q}^2}{c^2}}. \tag{F.27}
 \end{aligned}$$

Since we assume cold dark matter the particle velocity in units of c is small and the term $\frac{\Phi \dot{q}^2}{c^4} = \mathcal{O}(2)$ can be neglected. To first order the action then becomes

$$\begin{aligned}
 S &= -m_0 c^2 \int dt (1 + \Phi/c^2) \left(1 - \frac{1}{2} a^2 \frac{\dot{q}^2}{c^2}\right) \\
 &= \int dt \left(-m_0 c^2 + \frac{m_0}{2} a^2 \dot{q}^2 - m_0 \Phi\right). \tag{F.28}
 \end{aligned}$$

Ignoring the rest mass energy and pulling out the particle mass m_0 , both of which are irrelevant for the equations of motion, we recover the one-particle Lagrangian

$$\mathcal{L}_t\left(\mathbf{q}, \frac{d\mathbf{q}}{dt}, t\right) = \frac{a^2}{2} \left(\frac{d\mathbf{q}}{dt}\right)^2 - \Phi(\mathbf{q}, t), \tag{F.29}$$

where the dynamics of the potential Φ are governed by (F.26). Having shown that these equations are in fact the non-relativistic limit of GR we can from now on forget about relativistic effects and treat them in the framework of non-relativistic Newtonian mechanics.

G

LAPLACE TRANSFORMS

G.1 SOME BASIC FACTS

The Laplace transform of a one-dimensional function $f(t): \mathbb{R} \rightarrow \mathbb{R}$ is defined by

$$F(s) = \mathcal{L}_{t \rightarrow s}[f(t)] := \int_0^{\infty} dt f(t) e^{-st}. \quad (\text{G.1})$$

For our application it is sufficient to calculate the special case where $f(t) = e^{\alpha t}$ for some $\alpha \in \mathbb{R}$, where straightforward integration shows that

$$F(s) = \mathcal{L}_{t \rightarrow s}[f(t)] = \int_0^{\infty} dt e^{(\alpha-s)t} = \frac{1}{s-\alpha} \quad \forall s: \Re(s) > \alpha. \quad (\text{G.2})$$

As a consequence, the inverse Laplace transform of a fraction can be determined by simple inspection and is given by

$$\mathcal{L}_{t \leftarrow s}^{-1}\left[\frac{1}{s-\alpha}\right] = e^{\alpha t}. \quad (\text{G.3})$$

Similar to Fourier transforms, the convolution of two functions is mapped onto the product of their respective Laplace transforms

$$\mathcal{L}_{t \rightarrow s}\left[\int_0^t dt' f(t')g(t-t')\right] = \int_0^{\infty} dt e^{-st} \int_0^t dt' f(t')g(t-t') \quad (\text{G.4})$$

$$= \int_0^{\infty} dt \int_0^{\infty} dt' e^{-st} \theta(t-t') f(t')g(t-t') \quad (\text{G.5})$$

$$= \int_{-t'}^{\infty} dt'' \int_0^{\infty} dt' e^{-s(t''+t')} \theta(t'') f(t')g(t'') \quad (\text{G.6})$$

$$= \int_0^{\infty} dt'' g(t'') e^{-st''} \int_0^{\infty} dt' e^{-st'} f(t') \quad (\text{G.7})$$

$$= \mathcal{L}_{t'' \rightarrow s}[g(t'')] \mathcal{L}_{t' \rightarrow s}[f(t')] \quad (\text{G.8})$$

G.2 APPLICATION

We can use the convolution theorem for Laplace transforms to solve the self-consistent equation for the retarded propagator (5.17)

$$\tilde{\Delta}_R(\tau_1, \tau_2) = f_{1,2} + \int_{\tau_2}^{\tau_1} d\tau_3 f_{1,3} \tilde{\Delta}_R(\tau_3, \tau_2) \quad (\text{G.9})$$

if we assume that $\tilde{\Delta}_R(\tau_1, \tau_2) = \tilde{\Delta}_R(\tau_1 - \tau_2, 0)$ and $f_{1,2} = f(\tau_1, \tau_2) = f(\tau_1 - \tau_2, 0)$. Since

$$f_{1,2} = 3\left(1 - e^{-\frac{1}{2}(\tau_1 - \tau_2)}\right), \quad (\text{G.10})$$

this assumption obviously holds, allowing us to rewrite the self-consistent equation to

$$\tilde{\Delta}_R(\tau, 0) = f(\tau, 0) + \int_0^\tau d\tau_3 f(\tau - \tau_3) \tilde{\Delta}_R(\tau_3, 0). \quad (\text{G.11})$$

Performing the Laplace transform, applying the convolution theorem and rearranging the terms results in

$$\tilde{\Delta}_R(\tau, 0) = \mathcal{L}_{\tau \leftarrow s}^{-1} \left[\frac{\mathcal{L}_{\tau \rightarrow s}[f(\tau, 0)]}{1 - \mathcal{L}_{\tau \rightarrow s}[f(\tau, 0)]} \right]. \quad (\text{G.12})$$

Applying the definition of the Laplace transform a short calculation shows that

$$\mathcal{L}_{\tau \rightarrow s}[f(\tau, 0)] = \int_0^\infty d\tau 3(1 - e^{-\frac{1}{2}\tau})e^{-s\tau} = \frac{3}{2} \frac{1}{s(s + 1/2)}, \quad (\text{G.13})$$

leading to

$$\tilde{\Delta}_R(\tau, 0) = \mathcal{L}_{\tau \leftarrow s}^{-1} \left[\frac{\mathcal{L}_{\tau \rightarrow s}[f(\tau, 0)]}{1 - \mathcal{L}_{\tau \rightarrow s}[f(\tau, 0)]} \right] \quad (\text{G.14})$$

$$= \mathcal{L}_{\tau \leftarrow s}^{-1} \left[\left(\frac{3}{2} \frac{1}{s^2 + s/2 - 3/2} \right) \right] \quad (\text{G.15})$$

$$= \mathcal{L}_{\tau \leftarrow s}^{-1} \left[\frac{3}{5} \left(\frac{1}{s-1} - \frac{1}{s+3/2} \right) \right] \quad (\text{G.16})$$

$$= \frac{3}{5} \left(e^\tau - e^{-\frac{3}{2}\tau} \right). \quad (\text{G.17})$$

BIBLIOGRAPHY

- [1] M. Bartelmann, F. Fabis, D. Berg, E. Kozlikin, R. Lilow, and C. Viermann. “A microscopic, non-equilibrium, statistical field theory for cosmic structure formation.” In: *New J. Phys.* 18.4, 043020 (Apr. 2016), p. 043020. DOI: [10.1088/1367-2630/18/4/043020](https://doi.org/10.1088/1367-2630/18/4/043020).
- [2] M. Bartelmann, F. Fabis, E. Kozlikin, R. Lilow, J. Dombrowski, and J. Mildenerger. “Kinetic field theory: effects of momentum correlations on the cosmic density-fluctuation power spectrum.” In: *New J. Phys.* 19.8 (2017), p. 083001. DOI: [10.1088/1367-2630/aa7e6f](https://doi.org/10.1088/1367-2630/aa7e6f). URL: <https://dx.doi.org/10.1088/1367-2630/aa7e6f>.
- [3] F. Fabis, E. Kozlikin, R. Lilow, and M. Bartelmann. “Kinetic field theory: exact free evolution of Gaussian phase-space correlations.” In: *J. Stat. Mech.: Theory Exp* 2018.4 (2018), p. 043214. DOI: [10.1088/1742-5468/aab850](https://doi.org/10.1088/1742-5468/aab850). URL: <https://dx.doi.org/10.1088/1742-5468/aab850>.
- [4] F. Fabis. “A statistical field theory for classical particles.” PhD thesis. Heidelberg University, Apr. 2015. DOI: [10.11588/heidok.00018676](https://doi.org/10.11588/heidok.00018676). URL: <http://www.ub.uni-heidelberg.de/archiv/18676>.
- [5] A. A. Penzias and R. W. Wilson. “A Measurement of Excess Antenna Temperature at 4080 Mc/s.” In: *Astrophys. J.* 142 (July 1965), pp. 419–421. DOI: [10.1086/148307](https://doi.org/10.1086/148307).
- [6] G. F. Smoot et al. “Structure in the COBE Differential Microwave Radiometer First-Year Maps.” In: *Astrophys. J. Lett.* 396 (Sept. 1992), p. L1. DOI: [10.1086/186504](https://doi.org/10.1086/186504).
- [7] S. Perlmutter et al. “Measurements of Ω and Λ from 42 High-Redshift Supernovae.” In: *Astrophys. J.* 517.2 (June 1999), pp. 565–586. DOI: [10.1086/307221](https://doi.org/10.1086/307221). arXiv: [astro-ph/9812133](https://arxiv.org/abs/astro-ph/9812133) [astro-ph].
- [8] A. G. Riess et al. “Observational Evidence from Supernovae for an Accelerating Universe and a Cosmological Constant.” In: *Astron. J.* 116.3 (1998), p. 1009. DOI: [10.1086/300499](https://doi.org/10.1086/300499). URL: <https://dx.doi.org/10.1086/300499>.
- [9] Planck Collaboration et al. “Planck 2018 results. VI. Cosmological parameters.” In: *Astron. Astrophys.* 641, A6 (Sept. 2020), A6. DOI: [10.1051/0004-6361/201833910](https://doi.org/10.1051/0004-6361/201833910). arXiv: [1807.06209](https://arxiv.org/abs/1807.06209) [astro-ph.CO].
- [10] A. G. Riess. “The expansion of the Universe is faster than expected.” In: *Nat. Rev. Phys.* 2.1 (2020), pp. 10–12. ISSN: 2522-5820. DOI: [10.1038/s42254-019-0137-0](https://doi.org/10.1038/s42254-019-0137-0). URL: <https://doi.org/10.1038/s42254-019-0137-0>.
- [11] F. Bernardeau, S. Colombi, E. Gaztañaga, and R. Scoccimarro. “Large-scale structure of the Universe and cosmological perturbation theory.” In: *Phys. Rep.* 367.1 (2002), pp. 1–248. ISSN: 0370-1573. DOI: [https://doi.org/10.1016/S0370-1573\(02\)00135-7](https://doi.org/10.1016/S0370-1573(02)00135-7). URL: <https://www.sciencedirect.com/science/article/pii/S0370157302001357>.
- [12] M. Crocce and R. Scoccimarro. “Renormalized cosmological perturbation theory.” In: *Phys. Rev. D* 73 (6 2006), p. 063519. DOI: [10.1103/PhysRevD.73.063519](https://doi.org/10.1103/PhysRevD.73.063519). URL: <https://link.aps.org/doi/10.1103/PhysRevD.73.063519>.

- [13] M. Crocce and R. Scoccimarro. “Memory of initial conditions in gravitational clustering.” In: *Phys. Rev. D* 73 (6 2006), p. 063520. DOI: [10.1103/PhysRevD.73.063520](https://doi.org/10.1103/PhysRevD.73.063520). URL: <https://link.aps.org/doi/10.1103/PhysRevD.73.063520>.
- [14] S. Matarrese and M. Pietroni. “Resumming cosmic perturbations.” In: *J. Cosmol. Astropart. Phys.* 2007.06 (2007), p. 026. DOI: [10.1088/1475-7516/2007/06/026](https://doi.org/10.1088/1475-7516/2007/06/026). URL: <https://dx.doi.org/10.1088/1475-7516/2007/06/026>.
- [15] S. Floerchinger, M. Garny, N. Tetradis, and U. A. Wiedemann. “Renormalization-group flow of the effective action of cosmological large-scale structures.” In: *J. Cosmol. Astropart. Phys.* 2017.01 (2017), p. 048. DOI: [10.1088/1475-7516/2017/01/048](https://doi.org/10.1088/1475-7516/2017/01/048). URL: <https://dx.doi.org/10.1088/1475-7516/2017/01/048>.
- [16] A. Erschfeld and S. Floerchinger. “Cosmological functional renormalization group, extended Galilean invariance, and approximate solutions to the flow equations.” In: *Phys. Rev. D* 105 (2 2022), p. 023506. DOI: [10.1103/PhysRevD.105.023506](https://doi.org/10.1103/PhysRevD.105.023506). URL: <https://link.aps.org/doi/10.1103/PhysRevD.105.023506>.
- [17] N. Afshordi. “How well can (renormalized) perturbation theory predict dark matter clustering properties?” In: *Phys. Rev. D* 75 (2 2007), p. 021302. DOI: [10.1103/PhysRevD.75.021302](https://doi.org/10.1103/PhysRevD.75.021302). URL: <https://link.aps.org/doi/10.1103/PhysRevD.75.021302>.
- [18] V. et al. Springel. “Simulations of the formation, evolution and clustering of galaxies and quasars.” In: *Nature* 435.7042 (2005), pp. 629–636. ISSN: 1476-4687. DOI: [10.1038/nature03597](https://doi.org/10.1038/nature03597). URL: <https://doi.org/10.1038/nature03597>.
- [19] P. C. Martin, E. D. Siggia, and H. A. Rose. “Statistical Dynamics of Classical Systems.” In: *Phys. Rev. A* 8 (1 1973), pp. 423–437. DOI: [10.1103/PhysRevA.8.423](https://doi.org/10.1103/PhysRevA.8.423). URL: <https://link.aps.org/doi/10.1103/PhysRevA.8.423>.
- [20] G. F. Mazenko. “Fundamental theory of statistical particle dynamics.” In: *Phys. Rev. E* 81 (6 2010), p. 061102. DOI: [10.1103/PhysRevE.81.061102](https://doi.org/10.1103/PhysRevE.81.061102). URL: <https://link.aps.org/doi/10.1103/PhysRevE.81.061102>.
- [21] S. P. Das and G. F. Mazenko. “Field Theoretic Formulation of Kinetic Theory: Basic Development.” In: *J. Stat. Phys.* 149.4 (2012), pp. 643–675. ISSN: 1572-9613. DOI: [10.1007/s10955-012-0610-y](https://doi.org/10.1007/s10955-012-0610-y). URL: <https://doi.org/10.1007/s10955-012-0610-y>.
- [22] R. Lilow, F. Fabis, E. Kozlikin, C. Viermann, and M. Bartelmann. “Resummed Kinetic Field Theory: general formalism and linear structure growth from Newtonian particle dynamics.” In: *J. Cosmol. Astropart. Phys.* 2019.04 (2019), p. 001. DOI: [10.1088/1475-7516/2019/04/001](https://doi.org/10.1088/1475-7516/2019/04/001). URL: <https://dx.doi.org/10.1088/1475-7516/2019/04/001>.
- [23] S. Dodelson. *Modern Cosmology*. Academic Press, Elsevier Science, 2003.
- [24] M. Bartelmann. *Das kosmologische Standardmodell*. Springer, 2019. ISBN: 978-3-662-59627-2. URL: <https://link.springer.com/book/10.1007/978-3-662-59627-2>.
- [25] S. Weinberg. *Cosmology*. Cosmology. OUP Oxford, 2008. ISBN: 9780191523601. URL: <https://books.google.de/books?id=nqQZdg020fsC>.
- [26] F. Zwicky. “On the Masses of Nebulae and of Clusters of Nebulae.” In: *Astrophys. J.* 86 (Oct. 1937), p. 217. DOI: [10.1086/143864](https://doi.org/10.1086/143864).

- [27] F. Chadha-Day, J. Ellis, and D. J. E. Marsh. “Axion dark matter: What is it and why now?” In: *Sci. Adv.* 8.8 (2022), eabj3618. DOI: [10.1126/sciadv.abj3618](https://doi.org/10.1126/sciadv.abj3618). eprint: <https://www.science.org/doi/pdf/10.1126/sciadv.abj3618>. URL: <https://www.science.org/doi/abs/10.1126/sciadv.abj3618>.
- [28] A. M. Green and B. J. Kavanagh. “Primordial black holes as a dark matter candidate.” In: *Journal of Physics G: Nuclear and Particle Physics* 48.4 (2021), p. 043001. DOI: [10.1088/1361-6471/abc534](https://doi.org/10.1088/1361-6471/abc534). URL: <https://dx.doi.org/10.1088/1361-6471/abc534>.
- [29] J. M. Bardeen, J. R. Bond, N. Kaiser, and A. S. Szalay. “The Statistics of Peaks of Gaussian Random Fields.” In: *Astrophys. J.* 304 (May 1986), p. 15. DOI: [10.1086/164143](https://doi.org/10.1086/164143).
- [30] B. Jain and E. Bertschinger. “Second-Order Power Spectrum and Nonlinear Evolution at High Redshift.” In: *Astrophys. J.* 431 (Aug. 1994), p. 495. DOI: [10.1086/174502](https://doi.org/10.1086/174502). arXiv: [astro-ph/9311070](https://arxiv.org/abs/astro-ph/9311070) [astro-ph].
- [31] J. Carlson, M. White, and N. Padmanabhan. “Critical look at cosmological perturbation theory techniques.” In: *Phys. Rev. D* 80 (4 2009), p. 043531. DOI: [10.1103/PhysRevD.80.043531](https://doi.org/10.1103/PhysRevD.80.043531). URL: <https://link.aps.org/doi/10.1103/PhysRevD.80.043531>.
- [32] T. Matsubara. “Resumming cosmological perturbations via the Lagrangian picture: One-loop results in real space and in redshift space.” In: *Phys. Rev. D* 77 (6 2008), p. 063530. DOI: [10.1103/PhysRevD.77.063530](https://doi.org/10.1103/PhysRevD.77.063530). URL: <https://link.aps.org/doi/10.1103/PhysRevD.77.063530>.
- [33] T. Matsubara. “Recursive solutions of Lagrangian perturbation theory.” In: *Phys. Rev. D* 92 (2 2015), p. 023534. DOI: [10.1103/PhysRevD.92.023534](https://doi.org/10.1103/PhysRevD.92.023534). URL: <https://link.aps.org/doi/10.1103/PhysRevD.92.023534>.
- [34] P. Valageas, T. Nishimichi, and A. Taruya. “Matter power spectrum from a Lagrangian-space regularization of perturbation theory.” In: *Phys. Rev. D* 87 (8 2013), p. 083522. DOI: [10.1103/PhysRevD.87.083522](https://doi.org/10.1103/PhysRevD.87.083522). URL: <https://link.aps.org/doi/10.1103/PhysRevD.87.083522>.
- [35] P. McDonald and Z. Vlah. “Large-scale structure perturbation theory without losing stream crossing.” In: *Phys. Rev. D* 97 (2 2018), p. 023508. DOI: [10.1103/PhysRevD.97.023508](https://doi.org/10.1103/PhysRevD.97.023508). URL: <https://link.aps.org/doi/10.1103/PhysRevD.97.023508>.
- [36] A. Cooray and R. Sheth. “Halo models of large scale structure.” In: *Phys. Rep.* 372.1 (Dec. 2002), pp. 1–129. DOI: [10.1016/S0370-1573\(02\)00276-4](https://doi.org/10.1016/S0370-1573(02)00276-4). arXiv: [astro-ph/0206508](https://arxiv.org/abs/astro-ph/0206508) [astro-ph].
- [37] R. Takahashi, M. Sato, T. Nishimichi, A. Taruya, and M. Oguri. “Revising the halofit model for the nonlinear matter power spectrum.” In: *Astrophys. J.* 761.2 (2012), p. 152. DOI: [10.1088/0004-637X/761/2/152](https://doi.org/10.1088/0004-637X/761/2/152). URL: <https://dx.doi.org/10.1088/0004-637X/761/2/152>.
- [38] R. E. Smith, J. A. Peacock, A. Jenkins, S. D. M. White, C. S. Frenk, F. R. Pearce, P. A. Thomas, G. Efstathiou, and H. M. P. Couchman. “Stable clustering, the halo model and non-linear cosmological power spectra.” In: *Mon. Notices Royal Astron. Soc.* 341.4 (June 2003), pp. 1311–1332. DOI: [10.1046/j.1365-8711.2003.06503.x](https://doi.org/10.1046/j.1365-8711.2003.06503.x). arXiv: [astro-ph/0207664](https://arxiv.org/abs/astro-ph/0207664) [astro-ph].

- [39] D. Baumann, A. Nicolis, L. Senatore, and M. Zaldarriaga. “Cosmological nonlinearities as an effective fluid.” In: *J. Cosmol. Astropart. Phys.* 2012.07 (2012), p. 051. DOI: [10.1088/1475-7516/2012/07/051](https://doi.org/10.1088/1475-7516/2012/07/051). URL: <https://dx.doi.org/10.1088/1475-7516/2012/07/051>.
- [40] J. J. M. Carrasco, M. P. Hertzberg, and L. Senatore. “The effective field theory of cosmological large scale structures.” In: *J. High Energy Phys.* 2012.9 (2012), p. 82. ISSN: 1029-8479. DOI: [10.1007/JHEP09\(2012\)082](https://doi.org/10.1007/JHEP09(2012)082). URL: [https://doi.org/10.1007/JHEP09\(2012\)082](https://doi.org/10.1007/JHEP09(2012)082).
- [41] J. J. M. Carrasco, S. Foreman, D. Green, and L. Senatore. “The Effective Field Theory of Large Scale Structures at two loops.” In: *J. Cosmol. Astropart. Phys.* 2014.07 (2014), p. 057. DOI: [10.1088/1475-7516/2014/07/057](https://dx.doi.org/10.1088/1475-7516/2014/07/057). URL: <https://dx.doi.org/10.1088/1475-7516/2014/07/057>.
- [42] J. Zinn-Justin. “Renormalization and stochastic quantization.” In: *Nucl. Phys. B* 275.1 (1986), pp. 135–159. ISSN: 0550-3213. DOI: [https://doi.org/10.1016/0550-3213\(86\)90592-4](https://doi.org/10.1016/0550-3213(86)90592-4). URL: <https://www.sciencedirect.com/science/article/pii/0550321386905924>.
- [43] E. Gozzi and M. Regini. “Addenda and corrections to work done on the path-integral approach to classical mechanics.” In: *Phys. Rev. D* 62 (6 2000), p. 067702. DOI: [10.1103/PhysRevD.62.067702](https://link.aps.org/doi/10.1103/PhysRevD.62.067702). URL: <https://link.aps.org/doi/10.1103/PhysRevD.62.067702>.
- [44] L. Heisenberg, S. Hemmatyar, and S. Zentarra. “Kinetic field theory: Higher-order perturbation theory.” In: *Phys. Rev. D* 106 (6 2022), p. 063513. DOI: [10.1103/PhysRevD.106.063513](https://link.aps.org/doi/10.1103/PhysRevD.106.063513). URL: <https://link.aps.org/doi/10.1103/PhysRevD.106.063513>.
- [45] B. Delamotte. “An Introduction to the Nonperturbative Renormalization Group.” In: *Lecture Notes in Physics, Berlin Springer Verlag*. Ed. by J. Polonyi and A. Schwenk. Vol. 852. 2012, p. 49. DOI: [10.1007/978-3-642-27320-9_2](https://doi.org/10.1007/978-3-642-27320-9_2).
- [46] C. Viermann, F. Fabis, E. Kozlikin, R. Lilow, and M. Bartelmann. “Nonequilibrium statistical field theory for classical particles: Basic kinetic theory.” In: *Phys. Rev. E* 91 (6 2015), p. 062120. DOI: [10.1103/PhysRevE.91.062120](https://link.aps.org/doi/10.1103/PhysRevE.91.062120). URL: <https://link.aps.org/doi/10.1103/PhysRevE.91.062120>.
- [47] R. Lilow. “Structure Formation in Dark and Baryonic Matter within Resummed Kinetic Field Theory.” PhD thesis. Heidelberg University, July 2018. URL: <http://www.ub.uni-heidelberg.de/archiv/24828>.
- [48] J. E. Mayer and E. Montroll. “Molecular Distribution.” In: *J. Chem. Phys.* 9.1 (Jan. 1941), pp. 2–16. DOI: [10.1063/1.1750822](https://doi.org/10.1063/1.1750822).
- [49] M. Bartelmann, J. Dombrowski, S. Konrad, E. Kozlikin, R. Lilow, C. Littek, C. Pixius, and F. Fabis. “Kinetic field theory: Non-linear cosmic power spectra in the mean-field approximation.” In: *SciPost Phys.* 10 (2021), p. 153. DOI: [10.21468/SciPostPhys.10.6.153](https://scipost.org/10.21468/SciPostPhys.10.6.153). URL: <https://scipost.org/10.21468/SciPostPhys.10.6.153>.
- [50] C. Pixius, S. Celik, and M. Bartelmann. “Kinetic field theory: perturbation theory beyond first order.” In: *J. Cosmol. Astropart. Phys.* 2022.12 (2022), p. 030. DOI: [10.1088/1475-7516/2022/12/030](https://dx.doi.org/10.1088/1475-7516/2022/12/030). URL: <https://dx.doi.org/10.1088/1475-7516/2022/12/030>.

- [51] E. Kozlikin, R. Lilow, F. Fabis, and M. Bartelmann. “A first comparison of Kinetic Field Theory with Eulerian Standard Perturbation Theory.” In: *J. Cosmol. Astropart. Phys.* 2021.06 (2021), p. 035. DOI: [10.1088/1475-7516/2021/06/035](https://doi.org/10.1088/1475-7516/2021/06/035). URL: <https://dx.doi.org/10.1088/1475-7516/2021/06/035>.

COLOPHON

This document was typeset using the typographical look-and-feel `classicthesis` developed by André Miede. The style was inspired by Robert Bringhurst's seminal book on typography "*The Elements of Typographic Style*". `classicthesis` is available for both \LaTeX and \LyX :

<https://bitbucket.org/amiede/classicthesis/>

Happy users of `classicthesis` usually send a real postcard to the author, a collection of postcards received so far is featured here:

<http://postcards.miede.de/>